

# Hofstadter Topology: Non-crystalline Topological Materials at High Flux

Jonah Herzog-Arbeitman<sup>1,\*</sup>, Zhi-Da Song<sup>1,\*</sup>, Nicolas Regnault<sup>1,2</sup>, and B. Andrei Bernevig<sup>1</sup>

<sup>1</sup>*Department of Physics, Princeton University, Princeton, NJ 08544 and*

<sup>2</sup>*Laboratoire de Physique de l'École normale supérieure,  
ENS, Université PSL, CNRS, Sorbonne Université,*

*Université Paris-Diderot, Sorbonne Paris Cité, Paris, France.*

(Dated: December 4, 2020)

The Hofstadter problem is the lattice analog of the quantum Hall effect and is the paradigmatic example of topology induced by an applied magnetic field. Conventionally, the Hofstadter problem involves adding  $\sim 10^4$  T magnetic fields to a *trivial* band structure. In this work, we show that when a magnetic field is added to an initially *topological* band structure, a wealth of possible phases emerges. Remarkably, we find topological phases which cannot be realized in any crystalline insulators. We prove that threading magnetic flux through a Hamiltonian with nonzero Chern number or Mirror Chern Number enforces a phase transition at fixed filling and that a 2D Hamiltonian with nontrivial Kane-Mele invariant can be classified a 3D TI or 3D weak TI phase in periodic flux. We then study fragile topology protected by the product of two-fold rotation and time-reversal and show that there exists a higher order TI phase where corner modes are pumped by flux. We show that a model of twisted bilayer graphene realizes this phase. Our results rely primarily on the magnetic translation group which exists at rational values of the flux. The advent of Moiré lattices renders our work relevant experimentally. Due to the enlarged Moiré unit cell, it is possible for laboratory-strength fields to reach one flux per plaquette and allow access to our proposed Hofstadter topological phase.

## I. INTRODUCTION

When a two dimensional crystalline lattice in which electrons have a trivial band structure is pierced by a uniform magnetic field, translational symmetry is broken and the energy spectrum develops a complex, fractal structure known as the Hofstadter Butterfly, which hosts a wealth of nontrivial Chern number topology despite the triviality of the original band structure [1–12]. In this work, we study the Hofstadter problem for an initially *topological* band structure and demonstrate new phases not possible in crystalline insulators. We prove that (1) a nonzero Chern number or mirror Chern number enforces a gapless point in the bulk of the Hofstadter Butterfly and (2) insulators with time-reversal symmetry  $\mathcal{T}$  (TRS) and nontrivial  $\mathbb{Z}_2$  invariant can be considered as either strong or weak 3D topological insulators (TIs) in flux and host gapless edge states. We then study insulators with fragile topology protected by  $C_{2z}\mathcal{T}$  symmetry and (3) show that the Hofstadter Hamiltonian can achieve a 3D Higher Order TI (HOTI) phase characterized by corner mode pumping. We then show that a model of twisted bilayer graphene (TBG) realizes the HOTI phase [13].

Recently, progress in the manufacture of two dimensional Moiré lattices with mesoscale effective unit cells has brought measurements of the Hofstadter Butterfly within reach by enabling access to large fluxes at laboratory-strength magnetic fields [13–25]. We expect our theoretical predictions to be verifiable in the near future, opening a new field of Hofstadter topology.

First we review the framework for introducing magnetic flux on a lattice using the Peierls substitution [26]. We consider a general tight-binding model with unit vectors  $\mathbf{a}_1, \mathbf{a}_2$  whose lattice points we call  $\mathbf{R}$ , with orbitals at  $\delta_\alpha, \alpha = 1, \dots, N_{orb}$ , and hopping elements given by  $t_{\alpha\beta}(\mathbf{r} - \mathbf{r}')$ ,  $\mathbf{r} = \mathbf{R} + \delta_\alpha, \mathbf{r}' = \mathbf{R}' + \delta_\beta$ . The number of occupied bands is  $N_{occ}$ . We write  $c_{\mathbf{R},\alpha}^\dagger$  ( $c_{\mathbf{R},\alpha}$ ) as the fermion creation (destruction) operator of the  $\alpha$  orbital at position  $\mathbf{R} + \delta_\alpha$ . We find it convenient to work in units where the area of the unit cell, the electron charge  $e$ , and  $\hbar$  are all set to one. By Peierls' substitution, the hoppings acquire a phase  $t_{\alpha\beta}(\mathbf{r} - \mathbf{r}') \rightarrow t_{\alpha\beta}(\mathbf{r} - \mathbf{r}') \exp[i \int_{\mathbf{r}'}^{\mathbf{r}} \mathbf{A} \cdot d\mathbf{r}]$ . The path of integration is a straight line between the orbitals when they are well localized (see App. A1). We work in the Landau gauge  $\mathbf{A}(\mathbf{r}) = -\phi \mathbf{b}_1(\mathbf{r} \cdot \mathbf{b}_2)$  where the reciprocal vectors  $\mathbf{b}_i$  satisfy  $\mathbf{b}_i \cdot \mathbf{a}_j = \delta_{ij}$  and  $\phi$  is the flux per unit cell. In this gauge, the hoppings retain translation invariance along  $\mathbf{a}_1$  but the translation symmetry along  $\mathbf{a}_2$  is broken. However, at rational values of the flux where  $\phi = \frac{2\pi p}{q}$  with  $q, p$  coprime, the hoppings recover an extended translational symmetry:  $\mathbf{r} \rightarrow \mathbf{r} + q\mathbf{a}_2$ . In this case, we can diagonalize the Hamiltonian in the  $1 \times q$  magnetic unit cell:

$$H^\phi = \sum_{k_1, k_2, \alpha, \beta, r_2, r_2'} c_{k_1, k_2, r_2, \alpha}^\dagger [\mathcal{H}^\phi(k_1, k_2)]_{r_2, \alpha, r_2', \beta} c_{k_1, k_2, r_2', \beta}. \quad (1)$$

Here  $r_2', r_2 = 0, \dots, q - 1$  are the coordinates of the magnetic unit cell in the  $\mathbf{a}_2$  direction,  $k_1 \in (-\pi, \pi)$  is the momentum along  $\mathbf{b}_1$ ,  $k_2$  is the momentum along  $\mathbf{b}_2$  and takes values in  $(0, \frac{2\pi}{q})$  due to the enlargement of the magnetic unit cell, and  $\mathcal{H}^\phi$  is the single-particle  $qN_{orb} \times qN_{orb}$  Hamiltonian which we will refer to as the Hofstadter Hamiltonian. Importantly, the Hofstadter

\* These authors contributed equally.

Hamiltonian is periodic in flux up to a unitary transformation:  $H^{\phi+\Phi} = UH^\phi U^\dagger$ , where  $\Phi = 2\pi n, n \in \mathbb{N}$  is determined by the condition that *all* closed hopping loops encircle an integer number of flux quanta. In simple models such as nearest-neighbor hopping on the square lattice,  $n = 1$ . We can show (see App. A 2) that

$$U = \exp \left[ i \sum_{\mathbf{R}\alpha} \int_{\mathbf{r}_0}^{\mathbf{R}+\delta_\alpha} \tilde{\mathbf{A}} \cdot d\mathbf{r} c_{\mathbf{R},\alpha}^\dagger c_{\mathbf{R},\alpha} \right], \quad \nabla \times \tilde{\mathbf{A}} = \Phi \quad (2)$$

where  $\mathbf{r}_0$  is the position of a fixed but arbitrary orbital of the Hamiltonian, and the integral may be taken along any sequence of Peierls paths due to the definition of  $\Phi$ .

A central feature of the Hofstadter Hamiltonian is the increased periodicity of its Brillouin Zone (BZ) which can be deduced from the magnetic translation group [27]. As shown in Eq. (1),  $k_2$  is  $2\pi/q$  periodic. Here we show that the energy bands are also  $2\pi/q$  periodic along  $k_1$ . The single-particle magnetic translation operators are

$$T_i(\phi) = \sum_{\mathbf{R}\alpha} e^{i \int_{\mathbf{R}+\delta_\alpha}^{\mathbf{R}+\delta_\alpha+\mathbf{a}_i} \mathbf{A} \cdot d\mathbf{r} + i\chi_i(\mathbf{R}+\delta_\alpha)} c_{\mathbf{R}+\mathbf{a}_i,\alpha}^\dagger c_{\mathbf{R},\alpha}, \quad (3)$$

where  $\chi_i(\mathbf{r}) = \phi(\mathbf{a}_i \times \mathbf{r}) \cdot \hat{z}$  has been determined by requiring  $[H^\phi, T_i(\phi)] = 0$  and the integral is taken along a straight-line path (see App. A 3). While the translation operators commute in the absence of flux, otherwise we find  $T_1(\phi)T_2(\phi) = e^{i\phi}T_2(\phi)T_1(\phi)$ . However, at rational flux  $\phi = \frac{2\pi p}{q}$ , we see  $[T_1(\phi), T_2^q(\phi)] = 0$ . Hence  $H^\phi, T_1(\phi)$ , and  $T_2^q(\phi)$  commute and eigenstates may be written as  $|m, k_1, k_2\rangle$  with corresponding eigenvalues  $\epsilon_m(\mathbf{k}), e^{ik_1}, e^{iqk_2}$ , with  $m = 1, \dots, qN_{orb}$  (see Eq. (1)). Because  $[H^\phi, T_2(\phi)] = 0$ , the states  $T_2^j(\phi)|m, k_1, k_2\rangle$  also have energy  $\epsilon_m(\mathbf{k})$ . The  $k_1$  momentum of such states is deduced from  $T_1(\phi)(T_2^j(\phi)|m, k_1, k_2\rangle) = e^{i(k_1+j\phi)}T_2^j(\phi)|m, k_1, k_2\rangle$  and hence they represent the new states at  $k_1 + j\phi$  (see App. D 2 b). Thus we find

$$T_2^j(\phi)|m, k_1, k_2\rangle \sim |m, k_1 + j\phi, k_2\rangle, \quad j = 0, \dots, q-1 \quad (4)$$

are all degenerate in energy. Recalling that  $k_2 \in (0, \frac{2\pi}{q})$ , we conclude that the magnetic BZ has an increased periodicity:  $\epsilon_n(\mathbf{k}) = \epsilon_n(\mathbf{k} + \frac{2\pi}{q}\mathbf{b}_i)$ ,  $i = 1, 2$ . This feature is essential in the following proofs.

## II. CHERN INSULATORS

As a warmup, we study the Hofstadter Butterfly of a Chern insulator. According to the Streda formula [5], the filling of a state with fixed nonzero Chern number changes as the flux is increased. In the paradigm of Hofstadter topology, we prove a complementary result: at *fixed* filling, the many-body gap of a Chern insulator has a discontinuity at  $\phi = 0$  enforced by a mismatch between the Chern number at zero flux and any infinitesimal flux.

Consider a Hamiltonian  $H^{\phi=0}$  which is gapped with a nonzero Chern number  $C^{\phi=0}$  at filling  $\nu = N_{occ}/N_{orb}$ .

We emphasize that we keep  $\nu$  fixed as the flux is increased. Now we choose a flux  $\phi = \frac{2\pi p}{q}$  such that  $C^{\phi=0}/q \notin \mathbb{Z}$ . The magnetic unit cell of  $H^\phi$  contains  $qN_{orb}$  orbitals and  $qN_{occ}$  occupied bands at filling  $\nu$ . First, we introduce an onsite potential term of overall amplitude  $M$  to  $H^{\phi=0}$  that creates an energy splitting between each of the orbitals. For sufficiently large  $M$ , the model will be split into  $N_{orb}$  trivial bands and it will reach a gapped atomic limit for all  $\phi$  (see App. B).

As we tune  $M$  from zero to infinity, gap closings occur which eventually cause  $H^{\phi=\frac{2\pi p}{q}}$  to undergo a series of phase transitions into a trivial atomic limit (see App. B) at filling  $\nu = qN_{occ}/qN_{orb}^1$ , recalling that the change in Chern number is determined locally by the closing bands [5, 28, 29]. If there is gap closing at the each of the points  $\mathbf{k}^* + j\phi\mathbf{b}_1 \bmod 2\pi, j = 1, \dots, q-1$  due to the magnetic BZ periodicity of Eq. (4). Because a multiple of  $q$  gap closings separate  $H^\phi$  from the trivial atomic limit at large  $M$  where the Chern number is zero, it must be that  $C^{\phi=\frac{2\pi p}{q}} \neq 0 \in q\mathbb{Z}$ , zero included. Hence we recover the result of Ref. [8] using a proof applicable to Sec. III.

Since we chose  $q$  such that  $C^{\phi=0} \notin q\mathbb{Z}$ , we find by construction that the Chern number has changed during an adiabatic perturbation of  $H^\phi$ . But this is only possible if the gap closes for  $\phi \in [0, \frac{2\pi p}{q}]$ . For every  $C^{\phi=0}$ , we may choose an arbitrarily large  $q$  allowing us to conclude that, at fixed filling, the many-body gap must close immediately when the flux is increased from the fine-tuned point at  $\phi = 0$  (see App. C 2). This enforces a discontinuity in the occupied states as shown for a typical Chern insulator in Fig. 1a. There is no protected gap closing if  $C^{\phi=0} = 0$  because a vanishing Chern number is possible for all flux at filling  $\nu = N_{occ}/N_{orb}$ .

We now extend this result to insulators with a nonzero Mirror Chern number [30, 31]. Because mirror symmetry  $M_z$  is not broken in the presence of flux,  $M_z$  remains well-defined at all  $\phi$ . Then we may block-diagonalize  $H^\phi$  at all  $\phi$  by its mirror eigenvalues. Each block has a nonzero Chern number at  $\phi = 0$ , and thus the gap closes immediately at  $\phi = 0$  and filling  $\nu$  within each individual block. Each block must have a branch of its spectrum connecting its valence and conduction bands. Hence for *any* Fermi energy in the zero-flux gap, there will be a gapless point at *finite* flux in the spectrum of the whole model (see App. C 3). In Fig. 1b, we consider the Quantum Spin Hall model  $H_{QSH}$  of Ref. [30] with a nonzero Mirror Chern number. We show numerical confirmation that although the Chern number is identically zero due to TRS, the gap still closes due to the Mirror Chern number.

<sup>1</sup>Note that the structure of an *onsite* potential is identical for the  $q$  unit cells within the magnetic unit cell

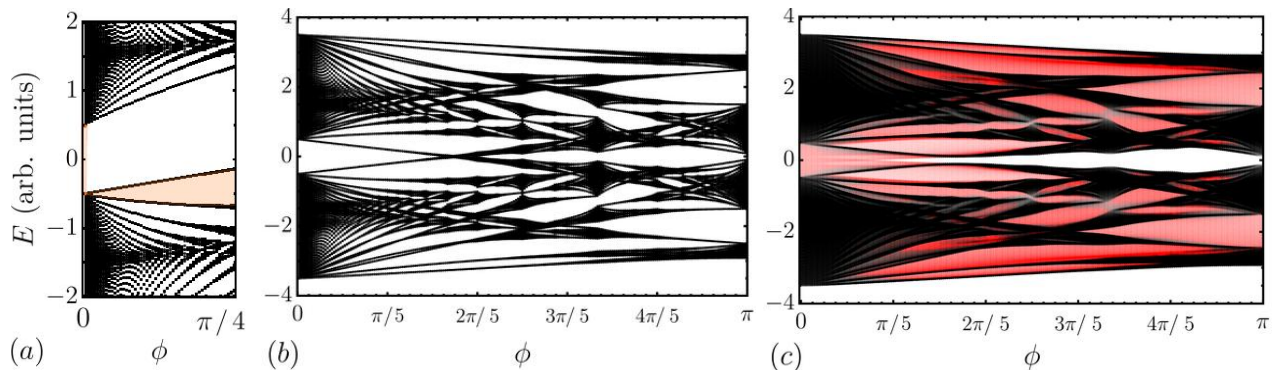


FIG. 1. (a) We consider a  $C = 1$  Chern insulator (see App. F) with the half-filling many-body gap shaded in orange. At zero flux, the gap is  $\sim 1$ , but when the flux is increased at constant filling, the gap discontinuously closes at infinitesimal  $\phi$ . Notably, this discontinuity is impossible to realize in *any* crystalline system and relies on the infinitely large magnetic unit cell as  $\phi \rightarrow 0$ . (b) We consider the Hofstadter spectrum of a model  $H'_{QSH}$  with nonzero Mirror Chern number and all symmetries broken except for  $M_z$  and  $\mathcal{T}$ . The gap closing at finite  $\phi$  is protected by  $M_z$ ; breaking it allows a gap to open in the bulk. (c) We show the Hofstadter Butterfly calculated on a  $30 \times 30$  lattice for  $H''_{QSH}$ , a variation where  $M_z$  is broken and  $\mathcal{T}$  is the only symmetry. The bulk spectrum (black) is gapped, but the edge spectrum (red) is gapless at  $\phi = 0$ . As the flux is increased to  $\phi = \pi$ , the edge states gap and move into the bulk. We also observe quantum hall states at all fluxes and fillings where  $\nu N_{orb} \notin \mathbb{N}$ . This is explained by the Diophantine equation, which can be written  $\frac{\phi}{2\pi}C = N_{orb}\nu \pmod{1}$  [8].

### III. TIME-REVERSAL INVARIANT INSULATORS

We show in this section that when a Hofstadter Hamiltonian with spinful TRS  $\mathcal{T}$  is topological (in a quantum spin hall state) at  $\phi = 0$ , it realizes a nontrivial 3D phase where the flux  $\phi$  is identified with  $k_z$  [30, 32, 33]. Recall that  $H^\phi$  is  $\Phi = 2\pi n$  periodic in flux. When  $n$  is odd,  $H^\phi$  is classified as a 3D TI, and may be a weak TI or 3D TI when  $n$  is even. However, it can never be 3D trivial.

The identification of  $\phi$  with  $k_z$  is deduced from its transformation under  $\mathcal{T}$ . Because  $\mathcal{T}$  is anti-unitary, it flips the sign of  $\phi$  in the Peierls substitution and hence

$$\mathcal{T}^{-1}\mathcal{H}^\phi(\mathbf{k})\mathcal{T} = \mathcal{H}^{-\phi}(-\mathbf{k}). \quad (5)$$

Let us first consider the simple case of  $\Phi = 2\pi$ , i.e.  $n = 1$ . Then  $\phi$  is  $2\pi$ -periodic and behaves as  $k_z$  would in a 3D Hamiltonian. Furthermore, we recall that  $H^{\phi+\Phi} = UH^\phi U^\dagger$  so from

$$(UT)H^\pi(UT)^\dagger = UH^{-\pi}U^\dagger = H^\pi, \quad (6)$$

we see that  $UT$  is a symmetry of  $H^{\phi=\pi}$ . It can be shown that  $(UT)^2 = \mathcal{T}^2 = -1$  (see App. D 1) so  $H^{\phi=\pi}$  also has a  $\mathbb{Z}_2$  topological classification.<sup>2</sup>

Considering  $H^\phi$  as a 3D model with  $\mathcal{T}$  symmetry, its topology is characterized by the magnetoelectric polarizability  $\theta \in \{0, \pi\}$  where  $\pi$  is the nontrivial value of the

3D TI phase.  $\theta$  is related to the Pfaffian  $\mathbb{Z}_2$  invariants by  $e^{i\theta} = \delta^{\phi=0} \times \delta^{\phi=\pi}$ , where  $\delta^\phi \in \{-1, 1\}$  is the protected by  $\mathcal{T}$  ( $UT$ ) at  $\phi = 0$  ( $\pi$ ) [34–36]. Because we assume that  $H^{\phi=0}$  is nontrivial, we need only show that  $\delta^{\phi=\pi} = +1$  in order to prove  $\theta = \pi$ . To do so, we introduce the parameter  $M$  which tunes the  $H^\phi$  to a trivial atomic limit as described in Sec. II. Now consider the magnetic BZ at  $\phi = \pi$  with  $k_1 \in (-\pi, \pi), k_2 \in (0, \pi)$ . Eq. (4) requires the BZ to be  $\pi$  periodic,  $\epsilon_m(\mathbf{k} + \pi\mathbf{b}_1) = \epsilon_m(\mathbf{k})$ . As  $M \rightarrow \infty$ , we determine the change in  $\delta^{\phi=\pi}$  by counting gap closings in *half* of the magnetic BZ defined by  $BZ_{1/2} = k_1 \in (-\pi, \pi), k_2 \in (0, \pi/2)$  [35, 37, 38]. If there is a gap closing at  $\mathbf{k}^* \in BZ_{1/2}$ , there is a second identical closing at  $\mathbf{k}^* + \pi\mathbf{b}_1 \in BZ_{1/2}$ . Each gap closing changes the sign of  $\delta^{\phi=\pi}$ , so it must be that  $\delta^{\pi-\phi} = +1$  because an even number of gap closings occur between  $M = 0$  and the trivial phase at  $M = \infty$ . We conclude  $\theta = \pi$ , proving that the Hofstadter Hamiltonian is a 3D TI. On open boundary conditions (OBC), such a model will pump gapless edge states into the bulk as  $\phi$  is increased, as exemplified in Fig. 1b. There, for a perturbed model with only  $\mathcal{T}$  symmetry  $H''_{QSH}$  (see App. F 1), we observe gapless edge states for small flux and their disappearance into the bulk.

The  $\pi$  periodicity in the magnetic BZ was crucial to proving that  $H^{\phi=\pi}$  is trivial. Generally, if  $\Phi = 2\pi n$  then the  $UT$ -symmetric point exists at  $\Phi/2 = n\pi$ . When  $n$  is odd, the energy spectrum is still  $\pi$  periodic along  $k_1$ , and we conclude that  $\delta^{\phi=n\pi} = +1$  (see App. D 2). However when  $n$  is even, this  $\pi$  periodicity is absent so our proof fails, and indeed,  $H^\phi$  can be a weak or strong 3D TI (see App. F 2).

<sup>2</sup>For pedagogical purposes, we assume that  $U$  is diagonal in momentum space. In the generic case, the algebra of  $UT$  and  $T_i(\phi)$  acquires a projective phase which leads to an off-diagonal representation of  $UT$  on the magnetic BZ (see App. D 2).

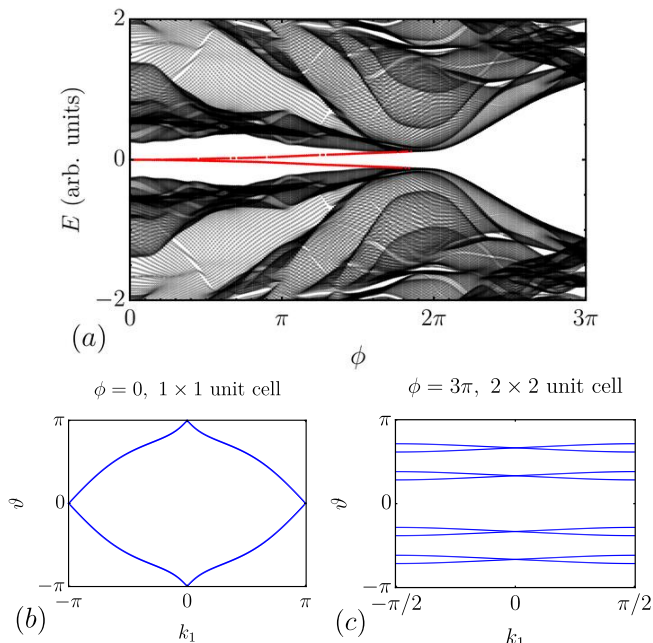


FIG. 2. (a) The Hofstadter Butterfly is calculated on a  $30 \times 30$  lattice for  $H'_{TBG}$  which has only  $C_{2z}\mathcal{T}$  symmetry (see App. G 1). The corner modes are shown in red over the gapped black bulk and edge spectrum, and pump between the nontrivial  $w_2 = 1$  phase at  $\phi = 0$  to the trivial phase at  $\phi = 3\pi$  where  $w_2 = 0$ . This model is classified as a HOTI. (b) We observe from the Wilson loop spectrum, with eigenvalues  $\exp i\vartheta(k_1)$ , that  $w_2^{\phi=0} = 1$  due to the odd number of crossings at  $\vartheta = 0$  and  $\vartheta = \pi$  [39]. (c) The Wilson spectrum at  $\phi = 3\pi$  is calculated in an extended  $2 \times 2$  unit cell where  $U$  is diagonal in momentum space (see App. G 3). Here,  $w_2^{\phi=3\pi} = 0$  because there are no crossings at  $\vartheta = 0$  and  $\vartheta = \pi$ .

#### IV. FRAGILE TOPOLOGICAL INSULATORS

So far we have studied the Hofstadter topology deriving from strong topological 2D phases with a nontrivial Chern number, the Mirror Chern number, or  $\mathbb{Z}_2$  index. We now consider a fragile invariant, the second Stiefel-Whitney index  $w_2 \in \{0, 1\}$  protected by  $C_{2z}\mathcal{T}$  (with  $(C_{2z}\mathcal{T})^2 = +1$ ) [13, 39–41]. A nontrivial value of  $w_2 = 1$  indicates fractional corner states [39, 42–45], and may be computed in the bulk from the Wilson loop eigenvalues or the nested Wilson loop [39, 46, 47].

The 3D HOTI phase is characterized by pumping corner states between a  $w_2$  nontrivial phase and trivial phase [31, 48]. Because  $(C_{2z}\mathcal{T})^{-1}\mathcal{H}^\phi(\mathbf{k})(C_{2z}\mathcal{T}) = \mathcal{H}^{-\phi}(\mathbf{k})$ , we can again identify  $\phi$  with  $k_z$  and use 3D topological invariants to classify  $H^\phi$ , which we now discuss.

We have assumed that  $C_{2z}\mathcal{T}$  is a symmetry of  $H^{\phi=0}$  and protects the invariant  $w_2^{\phi=0}$ . For a Hofstadter Hamiltonian that has a  $\Phi = 2\pi n$  periodicity in flux, the other symmetric point occurs at  $\phi = \Phi/2$  where  $H^{\Phi/2}$  has the symmetry  $UC_{2z}\mathcal{T}$ . We can show that  $(UC_{2z}\mathcal{T})^2 = \pm 1$  where the sign must be calculated from the Peierls paths (see App. E 1). The Hofstadter topological invariant de-

pends on this sign. If  $(UC_{2z}\mathcal{T})^2 = +1$ , a nonzero value of  $\frac{\theta}{\pi} = w_2^{\phi=0} - w_2^{\phi=\Phi/2}$  indicates corner state flow.<sup>3</sup> [48].

If  $(UC_{2z}\mathcal{T})^2 = -1$ , there is no  $w_2$  index at  $\phi = \Phi/2$  [39]. However, we can diagnose the topology directly with the nested Wilson loop and Kramers' theorem for  $(UC_{2z}\mathcal{T})^2 = -1$  (see App. E 3), showing there are no protected corner states at  $\phi = \Phi/2$  and the Hofstadter HOTI invariant depends only on the zero-field topology, i.e.  $\frac{\theta}{\pi} = w_2^{\phi=0}$ .

To exemplify the Hofstadter HOTI phase, we now consider  $H_{TBG}$ : a 4-band model of TBG with  $C_{2x}, C_{3z}, C_{2z}$ , and  $\mathcal{T}$  symmetries which possesses fragile Wilson loop winding yielding  $w_2^{\phi=0} = 1$  [13, 49]. We study a perturbed model  $H'_{TBG}$  which has only  $C_{2z}\mathcal{T}$  to protect the fragile topology (see App. G 1). The Hofstadter Hamiltonian has  $\Phi = 6\pi$  and  $(UC_{2z}\mathcal{T})^2 = +1$  (see App. G 1). In Fig. 2a, we calculate the Hofstadter Butterfly with OBC and observe the pumping of corner modes (with a gapped bulk and edge) that characterizes a HOTI. We show that  $\theta = \pi$  by calculating the  $w_2$  indices at  $\phi = 0, \Phi/2$  from the Wilson loop spectra shown in Fig. 2b,c.<sup>4</sup> Breaking the  $C_{2z}$  and  $C_{2x}\mathcal{T}$  symmetries of  $H_{TBG}$  (which are *not* true symmetries of TBG) is crucial. Both symmetries are preserved at all  $\phi$  and can enforce a bulk gap closing [50–52], which would disrupt the appearance of the HOTI phase (see Apps. G 5 and G 4).

#### V. DISCUSSION

The topological phases of the Hofstadter Hamiltonian can be computed in the momentum-flux manifold. We demonstrated that a nonzero Chern number or mirror Chern number enforces a level crossing in the bulk as flux is pumped through the crystal. In analogy to the 3D classifications, we call this a topologically protected Hofstadter semimetal. The Hofstadter topology of a Hamiltonian with a nontrivial  $\mathbb{Z}_2$  index depended on the flux periodicity  $\Phi = 2\pi n$ . When  $n$  is odd, we proved that the Hofstadter realized a 3D TI phase where flux pumps edge states into the bulk. Finally, we considered fragile topology at zero flux given by nonzero  $w_2$  index and found that the topological index of the Hofstadter Hamiltonian depended on the sign of  $(UC_{2z}\mathcal{T})^2 = \pm 1$  through the Peierls paths. This is notably different from crystalline systems where  $(C_{2z}\mathcal{T})^2 = +1$  with and without SOC. In the strong Hofstadter HOTI phase, realized by a model of TBG, flux pumps corner states into the bulk.

<sup>3</sup>The nontrivial phase with  $\theta = \pi$  is a “strong” symmetry-protected topological phase with corner state pumping. If both  $w_2^{\phi=0} = w_2^{\phi=\Phi/2} = 1$ , then  $\theta = 0$  but both  $H^{\phi=0}$  and  $H^{\phi=\Phi/2}$  have nontrivial corner states, which is a “weak” 3D fragile state.

<sup>4</sup>At  $\Phi/2$ , we have artificially doubled the magnetic unit cell along the  $\mathbf{a}_1$  direction so that  $UC_{2z}\mathcal{T}$  is diagonal in momentum space (see App. G 3)

We expect the results of this work to be experimentally verifiable using Moiré lattices, which have very large unit cells at small twist angles [18]. Indeed, after the submission of this work, Ref. [53] observed signatures of fragile Hofstadter topology in a TBG system, and Ref. [54] identified the flux-induced gap closings indicative of a Hofstadter semimetal protected by a valley Chern number in twisted double bilayer graphene. Both experiments show that realistic magnetic fields can probe the Hofstadter phase.

## VI. ACKNOWLEDGEMENTS

We thank Fang Xie, Biao Lian, Christopher Mora, and

Benjamin Wieder for helpful discussions. We also thank one of our referees for pointing out Ref. [8]. B. A. B., N.R., and S. Z.-D. were supported by the Department of Energy Grant No. desc0016239, the Schmidt Fund for Innovative Research, Simons Investigator Grant No. 404513, and the Packard Foundation. Further support was provided by the National Science Foundation EAGER Grant No. DMR 1643312, NSF-MRSEC DMR-1420541, BSF Israel US foundation No. 2018226, and ONR No. N00014-20-1-2303.

- 
- [1] Douglas R. Hofstadter. Energy levels and wave functions of bloch electrons in rational and irrational magnetic fields. *Phys. Rev. B*, 14:2239–2249, Sep 1976. doi:10.1103/PhysRevB.14.2239.
- [2] D. J. Thouless, M. Kohmoto, M. P. Nightingale, and M. den Nijs. Quantized hall conductance in a two-dimensional periodic potential. *Phys. Rev. Lett.*, 49:405–408, Aug 1982. doi:10.1103/PhysRevLett.49.405.
- [3] P G Harper. The general motion of conduction electrons in a uniform magnetic field, with application to the diamagnetism of metals. *Proceedings of the Physical Society. Section A*, 68(10):879–892, oct 1955. doi:10.1088/0370-1298/68/10/305.
- [4] Gerardo Naumis. Higher-dimensional quasicrystalline approach to the Hofstadter butterfly topological-phase band conductances: Symbolic sequences and self-similar rules at all magnetic fluxes. *Phys. Rev. B*, 100(16):165101, October 2019. doi:10.1103/PhysRevB.100.165101.
- [5] B. Andrei Bernevig and Taylor L. Hughes. *Topological Insulators and Topological Superconductors*. Princeton University Press, student edition edition, 2013. ISBN 9780691151755.
- [6] P. Wang, B. Cheng, O. Martynov, T. Miao, L. Jing, T. Taniguchi, K. Watanabe, V. Aji, C. N. Lau, and M. Bockrath. Topological Winding Number Change and Broken Inversion Symmetry in a Hofstadter’s Butterfly. *Nano Letters*, 15:6395–6399, October 2015. doi:10.1021/acs.nanolett.5b01568.
- [7] C. Albrecht, J. H. Smet, K. von Klitzing, D. Weiss, V. Umansky, and H. Schweizer. Evidence of hofstadter’s fractal energy spectrum in the quantized hall conductance. *Phys. Rev. Lett.*, 86:147–150, Jan 2001. doi:10.1103/PhysRevLett.86.147.
- [8] I Dana, Y Avron, and J Zak. Quantised hall conductance in a perfect crystal. *Journal of Physics C: Solid State Physics*, 18(22):L679–L683, aug 1985. doi:10.1088/0022-3719/18/22/004. URL <https://doi.org/10.1088/0022-3719/18/22/004>.
- [9] Yuria Otaki and Takahiro Fukui. Higher-order topological insulators in a magnetic field. *Phys. Rev. B*, 100(24):245108, December 2019. doi:10.1103/PhysRevB.100.245108.
- [10] Yujun Deng, Yijun Yu, Meng Zhu Shi, Zhongxun Guo, Zihan Xu, Jing Wang, Xian Hui Chen, and Yuanbo Zhang. Quantum anomalous Hall effect in intrinsic magnetic topological insulator MnBi<sub>2</sub>Te<sub>4</sub>. *Science*, 367(6480):895–900, February 2020. doi:10.1126/science.aax8156.
- [11] Cui-Zu Chang, Jinsong Zhang, Xiao Feng, Jie Shen, Zuocheng Zhang, Minghua Guo, Kang Li, Yunbo Ou, Pang Wei, Li-Li Wang, Zhong-Qing Ji, Yang Feng, Shuaihua Ji, Xi Chen, Jinfeng Jia, Xi Dai, Zhong Fang, Shou-Cheng Zhang, Ke He, Yayu Wang, Li Lu, Xu-Cun Ma, and Qi-Kun Xue. Experimental Observation of the Quantum Anomalous Hall Effect in a Magnetic Topological Insulator. *Science*, 340(6129):167–170, April 2013. doi:10.1126/science.1234414.
- [12] Peng Cheng, Canli Song, Tong Zhang, Yanyi Zhang, Yilin Wang, Jin-Feng Jia, Jing Wang, Yayu Wang, Bang-Fen Zhu, Xi Chen, Xucun Ma, Ke He, Lili Wang, Xi Dai, Zhong Fang, Xincheng Xie, Xiao-Liang Qi, Chao-Xing Liu, Shou-Cheng Zhang, and Qi-Kun Xue. Landau Quantization of Topological Surface States in Bi<sub>2</sub>Se<sub>3</sub>. *Phys. Rev. Lett.*, 105(7):076801, August 2010. doi:10.1103/PhysRevLett.105.076801.
- [13] Zhi-Da Song, Zhijun Wang, Wujun Shi, Gang Li, Chen Fang, and B. Andrei Bernevig. All Magic Angles in Twisted Bilayer Graphene are Topological. *Phys. Rev. Lett.*, 123(3):036401, Jul 2019. doi:10.1103/PhysRevLett.123.036401.
- [14] Xiang Ni, Kai Chen, Matthew Weiner, David J. Apigo, Camelia Prodan, Andrea Alù, Emil Prodan, and Alexander B. Khanikaev. Observation of hofstadter butterfly and topological edge states in reconfigurable quasi-periodic acoustic crystals. *Communications Physics*, 2(1):55, 2019. doi:10.1038/s42005-019-0151-7.
- [15] C. R. Dean, L. Wang, P. Maher, C. Forsythe, F. Ghahari, Y. Gao, J. Katoch, M. Ishigami, P. Moon, M. Koshino, T. Taniguchi, K. Watanabe, K. L. Shepard, J. Hone, and P. Kim. Hofstadter’s butterfly and the fractal quantum hall effect in moirésuperlattices. *Nature*, 497:598 EP –, 05 2013.
- [16] B. Hunt, J. D. Sanchez-Yamagishi, A. F. Young, M. Yankowitz, B. J. LeRoy, K. Watanabe, T. Taniguchi, P. Moon, M. Koshino, and P. Jarillo-Herrero. Massive Dirac Fermions and Hofstadter Butterfly in a van der Waals Heterostructure. *Science*, 340(6139):1427–1430,

- Jun 2013. doi:10.1126/science.1237240.
- [17] L. A. Ponomarenko, R. V. Gorbachev, G. L. Yu, D. C. Elias, R. Jalil, A. A. Patel, A. Mishchenko, A. S. Mayorov, C. R. Woods, and J. R. Wallbank. Cloning of Dirac fermions in graphene superlattices. *Nature (London)*, 497(7451):594–597, May 2013. doi:10.1038/nature12187.
- [18] Rafi Bistritzer and Allan H. MacDonald. Moiré bands in twisted double-layer graphene. *Proceedings of the National Academy of Science*, 108(30):12233–12237, Jul 2011. doi:10.1073/pnas.1108174108.
- [19] C. R. Dean, A. F. Young, I. Meric, C. Lee, L. Wang, S. Sorgenfrei, K. Watanabe, T. Taniguchi, P. Kim, K. L. Shepard, and J. Hone. Boron nitride substrates for high-quality graphene electronics. *Nature Nanotechnology*, 5(10):722–726, Oct 2010. doi:10.1038/nnano.2010.172.
- [20] Yuan Cao, Valla Fatemi, Ahmet Demir, Shiang Fang, Spencer L. Tomarken, Jason Y. Luo, Javier D. Sanchez-Yamagishi, Kenji Watanabe, Takashi Taniguchi, Efthimios Kaxiras, Ray C. Ashoori, and Pablo Jarillo-Herrero. Correlated insulator behaviour at half-filling in magic-angle graphene superlattices. *Nature (London)*, 556(7699):80–84, Apr 2018. doi:10.1038/nature26154.
- [21] Yonglong Xie, Biao Lian, Berthold Jäck, Xiaomeng Liu, Cheng-Li Chiu, Kenji Watanabe, Takashi Taniguchi, B. Andrei Bernevig, and Ali Yazdani. Spectroscopic signatures of many-body correlations in magic-angle twisted bilayer graphene. *Nature (London)*, 572(7767):101–105, Jul 2019. doi:10.1038/s41586-019-1422-x.
- [22] V A Skachkova, M S Baranova, D C Hvezdouski, and V R Stempitsky. Electronic properties of graphene-based heterostructures. *Journal of Physics: Conference Series*, 917:092012, nov 2017. doi:10.1088/1742-6596/917/9/092012.
- [23] I. Meric, C. R. Dean, A. F. Young, J. Hone, P. Kim, and K. L. Shepard. Graphene field-effect transistors based on boron nitride gate dielectrics. *arXiv e-prints*, art. arXiv:1101.4712, January 2011.
- [24] B. Hunt, J. D. Sanchez-Yamagishi, A. F. Young, M. Yankowitz, B. J. LeRoy, K. Watanabe, T. Taniguchi, P. Moon, M. Koshino, P. Jarillo-Herrero, and R. C. Ashoori. Massive dirac fermions and hofstadter butterfly in a van der waals heterostructure. *Science*, 340(6139):1427–1430, 2013. ISSN 0036-8075. doi:10.1126/science.1237240.
- [25] I. Meric, C. R. Dean, A. F. Young, J. Hone, P. Kim, and K. L. Shepard. Graphene field-effect transistors based on boron nitride gate dielectrics. *arXiv e-prints*, art. arXiv:1101.4712, Jan 2011.
- [26] R. Peierls. Zur Theorie des Diamagnetismus von Leitungselektronen. *Zeitschrift fur Physik*, 80:763–791, November 1933. doi:10.1007/BF01342591.
- [27] J. Zak. Magnetic translation group. *Phys. Rev.*, 134:A1602–A1606, Jun 1964. doi:10.1103/PhysRev.134.A1602.
- [28] Siddharth A. Parameswaran, Rahul Roy, and Shivaji L. Sondhi. Fractional quantum Hall physics in topological flat bands. *Comptes Rendus Physique*, 14(9):816–839, November 2013. doi:10.1016/j.crhy.2013.04.003.
- [29] Christian Brouder, Gianluca Panati, Matteo Calandra, Christophe Mourougane, and Nicola Marzari. Exponential localization of wannier functions in insulators. *Physical Review Letters*, 98(4), Jan 2007. ISSN 1079-7114. doi:10.1103/physrevlett.98.046402.
- [30] B. Andrei Bernevig, Taylor L. Hughes, and Shou-Cheng Zhang. Quantum Spin Hall Effect and Topological Phase Transition in HgTe Quantum Wells. *Science*, 314(5806):1757, Dec 2006. doi:10.1126/science.1133734.
- [31] Frank Schindler, Ashley M. Cook, Maia G. Vergniory, Zhijun Wang, Stuart S. P. Parkin, B. Andrei Bernevig, and Titus Neupert. Higher-order topological insulators. *Science Advances*, 4(6):eaat0346, Jun 2018. doi:10.1126/sciadv.aat0346.
- [32] Alexei Kitaev. Periodic table for topological insulators and superconductors. In Vladimir Lebedev and Mikhail Feigel’Man, editors, *American Institute of Physics Conference Series*, volume 1134 of *American Institute of Physics Conference Series*, pages 22–30, May 2009. doi:10.1063/1.3149495.
- [33] Shinsei Ryu, Andreas P. Schnyder, Akira Furusaki, and Andreas W. W. Ludwig. Topological insulators and superconductors: tenfold way and dimensional hierarchy. *New Journal of Physics*, 12(6):065010, Jun 2010. doi:10.1088/1367-2630/12/6/065010.
- [34] Liang Fu, C. L. Kane, and E. J. Mele. Topological Insulators in Three Dimensions. *Phys. Rev. Lett.*, 98(10):106803, Mar 2007. doi:10.1103/PhysRevLett.98.106803.
- [35] C. L. Kane and E. J. Mele.  $Z_2$  Topological Order and the Quantum Spin Hall Effect. *Phys. Rev. Lett.*, 95(14):146802, Sep 2005. doi:10.1103/PhysRevLett.95.146802.
- [36] Rui Yu, Xiao Liang Qi, Andrei Bernevig, Zhong Fang, and Xi Dai. Equivalent expression of  $Z_2$  topological invariant for band insulators using the non-Abelian Berry connection. *Phys. Rev. B*, 84(7):075119, Aug 2011. doi:10.1103/PhysRevB.84.075119.
- [37] Rahul Roy. Topological phases and the quantum spin Hall effect in three dimensions. *Phys. Rev. B*, 79(19):195322, May 2009. doi:10.1103/PhysRevB.79.195322.
- [38] Liang Fu and C. L. Kane. Time reversal polarization and a  $Z_2$  adiabatic spin pump. *Phys. Rev. B*, 74(19):195312, November 2006. doi:10.1103/PhysRevB.74.195312.
- [39] J. Ahn, S. Park, and B.-J. Yang. Failure of Nielsen-Ninomiya Theorem and Fragile Topology in Two-Dimensional Systems with Space-Time Inversion Symmetry: Application to Twisted Bilayer Graphene at Magic Angle. *Physical Review X*, 9(2):021013, April 2019. doi:10.1103/PhysRevX.9.021013.
- [40] Hoi Chun Po, Liujun Zou, T. Senthil, and Ashvin Vishwanath. Faithful Tight-binding Models and Fragile Topology of Magic-angle Bilayer Graphene. *arXiv e-prints*, art. arXiv:1808.02482, August 2018.
- [41] Zhijun Wang, Benjamin J. Wieder, Jian Li, Binghai Yan, and B. Andrei Bernevig. Higher-Order Topology, Monopole Nodal Lines, and the Origin of Large Fermi Arcs in Transition Metal Dichalcogenides  $XTe_2$  ( $X=Mo,W$ ). *arXiv e-prints*, art. arXiv:1806.11116, June 2018.
- [42] Zhida Song, L. Elcoro, Nicolas Regnault, and B. Andrei Bernevig. Fragile Phases As Affine Monoids: Classification and Material Examples. *arXiv e-prints*, art. arXiv:1905.03262, May 2019.
- [43] Adrien Bouhon, Annica M. Black-Schaffer, and Robert-Jan Slager. Wilson loop approach to fragile topology of split elementary band representations and topological crystalline insulators with time-reversal symmetry. *Phys. Rev. B*, 100(19):195135, November 2019. doi:10.1103/PhysRevB.100.195135.
- [44] Zhi-Da Song, Zhong Fang, and Chen Fang.  $(d - 2)$ -dimensional edge states of rotation symmetry protected

- topological states. *Phys. Rev. Lett.*, 119:246402, Dec 2017. doi:10.1103/PhysRevLett.119.246402.
- [45] Wladimir A. Benalcazar, B. Andrei Bernevig, and Taylor L. Hughes. Quantized electric multipole insulators. *Science*, 357(6346):61–66, Jul 2017. doi:10.1126/science.aah6442.
- [46] Wladimir A. Benalcazar, B. Andrei Bernevig, and Taylor L. Hughes. Electric multipole moments, topological multipole moment pumping, and chiral hinge states in crystalline insulators. *Phys. Rev. B*, 96(24):245115, Dec 2017. doi:10.1103/PhysRevB.96.245115.
- [47] A. Alexandradinata, Xi Dai, and B. Andrei Bernevig. Wilson-Loop Characterization of Inversion-Symmetric Topological Insulators. *Phys. Rev.*, B89(15):155114, 2014. doi:10.1103/PhysRevB.89.155114.
- [48] Benjamin J. Wieder and B. Andrei Bernevig. The Axion Insulator as a Pump of Fragile Topology. *arXiv e-prints*, art. arXiv:1810.02373, October 2018.
- [49] Biao Lian, Fang Xie, and B. Andrei Bernevig. The Landau Level of Fragile Topology. *arXiv e-prints*, art. arXiv:1811.11786, November 2018.
- [50] Barry Bradlyn, L. Elcoro, Jennifer Cano, M. G. Vergniory, Zhijun Wang, C. Felser, M. I. Aroyo, and B. Andrei Bernevig. Topological quantum chemistry. *Nature (London)*, 547(7663):298–305, Jul 2017. doi:10.1038/nature23268.
- [51] Jennifer Cano, Barry Bradlyn, Zhijun Wang, L. Elcoro, M. G. Vergniory, C. Felser, M. I. Aroyo, and B. Andrei Bernevig. Building blocks of topological quantum chemistry: Elementary band representations. *Phys. Rev. B*, 97(3):035139, Jan 2018. doi:10.1103/PhysRevB.97.035139.
- [52] M. G. Vergniory, L. Elcoro, Zhijun Wang, Jennifer Cano, C. Felser, M. I. Aroyo, B. Andrei Bernevig, and Barry Bradlyn. Graph theory data for topological quantum chemistry. *Phys. Rev. E*, 96:023310, Aug 2017. doi:10.1103/PhysRevE.96.023310.
- [53] Xiaobo Lu, Biao Lian, Gaurav Chaudhary, Benjamin A. Piot, Giulio Romagnoli, Kenji Watanabe, Takashi Taniguchi, Martino Poggio, Allan H. MacDonald, B. Andrei Bernevig, and Dmitri K. Efetov. Fingerprints of Fragile Topology in the Hofstadter spectrum of Twisted Bilayer Graphene Close to the Second Magic Angle. *arXiv e-prints*, art. arXiv:2006.13963, June 2020.
- [54] G. William Burg, Biao Lian, Takashi Taniguchi, Kenji Watanabe, B. Andrei Bernevig, and Emanuel Tutuc. Evidence of Emergent Symmetry and Valley Chern Number in Twisted Double-Bilayer Graphene. *arXiv e-prints*, art. arXiv:2006.14000, June 2020.
- [55] J. M. Luttinger. The effect of a magnetic field on electrons in a periodic potential. *Phys. Rev.*, 84:814–817, Nov 1951. doi:10.1103/PhysRev.84.814.
- [56] A. Alexandradinata, Chen Fang, Matthew J. Gilbert, and B. Andrei Bernevig. Spin-orbit-free topological insulators without time-reversal symmetry. *Phys. Rev. Lett.*, 113:116403, Sep 2014. doi:10.1103/PhysRevLett.113.116403.
- [57] Kai Sun, Zhengcheng Gu, Hosho Katsura, and S. Das Sarma. Nearly flatbands with nontrivial topology. *Phys. Rev. Lett.*, 106:236803, Jun 2011. doi:10.1103/PhysRevLett.106.236803.
- [58] B. Andrei Bernevig and N. Regnault. Emergent many-body translational symmetries of abelian and non-abelian fractionally filled topological insulators. *Phys. Rev. B*, 85:075128, Feb 2012. doi:10.1103/PhysRevB.85.075128.
- [59] Taylor L. Hughes, Emil Prodan, and B. Andrei Bernevig. Inversion-symmetric topological insulators. *Phys. Rev. B*, 83(24):245132, Jun 2011. doi:10.1103/PhysRevB.83.245132.
- [60] Jonah Herzog-Arbeitman, Zhida Song, and Andrei Bernevig. Symmetry-protected hofstadter topology: Signatures of the fragile phase, in preparation.
- [61] Zhi-Da Song, Luis Elcoro, and B. Andrei Bernevig. Twisted bulk-boundary correspondence of fragile topology. *Science*, 367(6479):794–797, February 2020. doi:10.1126/science.aaz7650.
- [62] Eslam Khalaf, Hoi Chun Po, Ashvin Vishwanath, and Haruki Watanabe. Symmetry Indicators and Anomalous Surface States of Topological Crystalline Insulators. *Physical Review X*, 8(3):031070, July 2018. doi:10.1103/PhysRevX.8.031070.
- [63] Max Geier, Luka Trifunovic, Max Hoskam, and Piet W. Brouwer. Second-order topological insulators and superconductors with an order-two crystalline symmetry. *Physical Review B*, 97(20), May 2018. ISSN 2469-9969. doi:10.1103/physrevb.97.205135.
- [64] Luka Trifunovic and Piet W. Brouwer. Higher-order bulk-boundary correspondence for topological crystalline phases. *Phys. Rev. X*, 9:011012, Jan 2019. doi:10.1103/PhysRevX.9.011012.
- [65] Eslam Khalaf. Higher-order topological insulators and superconductors protected by inversion symmetry. *Physical Review B*, 97(20), May 2018. ISSN 2469-9969. doi:10.1103/physrevb.97.205136.
- [66] MI Aroyo, JM Perez-Mato, Cesar Capillas, Eli Kroumova, Svetoslav Ivantchev, Gotzon Madariaga, Asen Kirov, and Hans Wondratschek. Bilbao crystallographic server: I. databases and crystallographic computing programs. *ZEITSCHRIFT FÜR KRISTALLOGRAPHIE*, 221:15–27, 01 2006. doi:10.1524/zkri.2006.221.1.15.
- [67] Mois I. Aroyo, Asen Kirov, Cesar Capillas, J. M. Perez-Mato, and Hans Wondratschek. Bilbao Crystallographic Server. II. Representations of crystallographic point groups and space groups. *Acta Crystallographica Section A*, 62(2):115–128, Mar 2006. doi:10.1107/S0108767305040286.

## Supplementary Appendices for "Hofstadter Topology: Non-crystalline Topological Materials in the Moiré Era"

For readers interested in the substantial additional calculations mentioned in the Main Text, we include a detailed and self-contained Supplementary Materials. For readers interested in specific supporting calculations for the individual sections, we provide a brief outline now.

Sec. I of the Main Text includes references to App. A 1 for a discussion of the Peierls paths, App. A 2 for a proof of  $U$  and the flux periodicity  $\Phi = 2\pi n$ , App. A 3 for a general definition of the magnetic translation group operators, and App. D 2 b for a precise discussion of the action of  $T_i(\phi)$  on states.

Sec. II of the Main Text includes references App. B 1 to prove the atomic limit of the Hofstadter, App. C 2 for detailed examples of the occupied state discontinuity of a Chern insulator, and App. C 3 for comparisons with a Mirror Chern insulator. The QSH model discuss is discussed at length in App. F.

Sec III of the Main Text references App. D 1 to prove the algebra of  $U$  and  $\mathcal{T}$ , App. E 2 a to discuss the off-diagonal representation of  $U$  in momentum space, App. D 3 for a Wilson loop proof of the 3D TI phase at  $\phi = 2\pi n$  for odd  $n$ , and exemplifies the weak TI phase for even  $n$  in App. F 2.

Sec. IV of the Main Text references App. E 1 to show the Peierls path dependence of the sign of  $UC_{2z}\mathcal{T}$ , App. E 2 to discussion the Wilson loop calculation at  $\phi = \Phi/2$ , App. E 3 for a proof of the triviality of the nested Wilson loop in the non-crystalline case. Finally, App. G contains the model of TBG and the calculation of the Wilson loops.

### CONTENTS

A. Features of the Hofstadter Hamiltonian	10
1. Peierls paths	10
2. Magnetic Periodicity and Gauge Invariance	10
3. The Magnetic Translation Group	12
4. Peierls Phases	15
5. Rationalization of the Flux	16
6. Residual $SL(2, \mathbb{Z})$ Gauge Freedom	18
7. Construction of the Hofstadter Hamiltonian	19
8. Embedding Matrices in Flux	20
B. Bounded Gaps in the Trivial Limit	23
1. Gershgorin circles	23
2. Hofstadter Hamiltonian on the Checkerboard Lattice	24
C. Wilson Loops	25
1. Definition of the Wilson Loop at Nonzero Flux	26
2. Wilson Loop Proof of Gap Closing in a Chern Insulator	28
3. Discussion of Gap Closing due to a Nonzero Mirror Chern Number	29
4. Alternative Proof of Gap Closing Using Inversion Eigenvalues	30
D. Hofstadter Topology Protected by Time Reversal symmetry	31
1. Properties of $U\mathcal{T}$	31
2. Gauge-Invariant Proof of the 3D TI phase	31
a. Proof of the Trivial Kane-Mele Index due to Gap Closings at the Phase Transition	31
b. Construction of the Gauge-invariant Eigenstates and the Projective Symmetry Algebra	33
3. Wilson Loop Proof of a Nontrivial $\mathbb{Z}_2$ Index with $\mathcal{T}$ symmetry	37
a. $U\mathcal{T}$ Constraints on the Wilson Loop	37
b. $\mathbb{Z}_2$ Index from the Wilson Loop	39
E. $C_{2z}\mathcal{T}$ symmetry	40
1. Symmetry Properties	40
2. Calculation of the $w_2$ invariant at $(UC_{2z}\mathcal{T})^2 = +1$	42
a. Construction of the Extended unit cell	43
b. Constraints on the Wilson loop at $\phi = \Phi/2$	45
3. Proof of a Trivial Phase when $(UC_{2z}\mathcal{T})^2 = -1$	47
F. The Quantum Spin Hall Model	49



1. Hofstadter Hamiltonian	49
2. Discussion of the Proof for $\mathcal{T}$ -symmetric TIs with General Flux Periodicity $\phi \rightarrow \phi + 2\pi n$	53
G. A Model of Twisted Bilayer Graphene	53
1. The Hofstadter Hamiltonian	54
2. Breaking Symmetries	57
3. Computing the $w_2$ index protected by $UC_{2z}\mathcal{T}$ symmetry	58
4. $C_{2z}$ Symmetry Eigenvalues	59
5. $C_{2x}\mathcal{T}$ -Protected Gap Closing	60

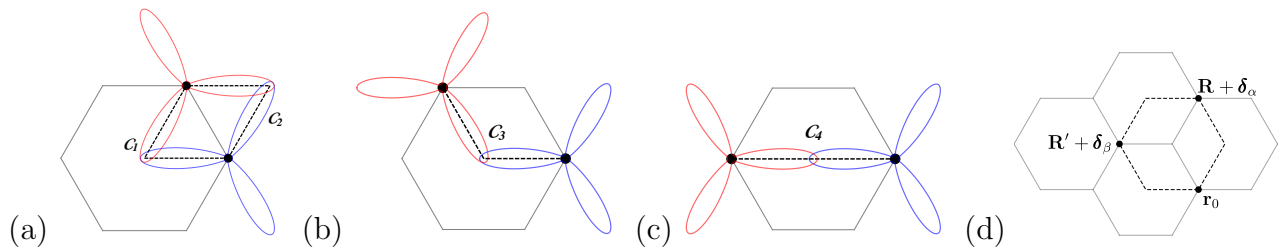


FIG. 3. We sketch the Wannier functions and Peierls paths for three different hoppings in the model of twisted bilayer graphene (introduced fully in App. G 1). (a) There are two symmetric paths,  $C_1$  and  $C_2$ , through the positions of maximum overlap, and thus the Peierls phase is calculated from these two paths *in superposition*. If the Peierls phases along  $C_1, C_2$  are denoted  $\varphi_1, \varphi_2$  respectively, then the hopping  $t$  between orbitals becomes  $t(e^{i\varphi_1} + e^{i\varphi_2})/2$ . (b) There is only one position of maximum overlap at the center of the honeycomb, and the path  $C_3$  (dashed) taken between the orbitals must go through it. (c) There is a straight-line path  $C_4$  (dashed) connecting the orbitals to the center of maximum overlap, matching the conventional Peierls substitution. (d) We show an example of the closed sequence of Peierls paths  $C_{\mathbf{r}_0}$  used in Eq. (A3). When  $\phi = \Phi$ , any such closed Peierls path encloses a multiple of  $2\pi$  flux.

## Appendix A: Features of the Hofstadter Hamiltonian

In this Appendix, we study Hofstadter Hamiltonian on an arbitrary lattice with arbitrary Peierls paths. We begin by discussing the Peierls substitution (App. A 1). Then we prove the periodicity in flux and the gauge invariance of the Hofstadter Hamiltonian (App. A 2). We derive the general form of the magnetic translation operators in App. A 3. In the remainder of the section, we discuss the momentum space features of the Hofstadter Hamiltonian in a suitable Landau gauge  $\mathbf{A}(\mathbf{r}) = -\phi \mathbf{b}_1(\mathbf{r} \cdot \mathbf{b}_2)$ . This choice of gauge is useful for numerical calculations of the spectrum, but has the disadvantage of generically requiring an *enlarged* magnetic unit cell that arises as an artifact of the gauge choice (Apps. A 4 and A 5). We discuss a residual  $SL(2, \mathbb{Z})$  gauge symmetry associated with the Landau gauge in App. A 6. We then construct the Hofstadter Hamiltonian in the Landau gauge (App. A 7) and we give expressions for the embedding matrices which implement the periodicity in flux across the magnetic BZ (App. A 8).

### 1. Peierls paths

To introduce a constant magnetic field to the lattice via the Peierls substitution, we must choose paths  $C_{\mathbf{r} \leftarrow \mathbf{r}'}$  connecting the orbitals at  $\mathbf{r} = \mathbf{R} + \boldsymbol{\delta}_\alpha, \mathbf{r}' = \mathbf{R}' + \boldsymbol{\delta}_\beta$  where  $\mathbf{R} = r_1 \mathbf{a}_1 + r_2 \mathbf{a}_2, \mathbf{R}' = r'_1 \mathbf{a}_1 + r'_2 \mathbf{a}_2$  with  $r_1, r'_1, r_2, r'_2 \in \mathbb{Z}$  and  $\boldsymbol{\delta}_\alpha$  is the position of an orbital  $\alpha$  within the unit cell. Given a path, we calculate the Peierls phases,

$$\varphi_{\mathbf{r}\mathbf{r}'} = \int_{C_{\mathbf{r} \leftarrow \mathbf{r}'}} \mathbf{A} \cdot d\mathbf{r}, \quad (\text{A1})$$

which modify the zero-field hoppings  $t_{\alpha\beta}(\mathbf{r} - \mathbf{r}') \rightarrow e^{i\varphi_{\mathbf{r}\mathbf{r}'}} t_{\alpha\beta}(\mathbf{r} - \mathbf{r}')$ . Conventionally, the Peierls substitution is for nearest neighbors and consists of straight-line paths between the orbitals. Ref. [49] discusses Peierls' approximation in more detail and demonstrated that the integral Eq. (A1) should be taken on piecewise straight paths from the orbitals through the points of greatest overlap of the local Wannier functions, possibly in superposition [55]. For instance, “*s*”  $\delta$ -function-like orbitals on sites should be connected by a straight-line path since they are centered on the atoms. In a more complicated example, our model of twisted bilayer graphene, the Wannier functions are extended and the paths are not straight but rather are taken through the center of the honeycomb [13, 49]. We show this in Fig. 3. We emphasize that the path  $C_{\mathbf{r} \leftarrow \mathbf{r}'}$  is physical; different paths lead to a different spectrum, resulting from the orbitals present in the model (see Ref. [49]). Of course, the additional gauge choice made in writing  $\mathbf{A}$  does affect the individual phases, but does not affect the spectrum.

### 2. Magnetic Periodicity and Gauge Invariance

A crucial feature of the Hofstadter Hamiltonian is its periodicity in the flux  $\phi$ , which we anticipate because the flux dependence enters the Hofstadter Hamiltonian only as a phase. For simplicity, we work in units of length such that the unit cell area  $\mathbf{a}_1 \times \mathbf{a}_2$  is set to 1. The flux periodicity is given by  $\Phi = 2\pi n, n \in \mathbb{N}$  such that taking  $\phi \rightarrow \phi + \Phi$  leaves the energy spectrum invariant.  $n$  is observable (in principle), gauge invariant, and exists so long as the Peierl's

paths are commensurate, meaning that all loops along Peierls paths enclose a rational area (given  $\mathbf{a}_1 \times \mathbf{a}_2 = 1$ ). As we will soon show,  $n$  is given by the least common denominator of the fractional area enclosed by all possible loops along the Peierls paths. For example, we consider the model of twisted bilayer graphene. Consulting the hoppings of the twisted bilayer graphene model in Fig. 3, we see all hoppings must pass through the center of the honeycomb and cannot go along the bonds. Examining the possible closed loops that can be constructed from the Peierls paths in Fig. 3, we see that all enclose multiples of  $1/3$  of a unit cell, so  $n = 3$ .

We prove the periodicity of  $H^\phi$  in flux by constructing the unitary transform  $U$  explicitly. Let  $\mathbf{A} \rightarrow \mathbf{A} + \tilde{\mathbf{A}}$  where the flux of  $\tilde{\mathbf{A}}$  through the unit cell, denoted  $\Omega$ , is

$$\nabla \times \tilde{\mathbf{A}} = \Phi \quad (\text{A2})$$

recalling that we take the cross product of 2D vectors to be a scalar, and that the magnetic field is constant. The Peierls phases  $\varphi_{\mathbf{R}+\delta_\alpha, \mathbf{R}'+\delta_\beta}$  acquire the additional contribution  $\int_{\mathbf{R}'+\delta_\beta}^{\mathbf{R}+\delta_\alpha} \tilde{\mathbf{A}} \cdot d\mathbf{r}$ . By the definition of  $n$ , all closed line integrals of  $\tilde{\mathbf{A}}$  which are taken along Peierls paths are pierced by an integer number of flux quanta. In what follows, we assume all integrals are taken along Peierls paths. Let  $\mathbf{r}_0$  be an arbitrary but fixed orbital of the Hamiltonian that is connected by a sequence of Peierls paths to orbitals at  $\mathbf{R} + \delta_\alpha$  and  $\mathbf{R}' + \delta_\beta$ , and let  $\mathcal{C}_{\mathbf{r}_0}$  be a closed loop along Peierls paths connecting  $\mathbf{R} + \delta_\alpha, \mathbf{R}' + \delta_\beta$ , and  $\mathbf{r}_0$  which we depict an example of in Fig. 3d. Then at  $\phi = \Phi$ , we have

$$\oint_{\mathcal{C}_{\mathbf{r}_0}} \tilde{\mathbf{A}} \cdot d\mathbf{r} = \left( \int_{\mathbf{R}+\delta_\alpha}^{\mathbf{R}'+\delta_\beta} + \int_{\mathbf{R}'+\delta_\beta}^{\mathbf{r}_0} + \int_{\mathbf{r}_0}^{\mathbf{R}+\delta_\alpha} \right) \tilde{\mathbf{A}} \cdot d\mathbf{r} = 0 \pmod{2\pi} \quad (\text{A3})$$

from which we conclude

$$\int_{\mathbf{R}'+\delta_\beta}^{\mathbf{R}+\delta_\alpha} \tilde{\mathbf{A}} \cdot d\mathbf{r} = \left( \int_{\mathbf{R}'+\delta_\beta}^{\mathbf{r}_0} + \int_{\mathbf{r}_0}^{\mathbf{R}+\delta_\alpha} \right) \tilde{\mathbf{A}} \cdot d\mathbf{r} \pmod{2\pi}. \quad (\text{A4})$$

This equation shows that the line integral of  $\tilde{\mathbf{A}}$ , generating  $\Phi$  flux, taken between two points  $\mathbf{R} + \delta_\alpha$  and  $\mathbf{R}' + \delta_\beta$  along Peierls paths may be deformed to any other point  $\mathbf{r}_0$  along Peierls paths without changing the value mod  $2\pi$ . Because of this, whenever integrals in the form Eq. (A4) appear in exponentials, the integral is path independent as long as it is taken along Peierls paths. Now we construct the unitary transformation

$$U^\dagger c_{\mathbf{R},\alpha} U = e^{i \int_{\mathbf{r}_0}^{\mathbf{R}+\delta_\alpha} \tilde{\mathbf{A}} \cdot d\mathbf{r}} c_{\mathbf{R},\alpha}, \quad U = \exp \left( i \sum_{\mathbf{R},\alpha} c_{\mathbf{R},\alpha}^\dagger c_{\mathbf{R},\alpha} \int_{\mathbf{r}_0}^{\mathbf{R}+\delta_\alpha} \tilde{\mathbf{A}} \cdot d\mathbf{r} \right), \quad (\text{A5})$$

which acts on  $c_{\mathbf{R},\alpha}^\dagger$  (resp.  $c_{\mathbf{R},\alpha}$ ), the fermion creation (resp. destruction) operator of the orbital  $\beta$  at  $\mathbf{R} + \delta_\alpha$ . We note that the path of integration is arbitrary *as long as it is taken along Peierls paths* as per the prior discussion. Using the definition of  $U$ , we compute

$$\begin{aligned} U^\dagger H^{\phi+\Phi} U &= U^\dagger \sum_{\mathbf{R}\mathbf{R}'\alpha\beta} t_{\alpha\beta}(\mathbf{R} + \delta_\alpha - (\mathbf{R}' + \delta_\beta)) e^{i\varphi_{\mathbf{R}+\delta_\alpha, \mathbf{R}'+\delta_\beta} + i \int_{\mathbf{R}'+\delta_\beta}^{\mathbf{R}+\delta_\alpha} \tilde{\mathbf{A}} \cdot d\mathbf{r}} c_{\mathbf{R},\alpha}^\dagger c_{\mathbf{R}',\beta} U \\ &= \sum_{\mathbf{R}\mathbf{R}'\alpha\beta} t_{\alpha\beta}(\mathbf{R} + \delta_\alpha - (\mathbf{R}' + \delta_\beta)) e^{i\varphi_{\mathbf{R}+\delta_\alpha, \mathbf{R}'+\delta_\beta} + i \int_{\mathbf{R}'+\delta_\beta}^{\mathbf{R}+\delta_\alpha} \tilde{\mathbf{A}} \cdot d\mathbf{r}} U^\dagger c_{\mathbf{R},\alpha}^\dagger U U^\dagger c_{\mathbf{R}',\beta} U \\ &= \sum_{\mathbf{R}\mathbf{R}'\alpha\beta} t_{\alpha\beta}(\mathbf{R} + \delta_\alpha - (\mathbf{R}' + \delta_\beta)) e^{i\varphi_{\mathbf{R}+\delta_\alpha, \mathbf{R}'+\delta_\beta} + i \int_{\mathbf{R}'+\delta_\beta}^{\mathbf{R}+\delta_\alpha} \tilde{\mathbf{A}} \cdot d\mathbf{r} - i \int_{\mathbf{R}'+\delta_\beta}^{\mathbf{r}_0} \tilde{\mathbf{A}} \cdot d\mathbf{r} + i \int_{\mathbf{r}_0}^{\mathbf{R}+\delta_\alpha} \tilde{\mathbf{A}} \cdot d\mathbf{r}} c_{\mathbf{R},\alpha}^\dagger c_{\mathbf{R}',\beta} \quad (\text{A6}) \\ &= \sum_{\mathbf{R}\mathbf{R}'\alpha\beta} t_{\alpha\beta}(\mathbf{R} + \delta_\alpha - (\mathbf{R}' + \delta_\beta)) e^{i\varphi_{\mathbf{R}+\delta_\alpha, \mathbf{R}'+\delta_\beta} + i \int_{\mathbf{r}_0}^{\mathbf{R}+\delta_\alpha} \tilde{\mathbf{A}} \cdot d\mathbf{r}} c_{\mathbf{R},\alpha}^\dagger c_{\mathbf{R}',\beta} \\ &= \sum_{\mathbf{R}\mathbf{R}'\alpha\beta} t_{\alpha\beta}(\mathbf{R} + \delta_\alpha - (\mathbf{R}' + \delta_\beta)) e^{i\varphi_{\mathbf{R}+\delta_\alpha, \mathbf{R}'+\delta_\beta}} c_{\mathbf{R},\alpha}^\dagger c_{\mathbf{R}',\beta} \\ &= H^\phi \end{aligned}$$

proving that the Hamiltonian is periodic in  $\Phi = 2\pi n$  up to a unitary transformation  $U$ . We may think of  $U$  as a kind of “embedding matrix” in the flux direction, in analogy to the embedding matrix along  $k_z$  of 3D Bloch Hamiltonians [56].

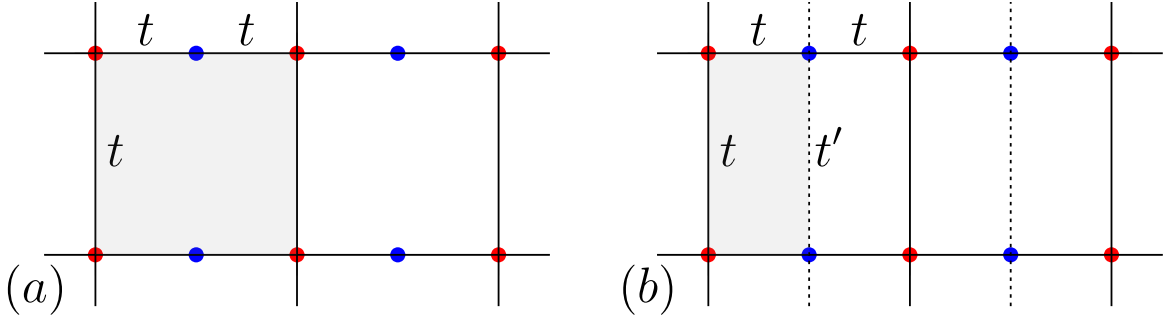


FIG. 4. (a) We show a square lattice with atoms at the 1a (red) and 1b (blue) positions. There are hoppings of amplitude  $t$  (solid lines) between the 1a atoms separated by  $(0, 1)$  and also between neighboring 1a and 1b atoms separated by  $(1/2, 0)$ . We take all Peierls paths to be straight lines between the atoms, so the paths are given by the lines shown in the figure. The smallest closed loop along Peierls paths encloses a single unit cell, and hence  $n = 1, \Phi = 2\pi$ . (b) We now allow the 1b atoms to be connected by a hopping of amplitude  $t'$ , shown by dotted lines. There is a closed loop that encloses half a unit cell (shaded in gray) by hopping between the 1b positions. In this case  $n = 2$  and  $\Phi = 4\pi$ .

A very similar proof can be used to show that the Hofstadter Hamiltonian is also gauge-invariant with respect to the electromagnetic field up to a unitary transform. For clarity, we momentarily denote the Hamiltonian's dependence on the gauge field as  $H(\mathbf{A})$ . If we change gauge to  $\mathbf{A} \rightarrow \mathbf{A} + \nabla\lambda$ , then we construct the new unitary transformation

$$\tilde{U} = \exp \left( i \sum_{\mathbf{R}\alpha} \lambda(\mathbf{R} + \boldsymbol{\delta}_\alpha) c_{\mathbf{R},\alpha}^\dagger c_{\mathbf{R},\alpha} \right) \quad (\text{A7})$$

and calculate

$$\begin{aligned} \tilde{U}^\dagger H(\mathbf{A} + \nabla\lambda) \tilde{U} &= \tilde{U}^\dagger \sum_{\mathbf{R}\mathbf{R}'\alpha\beta} t_{\alpha\beta}(\mathbf{r} - \mathbf{r}') e^{i\varphi_{\mathbf{R}+\boldsymbol{\delta}_\alpha, \mathbf{R}'+\boldsymbol{\delta}_\beta} + i \int_{\mathbf{R}'+\boldsymbol{\delta}_\beta}^{\mathbf{R}+\boldsymbol{\delta}_\alpha} \nabla\lambda \cdot d\mathbf{r}} c_{\mathbf{R},\alpha}^\dagger c_{\mathbf{R}',\beta} \tilde{U} \\ &= \sum_{\mathbf{R}\mathbf{R}'\alpha\beta} t_{\alpha\beta}(\mathbf{r} - \mathbf{r}') e^{i\varphi_{\mathbf{R}+\boldsymbol{\delta}_\alpha, \mathbf{R}'+\boldsymbol{\delta}_\beta} + i\lambda(\mathbf{R}+\boldsymbol{\delta}_\alpha) - i\lambda(\mathbf{R}'+\boldsymbol{\delta}_\beta)} \tilde{U}^\dagger c_{\mathbf{R},\alpha}^\dagger \tilde{U} \tilde{U}^\dagger c_{\mathbf{R}',\beta} \tilde{U} \\ &= \sum_{\mathbf{R}\mathbf{R}'\alpha\beta} t_{\alpha\beta}(\mathbf{r} - \mathbf{r}') e^{i\varphi_{\mathbf{R}+\boldsymbol{\delta}_\alpha, \mathbf{R}'+\boldsymbol{\delta}_\beta} + i\lambda(\mathbf{R}+\boldsymbol{\delta}_\alpha) - i\lambda(\mathbf{R}'+\boldsymbol{\delta}_\beta) - i\lambda(\mathbf{R}+\boldsymbol{\delta}_\alpha) + i\lambda(\mathbf{R}'+\boldsymbol{\delta}_\beta)} c_{\mathbf{R},\alpha}^\dagger c_{\mathbf{R}',\beta} \\ &= H(\mathbf{A}) . \end{aligned} \quad (\text{A8})$$

The transformation  $\tilde{U}$  is the straightforward implementation of the  $U(1)$  gauge symmetry of continuum electromagnetic to lattice fermions and is an important consistency check on the Peierls substitution.

We conclude this section with an example of a simple model with  $n \neq 1$  (thus  $\Phi \neq 2\pi$ ). Starting from the familiar square lattice Hofstadter model, we add atoms at the 1b position as shown in Fig. 4. If we connect the 1b sites with a hopping  $t'$  taken along a straight-line Peierls path (shown with a dotted line in Fig. 4) then there is a closed loop along Peierls paths enclosing half a unit cell, so  $n = 2$ . Accordingly, shifting  $\phi \rightarrow \phi + 2 \times 2\pi$  leaves the spectrum invariant and we identify  $\Phi = 2\pi n = 4\pi$ .

### 3. The Magnetic Translation Group

We now discuss the magnetic translation operators that commute with the Hamiltonian  $H^\phi$  in the presence of flux. We will prove that the single-particle operators

$$T_i(\phi) = \sum_{\mathbf{R}\alpha} \exp \left( i \int_{\mathbf{R}+\boldsymbol{\delta}_\alpha}^{\mathbf{R}+\boldsymbol{\delta}_\alpha+\mathbf{a}_i} \mathbf{A} \cdot d\mathbf{r} + i\chi_i(\mathbf{R} + \boldsymbol{\delta}_\alpha) \right) c_{\mathbf{R}+\mathbf{a}_i,\alpha}^\dagger |0\rangle \langle 0| c_{\mathbf{R},\alpha}, \quad \chi_i(\mathbf{r}) = \phi \mathbf{a}_i \times \mathbf{r} \quad (\text{A9})$$

commute with  $H^\phi$ . We have inserted a projector  $|0\rangle \langle 0|$  into Eq. (3) to arrive at Eq. (A9), which insures that  $T_i^\dagger(\phi) c_{\mathbf{R},\boldsymbol{\delta}_\alpha}^\dagger T_i(\phi)$  is still a single-particle operator. Note that  $T_i(\phi)$  is unitary on the single-particle Hilbert space. The path of integration in Eq. (A9) is taken to be a straight line between  $\mathbf{R} + \boldsymbol{\delta}_\alpha$  and  $\mathbf{R} + \mathbf{a}_i + \boldsymbol{\delta}_\alpha$ , although this is *not*

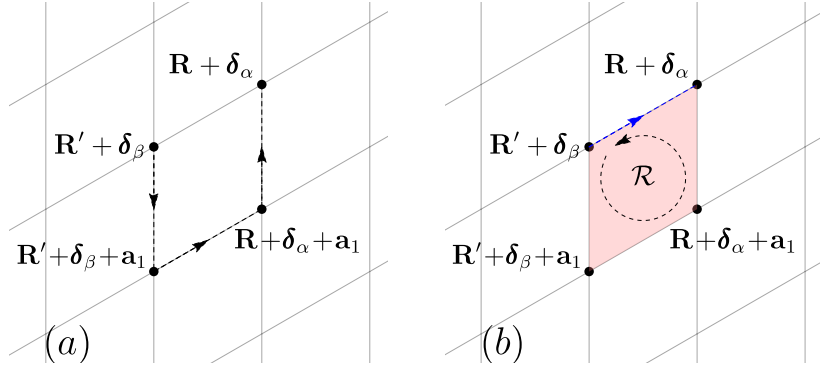


FIG. 5. (a) We depict an example of the open path of the line integral on the righthand side of Eq. (A11). (b) Such a path is equivalent to the one on the lefthand side of Eq. (A11), which is a closed path  $\mathcal{C}$  encircling  $\mathcal{R}$ , depicted in pink, with a segment going backwards as shown in blue.

necessarily a Peierls path if the local Wannier functions are supported off the orbital sites and the Peierls path is not a straight line (see App. A 1). We will prove  $[T_i(\phi), H^\phi] = 0$  by showing  $T_i^\dagger(\phi)H^\phi T_i(\phi) = H^\phi$  in the single-particle Hilbert space. We expand the LHS to find

$$\begin{aligned}
T_i^\dagger(\phi)H^\phi T_i(\phi) &= \sum_{\mathbf{R}, \alpha, \mathbf{R}', \beta} \exp\left(i \int_{\mathbf{R}'+\delta_\beta}^{\mathbf{R}+\delta_\alpha} \mathbf{A} \cdot d\mathbf{r}\right) t_{\alpha\beta}(\mathbf{R} + \delta_\alpha - (\mathbf{R}' + \delta_\beta)) T_i^\dagger(\phi) c_{\mathbf{R}, \alpha}^\dagger T_i(\phi) T_i^\dagger(\phi) c_{\mathbf{R}', \beta} T_i(\phi) \\
&= \sum_{\mathbf{R}, \alpha, \mathbf{R}', \beta} \exp\left(i \int_{\mathbf{R}'+\mathbf{a}_i+\delta_\beta}^{\mathbf{R}+\mathbf{a}_i+\delta_\alpha} \mathbf{A} \cdot d\mathbf{r} - i \int_{\mathbf{R}+\delta_\alpha}^{\mathbf{R}+\delta_\alpha+\mathbf{a}_i} \mathbf{A} \cdot d\mathbf{r} - i\chi_i(\mathbf{R} + \delta_\alpha) + i \int_{\mathbf{R}'+\delta_\beta}^{\mathbf{R}'+\delta_\beta+\mathbf{a}_i} \mathbf{A} \cdot d\mathbf{r} + i\chi_i(\mathbf{R}' + \delta_\beta)\right) \\
&\quad \times t_{\alpha\beta}(\mathbf{R} + \mathbf{a}_i + \delta_\alpha - (\mathbf{R}' + \mathbf{a}_i + \delta_\beta)) c_{\mathbf{R}, \alpha}^\dagger c_{\mathbf{R}', \beta} \\
&= \sum_{\mathbf{R}, \alpha, \mathbf{R}', \beta} \exp\left(i \left( \int_{\mathbf{R}'+\mathbf{a}_i+\delta_\beta}^{\mathbf{R}+\mathbf{a}_i+\delta_\alpha} + \int_{\mathbf{R}+\delta_\alpha}^{\mathbf{R}+\delta_\alpha+\mathbf{a}_i} + \int_{\mathbf{R}'+\delta_\beta}^{\mathbf{R}'+\delta_\beta+\mathbf{a}_i} \right) \mathbf{A} \cdot d\mathbf{r} - i\chi_i(\mathbf{R} + \delta_\alpha) + i\chi_i(\mathbf{R}' + \delta_\beta)\right) \\
&\quad \times t_{\alpha\beta}(\mathbf{R} + \delta_\alpha - (\mathbf{R}' + \delta_\beta)) c_{\mathbf{R}, \alpha}^\dagger c_{\mathbf{R}', \beta}. \tag{A10}
\end{aligned}$$

The path of the open line integral (e.g. Fig. 5a) in Eq. (A10) can be rewritten as a closed path that doubles back on itself (e.g. Fig. 5b). Written out, we have

$$\begin{aligned}
\left( \int_{\mathbf{R}'+\delta_\beta}^{\mathbf{R}'+\delta_\beta+\mathbf{a}_i} + \int_{\mathbf{R}'+\mathbf{a}_i+\delta_\beta}^{\mathbf{R}+\mathbf{a}_i+\delta_\alpha} + \int_{\mathbf{R}+\delta_\alpha}^{\mathbf{R}+\delta_\alpha+\mathbf{a}_i} \right) \mathbf{A} \cdot d\mathbf{r} &= \left( \int_{\mathbf{R}'+\mathbf{a}_i+\delta_\beta}^{\mathbf{R}+\mathbf{a}_i+\delta_\alpha} + \int_{\mathbf{R}+\delta_\alpha}^{\mathbf{R}+\delta_\alpha+\mathbf{a}_i} + \int_{\mathbf{R}'+\delta_\beta}^{\mathbf{R}'+\delta_\beta+\mathbf{a}_i} + \int_{\mathbf{R}+\delta_\alpha}^{\mathbf{R}'+\delta_\beta} + \int_{\mathbf{R}'+\delta_\beta}^{\mathbf{R}+\delta_\alpha} \right) \mathbf{A} \cdot d\mathbf{r} \\
&= \oint_{\mathcal{C}} \mathbf{A} \cdot d\mathbf{r} + \int_{\mathbf{R}'+\delta_\beta}^{\mathbf{R}+\delta_\alpha} \mathbf{A} \cdot d\mathbf{r} \tag{A11}
\end{aligned}$$

where the closed loop  $\mathcal{C}$  (e.g. the boundary of the pink region in Fig. 5b) is formed from the straight-line paths  $\mathbf{R} + \delta_\alpha + \mathbf{a}_i \rightarrow \mathbf{R} + \delta_\alpha$ ,  $\mathbf{R}' + \delta_\beta \rightarrow \mathbf{R}' + \delta_\beta + \mathbf{a}_i$  of the magnetic translation operator and the Peierls path from  $\mathbf{R} + \delta_\alpha + \mathbf{a}_i \rightarrow \mathbf{R}' + \delta_\beta + \mathbf{a}_i$ . In Fig. 5, the Peierls path shown in the example happens to be a straight-line path.

We now want to use Stokes' theorem to reduce the closed line integral in Eq. (A11) to a surface integral over  $\mathcal{R}$ , the area enclosed by  $\mathcal{C}$ .  $\mathcal{R}$  is a polygon formed from two parallel sides of length  $\mathbf{a}_i$  (corresponding to the straight-line paths of integration in the magnetic translation operator  $T_i(\phi)$  of Eq. (A9)) and two identical Peierls paths connecting the points  $\mathbf{R} + \delta_\alpha$  and  $\mathbf{R}' + \delta_\beta$  and the points  $\mathbf{R} + \delta_\alpha + \mathbf{a}_i$  and  $\mathbf{R}' + \delta_\beta + \mathbf{a}_i$ , which we call  $\mathcal{P}_1$  and  $\mathcal{P}_2$  respectively. An example of such a region is shown in Fig. 6. If  $\mathcal{P}_1$  and  $\mathcal{P}_2$  were straight lines, then  $\mathcal{R}$  would be a parallelogram with area  $(\mathbf{R}' + \delta_\beta - (\mathbf{R} + \delta_\alpha)) \times \mathbf{a}_i$ . In fact,  $\mathcal{R}$  still has area  $(\mathbf{R}' + \delta_\beta - (\mathbf{R} + \delta_\alpha)) \times \mathbf{a}_i$  for any (possibly piecewise-straight) Peierls path. This follows because any deviation in area due to  $\mathcal{P}_1$  not being straight and is canceled by the same deviation of  $\mathcal{P}_2$ , as shown for example by the blue dashed lines in Fig. 6 for the Peierls paths of the twisted bilayer graphene model in App. G 1. Using this geometrical fact, we find that

$$\oint_{\mathcal{C}} \mathbf{A} \cdot d\mathbf{r} = \phi \int_{\mathcal{R}} dS = \phi (\mathbf{R}' + \delta_\beta - (\mathbf{R} + \delta_\alpha)) \times \mathbf{a}_i. \tag{A12}$$

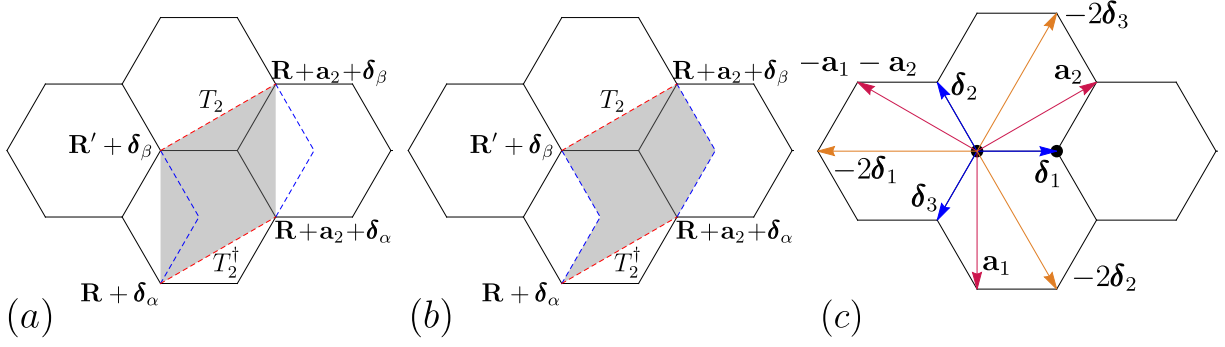


FIG. 6. We show an example of the area enclosed by the integral in Eq. (A12) for the Peierls paths of our model of twisted bilayer graphene (as shown in Fig. 3) and the magnetic translation operator  $T_2$ . The blue dashed lines are the Peierls' paths  $\mathcal{P}_1$  and  $|\mathcal{P}_2$  of the hoppings connecting the orbitals, and the red dashed lines show the path of integration in the  $T_2$  operator (which is not generically a Peierls path). (a) We depict the area of the parallelogram formed by the vectors  $(\mathbf{R}' + \boldsymbol{\delta}_\beta) - (\mathbf{R} + \boldsymbol{\delta}_\alpha)$  and  $\mathbf{a}_2$  in grey. (b) We depict the area enclosed by the contiguous integration paths, which has the same value as the area in (a). (c) We depict the lattice vectors  $\mathbf{a}_1$ , the nearest-neighbor vectors  $\boldsymbol{\delta}_i$ , and the third-nearest neighbor vectors  $-2\boldsymbol{\delta}_i$ .

We return to Eq. (A10) and using the results of Eqs. (A12) and (A11), we find

$$T_i^\dagger(\phi)H^\phi T_i(\phi) = \sum_{\mathbf{R}, \alpha, \mathbf{R}', \beta} \exp \left( i \int_{\mathbf{R}' + \boldsymbol{\delta}_\beta}^{\mathbf{R} + \boldsymbol{\delta}_\alpha} \mathbf{A} \cdot d\mathbf{r} + i\phi (\mathbf{R}' + \boldsymbol{\delta}_\beta - (\mathbf{R} + \boldsymbol{\delta}_\alpha)) \times \mathbf{a}_i - i\chi_i(\mathbf{R} + \boldsymbol{\delta}_\alpha) + i\chi_i(\mathbf{R}' + \boldsymbol{\delta}_\beta) \right) \times t_{\alpha\beta}(\mathbf{R} + \boldsymbol{\delta}_\alpha - (\mathbf{R}' + \boldsymbol{\delta}_\beta)) c_{\mathbf{R}, \alpha}^\dagger c_{\mathbf{R}', \beta}. \quad (\text{A13})$$

Now we recall our choice of  $\chi_i(\mathbf{r}) = \phi \mathbf{a}_i \times \mathbf{r}$  in Eq. (A9) and notice

$$\phi (\mathbf{R}' + \boldsymbol{\delta}_\beta - (\mathbf{R} + \boldsymbol{\delta}_\alpha)) \times \mathbf{a}_i - \chi_i(\mathbf{R} + \boldsymbol{\delta}_\alpha) + \chi_i(\mathbf{R}' + \boldsymbol{\delta}_\beta) = \phi (\mathbf{R}' + \boldsymbol{\delta}_\beta - (\mathbf{R} + \boldsymbol{\delta}_\alpha)) \times \mathbf{a}_i + \phi \mathbf{a}_i \times (\mathbf{R}' + \boldsymbol{\delta}_\beta - (\mathbf{R} + \boldsymbol{\delta}_\alpha)) = 0. \quad (\text{A14})$$

Hence, we find that Eq. (A13) simplifies to

$$T_i^\dagger(\phi)H^\phi T_i(\phi) = \sum_{\mathbf{R}, \alpha, \mathbf{R}', \beta} \exp \left( i \int_{\mathbf{R}' + \boldsymbol{\delta}_\beta}^{\mathbf{R} + \boldsymbol{\delta}_\alpha} \mathbf{A} \cdot d\mathbf{r} \right) t_{\alpha\beta}(\mathbf{R} + \boldsymbol{\delta}_\alpha - (\mathbf{R}' + \boldsymbol{\delta}_\beta)) c_{\mathbf{R}, \alpha}^\dagger c_{\mathbf{R}', \beta} = H^\phi. \quad (\text{A15})$$

We have proven that the magnetic translation operators  $T_i(\phi)$  commute with  $H^\phi$  at all  $\phi$ . To derive the magnetic translation group algebra, we start from Eq. (A9) and calculate

$$T_1(\phi)T_2(\phi) = \sum_{\mathbf{R}\alpha} \exp \left( i \int_{\mathbf{R} + \boldsymbol{\delta}_\alpha + \mathbf{a}_2}^{\mathbf{R} + \boldsymbol{\delta}_\alpha + \mathbf{a}_1 + \mathbf{a}_2} \mathbf{A} \cdot d\mathbf{r} + i\chi_1(\mathbf{R} + \mathbf{a}_2 + \boldsymbol{\delta}_\alpha) + i \int_{\mathbf{R} + \boldsymbol{\delta}_\alpha}^{\mathbf{R} + \boldsymbol{\delta}_\alpha + \mathbf{a}_2} \mathbf{A} \cdot d\mathbf{r} + i\chi_2(\mathbf{R} + \boldsymbol{\delta}_\alpha) \right) c_{\mathbf{R} + \mathbf{a}_1 + \mathbf{a}_2, \alpha}^\dagger c_{\mathbf{R}, \alpha},$$

$$T_2(\phi)T_1(\phi) = \sum_{\mathbf{R}\alpha} \exp \left( i \int_{\mathbf{R} + \boldsymbol{\delta}_\alpha + \mathbf{a}_1}^{\mathbf{R} + \boldsymbol{\delta}_\alpha + \mathbf{a}_1 + \mathbf{a}_2} \mathbf{A} \cdot d\mathbf{r} + i\chi_2(\mathbf{R} + \mathbf{a}_1 + \boldsymbol{\delta}_\alpha) + i \int_{\mathbf{R} + \boldsymbol{\delta}_\alpha}^{\mathbf{R} + \boldsymbol{\delta}_\alpha + \mathbf{a}_1} \mathbf{A} \cdot d\mathbf{r} + i\chi_1(\mathbf{R} + \boldsymbol{\delta}_\alpha) \right) c_{\mathbf{R} + \mathbf{a}_1 + \mathbf{a}_2, \alpha}^\dagger c_{\mathbf{R}, \alpha}, \quad (\text{A16})$$

which we use to find that, on the single-particle Hilbert space,

$$(T_2(\phi)T_1(\phi))^\dagger T_1(\phi)T_2(\phi) = \sum_{\mathbf{R}\alpha} \exp \left[ i \int_{\mathbf{R} + \boldsymbol{\delta}_\alpha + \mathbf{a}_2}^{\mathbf{R} + \boldsymbol{\delta}_\alpha + \mathbf{a}_1 + \mathbf{a}_2} \mathbf{A} \cdot d\mathbf{r} + i\chi_1(\mathbf{R} + \mathbf{a}_2 + \boldsymbol{\delta}_\alpha) + i \int_{\mathbf{R} + \boldsymbol{\delta}_\alpha}^{\mathbf{R} + \boldsymbol{\delta}_\alpha + \mathbf{a}_2} \mathbf{A} \cdot d\mathbf{r} + i\chi_2(\mathbf{R} + \boldsymbol{\delta}_\alpha) - i \int_{\mathbf{R} + \boldsymbol{\delta}_\alpha + \mathbf{a}_1}^{\mathbf{R} + \boldsymbol{\delta}_\alpha + \mathbf{a}_1 + \mathbf{a}_2} \mathbf{A} \cdot d\mathbf{r} - i\chi_2(\mathbf{R} + \mathbf{a}_1 + \boldsymbol{\delta}_\alpha) - i \int_{\mathbf{R} + \boldsymbol{\delta}_\alpha}^{\mathbf{R} + \boldsymbol{\delta}_\alpha + \mathbf{a}_1} \mathbf{A} \cdot d\mathbf{r} - i\chi_1(\mathbf{R} + \boldsymbol{\delta}_\alpha) \right] c_{\mathbf{R}, \alpha}^\dagger c_{\mathbf{R}, \alpha}. \quad (\text{A17})$$

Collecting the integrals, we see

$$\begin{aligned}
\left( \int_{\mathbf{R}+\boldsymbol{\delta}_\alpha+\mathbf{a}_2}^{\mathbf{R}+\boldsymbol{\delta}_\alpha+\mathbf{a}_1+\mathbf{a}_2} + \int_{\mathbf{R}+\boldsymbol{\delta}_\alpha}^{\mathbf{R}+\boldsymbol{\delta}_\alpha+\mathbf{a}_2} - \int_{\mathbf{R}+\boldsymbol{\delta}_\alpha+\mathbf{a}_1}^{\mathbf{R}+\boldsymbol{\delta}_\alpha+\mathbf{a}_1+\mathbf{a}_2} - \int_{\mathbf{R}+\boldsymbol{\delta}_\alpha}^{\mathbf{R}+\boldsymbol{\delta}_\alpha+\mathbf{a}_1} \right) \mathbf{A} \cdot d\mathbf{r} &= - \oint_{\text{unit cell}} \mathbf{A} \cdot d\mathbf{r} \\
&= -\phi \int_{\text{unit cell}} dS \\
&= -\phi
\end{aligned} \tag{A18}$$

where the minus sign has appeared because the path of integration is clockwise, and we recall that the area of the unit cell is one. Collecting the  $\chi_i$  terms from Eq. (A17), we find

$$\begin{aligned}
\chi_1(\mathbf{R} + \mathbf{a}_2 + \boldsymbol{\delta}_\alpha) + \chi_2(\mathbf{R} + \boldsymbol{\delta}_\alpha) - \chi_2(\mathbf{R} + \mathbf{a}_1 + \boldsymbol{\delta}_\alpha) - \chi_1(\mathbf{R} + \boldsymbol{\delta}_\alpha) &= \phi \mathbf{a}_1 \times (\mathbf{R} + \mathbf{a}_2 + \boldsymbol{\delta}_\alpha - (\mathbf{R} + \boldsymbol{\delta}_\alpha)) \\
&\quad + \phi \mathbf{a}_2 \times (\mathbf{R} + \boldsymbol{\delta}_\alpha - (\mathbf{R} + \mathbf{a}_1 + \boldsymbol{\delta}_\alpha)) \\
&= \phi \mathbf{a}_1 \times \mathbf{a}_2 - \phi \mathbf{a}_2 \times \mathbf{a}_1 \\
&= 2\phi \mathbf{a}_1 \times \mathbf{a}_2 \\
&= 2\phi
\end{aligned} \tag{A19}$$

because we have normalized the unit cell to be  $\mathbf{a}_1 \times \mathbf{a}_2 = 1$ . Using the results of Eqs. (A18) and (A19), we return to Eq. (A17) and find

$$(T_2(\phi)T_1(\phi))^\dagger T_1(\phi)T_2(\phi) = \sum_{\mathbf{R}\alpha} e^{-i\phi+2i\phi} c_{\mathbf{R},\alpha}^\dagger c_{\mathbf{R},\alpha} = e^{i\phi} \tag{A20}$$

recalling that  $\sum_{\mathbf{R}\alpha} c_{\mathbf{R},\alpha}^\dagger c_{\mathbf{R},\alpha} = 1$  when acting on single particle states. Eq. (A20) is the usual single-particle algebra of the magnetic translation operators.

#### 4. Peierls Phases

So far, we have discussed the magnetic translation group in position space which demonstrates the existence of a  $1 \times q$  magnetic unit cell at  $\phi = \frac{2\pi p}{q}$ ,  $p, q$  coprime. We now discuss a particular gauge choice, a certain Landau gauge, that will makes explicit calculations in momentum space tractable. We work in the Landau gauge  $\mathbf{A}(\mathbf{r}) = -\phi \mathbf{b}_1(\mathbf{r} \cdot \mathbf{b}_2)$  which obeys

$$\nabla \times \mathbf{A}(\mathbf{r}) = -\phi \mathbf{b}_2 \times \mathbf{b}_1 = \phi \tag{A21}$$

where we have used that  $\mathbf{b}_1 \times \mathbf{b}_2 = \mathbf{a}_1 \times \mathbf{a}_2 = 1$ . This choice of gauge is practical. We will see that the Peierls phases do not depend on  $r_1$ , the coordinate along  $\mathbf{a}_1$ , so the unit cell of the Hofstadter Hamiltonian is only extended along one direction. Thus we may Fourier transform along  $\mathbf{a}_1$  and obtain an effective 1D chain along  $\mathbf{a}_2$  which is *not* a priori periodic because of the dependence on  $r_2$ . However, for a certain choice of *rational* flux (in this specific gauge choice), an extended spatial periodicity reappears and enables the Hamiltonian to be Fourier transformed into momentum space. Importantly, at  $\phi = \frac{2\pi p}{q}$ ,  $p, q$  coprime, the Landau gauge does *not* permit a  $1 \times q$  unit cell on a general lattice, and may need to be enlarged to a  $1 \times q'$  unit cell for  $q' > q$ . We will discuss this extensively in App. A 5. In App. D 2, we introduce a gauge-invariant formalism where the minimal  $1 \times q$  magnetic unit cell is manifest. However, the Landau gauge is a much more convenient choice for numerical calculations because we can derive explicit expressions for the Peierls phases.

First we show that in our Landau gauge, all Peierls phases (Eq. (A1)) must be of the form  $\varphi_{\mathbf{r}\mathbf{r}'} = \phi(\rho_{\mathbf{r}\mathbf{r}'} r_2 + \rho'_{\mathbf{r}\mathbf{r}'})$  with  $\rho_{\mathbf{r}\mathbf{r}'} \in \mathbb{Q}$  so long as the orbitals are commensurate, meaning that  $\mathbf{R}' + \boldsymbol{\delta}_\beta - (\mathbf{R} + \boldsymbol{\delta}_\alpha)$  is a rational linear combination of the lattice vectors. As an example of an incommensurate orbitals, consider a lattice with atoms at the positions  $r_1 \mathbf{a}_1 + r_2 \mathbf{a}_2$  and  $r_1 \mathbf{a}_1 + r_2 \mathbf{a}_2 + 1/\sqrt{5} \mathbf{a}_1$  which are connected by straight-line Peierls paths. No magnetic unit cell exists on this lattice because there is no periodicity in its Peierls phases.

Let the Peierls path  $\mathcal{C}$  be from  $\mathbf{R} + \boldsymbol{\delta}_\alpha$  to  $\mathbf{R}' + \boldsymbol{\delta}_\beta$ , taken along the piecewise straight path connecting the points  $\mathbf{x}_1, \dots, \mathbf{x}_N$  (noting that the beginning and ending points are  $\mathbf{x}_1 = \mathbf{R} + \boldsymbol{\delta}_\alpha$  and  $\mathbf{x}_N = \mathbf{R}' + \boldsymbol{\delta}_\beta$  respectively). We now calculate the Peierls phase accumulated along the path  $\mathcal{C}$ . Breaking up the integral Eq. (A1) along the piecewise-straight path, we find

$$\varphi_{\mathbf{x}_1 \mathbf{x}_N} = \int_{\mathcal{C}} \mathbf{A} \cdot d\mathbf{r} = \sum_{i=1}^{N-1} \int_{\mathbf{x}_i}^{\mathbf{x}_{i+1}} \mathbf{A} \cdot d\mathbf{r} . \tag{A22}$$

We compute

$$\begin{aligned}
\int_{\mathbf{x}_i}^{\mathbf{x}_{i+1}} \mathbf{A} \cdot d\mathbf{r} &= -\phi \int_0^1 \mathbf{b}_2 \cdot (\mathbf{x}_i + t(\mathbf{x}_{i+1} - \mathbf{x}_i)) \mathbf{b}_1 \cdot (\mathbf{x}_{i+1} - \mathbf{x}_i) dt \\
&= -\phi \mathbf{b}_1 \cdot (\mathbf{x}_{i+1} - \mathbf{x}_i) \int_0^1 (\mathbf{b}_2 \cdot \mathbf{x}_i + t \mathbf{b}_2 \cdot (\mathbf{x}_{i+1} - \mathbf{x}_i)) dt \\
&= -\phi \mathbf{b}_1 \cdot (\mathbf{x}_{i+1} - \mathbf{x}_i) \left( \mathbf{b}_2 \cdot \mathbf{x}_i + \frac{1}{2} \mathbf{b}_2 \cdot (\mathbf{x}_{i+1} - \mathbf{x}_i) \right) \\
&= -\frac{\phi}{2} \mathbf{b}_1 \cdot (\mathbf{x}_{i+1} - \mathbf{x}_i) (\mathbf{b}_2 \cdot (\mathbf{x}_{i+1} + \mathbf{x}_i)) .
\end{aligned} \tag{A23}$$

We work with a fixed reference point (“origin”) at  $r_1 \mathbf{a}_1 + r_2 \mathbf{a}_2$ ,  $r_1, r_2 \in \mathbb{Z}$  and define  $\mathbf{t}_i = \mathbf{x}_i - (r_1 \mathbf{a}_1 + r_2 \mathbf{a}_2)$ . Note that because the  $\mathbf{x}_i$  are assumed commensurate, each  $\mathbf{t}_i$  is also commensurate. Then we have

$$\begin{aligned}
\int_{\mathbf{x}_i}^{\mathbf{x}_{i+1}} \mathbf{A} \cdot d\mathbf{r} &= -\phi \mathbf{b}_1 \cdot (\mathbf{t}_{i+1} - \mathbf{t}_i) \left( \mathbf{b}_2 \cdot (r_1 \mathbf{a}_1 + r_2 \mathbf{a}_2 + \frac{1}{2} (\mathbf{t}_{i+1} + \mathbf{t}_i)) \right) \\
&= -\phi \mathbf{b}_1 \cdot (\mathbf{t}_{i+1} - \mathbf{t}_i) \left( r_2 + \frac{\mathbf{b}_2}{2} \cdot (\mathbf{t}_{i+1} + \mathbf{t}_i) \right)
\end{aligned} \tag{A24}$$

using  $\mathbf{a}_i \cdot \mathbf{b}_2 = \delta_{i2}$ . Then by Eq. (A22), we find

$$\begin{aligned}
\varphi_{\mathbf{x}_1 \mathbf{x}_N} &= -\phi \sum_{i=1}^{N-1} \mathbf{b}_1 \cdot (\mathbf{t}_{i+1} - \mathbf{t}_i) \left( r_2 + \frac{\mathbf{b}_2}{2} \cdot (\mathbf{t}_{i+1} + \mathbf{t}_i) \right) \\
&= -\phi r_2 \left[ \mathbf{b}_1 \cdot \sum_{i=1}^{N-1} (\mathbf{t}_{i+1} - \mathbf{t}_i) \right] - \phi \left[ \sum_{i=1}^{N-1} \mathbf{b}_1 \cdot (\mathbf{t}_{i+1} - \mathbf{t}_i) \left( \frac{\mathbf{b}_2}{2} \cdot (\mathbf{t}_{i+1} + \mathbf{t}_i) \right) \right]
\end{aligned} \tag{A25}$$

We recognize

$$\rho_{\mathbf{r}\mathbf{r}'} = - \sum_{i=1}^{N-1} \mathbf{b}_1 \cdot (\mathbf{t}_{i+1} - \mathbf{t}_i), \quad \rho'_{\mathbf{r}\mathbf{r}'} = - \sum_{i=1}^{N-1} \mathbf{b}_1 \cdot (\mathbf{t}_{i+1} - \mathbf{t}_i) \left( \mathbf{b}_2 \cdot \frac{\mathbf{t}_{i+1} + \mathbf{t}_i}{2} \right), \tag{A26}$$

Additionally, we observe that our expression for  $\rho_{\mathbf{r}\mathbf{r}'}$  can be simplified because the sum telescopes, canceling term by term:

$$\begin{aligned}
\rho_{\mathbf{r}\mathbf{r}'} &= - \sum_{i=1}^{N-1} \mathbf{b}_1 \cdot (\mathbf{t}_{i+1} - \mathbf{t}_i) \\
&= -\mathbf{b}_1 \cdot (\mathbf{t}_N - \mathbf{t}_1) \\
&= -\mathbf{b}_1 \cdot (r_1 \mathbf{a}_1 + r_2 \mathbf{a}_2 + \mathbf{t}_N - (r_1 \mathbf{a}_1 + r_2 \mathbf{a}_2 + \mathbf{t}_1)) \\
&= -\mathbf{b}_1 \cdot ((\mathbf{R} + \boldsymbol{\delta}_\alpha) - (\mathbf{R}' + \boldsymbol{\delta}_\beta)) .
\end{aligned} \tag{A27}$$

and hence  $\rho_{\mathbf{r}\mathbf{r}'}$  is rational because  $\mathbf{b}_1 \cdot \mathbf{a}_i = \delta_{1i}$  and  $(\mathbf{R} + \boldsymbol{\delta}_\alpha) - (\mathbf{R}' + \boldsymbol{\delta}_\beta)$  is assumed to be a rational linear combination of the lattice vectors because the orbitals are commensurate. Eq. (A27) will be useful as we now determine the magnetic unit cell. We emphasize that the Peierls phases are calculated on open paths and hence are gauge-dependent.

## 5. Rationalization of the Flux

In this section we will demonstrate how to determine the magnetic unit cell in the Landau gauge at rational values of the flux  $\phi$ . We begin by recalling the well-known procedure on the square lattice. When the Peierls paths are taken along the bonds in the Landau gauge  $\mathbf{A}(\mathbf{r}) = -\phi(y, 0)$ , only the  $x$ -directed hoppings acquire nontrivial Peierls phases such that the hopping term becomes  $\exp(-\phi y) c_{x+1,y}^\dagger c_{x,y}$ . For  $\phi \neq 0$ , the unit cell is broken. However, we can recover a  $1 \times q$  unit cell where  $y \rightarrow y + q$  leaves all the Peierls phases invariant when  $\phi$  takes the values  $\phi = \frac{2\pi p}{q}$ ,  $p, q$  coprime. We emphasize that this specific magnetic unit cell derives from our Landau gauge choice. Because we can find  $p, q$  such that  $\phi$  is arbitrarily close to any real number, we are able to form the Hofstadter Hamiltonian in



momentum space arbitrarily close to any flux (potentially at the cost of a large magnetic unit cell.) We now consider the magnetic unit cell in a more complicated lattice. It is always possible in principle to choose a  $1 \times q$  magnetic unit cell since  $[T_1(\phi), T_2^q(\phi)] = [H, T_i(\phi)] = 0$ . However, since we wish to work *in a specific gauge*, the Landau gauge  $\mathbf{A}(\mathbf{r}) = -\phi \mathbf{b}_1(\mathbf{r} \cdot \mathbf{b}_2)$ , the Peierls phases are not generally periodic in the  $1 \times q$  magnetic unit cell. In our Landau gauge, all Peierls phases are in the form  $\varphi_{\mathbf{r}\mathbf{r}'} = \phi(\rho_{\mathbf{r}\mathbf{r}'} r_2 + \rho'_{\mathbf{r}\mathbf{r}'})$  (Eq. (A26)). Under a translation by  $T_2^q$  which amounts to taking  $r_2 \rightarrow r_2 + q$ , we have  $\varphi_{\mathbf{r}\mathbf{r}'} \rightarrow \varphi_{\mathbf{r}\mathbf{r}'} + 2\pi p \rho_{\mathbf{r}\mathbf{r}'}$  with  $\phi = 2\pi p/q$ . Generically,  $p \rho_{\mathbf{r}\mathbf{r}'}$  is not an integer and hence the Peierls phase is *not* periodic in the  $1 \times q$  magnetic unit cell. We now show that the Peierls phases *are* periodic for our gauge choice over a  $1 \times q'$  magnetic unit cell with  $q' \geq q$  if the flux is rationalized to be  $\phi = \mu \frac{2\pi p'}{q'}$  where  $\mu \in \mathbb{N}$  depends on the orbital positions and the choice of Landau gauge. (Note that  $\mu$  depends on the gauge and is unrelated to  $n$  and the flux periodicity  $\Phi = 2\pi n$ .)

Now we give an expression for  $\mu$  in the Landau gauge. Let  $\mu \in \mathbb{N}$  be the least common denominator (lcd) — equivalently the greatest common factor of the denominators — of  $\{\rho_{\mathbf{r}\mathbf{r}'}\}$  for each hopping of the model. Because  $\mathbf{R}$  and  $\mathbf{R}'$  are lattice vectors and  $\mathbf{b}_1 \cdot \mathbf{a}_i = \delta_{i1}$ ,  $\mathbf{b}_1 \cdot (\mathbf{R} - \mathbf{R}')$  is an integer, the rational part of  $\rho_{\mathbf{r}\mathbf{r}'}$  is  $-\mathbf{b}_1 \cdot (\boldsymbol{\delta}_\alpha - \boldsymbol{\delta}_\beta)$  and hence

$$\mu = \text{lcd} \{ \mathbf{b}_1 \cdot (\boldsymbol{\delta}_\beta - \boldsymbol{\delta}_\alpha) \} \text{ for all hoppings connecting } \mathbf{R} + \boldsymbol{\delta}_\alpha \text{ and } \mathbf{R}' + \boldsymbol{\delta}_\beta . \quad (\text{A28})$$

We seek to determine what (rational) value of the flux  $\phi$  permits a spatial periodicity in the Peierls phases Eq. (A25) along  $r_2$ . For a  $1 \times q'$  unit cell, meaning that all Peierls phases at  $r_2$  and  $r_2 + q'$  are identical modulo  $2\pi$ , we will prove that we must rationalize the flux to be

$$\phi = \mu \frac{2\pi p'}{q'}, \quad p', q' \in \mathbb{Z}, \text{ coprime} . \quad (\text{A29})$$

We see that the minimal  $1 \times q$  magnetic unit cell at  $\phi = \frac{2\pi p}{q}$  given by the magnetic translation group does not generically coincide with the  $1 \times q'$  magnetic unit cell which results from choosing the Landau gauge. Throughout this section, we define  $p'$  and  $q'$  by  $p/q = \mu p'/q'$  with  $\mu$  fixed by Eq. (A29) at  $\phi = \frac{2\pi p}{q}$ . Note that  $q$  and  $q'$  are related by  $q = q'/\text{gcd}(q', \mu)$  so  $q'$  is an integer multiple of  $q$  and  $q' \geq q$ .

In the  $1 \times q'$  magnetic unit cell, the Peierls phases are periodic and we can diagonalize the Hofstadter hamiltonian in momentum space. The  $1 \times q'$  unit cell is more convenient for practical purposes, such as determining the spectrum numerically. We emphasize that  $\mu$ , and hence the magnetic unit cell defined by  $q'$ , *are both gauge-dependent*. It is only the quantity  $\mu p'/q' = \phi/(2\pi)$  that is gauge-invariant.

We prove Eq. (A29) now. For brevity, we denote the Peierls phases  $\varphi_{\mathbf{R}+\boldsymbol{\delta}_\alpha, \mathbf{R}'+\boldsymbol{\delta}_\beta}$  as  $\varphi_{r_2\alpha, r_2'\beta}$ , recalling that  $\mathbf{R} = r_1 \mathbf{a}_1 + r_2 \mathbf{a}_2$  is the reference point as in Eq. (A25) and  $\mathbf{R}' = r_1' \mathbf{a}_1 + r_2' \mathbf{a}_2$  is the unit cell of the second orbital. We have used Eq. (A25) to show that  $\varphi_{\mathbf{R}+\boldsymbol{\delta}_\alpha, \mathbf{R}'+\boldsymbol{\delta}_\beta}$  does not depend on  $r_1$ . Then we have, under  $r_2 \rightarrow r_2 + q'$ ,

$$\begin{aligned} \varphi_{r_2\alpha, r_2'\beta} &= (\rho_{\mathbf{r}\mathbf{r}'} r_2 + \rho'_{\mathbf{r}\mathbf{r}'}) \phi \rightarrow (\rho_{\mathbf{r}\mathbf{r}'} (r_2 + q') + \rho'_{\mathbf{r}\mathbf{r}'}) \phi \\ &= \varphi_{r_2\alpha, r_2'\beta} + \phi q' \rho_{\mathbf{r}\mathbf{r}'} \\ &= \varphi_{r_2\alpha, r_2'\beta} + \mu \frac{2\pi p'}{q'} q' \rho_{\mathbf{r}\mathbf{r}'} \\ &= \varphi_{r_2\alpha, r_2'\beta} + 2\pi p' \rho_{\mathbf{r}\mathbf{r}'} \mu \\ &= \varphi_{r_2\alpha, r_2'\beta} \pmod{2\pi} . \end{aligned} \quad (\text{A30})$$

Thus  $\varphi_{r_2\alpha, r_2'\beta}$  only depends on  $r_2 \pmod{q'}$ , showing that the Peierls paths, and hence the Hofstadter Hamiltonian, has a  $1 \times q'$  unit cell. In many simple examples of the Hofstadter Butterfly [1, 9], the orbitals are all on the atomic sites, so  $\boldsymbol{\delta}_\alpha = 0$  for all  $\alpha$ . In this case, Eq. (A28) trivially gives  $\mu = 1$ , and the flux takes the familiar form  $\phi = \frac{2\pi p'}{q'} = \frac{2\pi p}{q}$ , so  $p = p'$  and  $q = q'$ .

We now turn to the example of the square lattice with 1b atoms (see Fig. 4) to discuss  $\mu \neq 1$ . If we choose the lattice vectors  $\mathbf{a}_1 = (1, 0)$ ,  $\mathbf{a}_2 = (0, 1)$  (noting  $\mathbf{a}_1 \times \mathbf{a}_2 = +1$ ), then  $\mathbf{b}_1 = (1, 0)$ . We calculate  $\mu$  using Eq. (A28) and find

$$\begin{aligned} \mu &= \text{lcd} \{ \mathbf{b}_1 \cdot (0, 0), \mathbf{b}_1 \cdot (1/2, 0), \mathbf{b}_1 \cdot (0, 0) \} \\ &= \text{lcd} \{ (1, 0) \cdot (0, 0), (1, 0) \cdot (1/2, 0), (1, 0) \cdot (0, 0) \} \\ &= 2 . \end{aligned} \quad (\text{A31})$$

This means that at  $\phi = 2 \frac{2\pi p'}{q'}$ , we can Fourier transform in the Landau gauge over a  $1 \times q'$  unit cell. Note that  $\mu = 2$  even when the  $t'$  hopping is zero, since it arises from the hopping connecting the 1a and 1b atoms (see Fig. 4). Thus we

see that when  $t' = 0$  we have  $n = 1, \mu = 2$  and when  $t' \neq 0$  we have  $n = 2, \mu = 2$  in this gauge. Alternatively, we could choose a different Landau gauge  $\mathbf{A}'(\mathbf{r}) = -\phi \mathbf{b}'_1(\mathbf{r} \cdot \mathbf{b}'_2)$  given by  $\mathbf{a}'_1 = (0, 1), \mathbf{a}'_2 = (-1, 0)$  (noting  $\mathbf{a}'_1 \times \mathbf{a}'_2 = +1$ ) where  $\mathbf{b}'_1 = (0, 1)$ . In this gauge, we compute

$$\begin{aligned} \mu' &= \text{lcd} \{ \mathbf{b}'_1 \cdot (0, 0), \mathbf{b}'_1 \cdot (1/2, 0), \mathbf{b}'_1 \cdot (0, 0) \} \\ &= \text{lcd} \{ (0, 1) \cdot (0, 0), (0, 1) \cdot (1/2, 0), (0, 1) \cdot (0, 0) \} \\ &= 1. \end{aligned} \quad (\text{A32})$$

Again, this result does not depend on  $t'$ . Hence in this gauge we have  $n = 1, \mu' = 1$  when  $t' = 0$  and  $n = 2, \mu' = 1$  when  $t' \neq 0$ . The values of  $\mu$  are distinct in the different gauges, but  $n$  is the same. Indeed,  $\Phi = 2\pi n$  is gauge-invariant, whereas  $\mu$  simply allowed us to Fourier transform the Peierls phases in a given gauge.

In some cases (but not all), it is possible to choose lattice vectors so that the Landau gauge  $\mathbf{A}(\mathbf{r}) = -\phi \mathbf{b}_1(\mathbf{r} \cdot \mathbf{b}_2)$  yields  $\mu = 1$ , which we discuss now.

## 6. Residual $SL(2, \mathbb{Z})$ Gauge Freedom

Despite fixing our gauge to the Landau gauge  $\mathbf{A}(\mathbf{r}) = -\phi \mathbf{b}_1(\mathbf{r} \cdot \mathbf{b}_2)$  which ensures a  $1 \times q'$  magnetic unit cell, there is a residual gauge freedom which arises due to the choice of reciprocal lattice vectors  $\mathbf{b}_i$ . In deriving Eq. (A27), the form of the Peierls phases which defines  $\mu$  (Eq. (A28)), we relied on the fact that  $\mathbf{b}_i \cdot \mathbf{a}_j = \delta_{ij}$ . For any given set of basis vectors  $\mathbf{a}_i$ ,  $\mathbf{b}_i$  is defined uniquely and our Landau gauge is fixed. However, we can gauge transform to a different Landau gauge  $\mathbf{A}'(\mathbf{r}) = -\phi \mathbf{b}'_1(\mathbf{r} \cdot \mathbf{b}'_2)$  while preserving the form of Eq. (A26) by choosing new lattice vectors

$$\mathbf{a}'_i = m_{i1} \mathbf{a}_1 + m_{i2} \mathbf{a}_2, \quad m_{ij} \in \mathbb{Z}. \quad (\text{A33})$$

For  $\mathbf{a}'_i$  to preserve the area of the unit cell, we require  $\mathbf{a}'_1 \times \mathbf{a}'_2 = \mathbf{b}'_1 \times \mathbf{b}'_2 = 1$  which holds iff  $\det[m] = m_{11}m_{22} - m_{12}m_{21} = 1$ . Thus  $[m] \in SL(2, \mathbb{Z})$ . The corresponding reciprocal lattice is spanned by  $\mathbf{b}'_i$  satisfying  $\mathbf{b}'_i \cdot \mathbf{a}'_j = \delta_{ij}$  and  $\nabla \times \mathbf{A}'(\mathbf{r}) = \phi \mathbf{b}'_1 \times \mathbf{b}'_2 = \phi$ . It can be checked using  $\det[m] = 1$  that the reciprocal vectors are given by

$$\begin{aligned} \mathbf{b}'_1 &= m_{22} \mathbf{b}_1 - m_{21} \mathbf{b}_2, \\ \mathbf{b}'_2 &= -m_{12} \mathbf{b}_1 + m_{11} \mathbf{b}_2. \end{aligned} \quad (\text{A34})$$

We find that even after fixing the form of our Landau gauge, there is still a nontrivial residual gauge symmetry

$$\mathbf{A}'(\mathbf{r}) = -\phi \mathbf{b}'_1(\mathbf{r} \cdot \mathbf{b}'_2) = \mathbf{A}(\mathbf{r}) + \nabla \Lambda \quad (\text{A35})$$

where one may verify that  $\Lambda = \frac{\phi}{2} \left( (\mathbf{r} \cdot \mathbf{b}_1)(\mathbf{r} \cdot \mathbf{b}_2) - (\mathbf{r} \cdot \mathbf{b}'_1)(\mathbf{r} \cdot \mathbf{b}'_2) \right)$  by direct computation. In the gauge  $\mathbf{A}'(\mathbf{r})$ , we find a new rationalization of the flux  $\phi = \mu' \frac{2\pi p''}{q''}$  where

$$\mu' = \text{lcd} \{ \mathbf{b}'_1 \cdot (\boldsymbol{\delta}_\beta - \boldsymbol{\delta}_\alpha) \} \text{ for all hoppings connecting } \mathbf{R} + \boldsymbol{\delta}_\alpha \text{ and } \mathbf{R}' + \boldsymbol{\delta}_\beta. \quad (\text{A36})$$

This is once again an illustration that  $\mu$  is gauge-dependent. It is tempting to think that with an appropriate  $SL(2, \mathbb{Z})$  gauge transformation, it is possible to find a basis where  $\mu' = 1$ . We prove a condition on the orbitals  $\boldsymbol{\delta}_\alpha$  demonstrating when it is possible to find such a basis, but we also show that in general it is impossible, i.e. that there is no choice of basis where  $\mu = 1$  in our Landau gauge.

$\mu$  is calculated from the distances between hoppings  $\{\boldsymbol{\delta}_\beta - \boldsymbol{\delta}_\alpha\}$ . Because we assume  $\boldsymbol{\delta}_\beta - \boldsymbol{\delta}_\alpha$  is a rational sum of lattice vectors, we have  $\boldsymbol{\delta}_\beta - \boldsymbol{\delta}_\alpha = \omega_{1,\alpha\beta} \mathbf{a}_1 + \omega_{2,\alpha\beta} \mathbf{a}_2$  for  $\omega_{1,\alpha\beta}, \omega_{2,\alpha\beta} \in \mathbb{Q}$ . By Eq. (A28), we have

$$\begin{aligned} \mu' &= \text{lcd} \{ \mathbf{b}'_1 \cdot (\omega_{1,\alpha\beta} \mathbf{a}_1 + \omega_{2,\alpha\beta} \mathbf{a}_2) \} \text{ for all hoppings connecting } \mathbf{R} + \boldsymbol{\delta}_\alpha \text{ and } \mathbf{R}' + \boldsymbol{\delta}_\beta \\ &= \text{lcd} \{ m_{22} \omega_{1,\alpha\beta} - m_{21} \omega_{2,\alpha\beta} \} \text{ for all hoppings connecting } \mathbf{R} + \boldsymbol{\delta}_\alpha \text{ and } \mathbf{R}' + \boldsymbol{\delta}_\beta. \end{aligned} \quad (\text{A37})$$

Let  $\mu_i = \text{lcd} \{ \omega_{i,\alpha\beta} \}$  for all hoppings connecting  $\mathbf{R} + \boldsymbol{\delta}_\alpha$  and  $\mathbf{R}' + \boldsymbol{\delta}_\beta$ . If  $\mu_1$  and  $\mu_2$  are coprime, *it is possible to set*  $\mu' = 1$ . We show this by explicitly constructing  $[m]$ . Set  $m_{22} = \mu_1$  and  $m_{21} = -\mu_2$  in which case  $m_{22} \omega_{1i} = \mu_1 \omega_{1i} \in \mathbb{Z}$  and  $-m_{21} \omega_{2i} = \mu_2 \omega_{2i} \in \mathbb{Z}$  for all  $i$ . Hence  $\mu' = 1$ . Additionally, there exist  $m_{11}, m_{12} \in \mathbb{Z}$  such that  $\det[m] = \mu_1 m_{11} + \mu_2 m_{12} = 1$ . Indeed,  $\mu_1$  and  $\mu_2$  are coprime. We can thus choose  $m_{12}$  to be the modular inverse of  $\mu_2$ , i.e.  $\mu_2 m_{12} = 1 \pmod{\mu_1}$ , simultaneously setting  $m_{11} \in \mathbb{Z}$  such that  $\mu_2 m_{12} = 1 - m_{11} \mu_1$ .

However, when  $\mu_1$  and  $\mu_2$  are not coprime, this proof fails. We now give an example of such a case where it is impossible to construct a basis where  $\mu = 1$ . Let there be three orbitals  $\boldsymbol{\delta}_i = (0, 0), (1/2, 1/2), (1/2, 1/4)$  in the

$\mathbf{a}_1, \mathbf{a}_2$  basis such that  $\boldsymbol{\delta}_1$  is connected to  $\boldsymbol{\delta}_2$  and  $\boldsymbol{\delta}_3$  so that  $\{\omega_{1,\alpha\beta}\} = \{1/2\}$  and  $\{\omega_{2,\alpha\beta}\} = \{1/2, 1/4\}$ . Then we find  $\mu_1 = 2, \mu_2 = 4$  which are not coprime. Assume for contradiction that coprime  $m_{22}$  and  $m_{21}$  exist such that  $\mu' = \text{lcd} \{\mathbf{b}'_1 \cdot (\boldsymbol{\delta}_1 - \boldsymbol{\delta}_2), \mathbf{b}'_1 \cdot (\boldsymbol{\delta}_1 - \boldsymbol{\delta}_3)\}$  is 1, recalling  $\mathbf{b}'_1 = m_{22}\mathbf{b}_1 - m_{21}\mathbf{b}_2$ . (Note that if  $m_{22}$  and  $m_{21}$  are not coprime, then  $\det[m] \neq 1$  and  $\nabla \times \mathbf{A}'(\mathbf{r}) \neq \phi$ .) This implies that each component of

$$\{\mathbf{b}'_1 \cdot (\boldsymbol{\delta}_1 - \boldsymbol{\delta}_2), \mathbf{b}'_1 \cdot (\boldsymbol{\delta}_1 - \boldsymbol{\delta}_3)\} = \left\{ \frac{1}{2}(m_{22} - m_{21}), \frac{1}{4}(2m_{22} - m_{21}) \right\} \quad (\text{A38})$$

is integer, so  $m_{22} - m_{21} \in 2\mathbb{Z}$ . We write  $m_{22} = m_{21} + 2s, s \in \mathbb{Z}$ . Then

$$\frac{1}{4}(2m_{22} - m_{21}) = \frac{1}{4}(m_{21} + 4s) \quad (\text{A39})$$

is an integer only if  $m_{21}$  is a multiple of 4. But  $m_{22} - m_{21} \in 2\mathbb{Z}$  implies  $m_{21}$  is then a multiple of 2, so  $m_{21}$  and  $m_{22}$  are not coprime.

In summary, we have shown that at  $\phi = \frac{2\pi p}{q} = \mu \frac{2\pi p'}{q'}$  for  $p', q'$  coprime, the Peierls phases are periodic in a  $1 \times q'$  magnetic unit cell *in our Landau gauge*.  $\mu$  is calculated from the positions of the orbitals and the choice of lattice vectors. We gave a simple criterion to determine if it is generically possible to find a basis where  $\mu = 1$ , but we showed that there exist lattices where it is impossible to find such a basis. In the remaining sections, we develop our theory for a general  $\mu$ .

## 7. Construction of the Hofstadter Hamiltonian

We have shown that our choice of Landau gauge preserves translation invariance along  $\mathbf{a}_1$ , but at  $\phi = \mu \frac{2\pi p'}{q'}$ , there is only translational invariance along  $\mathbf{a}_2$  given by  $r_2 \rightarrow r_2 + q'$  *even if  $\mu$  and  $q'$  are not coprime*. By choosing the Landau gauge, we are able to easily calculate the Peierls phases and form the Hofstadter Hamiltonian in a  $1 \times q'$  magnetic unit cell. From the magnetic translation group, we know that it is possible to make a gauge transformation and diagonalize  $H^\phi$  in the minimal  $1 \times q$  unit cell at  $\phi = \frac{2\pi p}{q}$ , but it is difficult to find such a gauge explicitly. The Landau gauge is much more convenient for numerics, even at the cost of a larger magnetic unit cell.

Redefining  $r_1$  and  $r_2$ , we write an atomic position in the crystal in the form  $r_1\mathbf{a}_1 + q'r_2\mathbf{a}_2 + \ell\mathbf{a}_2 + \boldsymbol{\delta}_\alpha$  where  $\ell = 0, \dots, q' - 1$  indexes the zero-field unit cells within the magnetic unit cell, and the orbitals are given by  $\alpha = 1, \dots, N_{orb}$  with positions  $\boldsymbol{\delta}_\alpha$ . Because the Peierls phases are periodic over the magnetic lattice, we have  $\varphi_{q'r_2+\ell, \alpha, q'r'_2+\ell', \beta} = \varphi_{\ell\alpha, \ell'\beta}$ .

The momentum space operators are defined as usual in the magnetic unit cell. In this notation, they are given by

$$c_{k_1, k_2, \ell, \alpha}^\dagger = \frac{1}{\sqrt{\mathcal{N}/q'}} \sum_{r_1 r_2} e^{-i\mathbf{k} \cdot (r_1\mathbf{a}_1 + r_2 q'\mathbf{a}_2 + \ell\mathbf{a}_2 + \boldsymbol{\delta}_\alpha)} c_{r_1, r_2, \ell, \alpha}^\dagger \quad (\text{A40})$$

where the sum is over  $r_1 = 1, \dots, \mathcal{N}_1, r_2 = 1, \dots, \mathcal{N}_2/q'$ , and  $\mathcal{N} = \mathcal{N}_1\mathcal{N}_2$  is the number of unit cells in the lattice. We assume that  $\mathcal{N}_2/q' \in \mathbb{Z}$  for the periodic boundary conditions to have an integer number of  $1 \times q'$  magnetic unit cells. The Hamiltonian can be written in terms of these operators

$$\begin{aligned} H^{\phi = \mu \frac{2\pi p'}{q'}} &= \sum_{r_1 r_2, r'_1 r'_2} \sum_{\ell\alpha, \ell'\beta} e^{i\varphi_{\ell\alpha, \ell'\beta}} t_{\alpha\beta} \left( (r_1 - r'_1)\mathbf{a}_1 + (r_2 - r'_2)q'\mathbf{a}_2 + (\ell - \ell')\mathbf{a}_2 + (\boldsymbol{\delta}_\alpha - \boldsymbol{\delta}_\beta) \right) c_{r_1, r_2, \ell, \alpha}^\dagger c_{r'_1, r'_2, \ell', \beta} \\ &= \sum_{k_1, k_2} \sum_{\ell\alpha, \ell'\beta} c_{k_1, k_2, \ell, \alpha}^\dagger [\mathcal{H}(k_1, k_2)]_{\ell, \alpha, \ell', \beta} c_{k_1, k_2, \ell', \beta}, \quad k_1 \in (-\pi, \pi), \quad k_2 \in \left(0, \frac{2\pi}{q'}\right) \end{aligned} \quad (\text{A41})$$

where  $\mathcal{H}$  is the Fourier transform over the *magnetic* lattice:

$$\begin{aligned} [\mathcal{H}(k_1, k_2)]_{\ell, \alpha, \ell', \beta} &= \frac{1}{\mathcal{N}/q'} \sum_{r_1, r'_1, r_2, r'_2} e^{i\varphi_{\ell\alpha, \ell'\beta} - i\mathbf{k} \cdot ((r_1 - r'_1)\mathbf{a}_1 + (r_2 - r'_2)q'\mathbf{a}_2 + (\ell - \ell')\mathbf{a}_2 + (\boldsymbol{\delta}_\alpha - \boldsymbol{\delta}_\beta))} \\ &\quad \times t_{\alpha\beta} \left( (r_1 - r'_1)\mathbf{a}_1 + (r_2 - r'_2)q'\mathbf{a}_2 + (\ell - \ell')\mathbf{a}_2 + (\boldsymbol{\delta}_\alpha - \boldsymbol{\delta}_\beta) \right) \end{aligned} \quad (\text{A42})$$

and the magnetic BZ is defined as  $k_1 = \frac{2\pi}{\mathcal{N}_x}(0, \dots, \mathcal{N}_x - 1), k_2 = \frac{2\pi}{\mathcal{N}_y}(0, \dots, \mathcal{N}_y/q' - 1)$ . We note that for an infinite crystal, i.e. taking  $\mathcal{N}_1, \mathcal{N}_2 \rightarrow \infty$ , the magnetic BZ is defined to be  $k_1 \in (-\pi, \pi), k_2 \in (0, 2\pi/q')$ . At a given momentum, the matrix Eq. (A42) can be diagonalized numerically to determine the  $q'n_{orb}$  band energies. We have separated the  $\ell, \alpha$  indices because it is useful to think of them in a tensor product basis.

We comment now on the apparent discontinuity that  $\mathcal{H}^\phi(\mathbf{k})$  suffers. Because commuting translation operators only exist when  $\phi$  is rational,  $\mathcal{H}^\phi(\mathbf{k})$  only exists at  $\phi = \mu \frac{2\pi p'}{q}$ . Additionally, the Fourier transform is only well-defined when the number of lattice sites (on periodic boundary conditions as we have assumed) is a multiple of  $q'$ . For two arbitrarily close values of  $\phi$ , their denominators may be arbitrarily different, and for any finite size lattice,  $\mathcal{H}^\phi(\mathbf{k})$  may not strictly exist. While  $\mathcal{H}$  and  $\mathbf{k}$  have very discontinuous behavior in  $\phi$ , the spectrum of  $H^\phi$  evolves smoothly. Ref. [1] proves that the spectrum is continuous for the simple Hamiltonian which it considers, but extending this proof to momentum space for a general Hamiltonian is beyond the scope of this work. Instead, we appeal to the position space representation of the Hofstadter Hamiltonian. It is clear that the spectrum evolves smoothly there because each term in  $H^\phi$  is an analytic function of  $\phi$ .

## 8. Embedding Matrices in Flux

Thus far, we have shown that at  $\phi = \mu \frac{2\pi p'}{q}$ , the Hofstadter Hamiltonian can be diagonalized in a  $1 \times q'$  magnetic unit cell, and the magnetic BZ may be taken as  $k_1 \in (-\pi, \pi), k_2 \in (0, 2\pi/q')$ . This establishes a  $2\pi/q'$  periodicity in  $k_2$ . In this section, we will show that the energy spectrum and eigenstates of the Hofstadter Hamiltonian are also periodic in  $k_1$  across the magnetic BZ with period  $\phi = \mu \frac{2\pi p'}{q}$ , with  $p', q'$  coprime. If  $\mu$  and  $q'$  are coprime, then iterating the  $\phi$  periodicity will give a  $\frac{2\pi}{q'}$  periodicity in  $k_1$ , matching the  $\frac{2\pi}{q'}$  periodicity along  $k_2$ . If  $\mu$  and  $q'$  are *not* coprime, then iterating the  $\phi$  periodicity will only yield a  $\frac{2\pi}{q} = \frac{2\pi}{q'/\text{gcd}(q', \mu)}$  periodicity along  $k_1$ . In contrast, there will always be a  $\frac{2\pi}{q'}$  periodicity along  $k_2$  because the magnetic unit cell is  $1 \times q'$  at  $\phi = \mu \frac{2\pi p'}{q}$ , so a  $\frac{2\pi}{q'}$  periodicity appears due to the definition of the magnetic BZ. We emphasize that the states at  $\mathbf{k}$  and  $\mathbf{k} + \frac{2\pi}{q} \mathbf{b}_1$  are independent states in the Hilbert space although they have the same energy, but states at  $\mathbf{k}$  and  $\mathbf{k} + \frac{2\pi}{q'} \mathbf{b}_2$  are not independent states due to the definition of the magnetic BZ (see Eq. (A41)). We sketch an example of the magnetic BZ when  $\mu = 2$ , as is the case for a simple choice of basis for the lattice in Fig. 4, and  $\phi = 2 \frac{2\pi \times 3}{4} = 3\pi$  in Fig. 7, where there is a  $\pi$  periodicity along  $k_1 \in (-\pi, \pi)$  and a  $\frac{2\pi}{q'} = \pi/2$  periodicity along  $k_2 \in (0, \frac{\pi}{2})$ .

In our Landau gauge  $\mathbf{A}(\mathbf{r}) = -\phi \mathbf{b}_1(\mathbf{r} \cdot \mathbf{b}_2)$ , we will find expressions for magnetic embedding matrices  $V_i(\phi)$  which obey

$$\mathcal{H}^\phi(\mathbf{k} + \phi \mathbf{b}_i) = V_i(\phi) \mathcal{H}^\phi(\mathbf{k}) V_i^\dagger(\phi) \quad (\text{A43})$$

and implement the  $\phi$  periodicity in the spectrum. This is the same  $\phi$  periodicity that was proved in Eq. (4) using the magnetic translation operators. The energy spectrum always has a  $\phi$  periodicity along both axes of the magnetic BZ, no matter what magnetic unit cell is chosen to diagonalize the Hamiltonian.

We begin with the expression for  $V_2(\phi)$  in our Landau gauge, noting that

$$\begin{aligned} c_{k_1, k_2 + \phi, \ell, \alpha} &= \frac{1}{\sqrt{\mathcal{N}/q'}} \sum_{r_1 r_2} e^{i(\mathbf{k} + \mathbf{b}_2 \phi) \cdot (r_1 \mathbf{a}_1 + q' r_2 \mathbf{a}_2 + \ell \mathbf{a}_2 + \delta_\alpha)} c_{r_1, r_2, \ell, \alpha} \\ &= \frac{1}{\sqrt{\mathcal{N}/q'}} \sum_{r_1 r_2} e^{i\mathbf{k} \cdot (r_1 \mathbf{a}_1 + q' r_2 \mathbf{a}_2 + \ell \mathbf{a}_2 + \delta_\alpha)} e^{i\phi(q' r_2 + \ell + \mathbf{b}_2 \cdot \delta_\alpha)} c_{r_1, r_2, \ell, \alpha} \\ &= \frac{1}{\sqrt{\mathcal{N}/q'}} \sum_{r_1 r_2} e^{i\mathbf{k} \cdot (r_1 \mathbf{a}_1 + q' r_2 \mathbf{a}_2 + \ell \mathbf{a}_2 + \delta_\alpha)} e^{i\phi(\ell + \mathbf{b}_2 \cdot \delta_\alpha)} c_{r_1, r_2, \ell, \alpha} \\ &= \sum_{\ell' \beta} [V_2(\phi)]_{\ell, \alpha, \ell', \beta} c_{k_1, k_2, \ell', \beta} \end{aligned} \quad (\text{A44})$$

where we have defined

$$[V_2(\phi)]_{\ell, \alpha, \ell', \beta} = \delta_{\ell \ell'} e^{i\phi \ell} \delta_{\alpha \beta} e^{i\phi \delta_\alpha \cdot \mathbf{b}_2} . \quad (\text{A45})$$

This allows us to deduce the action of  $V_2$  on the Hamiltonian:

$$\begin{aligned} H^\phi &= \sum_{k_1, k_2} \sum_{\ell \alpha, \ell' \beta} c_{k_1, k_2, \ell, \alpha}^\dagger [\mathcal{H}(k_1, k_2)]_{\ell, \alpha, \ell', \beta} c_{k_1, k_2, \ell', \beta} \\ &= \sum_{k_1, k_2} \sum_{\ell \alpha, \ell' \beta} c_{k_1, k_2 + \phi, \ell, \alpha}^\dagger [\mathcal{H}(k_1, k_2 + \phi)]_{\ell, \alpha, \ell', \beta} c_{k_1, k_2 + \phi, \ell', \beta} \\ &= \sum_{k_1, k_2} \sum_{\ell \alpha, \ell' \beta} \sum_{\ell'' \ell''', \alpha' \beta'} c_{k_1, k_2, \ell''', \alpha'}^\dagger [V_2^\dagger(\phi)]_{\ell''', \alpha', \ell, \alpha} [\mathcal{H}(k_1, k_2 + \phi)]_{\ell, \alpha, \ell', \beta} [V_2(\phi)]_{\ell', \beta, \ell'', \beta'} c_{k_1, k_2, \ell'', \beta'} . \end{aligned} \quad (\text{A46})$$

Matching terms, we see that Eq. (A43) is satisfied. We note that  $V_2(\phi)$  is a diagonal matrix of phases, and so is unitary.

To derive  $V_1(\phi)$  in our Landau gauge, we focus without loss of generality on a generic hopping of  $H^\phi$  from  $r_1\mathbf{a}_1 + (q'r_2 + \ell)\mathbf{a}_2 + \boldsymbol{\delta}_\alpha$  to  $r'_1\mathbf{a}_1 + (q'r'_2 + \ell')\mathbf{a}_2 + \boldsymbol{\delta}_\beta$ . Let  $(\Delta_1, \Delta_2) = (r_1 - r'_1, q'(r_2 - r'_2) + \ell - \ell')$  denote the distance between the unit cells of the orbitals in the hopping, and let  $t$  denote the amplitude of the hopping. After Fourier transforming this hopping, we get a term in the Hamiltonian Eq. (A42) given by

$$[\mathcal{H}_t^\phi(\mathbf{k})]_{\ell, \alpha, \ell', \beta} = t e^{i\varphi_{\ell, \alpha, \ell', \beta} - ik_1 \mathbf{b}_1 \cdot (\Delta_1 \mathbf{a}_1 + \boldsymbol{\delta}_\alpha - \boldsymbol{\delta}_\beta) - ik_2 \mathbf{b}_2 \cdot (\Delta_2 \mathbf{a}_2 + \boldsymbol{\delta}_\alpha - \boldsymbol{\delta}_\beta)}, \quad (\text{A47})$$

and the whole Hamiltonian  $\mathcal{H}^\phi(\mathbf{k})$  consists of a sum over the hoppings  $t$  of  $\mathcal{H}_t^\phi(\mathbf{k})$ . We recall that  $\varphi_{\ell, \alpha, \ell', \beta}$  is the Peierls phase (see Eq. (A30) and the following discussion). Using the expression for  $\mathcal{H}_t^\phi(k_1, k_2)$  in Eq. (A47), we see that

$$[\mathcal{H}_t^\phi(k_1 + \phi, k_2)]_{\ell-1, \alpha, \ell'-1, \beta} = t e^{i\varphi_{\ell-1, \alpha, \ell'-1, \beta} - i(k_1 + \phi) \mathbf{b}_1 \cdot (\Delta_1 \mathbf{a}_1 + \boldsymbol{\delta}_\alpha - \boldsymbol{\delta}_\beta) - ik_2 \mathbf{b}_2 \cdot (\Delta_2 \mathbf{a}_2 + \boldsymbol{\delta}_\alpha - \boldsymbol{\delta}_\beta)} \quad (\text{A48})$$

where  $\ell$  and  $\ell'$  are defined mod  $q'$ . Now we calculate that

$$\begin{aligned} \varphi_{\ell-1, \alpha, \ell'-1, \beta} - \phi \mathbf{b}_1 \cdot (\Delta_1 \mathbf{a}_1 + \boldsymbol{\delta}_\alpha - \boldsymbol{\delta}_\beta) &= -\phi \int_{r'_1 \mathbf{a}_1 + (\ell'-1+q'r'_2)\mathbf{a}_2 + \boldsymbol{\delta}_\beta}^{r_1 \mathbf{a}_1 + (\ell-1+q'r_2)\mathbf{a}_2 + \boldsymbol{\delta}_\alpha} (\mathbf{r} \cdot \mathbf{b}_2) \mathbf{b}_1 \cdot d\mathbf{r} - \phi \mathbf{b}_1 \cdot (\Delta_1 \mathbf{a}_1 + \boldsymbol{\delta}_\alpha - \boldsymbol{\delta}_\beta) \\ &= -\phi \int_{r'_1 \mathbf{a}_1 + (\ell'+q'r'_2)\mathbf{a}_2 + \boldsymbol{\delta}_\beta}^{r_1 \mathbf{a}_1 + (\ell+q'r_2)\mathbf{a}_2 + \boldsymbol{\delta}_\alpha} ((\mathbf{r} - \mathbf{a}_2) \cdot \mathbf{b}_2) \mathbf{b}_1 \cdot d\mathbf{r} - \phi \mathbf{b}_1 \cdot (\Delta_1 \mathbf{a}_1 + \boldsymbol{\delta}_\alpha - \boldsymbol{\delta}_\beta) \\ &= \varphi_{\ell, \alpha, \ell', \beta} + \phi \int_{r'_1 \mathbf{a}_1 + (\ell'+q'r'_2)\mathbf{a}_2 + \boldsymbol{\delta}_\beta}^{r_1 \mathbf{a}_1 + (\ell+q'r_2)\mathbf{a}_2 + \boldsymbol{\delta}_\alpha} \mathbf{b}_1 \cdot d\mathbf{r} - \phi \mathbf{b}_1 \cdot (\Delta_1 \mathbf{a}_1 + \boldsymbol{\delta}_\alpha - \boldsymbol{\delta}_\beta) \\ &= \varphi_{\ell, \alpha, \ell', \beta} + \phi \mathbf{b}_1 \cdot (\Delta_1 \mathbf{a}_1 + \boldsymbol{\delta}_\alpha - \boldsymbol{\delta}_\beta) - \phi \mathbf{b}_1 \cdot (\Delta_1 \mathbf{a}_1 + \boldsymbol{\delta}_\alpha - \boldsymbol{\delta}_\beta) \\ &= \varphi_{\ell, \alpha, \ell', \beta} \end{aligned} \quad (\text{A49})$$

where we have used  $\mathbf{a}_2 \cdot \mathbf{b}_2 = 1$ . We observe that the cancelation of the  $\Delta_1$ -dependent terms is due to the structure of our Landau gauge. Comparing Eqs. (A47) and (A48), we see that

$$[\mathcal{H}_t^\phi(k_1 + \phi, k_2)]_{\ell-1, \alpha, \ell'-1, \beta} = [\mathcal{H}_t^\phi(k_1, k_2)]_{\ell, \alpha, \ell', \beta}. \quad (\text{A50})$$

Hence, defining

$$[V_1(\phi)]_{\ell, \alpha, \ell', \beta} = \delta_{\ell, \ell'-1} \delta_{\alpha\beta}, \quad (\text{A51})$$

emphasizing again that  $\ell$  and  $\ell'$  are defined mod  $q'$  in the Kronecker delta. We find that  $\mathcal{H}_t^\phi(k_1 + \phi, k_2) = V_1(\phi) \mathcal{H}_t^\phi(k_1, k_2) V_1^\dagger(\phi)$ . Note that  $V_1(\phi)$  is unitary because it is the tensor product of a permutation matrix and the identity. Thus we have proven Eq. (A43) holds for  $H^\phi$  when focusing on a single generic hopping. It is simple to extend this result for  $H^\phi$  having arbitrary hoppings. We observe that

$$\begin{aligned} \mathcal{H}^\phi(k_1, k_2) &= \sum_{\text{hoppings } t} \mathcal{H}_t^\phi(k_1, k_2) \\ \mathcal{H}^\phi(k_1 + \phi, k_2) &= \sum_{\text{hoppings } t} \mathcal{H}_t^\phi(k_1 + \phi, k_2) \\ &= \sum_{\text{hoppings } t} V_1(\phi) \mathcal{H}_t^\phi(k_1, k_2) V_1^\dagger(\phi) \\ &= V_1(\phi) \left( \sum_{\text{hoppings } t} \mathcal{H}_t^\phi(k_1, k_2) \right) V_1^\dagger(\phi) \\ &= V_1(\phi) \mathcal{H}^\phi(k_1, k_2) V_1^\dagger(\phi). \end{aligned} \quad (\text{A52})$$

By explicit computation, we obtain the braiding relation of the embedding matrices,

$$V_1(\phi) V_2(\phi) = e^{i\phi} V_2(\phi) V_1(\phi). \quad (\text{A53})$$

According to Eq. (A43), the embedding matrices  $V_i(\phi)$  establish a  $\phi$  periodicity along  $k_1$  and  $k_2$  in the energy spectrum.

At zero flux, we also have an  $N_{orb} \times N_{orb}$  embedding matrix corresponding to the  $2\pi$  periodicity in the BZ. The embedding matrix  $[\mathcal{V}_i]_{\alpha\beta} = \delta_{\alpha\beta} e^{2\pi i \boldsymbol{\delta}_\alpha \cdot \mathbf{b}_i}$  satisfies

$$\mathcal{H}^{\phi=0}(\mathbf{k} + 2\pi \mathbf{b}_i) = \mathcal{V}_i \mathcal{H}^{\phi=0}(\mathbf{k}) \mathcal{V}_i^\dagger. \quad (\text{A54})$$

We extend this embedding matrix to the nonzero flux case to recover the usual  $2\pi$  periodicity in the magnetic BZ by defining its action on the Hofstadter Hamiltonian as the identity on the  $\ell$  indices, i.e.  $[\mathcal{V}_i]_{\alpha\beta} \rightarrow [\mathcal{V}_i]_{\ell\alpha, \ell'\beta} = \delta_{\ell\ell'} \delta_{\alpha\beta} e^{2\pi i \boldsymbol{\delta}_\alpha \cdot \mathbf{b}_i}$  such that

$$\mathcal{H}^\phi(\mathbf{k} + 2\pi \mathbf{b}_i) = \mathcal{V}_i \mathcal{H}^\phi(\mathbf{k}) \mathcal{V}_i^\dagger. \quad (\text{A55})$$

It is sometimes useful to combine the  $2\pi$  periodicity given by  $\mathcal{V}_i$  and the  $\phi$  periodicity given by  $V_i(\phi)$ . For example at  $\phi = \frac{4\pi}{3}$ , the spectrum is actually  $\frac{2\pi}{3}$ -periodic, as we see from iterating the  $\phi = \frac{4\pi}{3}$  periodicity twice, and then applying the  $2\pi$  periodicity of  $k_1$  given by  $\mathcal{V}_i$ . The embedding matrix  $\mathcal{V}_i^\dagger V_i(\phi)^2$  establishes this  $\frac{2\pi}{3}$ -periodicity. By combining the  $\phi$  periodicity and the  $2\pi$  periodicity, we will show that there is a  $\frac{2\pi}{q}$  periodicity along  $k_1$  at  $\phi = \frac{2\pi p}{q} = \mu \frac{2\pi p'}{q'}$ . Note that the periodicity along  $k_1$  depends on  $q$  and is gauge-independent. This  $2\pi/q$  periodicity along  $k_1$  is the same as the periodicity established by the magnetic translation group in Eq. (4).

To find expressions for the embedding matrices that implement the  $\frac{2\pi}{q}$  periodicity, we define  $\zeta, s \in \mathbb{Z}$  by

$$\zeta\phi = \frac{2\pi}{q} + 2\pi s \quad (\text{A56})$$

or equivalently  $\zeta\phi = 2\pi/q \pmod{2\pi}$ . To prove the  $\frac{2\pi}{q}$  periodicity along  $k_1$ , we first note that

$$\mathcal{H}^\phi(\mathbf{k} + \zeta\phi \mathbf{b}_i) = [V_1(\phi)]^\zeta \mathcal{H}^\phi(\mathbf{k}) [V_1^\dagger(\phi)]^\zeta. \quad (\text{A57})$$

Additionally, we see

$$\begin{aligned} \mathcal{H}^\phi(\mathbf{k} + \zeta\phi \mathbf{b}_1) &= \mathcal{H}^\phi(\mathbf{k} + \frac{2\pi}{q} \mathbf{b}_1 + 2\pi s \mathbf{b}_1) \\ &= [\mathcal{V}_1]^s \mathcal{H}^\phi(\mathbf{k} + \frac{2\pi}{q} \mathbf{b}_1) [\mathcal{V}_1^\dagger]^s. \end{aligned} \quad (\text{A58})$$

Combining Eqs. (A57) and (A58), we obtain

$$\mathcal{H}^\phi(\mathbf{k} + \frac{2\pi}{q} \mathbf{b}_1) = \tilde{V}_1(\phi) \mathcal{H}^\phi(\mathbf{k}) \tilde{V}_1^\dagger(\phi), \quad \tilde{V}_1(\phi) = [\mathcal{V}_1^\dagger]^s [V_1(\phi)]^\zeta \quad (\text{A59})$$

which shows the spectrum is  $2\pi/q$ -periodic along  $k_1$ . We remark that  $[\mathcal{V}_i, V_i(\phi)] = 0$ . The algebra of  $\tilde{V}_1$  and  $\tilde{V}_2$  is readily obtained by repeated application of Eq. (A53) and Eq. (A56). We find

$$\tilde{V}_1(\phi) \tilde{V}_2(\phi) = e^{i\zeta \frac{2\pi}{q}} \tilde{V}_2(\phi) \tilde{V}_1(\phi). \quad (\text{A60})$$

We have thus far shown that  $V_1(\phi)$  and  $V_2(\phi)$  give a  $\phi$  periodicity along  $k_1$  and  $k_2$ . Also we combined the  $\phi$  and  $2\pi$  periodicity along  $k_1$  to show that  $\tilde{V}_1(\phi)$  gives a minimal  $\frac{2\pi}{q}$  periodicity along  $k_1$  at  $\phi = \frac{2\pi p}{q}$ . Recall from App. A 5 that  $q'$  is an integer multiple of  $q$ , and  $q = q'$  when  $\mu$  and  $q'$  are coprime. We emphasize that  $k_1$  is periodic in  $\frac{2\pi}{q}$ . However, we will now show that because the magnetic BZ is given by  $k_1 \in (-\pi, \pi), k_2 \in (0, 2\pi/q')$ ,  $k_2$  is periodic in  $\frac{2\pi}{q'}$  which is a finer periodicity, and implies a larger  $\frac{2\pi}{q}$  periodicity along  $k_2$  when iterated. We now construct the embedding matrix  $\bar{V}_2(\phi)$  that gives the  $\frac{2\pi}{q'}$  periodicity along  $k_2$ . This periodicity arises because we diagonalized the Hamiltonian in a  $1 \times q'$  magnetic unit cell and is gauge dependent.  $\bar{V}_2(\phi)$  satisfies

$$\mathcal{H}^\phi(\mathbf{k} + \frac{2\pi}{q'} \mathbf{b}_2) = [\bar{V}_2(\phi)] \mathcal{H}^\phi(\mathbf{k}) [\bar{V}_2(\phi)]^\dagger. \quad (\text{A61})$$

We follow the steps of Eq. (A44) and find

$$\begin{aligned} c_{k_1, k_2 + \frac{2\pi}{q'}, \ell, \alpha} &= \sum_{r_1 r_2} e^{i(\mathbf{k} + \mathbf{b}_2 \frac{2\pi}{q'}) \cdot (r_1 \mathbf{a}_1 + q' r_2 \mathbf{a}_2 + \ell \mathbf{a}_2 + \boldsymbol{\delta}_\alpha)} c_{r_1, r_2, \ell, \alpha} \\ &= \sum_{r_1 r_2} e^{i\mathbf{k} \cdot (r_1 \mathbf{a}_1 + q' r_2 \mathbf{a}_2 + \ell \mathbf{a}_2 + \boldsymbol{\delta}_\alpha)} e^{i \frac{2\pi}{q'} (q' r_2 + \ell + \mathbf{b}_2 \cdot \boldsymbol{\delta}_\alpha)} c_{r_1, r_2, \ell, \alpha} \\ &= [\bar{V}_2(\phi)]_{\ell, \alpha, \ell', \beta} c_{k_1, k_2, \ell', \beta}, \end{aligned} \quad (\text{A62})$$

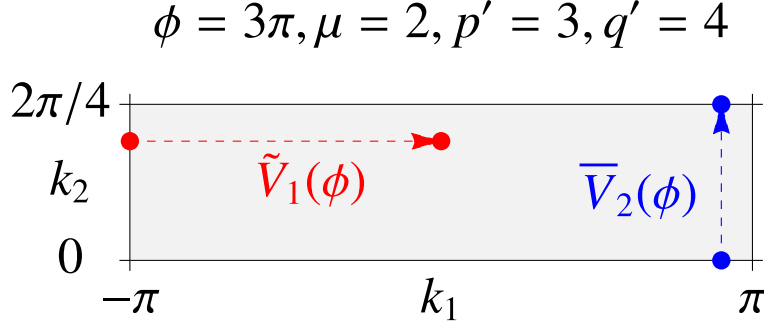


FIG. 7. We show the magnetic BZ at  $\phi = 2\frac{2\pi \times 3}{4} = 3\pi$  with  $\mu = 2$  and  $q' = 4$  not coprime, and  $p' = 3$ . There is a  $\pi$  periodicity along  $k_1$  implemented by  $\tilde{V}_1(\phi)$ , but a  $\pi/2 = 2\pi/q'$  periodicity along  $k_2$  implemented by  $\bar{V}_2(\phi)$  because the magnetic BZ is defined as  $k_1 \in (-\pi, \pi), k_2 \in (0, \pi/2)$ . The embedding matrices  $\tilde{V}_2(\phi) = [\bar{V}_2(\phi)]^2$  or  $V_2(\phi) = [\bar{V}_2(\phi)]^6$  implement periodicities that are larger than the domain of  $k_2$ .

with

$$[\bar{V}_2(\phi)]_{\ell, \alpha, \ell', \beta} = \delta_{\ell \ell'} e^{i\frac{2\pi}{q'} \ell} \delta_{\alpha \beta} e^{i\frac{2\pi}{q'} \delta_{\alpha} \cdot \mathbf{b}_2}. \quad (\text{A63})$$

We observe from Eqs. (A63) and (A45) that  $\bar{V}_2(\phi)^{\mu p'} = V_2(\phi)$ . The algebra with  $V_1(\phi)$  can be directly computed and reads

$$V_1(\phi) \bar{V}_2(\phi) = e^{i\frac{2\pi}{q'}} \bar{V}_2(\phi) V_1(\phi). \quad (\text{A64})$$

In App. C1, we will need the algebra of  $\bar{V}_2(\phi)$  with  $\tilde{V}_1(\phi)$  to study the Wilson loop in the magnetic BZ. Using Eq. (A64) and the definition of  $\tilde{V}_1(\phi)$  in Eq. (A59), we arrive at

$$\tilde{V}_1(\phi) \bar{V}_2(\phi) = e^{i\frac{2\pi}{q'} \zeta} \bar{V}_2(\phi) \tilde{V}_1(\phi). \quad (\text{A65})$$

We depict the magnetic BZ and embedding matrices for  $\phi = 2\frac{2\pi \times 3}{4} = 3\pi$ , with  $\mu = 2$  and  $p = 3, q' = 4$  in Fig. 7. Note that  $\mu$  and  $q'$  are not coprime, so the periodicities along  $k_1$  (which is  $\pi$ ) and  $k_2$  (which is  $\pi/2$ ) are not equal.

We now give a brief example illustrating the different embedding matrices. In App. A5, we discussed a model on the square lattice with 1a and 1b atoms (see Fig. 4) where  $\mu = 2$  for  $\mathbf{a}_1 = (1, 0), \mathbf{a}_2 = (0, 1)$ . In our Landau gauge defined by  $\mathbf{A}(\mathbf{r}) = -\phi \mathbf{b}_1(\mathbf{r} \cdot \mathbf{b}_2) = \phi(-y, 0)$ , the Hofstadter Hamiltonian could be formed by taking  $\phi = 2\frac{2\pi p'}{q'}$  for  $p'$  and  $q'$  coprime, and defining the magnetic BZ as  $k_1 \in (-\pi, \pi), k_2 \in (0, 2\pi/q')$ . The  $\tilde{V}_1(\phi)$  embedding matrix provides a  $2\pi/q$  periodicity in the energy spectrum along  $k_1$  and  $k_2$ , where  $\phi = \frac{2\pi p}{q}$ ,  $p$  and  $q$  coprime. Due to  $\bar{V}_2(\phi)$ , there is always a  $2\pi/q'$  periodicity along  $k_2$ . In this example, when  $q'$  and  $\mu = 2$  are not coprime (i.e.  $q'$  is even), we have  $\frac{2\pi}{q'} = \frac{2\pi}{2q}$ , and so  $k_2$  has twice a fine a periodicity as  $k_1$ . When  $q'$  and  $\mu = 2$  are coprime, both  $k_1$  and  $k_2$  have the same periodicity.

## Appendix B: Bounded Gaps in the Trivial Limit

In this Appendix, we prove that a Hamiltonian with a large enough on-site, per orbital, potential has a gapped Hofstadter Butterfly spectrum for any flux and hence is adiabatically connected to the atomic limit for all flux (App. B1). Such a property was mentioned in the derivation of the bulk gap closing of an insulator with nonzero Chern number in Sec. II of the main text. We exemplify this feature on the checkerboard lattice model in App. B2.

### 1. Gershgorin circles

We first consider the Hamiltonian at zero field. We add to the lattice model described by the hopping amplitudes  $t_{\alpha\beta}(\mathbf{r} - \mathbf{r}')$  an on-site, per-orbital potential

$$\mu_{\alpha} = (2\alpha - N_{orb} - 1)M \quad (\text{B1})$$

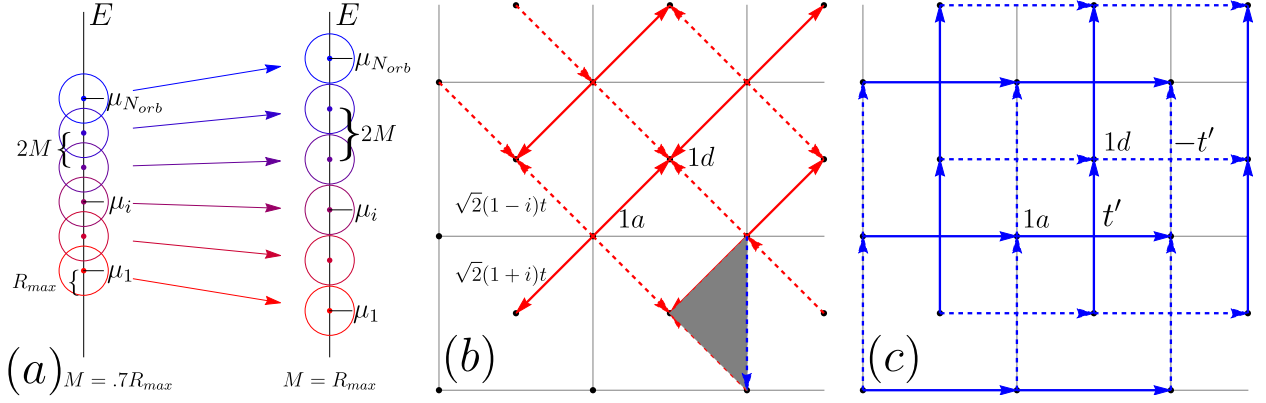


FIG. 8. (a) We illustrate the Gershgorin circles  $\mathcal{D}_\alpha$  with centers  $\mu_\alpha$  and radii  $R_\alpha \leq R_{max}$ . For clarity, we draw all the circles with radius  $R_{max}$ . The onsite potential (proportional to  $M$ ) sets the distance between the centers  $\mu_\alpha$  to be  $2M$ . By increasing  $M$  to  $M > R_{max}$ , we can make all Gershgorin circles disjoint. We depict the two hoppings of the checkerboard model (Eq. (B3)) in (b), which shows nearest-neighbor hoppings from the  $1a$  position to the  $1d$  position, and in (c), which shows next nearest-neighbor hoppings from  $1a$  to  $1a$  and  $1d$  to  $1d$ . In (b), we also provide an example of the minimal area ( $1/4$  of the unit cell) enclosed by Peierls paths as a grey triangle.

where  $\alpha = 1, \dots, N_{orb}$  labels the orbitals and  $M$  is the on-site amplitude. Let  $H$  be the matrix representation of the tight-binding hamiltonian in real space including both  $\mu_\alpha$  and the hopping amplitudes.  $H$  is a  $(N_{orb}\mathcal{N}) \times (N_{orb}\mathcal{N})$  hermitian matrix where  $\mathcal{N}$  is the number of unit cells. We want to focus on the eigenvalues of  $H$ . Thanks to the translation invariance, we can define  $N_{orb}$  Gershgorin circles  $\mathcal{D}_\alpha$  of center  $\mu_\alpha$  and radius  $R_\alpha$  with

$$R_\alpha = \sum_{\beta \neq \alpha} \sum_{\mathbf{r}} |t_{\alpha\beta}(\mathbf{r})|. \quad (\text{B2})$$

We assume that these series appearing in Eq. (B2) do converge, which is true for any system with only finite range hopping terms or exponentially decaying hoppings  $|t_{\alpha\beta}(\mathbf{r})| \sim \exp(-\kappa|\mathbf{r}|)$ ,  $\kappa > 0$ , as may arise in the case of flat Chern bands [28, 29]. From there we define  $R_{max} = \max\{R_\alpha; \alpha = 1, \dots, N_{orb}\}$ . The Gershgorin circle theorem states that any eigenvalue of  $H$  lies within at least one of the Gershgorin circles, and a union of  $m$  circles disjoint from all other circles must contain exactly  $m$  eigenvalues of  $H$ . For  $|M|$  large, i.e., in the atomic limit, we have exactly  $\mathcal{N}$  eigenvalues lying in each  $\mathcal{D}_\alpha$  circle, forming  $N_{orb}$  separated trivial bands. As long as  $|M| > R_{max}$ , we are guaranteed that all the  $\mathcal{D}_\alpha$  circles are disjoint and thus all bands are separated by a gap from above and below, as we sketch in Fig. 8a.

Turning on the magnetic field, the hopping terms acquire a phase  $t_{\alpha\beta}(\mathbf{r}-\mathbf{r}') \rightarrow t_{\alpha\beta}(\mathbf{r}-\mathbf{r}') \exp\left[i \int_{\mathbf{R}+\delta_\beta}^{\mathbf{R}+\delta_\alpha} \mathbf{A} \cdot d\mathbf{r}\right]$  from the Peierls substitution as discussed in App. A 1. Note that  $\mu_\alpha$  and  $R_\alpha$  are unchanged under this substitution and so are the  $\mathcal{D}_\alpha$  circles. This implies that for  $|M| > R_{max}$  and irrespective of the magnetic field, the Gershgorin circles remain disjoint and each band is gapped. As a consequence, if we start with  $N_{occ}$  occupied bands at  $\phi = 0$ , these bands will stay gapped for any  $\phi \neq 0$  if  $|M| > R_{max}$ . This is valid subject to the convergence of the sum in Eq. (B2). This is not in contradiction to Sec. II where we proved that a model with nonzero Chern number necessarily has a gap closing: for large enough  $|M|$ , i.e.  $|M| > R_{max}$ , the model cannot host nontrivial bands because it is adiabatically connected to an atomic limit. When  $M < R_{max}$ , a gap closing is not forbidden in the Hofstadter spectrum.

## 2. Hofstadter Hamiltonian on the Checkerboard Lattice

We consider a checkerboard lattice with  $s$  orbitals at the  $1a = (0, 0)$  and  $1d = (1/2, 1/2)$  positions [57, 58]. In the basis  $c_{\mathbf{R}}^\dagger = (c_{\mathbf{R},1a}^\dagger, c_{\mathbf{R},1d}^\dagger)$ , the Hamiltonian is given by

$$H^{\phi=0} = \sum_{\mathbf{R}} M c_{\mathbf{R}}^\dagger \sigma_z c_{\mathbf{R}} + t \sum_{\mathbf{R}} \sum_j c_{\mathbf{R}+\mathbf{d}_j}^\dagger (\sigma_1 \cos \theta + (-1)^j \sigma_2 \sin \theta) c_{\mathbf{R}} + t' \sum_{\mathbf{R}} c_{\mathbf{R}+\hat{x}}^\dagger \sigma_z c_{\mathbf{R}} - c_{\mathbf{R}+\hat{y}}^\dagger \sigma_z c_{\mathbf{R}} + h.c. \quad (\text{B3})$$

where  $\mathbf{d}_j$  are defined by  $\mathbf{d}_0 = 0$ ,  $\mathbf{d}_1 = -\hat{x}$ ,  $\mathbf{d}_2 = -\hat{x} - \hat{y}$ ,  $\mathbf{d}_3 = -\hat{y}$ . The hoppings  $t$  ( $t'$ ) represent nearest (next-nearest) neighbor hoppings as shown in Fig. 8b and Fig. 8c. Note that the parameter  $M$  matches the definition of the on-site



potential  $\mu_\alpha$  Eq. B1. We use the parameters  $t = 1, t' = 1/2, \theta = \pi/4$ . At  $\phi = 0$ , the model is topological with  $C = 1$  for  $|M| < 2$ , and for  $|M| > 2$ , the model is in a trivial atomic limit.

We introduce magnetic flux through the lattice in our Landau gauge  $\mathbf{A} = -\phi(y, 0)$  and take each Peierls integral along the straight-line paths between the endpoints. This is the conventional choice for  $s$  orbitals. Our choice for the Peierls paths allows minimal loops that enclose  $1/4$  of the unit cell, as depicted for instance in Fig. 8b as a grey triangle, so the periodicity of the Hofstadter spectrum is  $\Phi = 4 \times 2\pi$ . The Hofstadter Hamiltonian is given in position space by

$$H^\phi = \sum_{\mathbf{R}} M c_{\mathbf{R}}^\dagger \sigma_z c_{\mathbf{R}} + \sum_{\mathbf{R}} \sum_j c_{\mathbf{R}+\mathbf{d}_j}^\dagger \left[ \begin{pmatrix} 0 & t_j(\phi)^* \\ t_j(\phi) & 0 \end{pmatrix} \cos \theta + (-1)^j \begin{pmatrix} 0 & -it_j(\phi)^* \\ it_j(\phi) & 0 \end{pmatrix} \sin \theta \right] c_{\mathbf{R}} \\ + \sum_{\mathbf{R}} c_{\mathbf{R}+\hat{x}}^\dagger \begin{pmatrix} t'_{1,a}(\phi) & 0 \\ 0 & -t'_{1,d}(\phi) \end{pmatrix} c_{\mathbf{R}} - t' c_{\mathbf{R}+\hat{y}}^\dagger \sigma_z c_{\mathbf{R}} + h.c. \quad (\text{B4})$$

where the Peierls phases are given by

$$t_j(\phi) = t e^{i \int_{\mathbf{R}}^{\mathbf{R}+\mathbf{d}_j} \mathbf{A} \cdot d\mathbf{r}} = \{t e^{-i\frac{\phi}{8} - i\phi\frac{y}{2}}, t e^{i\frac{\phi}{8} + i\phi\frac{y}{2}}, t e^{-i\frac{\phi}{8} + i\phi\frac{y}{2}}, t e^{i\frac{\phi}{8} - i\phi\frac{y}{2}}\}_j, \\ t'_{1,a}(\phi) = t' e^{i \int_{\mathbf{R}}^{\mathbf{R}+\hat{x}} \mathbf{A} \cdot d\mathbf{r}} = t' e^{-i\phi y}, \quad t'_{1,d}(\phi) = t' e^{i \int_{\mathbf{R}+\frac{1}{2}(\hat{x}+\hat{y})}^{\mathbf{R}+\frac{1}{2}(3\hat{x}+\hat{y})} \mathbf{A} \cdot d\mathbf{r}} = t' e^{-i\phi(y+1/2)}, \\ t'_{2,a}(\phi) = t' e^{i \int_{\mathbf{R}}^{\mathbf{R}+\hat{y}} \mathbf{A} \cdot d\mathbf{r}} = t', \quad t'_{2,d}(\phi) = t' e^{i \int_{\mathbf{R}}^{\mathbf{R}+\hat{y}} \mathbf{A} \cdot d\mathbf{r}} = t' \quad (\text{B5})$$

Using Eq. (A28), we calculate  $\mu = \text{lcd} \{\mathbf{b}_1 \cdot (\boldsymbol{\delta}_\beta - \boldsymbol{\delta}_\alpha)\} = \text{lcd} \{1, 1/2\} = 2$  because there are orbitals at  $1a = (0, 0)$  and  $1a = (1/2, 1/2)$  connected by a hopping. Indeed, from the Peierls phases themselves, we see that setting  $\phi = 2\frac{2\pi p'}{q'}$  gives a  $1 \times q'$  unit cell, meaning the phases Eq. (B5) are invariant under  $y \rightarrow y + q'$ .

We define the Hermitian matrices

$$\Sigma_j(k_x, k_y) = \left[ \begin{pmatrix} 0 & t_j(\phi)^* e^{i\mathbf{k} \cdot (\boldsymbol{\delta} + \mathbf{d}_j)} \\ t_j(\phi) e^{-i\mathbf{k} \cdot (\boldsymbol{\delta} + \mathbf{d}_j)} & 0 \end{pmatrix} \cos \theta + (-1)^j \begin{pmatrix} 0 & -it_j(\phi)^* e^{i\mathbf{k} \cdot (\boldsymbol{\delta} + \mathbf{d}_j)} \\ it_j(\phi) e^{-i\mathbf{k} \cdot (\boldsymbol{\delta} + \mathbf{d}_j)} & 0 \end{pmatrix} \sin \theta \right] \\ = \begin{pmatrix} 0 & e^{-i(-1)^j \theta} t_j(\phi)^* e^{i\mathbf{k} \cdot (\boldsymbol{\delta} + \mathbf{d}_j)} \\ e^{i(-1)^j \theta} t_j(\phi) e^{-i\mathbf{k} \cdot (\boldsymbol{\delta} + \mathbf{d}_j)} & 0 \end{pmatrix} \quad (\text{B6})$$

where the location of the  $1d$  Wyckoff position is  $\boldsymbol{\delta} = (1/2, 1/2)$ . We Fourier transform over the magnetic unit cell at  $\phi = 2\frac{2\pi p'}{q'}$  to find

$$\mathcal{H}_{y,y'}^\phi = \delta_{y,y'} h_y + \delta_{y,y'+1} T_y + \delta_{y+1,y'} T_{y'}^\dagger \\ h_y = M \sigma_z + \Sigma_0(k_x, k_y) + \Sigma_1(k_x, k_y) + 2t' \begin{pmatrix} \cos(k_x + \phi y) & 0 \\ 0 & -\cos(k_x + \phi y + \phi/2) \end{pmatrix} \\ T_{y+1} = \begin{pmatrix} 0 & e^{-i\theta} t_2(\phi)^* e^{i\mathbf{k} \cdot (\boldsymbol{\delta} + \mathbf{d}_2)} + e^{i\theta} t_3(\phi)^* e^{i\mathbf{k} \cdot (\boldsymbol{\delta} + \mathbf{d}_3)} \\ 0 & 0 \end{pmatrix} - t' \sigma_z e^{-ik_y} \quad (\text{B7})$$

where  $y = 0, \dots, q' - 1$  at  $\phi = 2\frac{2\pi p'}{q'}$ .

We numerically diagonalize this Hofstadter Hamiltonian Eq. (B7) to compute the Hofstadter Butterfly at  $M = 2.4$  in Fig. 9. The two Gershgorin circles for the checkerboard lattice model are defined by the two centers  $\mu_{1a} = |M|$  and  $\mu_{1d} = -|M|$ , and the Gershgorin radius  $R_{max} = R_{1a} = R_{1d} = 4(|t| + |t'|)$  (each site being connected to four nearest neighbors and four next nearest neighbors). For the parameters used in Fig. 9, we get  $R_{max} = 6$ . For any  $|M| > 6$ , we are guaranteed that the system at half filling will have a gap irrespective of  $\phi$ . Note that this value is *only* an upper bound of the minimal  $|M|$  value where this gap can appear. As already mentioned previously, the transition from a  $C = 1$  topological band to a trivial band occurs at  $|M| = 2$ , and for  $M > 2$  the Hofstadter Butterfly is gapped everywhere. We show an example of the Hofstadter Butterfly in this phase in Fig. 9. It is hence expected that further analysis can produce tighter bounds.

### Appendix C: Wilson Loops

In this Appendix, we define the Wilson loop at nonzero flux and determine the constraints on its eigenvalues, the Wannier centers of the magnetic unit cell, due to the magnetic translation group (App. C1). In App. C2, we provide

$$H_{Ch}, M = 2.4$$

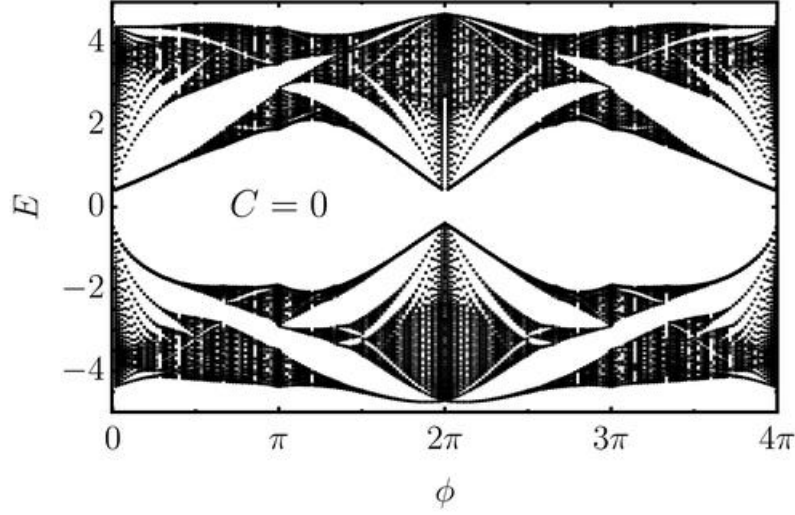


FIG. 9. We show the the Hofstadter Butterflies for  $H_{ch}$  (Eq. (B3)) at  $M = 2.4$  in the trivial phase. Because  $H_{ch}^{\phi=0}$  is trivial, the Hofstadter spectrum may be gapped everywhere.

an alternative proof of the major claim in Sec. II, that  $C^{\phi=\frac{2\pi p}{q}} \in q\mathbb{Z}$ , which leads to a proof of gap closing in the bulk of the Hofstadter Butterfly when the  $\phi = 0$  model has a nonzero Chern number. We also discuss in depth the behavior of the occupied bands as the flux is pumped. In App. C 3, we show that a Mirror Chern number also enforces a gap closing. We provide an alternative proof of the gap closing for a nonzero Chern number using only inversion eigenvalues (App. C 4).

### 1. Definition of the Wilson Loop at Nonzero Flux

The Wilson loop at  $\phi = 0$  is calculated from the eigenvectors of  $\mathcal{H}^0(\mathbf{k})$ . Denote the  $j$ th eigenvector as  $|u_j(\mathbf{k})\rangle$ , which is a vector with  $N_{orb}$  components corresponding to the  $j$ th eigenvalue  $\epsilon_j(\mathbf{k})$ . (Note that this is a slight abuse of the ket notation, which usually specifies a state in the Hilbert space, as opposed to merely a vector in  $\mathbb{R}^{N_{orb}}$ .) We denote the  $i$ th element of the  $j$ th (ordered by energy) eigenvector by  $|u_j(\mathbf{k})\rangle_i$ ,  $i = 1, \dots, N_{orb}$ . When the bulk spectrum is gapped, we may consider only the  $N_{occ} < N_{orb}$  occupied bands which determine the topology of the Hamiltonian at a given filling  $\nu = N_{occ}/N_{orb}$ . For brevity, we write  $[U_{\mathbf{k}}]_{ij} = |u_j(\mathbf{k})\rangle_i$  as the matrix of occupied eigenvectors. (Here we assume the bulk spectrum is gapped so the occupied spectrum is well-defined.) Then the Wilson loop is defined by

$$W^{\phi=0}(k_1) = U_{(k_1, 2\pi)}^\dagger \left[ \prod_{k_2}^{2\pi \leftarrow 0} \mathcal{P}_{(k_1, k_2)} \right] U_{(k_1, 0)}, \quad \mathcal{P}_{(k_1, k_2)} = U_{(k_1, k_2)} U_{(k_1, k_2)}^\dagger \quad (C1)$$

where the ordered product is understood to be discretized:  $\prod_{k_2}^{2\pi \leftarrow 0} \mathcal{P}_{(k_1, k_2)} \equiv \lim_{\epsilon \rightarrow 0} \mathcal{P}_{(k_1, 2\pi)} \mathcal{P}_{(k_1, 2\pi - \epsilon)} \dots \mathcal{P}_{(k_1, 0)}$ . It is convenient to fix the  $U(1)$  gauge symmetry of the eigenvalues by requiring  $U_{(k_1, 2\pi)} = \mathcal{V}_2 U_{(k_1, 0)}$ .

When we add flux to the model in our Landau gauge, the magnetic BZ can be chosen to be  $k_1 \in (-\pi, \pi)$ ,  $k_2 \in (0, \frac{2\pi}{q'})$  as discussed in App. A 7. To define the Wilson loop along the  $k_2$  direction of the BZ at  $\phi = \frac{2\pi p}{q}$ , we assume there is a set of  $N_{occ}^\phi$  occupied bands which are gapped from the higher energy bands whose eigenvectors form the matrix  $[U_{\mathbf{k}}^\phi]_{ij} = |u_j^\phi(\mathbf{k})\rangle_i$ . Then we may calculate the Wilson loop according to

$$W_{(k_1, \frac{2\pi}{q'}) \leftarrow (k_1, 0)} \equiv W^{\phi=\frac{2\pi p}{q}}(k_1) = [U_{(k_1, \frac{2\pi}{q'})}^\phi]^\dagger \left[ \prod_{k_2}^{\frac{2\pi}{q'} \leftarrow 0} \mathcal{P}_{(k_1, k_2)}^\phi \right] U_{(k_1, 0)}^\phi \quad (C2)$$

We have chosen to take the Wilson loop along the  $k_2$  direction so the Wilson loop eigenvalues correspond to positions along the extended  $\mathbf{a}_2$  direction of the magnetic unit cell [47]. We will usually be interested in the Wilson loop at the

fixed filling  $\nu = N_{occ}/N_{orb}$  of the zero-field Hamiltonian. In this case at filling  $\nu$ ,  $N_{occ}^{\phi=\mu\frac{2\pi p'}{q'}} = q'N_{occ}$  because there are  $q'N_{orb}$  bands in  $H^\phi$  due to the magnetic unit cell being  $1 \times q'$ . (Of course, it is possible for gaps to exist at other fillings in the Hofstadter Hamiltonian at a given flux.) As in the zero-field case, it is convenient to fix the gauge by requiring

$$U_{(k_1, \frac{2\pi}{q'})}^\phi = \bar{V}_2(\phi)U_{(k_1, 0)}^\phi \quad (\text{C3})$$

with the embedding matrix  $\bar{V}_2(\phi)$  providing the  $2\pi/q'$  periodicity in  $k_2$  (see Eq. (A62)).

We study the effect of the magnetic translation group on the Wilson loop following the presentation of Ref. [46] (App. VII D) which develops constraints on the Wilson loop for tight-binding models with the general symmetry

$$g_{\mathbf{k}}\mathcal{H}(\mathbf{k})g_{\mathbf{k}}^\dagger = \mathcal{H}(D_g\mathbf{k}) \quad (\text{C4})$$

where  $D_g$  is an operator acting on the momentum vector. In the Hofstadter Hamiltonian, the magnetic translation group requires  $\tilde{V}_1(\phi)\mathcal{H}^\phi(\mathbf{k})\tilde{V}_1^\dagger(\phi) = \mathcal{H}^\phi(\mathbf{k} + \frac{2\pi}{q}\mathbf{b}_i)$  where  $\phi = \frac{2\pi p}{q}$ ,  $p, q$  coprime (see Eq. (A59)). This allows us to form a sewing matrix between the occupied bands at  $\mathbf{k}$  and  $\mathbf{k} + \frac{2\pi}{q}\mathbf{b}_1$  defined by

$$B_{\mathbf{k}}^{ij} = \langle u_i^\phi(\mathbf{k} + \frac{2\pi}{q}\mathbf{b}_1) | \tilde{V}_1(\phi) | u_j^\phi(\mathbf{k}) \rangle, \quad i, j = 1, \dots, q'N_{occ}. \quad (\text{C5})$$

This matrix is unitary as long as there is a gap above the occupied bands [47] (if there is a gap at  $k_1$ , there is also a gap at  $k_1 + \frac{2\pi}{q}$ ). Ref. [46] demonstrates that the sewing matrix also obeys

$$|u_j^\phi(\mathbf{k})\rangle = \sum_i \tilde{V}_1^\dagger(\phi) |u_i^\phi(\mathbf{k} + \frac{2\pi}{q}\mathbf{b}_1)\rangle B_{\mathbf{k}}^{ij}. \quad (\text{C6})$$

This prepares us to calculate a small segment of a Wilson line. We find

$$\begin{aligned} [W_{\mathbf{k}'_1 \leftarrow \mathbf{k}_1}^\phi]^{ij} &= \langle u_i^\phi(\mathbf{k}'_1) | u_j^\phi(\mathbf{k}_1) \rangle \\ &= \sum_{rs} B_{\mathbf{k}_2}^{\dagger ir} \langle u_r^\phi(\mathbf{k}'_1 + \frac{2\pi}{q}\mathbf{b}_1) | V_1(\phi)V_1(\phi)^\dagger | u_s^\phi(\mathbf{k}_1 + \frac{2\pi}{q}\mathbf{b}_1) B_{\mathbf{k}_1}^{sj} \rangle \\ &= \sum_{rs} B_{\mathbf{k}_2}^{\dagger ir} [W_{\mathbf{k}'_1 + \frac{2\pi}{q}\mathbf{b}_1 \leftarrow \mathbf{k}_1 + \frac{2\pi}{q}\mathbf{b}_1}^\phi]^{rs} B_{\mathbf{k}_1}^{sj}. \end{aligned} \quad (\text{C7})$$

We are interested in the Wilson loops  $W^\phi(k_1) = W_{(k_1, \frac{2\pi}{q'}) \leftarrow (k_1, 0)}^\phi$ . Piecing together the single Wilson line transformations, we find

$$B_{(k_1, \frac{2\pi}{q'})} W^\phi(k_1) B_{(k_1, 0)}^\dagger = W^\phi(k_1 + \frac{2\pi}{q}). \quad (\text{C8})$$

Now we must relate  $B_{(k_1, \frac{2\pi}{q'})}$  to  $B_{(k_1, 0)}$  to establish a unitary relation between the Wilson loops at  $k_1$  and  $k_1 + \frac{2\pi}{q}$ . By Eq. (A62),  $|u_j^\phi(k_1, \frac{2\pi}{q'})\rangle = \bar{V}_2(\phi) |u_j^\phi(k_1, 0)\rangle$ , so returning to Eq. (C5), we obtain

$$\begin{aligned} B_{(k_1, \frac{2\pi}{q'})}^{ij} &= \langle u_i^\phi(k_1 + \frac{2\pi}{q}, \frac{2\pi}{q'}) | \tilde{V}_1(\phi) | u_j^\phi(k_1, \frac{2\pi}{q'}) \rangle \\ &= \langle u_i^\phi(k_1 + \frac{2\pi}{q}, 0) | \bar{V}_2^\dagger(\phi) \tilde{V}_1(\phi) \bar{V}_2(\phi) | u_j^\phi(k_1, 0) \rangle \end{aligned} \quad (\text{C9})$$

We simplify the product  $\bar{V}_2^\dagger(\phi)\tilde{V}_1(\phi)\bar{V}_2(\phi)$  using the algebra in Eq. (A65). We find

$$\begin{aligned} B_{(k_1, \frac{2\pi}{q'})}^{ij} &= \langle u_i(k_1 + \frac{2\pi}{q}, 0) | \bar{V}_2^\dagger(\phi) e^{i\zeta\frac{2\pi}{q'}} \bar{V}_2(\phi) \tilde{V}_1(\phi) | u_j(k_1, 0) \rangle \\ &= e^{i\zeta\frac{2\pi}{q'}} B_{(k_1, 0)}^{ij}, \end{aligned} \quad (\text{C10})$$

relating the sewing matrix  $B$  at  $k_2 = 0$  and  $k_2 = 2\pi/q'$ . We remind the reader that  $\zeta \in \mathbb{Z}$  satisfies  $\zeta\phi = 2\pi/q \pmod{2\pi}$ . Plugging in this result to Eq. (C8), we establish

$$W^\phi(k_1 + \frac{2\pi}{q}) = e^{i\frac{2\pi}{q'}\zeta} B_{(k_1, 0)}^\dagger W^\phi(k_1) B_{(k_1, 0)} \quad (\text{C11})$$

and hence the eigenvalues  $e^{i\vartheta_j(k_1)}$  of the Wilson loop, also called the Wannier centers [47], must satisfy

$$\{\vartheta_j(k_1 + \frac{2\pi}{q})\} = \{\vartheta_j(k_1) + \frac{2\pi}{q'}\zeta\}. \quad (\text{C12})$$

This feature of Wilson spectrum can be used to prove topological properties of the Hamiltonian. Below, we show how these results allow an alternative proof of gap closing in a Chern insulator.

## 2. Wilson Loop Proof of Gap Closing in a Chern Insulator

The winding of the determinant of the Wilson loop is equal to the Chern number, and we may leverage this fact to constrain  $C^\phi$  at the filling of  $H^{\phi=0}$ ,  $\nu = N_{occ}/N_{orb}$ , with the results of App. C1. Let us again define  $q$  as the denominator of  $\phi$ , i.e.  $\phi = \mu \frac{2\pi p'}{q} = \frac{2\pi p}{q}$ . Then assuming a gap exists so that the Wilson loop is well-defined, we establish that

$$\begin{aligned} \det \left[ W^\phi(k_1 + \frac{2\pi}{q}) \right] &= \prod_{j=1}^{q' N_{occ}} e^{i\vartheta_j(k_1 + \frac{2\pi}{q})} \\ &= \exp \left( i \sum_{j=1}^{q' N_{occ}} \left( \vartheta_j(k_1) + \zeta \frac{2\pi}{q'} \right) \right) \\ &= \exp \left( i \sum_{j=1}^{q' N_{occ}} \vartheta_j(k_1) + 2\pi i \zeta N_{occ} \right) \\ &= \prod_{j=1}^{q' N_{occ}} e^{i\vartheta_j(k_1)} \\ &= \det[W^\phi(k_1)] \end{aligned} \quad (\text{C13})$$

using Eq. (C12). We see that the determinant is periodic in  $k_1$  with period  $\frac{2\pi}{q}$  and consequently must wind a multiple of  $q$  times across the magnetic BZ. This proves  $C^{\phi=\frac{2\pi p}{q}} \in q\mathbb{Z}$  at the filling  $\nu = N_{occ}/N_{orb}$ . If we were to consider another filling where  $H^\phi$  is gapped, we see from the above calculation that the determinant would not necessarily be  $\frac{2\pi}{q}$  periodic, and the Chern number is not required to be quantized in multiples of  $q$ .

We now discuss in more detail what it means for  $H^{\phi=0}$  to be an insulator with a gap at filling  $\nu$ , and yet have a gap closing at  $\phi \rightarrow 0$  enforced by a nonzero Chern number at filling  $\nu$ . This apparent discrepancy is due to the discontinuity in the energy spectrum at a fixed filling of  $H^\phi$ . While the entire spectrum evolves continuously in  $\phi$ , there is no guarantee that the spectrum at a given filling is continuous in  $\phi$ . This is because the filling is determined by the number of bands, and as we have seen in App. A7, the number of bands of  $H^{\phi=\mu \frac{2\pi p'}{q}}$  depends on  $q'$  and thus is discontinuous everywhere.

To illustrate this, we show examples of Hofstadter Butterflies in Fig. 10 calculated from the Hamiltonian  $H_{ch}$  (Eq. (B3)). The phases of  $H_{ch}^{\phi=0}$  are controlled by a single parameter  $M$ . When  $|M| < 2$ ,  $H_{ch}^{\phi=0}$  has a Chern number  $C^{\phi=0} = 1$  at half filling, and when  $|M| > 2$ , the Hamiltonian is trivial. In addition to the bulk spectrum, we color the maximum (minimum) of the valence (conduction) bands red in order to show that a branch of the conduction bands connects to the valence bands as  $\phi$  approaches zero. Thus, the conduction spectrum is discontinuous at  $\phi = 0$ , although the valence spectrum is continuous. A gapped Hamiltonian  $H^{\phi_1}$  with nonzero Chern number at filling  $\nu$  cannot be adiabatically connected to another gapped Hamiltonian  $H^{\phi_2}$  at filling  $\nu$  in the Hofstadter Butterfly as we argued in Sec. II. We note that  $C^{\phi=\frac{2\pi p}{q}} = 0$  is the only number satisfying  $C^\phi \in q\mathbb{Z}$  for all  $\phi$ , and hence a gap which exists at filling  $\nu$  for a range of  $\phi$  can only have  $C^\phi = 0$ . This is illustrated in Fig. 10. It appears there that there are continuously connected gaps with  $C^\phi = 1$ . However, these gaps are not at the same filling, and hence can be connected without a gap closing. For instance in Fig. 10c, the  $C = 1$  gap occurs at filling  $5/8$  at  $\phi = \pi/2$  and filling  $3/4$  at  $\phi = \pi$ , which are in accordance with the Streda formula  $\nu = C \frac{\phi}{4\pi} + \nu_0$  where  $\nu_0 = 1/2$  is the filling of the gap at  $\phi = 0$ .

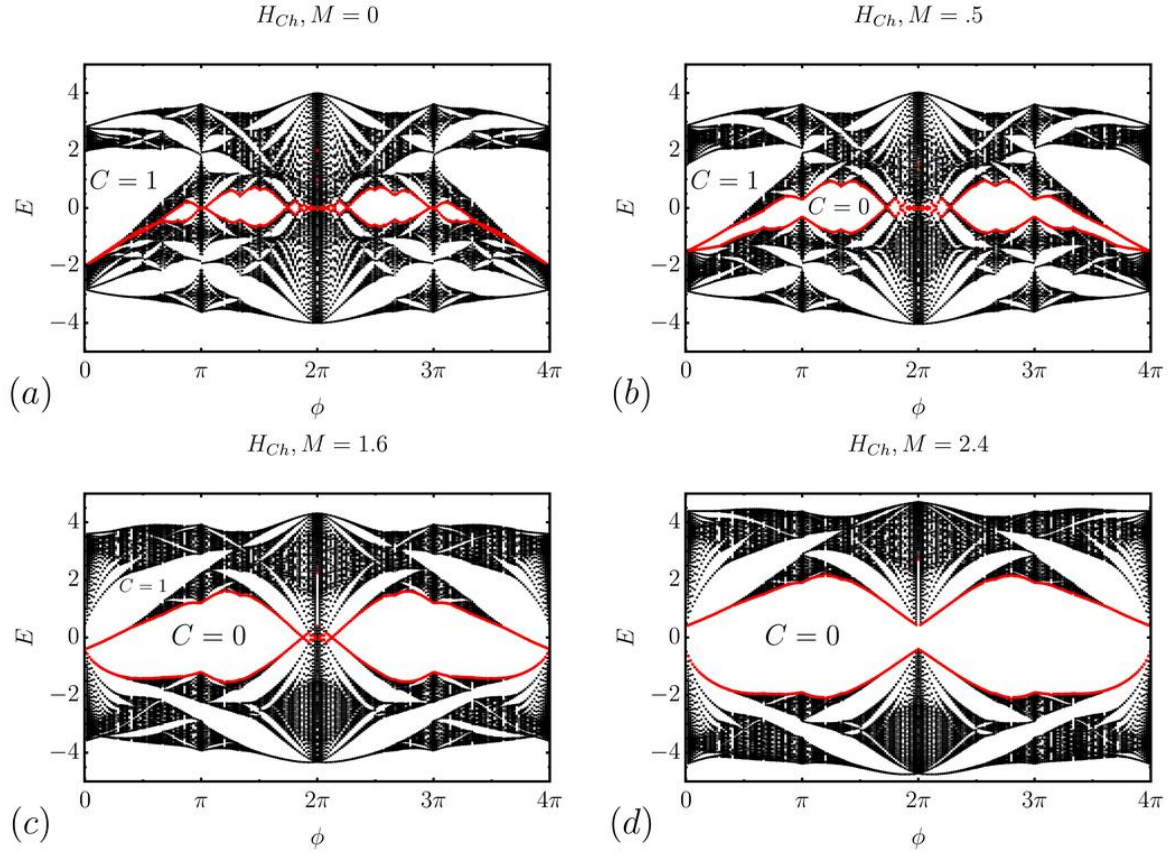


FIG. 10. We show the Hofstadter Butterflies for  $H_{ch}$  (Eq. (B3)) for (a) the topological phase,  $M = 0$ , (b) the topological phase,  $M = .5$ , (c) the topological phase,  $M = 1.6$ , (d) the trivial phase,  $M = 2.4$ . We indicate the highest occupied state at half filling and the lowest unoccupied state in red, so the half filling gap occurs between the red lines. In (a), (b), (c), we see that the occupied spectrum at half filling *does* connect smoothly to the occupied spectrum at  $\phi = 0$ , but the unoccupied spectrum is *discontinuous* at  $\phi = 0$ . In particular, there are conduction bands (those above filling  $\nu$ ) that connect to the valence bands (those at or below filling  $\nu$ ) as  $\phi$  approaches 0 despite the zero-field Hamiltonian being a gapped insulator at half filling. We have proven that this is required by the nonzero Chern number of the zero-field Hamiltonian. In (a) where  $M = 0$ , we see an extreme case where the half-filling gap closes, as it must, at  $\phi$  but remains extremely small up until  $\phi \sim \frac{3\pi}{4}$ . (b) The Hofstadter Butterfly is visibly gapped at half-filling for  $0 < \phi < \pi$ , and the gap closing at  $\phi = 0^+$  is clearer. This is even more exaggerated in (c), closer to the  $\phi = 0$  phase transition which happens at  $M = 2$ . Between (c) and (d), the  $\phi = 0$  gap closes, and  $H^0$  undergoes a transition from a topological insulator to a trivial insulator. In the Hofstadter Butterfly, this transition manifests itself as the conduction branch detaching from the valence branch at  $\phi = 0^+$  at the  $M = 2$  phase transition and reconnecting with the conduction branch. In the trivial phase, the half filling gap remains open at all  $\phi$ .

### 3. Discussion of Gap Closing due to a Nonzero Mirror Chern Number

We now consider the generalization of this theorem to deduce a gap closing in the bulk spectrum of the Hofstadter Butterfly with a nonzero mirror Chern number at  $\phi = 0$ . However, unlike the case of a true Chern number, a mirror Chern number does *not* cause the gap to close immediately at  $\phi = 0$ , as we see in Fig. 1b of the Main Text.

The proof for the bulk gap closing at finite  $\phi$  in a model with nonzero mirror Chern number reduces to the Chern number case because the Hamiltonian may be block-diagonalized using the mirror eigenvalues  $\pm i$ . Additionally, the Hofstadter Hamiltonian may still be block-diagonalized by the mirror symmetry  $M_z$ . Being the product of inversion and a two-fold rotation,  $M_z$  is not broken by flux. We assume the total Chern number is zero, or else there would be a gap closing at  $\phi = 0^+$ . Then the mirror Chern number is defined by

$$C_{M_z} = \frac{C_{m=+i} - C_{m=-i}}{2} \quad (\text{C14})$$

where  $C_{m=\pm i}$  is the Chern number calculated over the occupied bands with mirror eigenvalue  $m = \pm i$ . The total Chern number is  $C = C_{m=+i} + C_{m=-i}$  which we assume to be zero (otherwise, we would have a gap closing as  $\phi \rightarrow 0$ ),

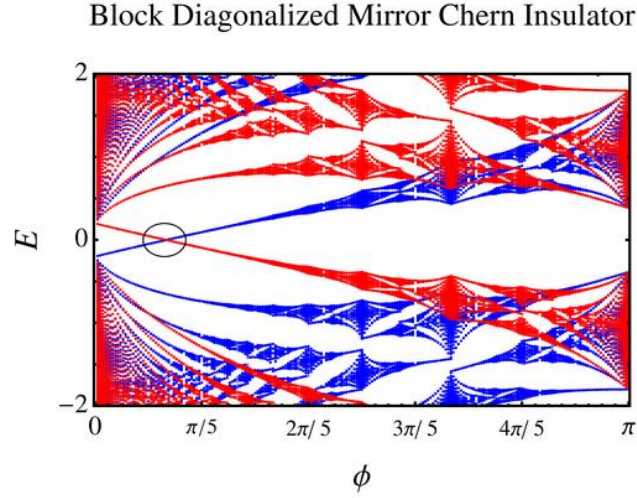


FIG. 11. We show a schematic spectrum of a mirror Chern insulator where each state is colored by its mirror eigenvalue,  $+i$  (resp.  $-i$ ) for red (resp. blue). If we consider the red and blue models individually, each has a nonzero and opposite Chern number. Thus the total Chern number of the full Hamiltonian is zero, but there is a nonzero mirror Chern number. The full Hamiltonian, i.e. the red and blue bands, has a gap closing (circled) at  $\nu = 1/2$  that occurs at a finite value of the flux where the branches of opposite mirror eigenvalues intersect. The intersection cannot be gapped out by any mirror-preserving perturbation.

so a nonzero value of  $C_{M_z}$  means  $C_{m=\pm i}$  must be nonzero. Thus both mirror eigenvalue blocks have opposite and nonzero Chern numbers. Considering each block individually at their own fillings, we use the standard Chern number result of Sec. II to show that a band in each must traverse their individual gaps. Considering the full model, the intersection of the Landau levels of different mirror eigenvalues closes the bulk gap at the  $\phi = 0$  filling of the whole model.

#### 4. Alternative Proof of Gap Closing Using Inversion Eigenvalues

We proved in Sec. II of the Main Text and independently in App. C2 that a Hamiltonian with a nonzero Chern number had a gap closing at the Fermi level. Here, we show that a weaker version of this statement may be proven with knowledge of only inversion (or  $C_{2z}$ ) eigenvalues. We prove now that an insulator with inversion symmetry and odd Chern number must also have a gap closing.

We will calculate the inversion eigenvalues of  $\mathcal{H}^\phi(\mathbf{k})$  at  $\phi = 0$  and  $\phi = \pi$ . We are able to do so because inversion is not broken by a magnetic field, i.e.

$$\mathcal{I}\mathcal{H}^\phi(\mathbf{k})\mathcal{I} = \mathcal{H}^\phi(-\mathbf{k}), \quad \mathcal{I}^2 = 1, \quad (\text{C15})$$

By assumption, the Chern number  $C^{\phi=0}$  (at filling  $\nu$ ) at  $\phi = 0$  is odd, and can be diagnosed by an odd number of  $-1$  inversion eigenvalues [59]. Hence to show a gap closing, we need only show that the Chern number at  $\phi = \pi$  is even (at the same filling  $\nu$ ), since a gap closing must occur between phases with differing Chern number under adiabatic evolution.

In the magnetic BZ at  $\phi = \pi$ , we consider the inversion invariant points  $\mathbf{k}^* = (k_1^*, k_2^*) = (0, 0), (0, \frac{\pi}{2}), (\pi, 0), (\pi, \frac{\pi}{2})$  which obey  $k_1^* = -k_1^* \bmod 2\pi$  and  $k_2^* = -k_2^* \bmod \pi$ . Now we study the eigenstates of  $H^{\phi=\pi}$  at these points. If  $\mathcal{I}|\mathbf{k}^*\rangle = \xi|\mathbf{k}^*\rangle$ , then

$$\mathcal{I}T_2(\pi)|\mathbf{k}^*\rangle = \xi T_2^\dagger(\pi)|\mathbf{k}^*\rangle = \xi T_2(\pi)T_2^\dagger(\pi)^2|\mathbf{k}^*\rangle = \xi e^{-2ik_2}T_2(\pi)|\mathbf{k}^*\rangle \quad (\text{C16})$$

where we have used that the magnetic translation operators satisfy  $\mathcal{I}T_i(\phi)\mathcal{I} = T_i(\phi)^\dagger$  which follows directly from Eq. (3). Recalling that  $T_2(\phi)|\mathbf{k}^*\rangle$  has momentum  $\mathbf{k}^* - \phi\mathbf{b}_1 = \mathbf{k}^* - \pi\mathbf{b}_1$ , we see that if there are  $n_1$  negative inversion eigenvalues at the points  $(0, 0)$ , then there are also  $n_1$  negative inversion eigenvalues at  $(\pi, 0)$ . Similarly, if there are  $n_2$  negative inversion eigenvalues at  $(0, \frac{\pi}{2})$ , then there are  $n_2$  positive ones at  $(\pi, \frac{\pi}{2})$ . Since there are  $2N_{occ}$  bands in the doubled magnetic unit cell at  $\phi = \pi$ , we find the total number of negative inversion eigenvalues to be  $2n_1 + n_2 + (2N_{occ} - n_2)$  which is even, so the Chern number must be even (zero included) [59]. Because the  $C^{\phi=0}$  is assumed odd, there must be a gap closing between  $\phi = 0$  and  $\phi = \pi$ .

## Appendix D: Hofstadter Topology Protected by Time Reversal symmetry

In this Appendix, we study the Hofstadter 3D TI phase in generality. First we determine the properties of  $UT$ , the effective time-reversal symmetry at  $\phi = \Phi/2$  (App. D 1). We then give two proofs showing that the  $\mathbb{Z}_2$  index protected by  $UT$  at  $\phi = \Phi/2$  is trivial: one in the magnetic BZ (App. D 2) and the other using the Wilson loop (App. D 3). These proofs are facilitated by a gauge-invariant formalism, introduced in App. D 2 b, which makes use of the magnetic translation group to construct the Hofstadter Hamiltonian. From this construction, we also find that  $UT$  symmetry at  $\phi = \Phi/2$  yields a projective representation of the magnetic space group.

### 1. Properties of $UT$

First, we discuss time-reversal symmetry (TRS) for the Hofstadter Hamiltonian with a  $\phi \rightarrow \phi + \Phi$  periodicity in the flux. If the  $\phi = 0$  model is  $\mathcal{T}$ -symmetric then the model at  $\phi = \Phi/2$  is  $UT$ -symmetric. This is because

$$UTH^{\Phi/2}(UT)^\dagger = UH^{-\Phi/2}U^\dagger = H^{\Phi/2}, \quad (\text{D1})$$

where  $U$  is given by Eq. (A5). We now define the anti-unitary operator  $\mathcal{T}$  in position space as

$$\mathcal{T}^{-1}c_{\mathbf{R},\alpha}\mathcal{T} = \sum_{\beta'} D_{\alpha\beta}(\mathcal{T})c_{\mathbf{R},\beta} \quad (\text{D2})$$

where the unitary matrix  $D_{\alpha\beta}(\mathcal{T})$  is only nonzero when  $\delta_\alpha = \delta_\beta$  (and  $\alpha$  and  $\beta$  are spin-flipped Kramers' pairs), i.e.  $\mathcal{T}$  is local, onsite.  $DD^* = \pm 1$  for spinful/spin-less electrons ( $\mathcal{T}^2 = \pm 1$ ). The action of  $\mathcal{T}$  flips the flux, taking  $\phi \rightarrow -\phi$  and hence

$$\mathcal{T}U\mathcal{T}^{-1} = U^\dagger \quad (\text{D3})$$

as may be verified using the position space representations of the operators. From here we conclude  $(UT)^2 = U\mathcal{T}U\mathcal{T} = UU^\dagger\mathcal{T}^2 = \mathcal{T}^2$ . This result holds for  $\Phi = 2\pi n$ ,  $n$  even or odd. Because we study insulators with a nontrivial Kane-Mele invariant, we have  $\mathcal{T}^2 = -1$ . We recall that  $UH^\phi U^\dagger = H^{\phi+\Phi}$  and thus  $UT$  also protects a topological classification at  $H^{\phi=\Phi/2}$  as per Eq. (6).

### 2. Gauge-Invariant Proof of the 3D TI phase

In the prior sections, we have worked explicitly in the Landau gauge which enables us do explicit, numerical computations such as computing the energy spectrum or the Wilson loop. In this section, we will prove the triviality of the Kane-Mele  $\mathbb{Z}_2$  index  $\delta^{\phi=\Phi/2}$ , and do not need to perform explicit computations. Hence we can avoid the cumbersome degeneracies caused by the extended  $1 \times q'$  magnetic unit cell (see App. A) by introducing a new formalism which makes use of the magnetic translation operators to study the Hofstadter Hamiltonian in the  $1 \times q$  without specifying a gauge. First in App. D 2 a, we will construct the Hofstadter Hamiltonian in this magnetic unit cell in a gauge-invariant manner to facilitate a simple proof that  $\delta^{\phi=\Phi/2} = +1$ , with the details of the calculations left to App. D 2 b.

#### a. Proof of the Trivial Kane-Mele Index due to Gap Closings at the Phase Transition

Recall from Sec. I that we may choose a simultaneous eigenbasis of  $T_1(\phi), T_2^q(\phi)$  where  $\phi = \frac{2\pi p}{q}$  for  $p, q$  coprime. At  $\phi = \Phi/2 = \pi n$  for odd  $n$ , this means  $q = 2$ . We study the single-particle states  $|\alpha, \ell, k_1, k_2\rangle$  with  $\alpha = 1, \dots, N_{orb}$ ,  $\ell = 0, 1$  which are eigenstates of  $T_1(\Phi/2)$  and  $T_2(\Phi/2)$ . Going forward, we write  $T_i(\Phi/2) = T_i$  for brevity unless otherwise specified. These states satisfy

$$T_1 |k_1, k_2, \ell, \alpha\rangle = e^{ik_1} |k_1, k_2, \ell, \alpha\rangle, \quad T_2^2 |k_1, k_2, \ell, \alpha\rangle = e^{i2k_2} |k_1, k_2, \ell, \alpha\rangle \quad (\text{D4})$$

where  $k_1 \in (-\pi, \pi)$  and we may choose  $k_2 \in (-\pi/2, \pi/2)$ . Note that these eigenstates differ from the conventional ‘‘momentum’’ eigenstates in Eq. (A40) which were used to diagonalize the Hofstadter Hamiltonian in App. A. Now we can form the Hofstadter Hamiltonian  $\mathcal{H}^{\Phi/2}(\mathbf{k})$  in this magnetic translation operator eigenbasis directly:

$$\mathcal{H}_{\ell\alpha, \ell'\beta}^{\Phi/2}(\mathbf{k})\delta_{\mathbf{k}, \mathbf{k}'} = \langle k_1, k_2, \ell, \alpha | H^{\Phi/2} | k'_1, k'_2, \ell', \beta \rangle, \quad k_1 \in (-\pi, \pi), k_2 \in (-\pi/2, \pi/2) \quad (\text{D5})$$

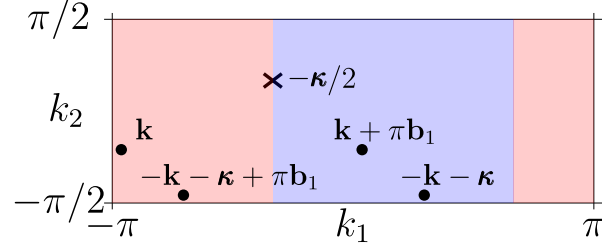


FIG. 12. We illustrate an example of  $BZ_{1/2, \kappa}$ , shown in red, with the rest of the magnetic BZ shown in blue. The point  $-\kappa/2$ , shown with an “X” is invariant under  $UT$ . If there is a gap closing at  $\mathbf{k} = -\frac{1}{2}\kappa + \mathbf{k}$ , then three more gap closings are generated under the application of  $UT$  and  $V_1(\Phi/2)$ . We denote these points with dots, and observe that exactly two points fall in  $BZ_{1/2, \kappa}$ .

which gives a representation of the Hamiltonian in the  $1 \times 2$  unit cell. We emphasize that the states Eq. (D4) give the minimal, gauge-independent  $1 \times 2$  unit cell, but we do not have an explicit expression for the Hofstadter Hamiltonian. We can derive the embedding matrices for  $\mathcal{H}^{\Phi/2}(\mathbf{k})$  that implement the  $k_1 \rightarrow k_1 + \pi$  periodicity following Sec. I. We prove in App. D 2 b that there is an embedding matrix  $[V_1(\Phi/2, k_2)]_{\ell, \alpha, \ell', \beta}$  satisfying

$$\mathcal{H}^{\Phi/2}(\mathbf{k} + \pi \mathbf{b}_1) = V_1(\Phi/2, k_2) \mathcal{H}^{\Phi/2}(\mathbf{k}) V_1^\dagger(\Phi/2, k_2). \quad (\text{D6})$$

We will not need an explicit expression for  $V_1(\Phi/2, k_2)$  in this section, but we provide one in App. D 2 b. Note that this embedding matrix depends on  $k_2$ , which we make explicit in the notation. This differs from the embedding matrices in App. A 8 where there was no momentum dependence.

So far we have constructed the Hofstadter Hamiltonian in a gauge-invariant manner that guarantees a magnetic BZ with  $k_1 \in (-\pi, \pi)$ ,  $k_2 \in (-\pi/2, \pi/2)$  with a  $k_1 \rightarrow k_1 + \pi$  periodicity in the spectrum implemented by  $V_1(\Phi/2, k_2)$ . Now we consider the  $UT$  symmetry that protects a  $\mathbb{Z}_2$  index, recalling that  $(UT)^2 = \mathcal{T}^2 = -1$ . We need to determine what properties this symmetry enforces. We will prove in App. D 2 b that

$$\sum_{\ell' \alpha', r' \beta'} [D(UT)^\dagger]_{\ell \alpha, \ell' \alpha'} \mathcal{H}_{\ell' \alpha', r' \beta'}^{\Phi/2}(\mathbf{k}) [D(UT)]_{r' \beta', r \beta} = \mathcal{H}_{\ell \alpha, r \beta}^{\Phi/2 * }(-\mathbf{k} - \kappa) \quad (\text{D7})$$

where  $D(UT)$  is the representation of  $UT$  on the single-particle Hilbert space satisfying  $D(UT)[D(UT)]^* = -1$  and  $\kappa$  is a momentum shift. We give a formula for  $\kappa$  in App. D 2 b where we show that it appears as a projective phase in the magnetic space group.

In Sec. III of the Main Text, we proved that the  $\mathbb{Z}_2$  invariant was always trivial,  $\delta^{\phi=\Phi/2} = +1$ , for  $\Phi = 2\pi n$ ,  $n$  odd when  $\kappa = 0$  by proving that all gap closings come in pairs in half the magnetic BZ. To prove the case with arbitrary  $\kappa$ , we note that we can rewrite Eq. (D7) in terms of a shifted momentum  $\mathbf{k} = -\frac{1}{2}\kappa + \tilde{\mathbf{k}}$ . In matrix notation, this reads

$$D(UT)^\dagger \mathcal{H}^{\Phi/2}(-\frac{1}{2}\kappa + \tilde{\mathbf{k}}) D(UT) = \mathcal{H}^{\Phi/2 * }(-\frac{1}{2}\kappa - \tilde{\mathbf{k}}) \quad (\text{D8})$$

from which we observe that  $\tilde{\mathbf{k}}$ , the momentum measured from  $-\frac{1}{2}\kappa$ , flips sign under  $UT$ . Thus we can replicate the gap closing proof in Sec. II Sec. III by choosing the half magnetic BZ defined by  $BZ_{1/2, \kappa} = \{-\frac{1}{2}\kappa + \tilde{\mathbf{k}} | \tilde{k}_1 \in (-\pi, 0), \tilde{k}_2 \in (-\pi/2, \pi/2)\}$ . Now we use the fact that  $n$  is odd, so there is a  $\pi$  periodicity in the spectrum along  $k_1$  given by Eq. (D6). In addition, due to Eq. (D8), the spectrum is invariant under  $\mathbf{k} \rightarrow -\mathbf{k} - \kappa$ . Hence gap closings in the *whole* magnetic BZ come in quartets, two due to the magnetic translation group and two due to  $UT$ , at the points

$$-\frac{1}{2}\kappa + \mathbf{k}, -\frac{1}{2}\kappa - \mathbf{k}, -\frac{1}{2}\kappa + \mathbf{k} + \pi \mathbf{b}_1, \text{ and } -\frac{1}{2}\kappa - \mathbf{k} + \pi \mathbf{b}_1 \quad (\text{D9})$$

as is shown for instance in Fig. 12. Note that for generic  $\mathbf{k}$ , exactly one of  $-\frac{1}{2}\kappa \pm \mathbf{k}$  is in  $BZ_{1/2, \kappa}$  and similarly exactly one of  $-\frac{1}{2}\kappa \mp \mathbf{k} + \pi \mathbf{b}_1$  is in  $BZ_{1/2, \kappa}$ . The degenerate points with  $k_1 = 0, \pm\pi/2$  or  $\pi$  and  $k_2 = 0$  or  $\pi/2$  reduce the quartet of points in Eq. (D9) to pairs of point where *doubly degenerate* gap closings occur. Thus all gap closings in the *half* BZ,  $BZ_{1/2, \kappa}$ , come in pairs and  $\delta^{\phi=\Phi/2} = +1$ .



b. Construction of the Gauge-invariant Eigenstates and the Projective Symmetry Algebra

To compute objects like  $T_i |\beta, \ell', k_1, k_2\rangle$  and  $UT |\beta, \ell', k_1, k_2\rangle$ , we note that there is an explicit expression for the momentum eigenstates given by the magnetic translation operators

$$|k_1, k_2, \ell, \alpha\rangle = \frac{1}{\sqrt{\mathcal{N}/2}} \sum_{mn} e^{-imk_1 - 2ink_2} T_1^m T_2^{2n} c_{\ell \mathbf{a}_2, \alpha}^\dagger |0\rangle, \quad \ell = 0, 1 \text{ and } \alpha = 1, \dots, N_{orb} \quad (\text{D10})$$

where  $T_i^{-m} = [T_i^\dagger]^m$ . (Recall that we have denoted  $T_i(\Phi/2)$  as  $T_i$  for brevity). It is straightforward to check that these states have the correct  $T_1, T_2^2$  eigenvalues. Here we have assumed  $n$  odd so there is a  $1 \times 2$  magnetic unit cell. We will first use Eq. (D10) to derive the embedding matrix  $V_1(\Phi/2, k_2)$  (see Eq. (D6)). We treat the cases of  $\ell = 0$  and  $\ell = 1$  separately. For  $\ell = 0$ , we find

$$\begin{aligned} T_2 |k_1, k_2, 0, \alpha\rangle &= \frac{1}{\sqrt{\mathcal{N}/2}} \sum_{mn} e^{-imk_1 - 2ink_2} T_2 T_1^m T_2^{2n} (\phi) c_{0, \alpha}^\dagger |0\rangle \\ &= \frac{1}{\sqrt{\mathcal{N}/2}} \sum_{mn} e^{-imk_1 - 2ink_2} (-1)^m T_1^m T_2^{2n} T_2 c_{0, \alpha}^\dagger |0\rangle \\ &= \frac{1}{\sqrt{\mathcal{N}/2}} \sum_{mn} e^{-im(k_1 + \pi) - 2ink_2} T_1^m T_2^{2n} T_2 c_{0, \alpha}^\dagger |0\rangle \end{aligned} \quad (\text{D11})$$

using the magnetic translation group and  $\exp(i\Phi/2) = -1$  for  $n$  odd. Now using Eq. (A9) to compute the action of  $T_2$  on the single-particle state, we find

$$T_2 c_{0 \mathbf{a}_2, \alpha}^\dagger |0\rangle = \exp\left(i \int_{\delta_\alpha}^{\mathbf{a}_2 + \delta_\alpha} \mathbf{A} \cdot d\mathbf{r} + i\chi_2(\delta_\alpha)\right) c_{\mathbf{a}_2, \alpha}^\dagger |0\rangle \quad (\text{D12})$$

and hence

$$T_2 |k_1, k_2, 0, \alpha\rangle = \exp\left(i \int_{\delta_\alpha}^{\mathbf{a}_2 + \delta_\alpha} \mathbf{A} \cdot d\mathbf{r} + i\chi_2(\delta_\alpha)\right) |k_1 + \pi, k_2, 1, \alpha\rangle \quad (\text{D13})$$

For  $\ell = 1$ , we calculate

$$\begin{aligned} T_2 |k_1, k_2, 1, \alpha\rangle &= \frac{1}{\sqrt{\mathcal{N}/2}} \sum_{mn} e^{-imk_1 - 2ink_2} T_2 T_1^m T_2^{2n} c_{\mathbf{a}_2, \alpha}^\dagger |0\rangle \\ &= \frac{1}{\sqrt{\mathcal{N}/2}} \sum_{mn} e^{-im(k_1 + \pi) - 2ink_2} T_1^m T_2^{2n+1} c_{\mathbf{a}_2, \alpha}^\dagger |0\rangle \\ &= \frac{1}{\sqrt{\mathcal{N}/2}} \sum_{mn} e^{-im(k_1 + \pi) - 2ink_2} T_1^m T_2^{2n+2} T_2^\dagger c_{\mathbf{a}_2, \alpha}^\dagger |0\rangle \\ &= \frac{1}{\sqrt{\mathcal{N}/2}} \sum_{mn} e^{-im(k_1 + \pi) - 2i(n-1)k_2} T_1^m T_2^{2n} T_2^\dagger c_{\mathbf{a}_2, \alpha}^\dagger |0\rangle \end{aligned} \quad (\text{D14})$$

Now using Eq. (A9) to compute the action of  $T_2^\dagger$  on the single-particle state, we find

$$T_2^\dagger c_{\mathbf{a}_2, \alpha}^\dagger |0\rangle = \exp\left(-i \int_{\delta_\alpha}^{\mathbf{a}_2 + \delta_\alpha} \mathbf{A} \cdot d\mathbf{r} - i\chi_2(\delta_\alpha)\right) c_{0, \alpha}^\dagger |0\rangle \quad (\text{D15})$$

and hence

$$T_2 |k_1, k_2, 1, \alpha\rangle = \exp\left(2ik_2 - i \int_{\delta_\alpha}^{\mathbf{a}_2 + \delta_\alpha} \mathbf{A} \cdot d\mathbf{r} - i\chi_2(\delta_\alpha)\right) |k_1 + \pi, k_2, 0, \alpha\rangle. \quad (\text{D16})$$

We collect Eqs. (D13) and (D16) into the following formula

$$T_2 |k_1, k_2, \ell, \alpha\rangle = \sum_{\ell', \beta} |k_1 + \pi, k_2, \ell', \beta\rangle [V_1(\Phi/2, k_2)]_{\ell', \beta, \ell \alpha} \quad (\text{D17})$$

where

$$[V_1(\Phi/2, k_2)]_{\ell'\beta, \ell\alpha} = \delta_{\alpha\beta} e^{ik_2} \left[ \cos \left( k_2 - \int_{\delta_\alpha}^{\mathbf{a}_2 + \delta_\alpha} \mathbf{A} \cdot d\mathbf{r} - \chi_2(\delta_\alpha) \right) \sigma_1 + \sin \left( k_2 - \int_{\delta_\alpha}^{\mathbf{a}_2 + \delta_\alpha} \mathbf{A} \cdot d\mathbf{r} - \chi_2(\delta_\alpha) \right) \sigma_2 \right]_{\ell, \ell'} \quad (\text{D18})$$

which by inspection is a unitary matrix. We remark that  $V_1(\Phi/2, k_2)$  is periodic along the magnetic BZ, i.e.  $V_1(\Phi/2, k_2) = V_1(\Phi/2, k_2 - \pi)$ , which we will make use of in App. D3a when considering the Wilson loop. We derive the corresponding transformation on the Hofstadter Hamiltonian to be

$$\mathcal{H}_{\ell\alpha, r\beta}^{\Phi/2}(k_1, k_2) = \sum_{\ell'\alpha', r'\beta} [V_1^\dagger(\Phi/2, k_2)]_{\ell\alpha, \ell'\alpha'} \mathcal{H}_{\ell'\alpha', r'\beta}^{\Phi/2}(k_1 + \pi, k_2) [V_1(\Phi/2, k_2)]_{r'\beta', r\beta}. \quad (\text{D19})$$

In matrix notation, this reads

$$\mathcal{H}^{\Phi/2}(\mathbf{k}) = V_1^\dagger(\Phi/2, k_2) \mathcal{H}^{\Phi/2}(\mathbf{k} + \pi \mathbf{b}_1) V_1(\Phi/2, k_2) \quad (\text{D20})$$

which proves Eq. (D6).

In a similar manner, we can compute the action of  $UT$  on the eigenstates Eq. (D10) once we know the algebra of  $UT$  and  $T_i(\Phi/2)$ . Using Eq. (A9), we compute

$$\mathcal{T} T_i \mathcal{T}^{-1} = \mathcal{T} \sum_{\mathbf{R}\alpha} e^{i \int_{\mathbf{R} + \delta_\alpha}^{\mathbf{R} + \delta_\alpha + \mathbf{a}_i} \mathbf{A} \cdot d\mathbf{r} + i\chi_i(\mathbf{R} + \delta_\alpha)} c_{\mathbf{R} + \mathbf{a}_i, \alpha}^\dagger c_{\mathbf{R}, \alpha} \mathcal{T}^{-1} \quad (\text{D21})$$

where the integral of  $\mathbf{A}$  is taken *over a straight-line path*, which is not necessarily a Peierls path. Using Eq. (D2), we compute

$$\begin{aligned} \mathcal{T} T_i(\Phi/2) \mathcal{T}^{-1} &= \sum_{\mathbf{R}\alpha} e^{-i \int_{\mathbf{R} + \delta_\alpha}^{\mathbf{R} + \delta_\alpha + \mathbf{a}_i} \mathbf{A} \cdot d\mathbf{r} - i\chi_i(\mathbf{R} + \delta_\alpha)} \mathcal{T} c_{\mathbf{R} + \mathbf{a}_i, \alpha}^\dagger c_{\mathbf{R}, \alpha} \mathcal{T}^{-1} \\ &= \sum_{\mathbf{R}\alpha, \alpha', \alpha''} e^{-i \int_{\mathbf{R} + \delta_\alpha}^{\mathbf{R} + \delta_\alpha + \mathbf{a}_i} \mathbf{A} \cdot d\mathbf{r} - i\chi_i(\mathbf{R} + \delta_\alpha)} c_{\mathbf{R} + \mathbf{a}_i, \alpha'}^\dagger D_{\alpha'\alpha}^\dagger(\mathcal{T}) D_{\alpha\alpha''}(\mathcal{T}) c_{\mathbf{R}, \alpha''} \\ &= \sum_{\mathbf{R}\alpha} e^{-i \int_{\mathbf{R} + \delta_\alpha}^{\mathbf{R} + \delta_\alpha + \mathbf{a}_i} \mathbf{A} \cdot d\mathbf{r} - i\chi_i(\mathbf{R} + \delta_\alpha)} c_{\mathbf{R} + \mathbf{a}_i, \alpha}^\dagger c_{\mathbf{R}, \alpha} \\ &= T_i(-\Phi/2) \end{aligned} \quad (\text{D22})$$

where we have used the fact that  $\mathcal{T}$  is onsite as discussed in App. D1. We see that the effect of  $\mathcal{T}$  is merely to complex conjugate  $T_i(\phi)$ , which is equivalent to reversing the flux. We now study  $UT T_i(\phi) (UT)^{-1} = UT_i(-\phi) U^\dagger$ . Using Eq. (A5), we find

$$\begin{aligned} UT_i(-\Phi/2) U^\dagger &= \sum_{\mathbf{R}\alpha} e^{-i \int_{\mathbf{R} + \delta_\alpha}^{\mathbf{R} + \delta_\alpha + \mathbf{a}_i} \mathbf{A} \cdot d\mathbf{r} - i\chi_i(\mathbf{R} + \delta_\alpha)} U c_{\mathbf{R} + \mathbf{a}_i, \alpha}^\dagger U^\dagger U c_{\mathbf{R}, \alpha} U^\dagger \\ &= \sum_{\mathbf{R}\alpha} \exp \left( -i \int_{\mathbf{R} + \delta_\alpha}^{\mathbf{R} + \delta_\alpha + \mathbf{a}_i} \mathbf{A} \cdot d\mathbf{r} - i\chi_i(\mathbf{R} + \delta_\alpha) + i \int_{\mathbf{r}_0}^{\mathbf{R} + \mathbf{a}_i + \delta_\alpha} \tilde{\mathbf{A}} \cdot d\mathbf{r} - i \int_{\mathbf{r}_0}^{\mathbf{R} + \delta_\alpha} \tilde{\mathbf{A}} \cdot d\mathbf{r} \right) c_{\mathbf{R} + \mathbf{a}_i, \alpha}^\dagger c_{\mathbf{R}, \alpha} \end{aligned} \quad (\text{D23})$$

where we emphasize that the integral of  $\tilde{\mathbf{A}}$  (generating  $\Phi$  flux) is taken over a Peierls path (see Eq. (2)) and the integral of  $\mathbf{A}$  (generating  $\phi = \Phi/2$  flux) is taken over a straight-line path (see Eq. (3)). We can re-sum the Peierls integrals using Eq. (A4)

$$UT_i(-\Phi/2) U^\dagger = \sum_{\mathbf{R}\alpha} \exp \left( -i \int_{\mathbf{R} + \delta_\alpha}^{\mathbf{R} + \delta_\alpha + \mathbf{a}_i} \mathbf{A} \cdot d\mathbf{r} - i\chi_i(\mathbf{R} + \delta_\alpha) + i \int_{\mathbf{R} + \delta_\alpha}^{\mathbf{R} + \delta_\alpha + \mathbf{a}_i} \tilde{\mathbf{A}} \cdot d\mathbf{r} \right) c_{\mathbf{R} + \mathbf{a}_i, \alpha}^\dagger c_{\mathbf{R}, \alpha}. \quad (\text{D24})$$

To proceed, we want to relate the gauge fields  $\mathbf{A}$  and  $\tilde{\mathbf{A}}$  in a convenient way. We have  $2\mathbf{A} = \tilde{\mathbf{A}}$  up to a gauge transformation because  $\nabla \times \mathbf{A} = \Phi/2$  and  $\nabla \times \tilde{\mathbf{A}} = \Phi$ . It is most convenient to take  $2\mathbf{A} = \tilde{\mathbf{A}}$ . We now note that the integrals can be combined. For clarity, we denote integrals over Peierls paths with a *P.P.* label, and the straight-line path with *straight*, and we also denote  $\mathbf{R} + \delta_\alpha = \mathbf{r}_\alpha$  as shorthand. Then the integrals in Eq. (D24) can be manipulated

to yield

$$\begin{aligned}
-\int_{\text{straight}}^{\mathbf{r}_\alpha \rightarrow \mathbf{r}_\alpha + \mathbf{a}_i} \mathbf{A} \cdot d\mathbf{r} + \int_{P.P.}^{\mathbf{r}_\alpha \rightarrow \mathbf{R} + \mathbf{a}_i + \boldsymbol{\delta}_\alpha} \tilde{\mathbf{A}} \cdot d\mathbf{r} &= \int_{\text{straight}}^{\mathbf{r}_\alpha \rightarrow \mathbf{r}_\alpha + \mathbf{a}_i} \mathbf{A} \cdot d\mathbf{r} - 2 \int_{\text{straight}}^{\mathbf{r}_\alpha \rightarrow \mathbf{r}_\alpha + \mathbf{a}_i} \mathbf{A} \cdot d\mathbf{r} + \int_{P.P.}^{\mathbf{r}_\alpha \rightarrow \mathbf{r}_\alpha + \mathbf{a}_i} \tilde{\mathbf{A}} \cdot d\mathbf{r} \\
&= \int_{\text{straight}}^{\mathbf{r}_\alpha \rightarrow \mathbf{r}_\alpha + \mathbf{a}_i} \mathbf{A} \cdot d\mathbf{r} + 2 \int_{\text{straight}}^{\mathbf{r}_\alpha + \mathbf{a}_i \rightarrow \mathbf{r}_\alpha} \mathbf{A} \cdot d\mathbf{r} + \int_{P.P.}^{\mathbf{r}_\alpha \rightarrow \mathbf{r}_\alpha + \mathbf{a}_i} \tilde{\mathbf{A}} \cdot d\mathbf{r} \quad (\text{D25}) \\
&= \int_{\text{straight}}^{\mathbf{r}_\alpha \rightarrow \mathbf{r}_\alpha + \mathbf{a}_i} \mathbf{A} \cdot d\mathbf{r} + \left( \int_{P.P.}^{\mathbf{r}_\alpha \rightarrow \mathbf{r}_\alpha + \mathbf{a}_i} + \int_{\text{straight}}^{\mathbf{r}_\alpha + \mathbf{a}_i \rightarrow \mathbf{r}_\alpha} \right) \tilde{\mathbf{A}} \cdot d\mathbf{r} .
\end{aligned}$$

Notice that the first integral is of the same form as in  $T_i(\Phi/2)$ , and the second is over a loop given by a Peierls path from  $\mathbf{r}_\alpha$  to  $\mathbf{r}_\alpha + \mathbf{a}_i$  (which may be taken along an arbitrary sequence of Peierls paths because  $\nabla \times \tilde{\mathbf{A}} = \Phi$ ) and then a straight-line path back from  $\mathbf{r}_\alpha + \mathbf{a}_i$  to  $\mathbf{r}_\alpha$ . We denote the area enclosed by such a path as  $\Omega_{i,\alpha}$ , as shown for example in Fig. 13a. Continuing, we find

$$\begin{aligned}
-\int_{\text{straight}}^{\mathbf{r}_\alpha \rightarrow \mathbf{r}_\alpha + \mathbf{a}_i} \mathbf{A} \cdot d\mathbf{r} + \int_{P.P.}^{\mathbf{r}_\alpha \rightarrow \mathbf{R} + \mathbf{a}_i + \boldsymbol{\delta}_\alpha} \tilde{\mathbf{A}} \cdot d\mathbf{r} &= \int_{\text{straight}}^{\mathbf{r}_\alpha \rightarrow \mathbf{r}_\alpha + \mathbf{a}_i} \mathbf{A} \cdot d\mathbf{r} + \oint_{\partial\Omega_{i,\alpha}} \tilde{\mathbf{A}} \cdot d\mathbf{r} \\
&= \int_{\text{straight}}^{\mathbf{r}_\alpha \rightarrow \mathbf{r}_\alpha + \mathbf{a}_i} \mathbf{A} \cdot d\mathbf{r} + \oint_{\Omega_{i,\alpha}} \Phi dS \quad (\text{D26}) \\
&= \int_{\text{straight}}^{\mathbf{r}_\alpha \rightarrow \mathbf{r}_\alpha + \mathbf{a}_i} \mathbf{A} \cdot d\mathbf{r} + \Phi \Omega_{i,\alpha}
\end{aligned}$$

and thus we find

$$UT_i(-\Phi/2)U^\dagger = \sum_{\mathbf{R}\alpha} \exp \left( i\Phi\Omega_{i,\alpha} + i \int_{\mathbf{R} + \boldsymbol{\delta}_\alpha}^{\mathbf{R} + \boldsymbol{\delta}_\alpha + \mathbf{a}_i} \mathbf{A} \cdot d\mathbf{r} - i\chi_i(\mathbf{R} + \boldsymbol{\delta}_\alpha) \right) c_{\mathbf{R} + \mathbf{a}_i, \alpha}^\dagger c_{\mathbf{R}, \alpha} . \quad (\text{D27})$$

We want to recover an expression proportional to the magnetic translation operator  $T_i(\Phi/2)$ . To make progress, we note that at  $\phi = \Phi/2$ , Eq. (A9) gives  $\chi_i(\mathbf{r}) = \Phi/2(\mathbf{a}_i \times \mathbf{r})$  and hence

$$\begin{aligned}
-\chi_i(\mathbf{R} + \boldsymbol{\delta}_\alpha) &= \chi_i(\mathbf{R} + \boldsymbol{\delta}_\alpha) - \Phi \mathbf{a}_i \times (\mathbf{R} + \boldsymbol{\delta}_\alpha) \\
&= \chi_i(\mathbf{R} + \boldsymbol{\delta}_\alpha) - \Phi \mathbf{a}_i \times \boldsymbol{\delta}_\alpha \quad \text{mod } 2\pi \quad (\text{D28})
\end{aligned}$$

and hence

$$UT_i(-\Phi/2)U^\dagger = \sum_{\mathbf{R}\alpha} \exp \left( i\Phi(\Omega_{i,\alpha} + \boldsymbol{\delta}_\alpha \times \mathbf{a}_i) + i \int_{\mathbf{R} + \boldsymbol{\delta}_\alpha}^{\mathbf{R} + \boldsymbol{\delta}_\alpha + \mathbf{a}_i} \mathbf{A} \cdot d\mathbf{r} + i\chi_i(\mathbf{R} + \boldsymbol{\delta}_\alpha) \right) c_{\mathbf{R} + \mathbf{a}_i, \alpha}^\dagger c_{\mathbf{R}, \alpha} . \quad (\text{D29})$$

We can now define the momentum shift  $\boldsymbol{\kappa}_\alpha$  by

$$\boldsymbol{\kappa}_{i,\alpha} = \Phi(\Omega_{i,\alpha} + \boldsymbol{\delta}_\alpha \times \mathbf{a}_i) . \quad (\text{D30})$$

It appears that the momentum shift depends on the orbital location. However, we will now prove that, in fact

$$\boldsymbol{\kappa}_\alpha - \boldsymbol{\kappa}_\beta = \Phi(\Omega_{i,\alpha} - \Omega_{i,\beta} + (\boldsymbol{\delta}_\alpha - \boldsymbol{\delta}_\beta) \times \mathbf{a}_i) = 0 \quad \text{mod } 2\pi \quad (\text{D31})$$

To prove Eq. (D31), we recall that any integral of  $\tilde{\mathbf{A}}$  over a closed loop of Peierls paths is equal a multiple of  $2\pi$ . We consider a closed loop  $\partial\mathcal{M}$  that is formed of Peierls paths connecting  $\boldsymbol{\delta}_\alpha, \boldsymbol{\delta}_\alpha + \mathbf{a}_i, \boldsymbol{\delta}_\beta + \mathbf{a}_i, \boldsymbol{\delta}_\beta$  in sequence, which we depict in Fig. 13a. Importantly, the Peierls paths connecting  $\boldsymbol{\delta}_\alpha, \boldsymbol{\delta}_\beta$  and  $\boldsymbol{\delta}_\alpha + \mathbf{a}_i, \boldsymbol{\delta}_\beta + \mathbf{a}_i$  can be chosen to be the same shape since they are related by a lattice vector. Now, as shown in Fig. 13b we can separate the line integral over  $\partial\mathcal{M}$  with *straight-line* paths connecting  $\boldsymbol{\delta}_\alpha, \boldsymbol{\delta}_\alpha + \mathbf{a}_i$  and  $\boldsymbol{\delta}_\beta, \boldsymbol{\delta}_\beta + \mathbf{a}_i$ :

$$\begin{aligned}
0 &= \oint_{\partial\mathcal{M}} \tilde{\mathbf{A}} \cdot d\mathbf{r} \quad \text{mod } 2\pi \\
&= \oint_{\partial\Omega_{i,\alpha}} \tilde{\mathbf{A}} \cdot d\mathbf{r} + \oint_{\partial\mathcal{R}} \tilde{\mathbf{A}} \cdot d\mathbf{r} + \oint_{-\partial\Omega_{i,\beta}} \tilde{\mathbf{A}} \cdot d\mathbf{r} \quad \text{mod } 2\pi \\
&= \Phi \oint_{\Omega_{i,\alpha}} dS + \Phi \oint_{\mathcal{R}} dS - \Phi \int_{\Omega_{i,\beta}} dS \quad \text{mod } 2\pi \\
&= \Phi(\Omega_{i,\alpha} - \Omega_{i,\beta}) + \Phi \oint_{\mathcal{R}} dS \quad \text{mod } 2\pi \quad (\text{D32})
\end{aligned}$$

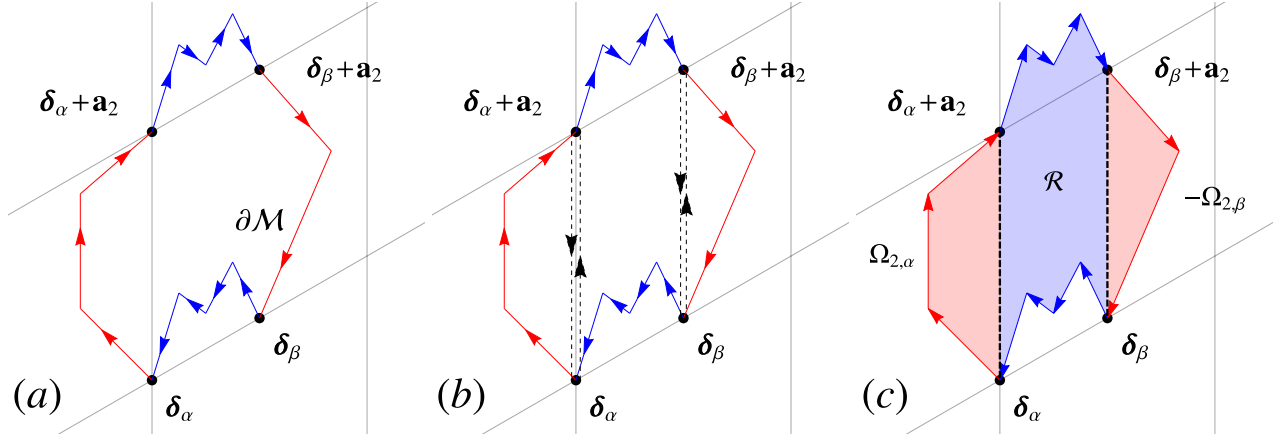


FIG. 13. We illustrate the manipulations of the integrals from Eq. (D26) to Eq. (D32) with  $\mathbf{a}_i = \mathbf{a}_2$ . (a) We show the closed loop along Peierls paths  $\partial\mathcal{M}$ . The loop is composed of (1) the Peierls paths connecting  $\delta_\alpha \rightarrow \delta_\alpha + \mathbf{a}_i$  and  $\delta_\beta + \mathbf{a}_i \rightarrow \delta_\beta$  shown in red which in general have different shapes, and (2) the Peierls paths connecting  $\delta_\alpha + \mathbf{a}_i \rightarrow \delta_\beta + \mathbf{a}_i$  and  $\delta_\beta \rightarrow \delta_\alpha$  shown in blue, which may be chosen to have the same shape because they are related by a lattice vector. (b) Without changing the value of the integral, we add and subtract straight-line paths, dashed in black, that connect  $\delta_\alpha, \delta_\alpha + \mathbf{a}_i$  and  $\delta_\beta, \delta_\beta + \mathbf{a}_i$ . (c) The line integral can be divided along the straight-line contours and separated into the areas  $\Omega_{i,\alpha}, \mathcal{R}, -\Omega_{i,\beta}$  where the minus sign is due to the opposite orientation. We see and can easily prove that  $\mathcal{R}$  can be deformed to a parallelogram with corners at  $\delta_\alpha, \delta_\alpha + \mathbf{a}_2, \delta_\beta + \mathbf{a}_2$ , and  $\delta_\beta$ .

where  $\mathcal{R}$ , shown in Fig. 13c, is the area formed by the straight-line paths and the Peierls paths connecting  $\delta_\alpha, \delta_\beta$  and  $\delta_\alpha + \mathbf{a}_i, \delta_\beta + \mathbf{a}_i$ . Because these Peierls paths are the same shape,  $\mathcal{R}$  can be deformed to a parallelogram without changing its area. Hence the area of  $\mathcal{R}$  is that of a parallelogram with sides given by  $\mathbf{a}_i$  and  $\delta_\beta - \delta_\alpha$ . Thus, Eq. (D32) reads

$$\Phi(\Omega_{i,\alpha} - \Omega_{i,\beta}) + \mathbf{a}_i \times (\delta_\beta - \delta_\alpha) = 0 \pmod{2\pi}, \quad (\text{D33})$$

proving Eq. (D31). Hence we can calculate  $\boldsymbol{\kappa} = \boldsymbol{\kappa}_\alpha$  at *any* orbital location. However, we must be consistent with the choice of origin which defines  $\delta_\alpha$ . Shifting the origin changes both  $\boldsymbol{\kappa}$  and the overall phase of  $T_i(\Phi/2)$ , which we have fixed throughout. Note however that Eq. (D31) remains invariant under such a shift.

With  $\boldsymbol{\kappa} = \kappa_1 \mathbf{b}_1 + \kappa_2 \mathbf{b}_2$  determined, we return to Eq. (D29) to obtain

$$\begin{aligned} U\mathcal{T}T_i(\Phi/2)(U\mathcal{T})^{-1} &= \left[ \sum_{\mathbf{R}\alpha} \exp \left( i\kappa_i + i \int_{\mathbf{R}+\delta_\alpha}^{\mathbf{R}+\delta_\alpha+\mathbf{a}_i} \mathbf{A} \cdot d\mathbf{r} + i\chi_i(\mathbf{R} + \delta_\alpha) \right) c_{\mathbf{R}+\mathbf{a}_i,\alpha}^\dagger c_{\mathbf{R},\alpha} \right] \\ &= \exp(i\boldsymbol{\kappa} \cdot \mathbf{b}_i) T_i(\Phi/2). \end{aligned} \quad (\text{D34})$$

We remark that this result, the algebra of  $U\mathcal{T}$  and  $T_i(\Phi/2)$  holds for  $n$  even or odd, and regardless of the sign of  $\mathcal{T}^2$ . Now assuming  $n$  odd so there is a  $1 \times 2$  unit cell, (Eq. (D34)) lets us calculate

$$\begin{aligned} U\mathcal{T} |k_1, k_2, \ell, \alpha\rangle &= \frac{1}{\sqrt{\mathcal{N}/2}} \sum_{mn} e^{+imk_1+2ink_2} U\mathcal{T}T_1^m T_2^{2n} (U\mathcal{T})^{-1} U\mathcal{T} c_{\ell\mathbf{a}_2,\alpha}^\dagger |0\rangle \\ &= \frac{1}{\sqrt{\mathcal{N}/2}} \sum_{mn} e^{+imk_1+2ink_2} e^{im\kappa_1+i2n\kappa_2} T_1^m T_2^{2n} U\mathcal{T} c_{\ell\mathbf{a}_2,\alpha}^\dagger |0\rangle \\ &= \frac{1}{\sqrt{\mathcal{N}/2}} \sum_{mn} e^{+im(k_1+\kappa_1)+2in(k_2+\kappa_2)} T_1^m T_2^{2n} U\mathcal{T} c_{\ell\mathbf{a}_2,\alpha}^\dagger |0\rangle \\ &= \sum_{\alpha', \ell'} |-(k_1 + \kappa_1), -(k_2 + \kappa_2), \ell', \alpha'\rangle K[D^\dagger(U\mathcal{T})]_{\ell'\alpha', \ell\alpha} \end{aligned} \quad (\text{D35})$$

where in the last line we defined  $D^\dagger(U\mathcal{T})$ , the single-particle representation of  $U\mathcal{T}$  (with  $K$  denoting complex conjugation).

gation). This follows from

$$\begin{aligned}
UTc_{\ell\mathbf{a}_2,\alpha}^\dagger|0\rangle &= UTC_{\ell\mathbf{a}_2,\alpha}^\dagger\mathcal{T}^{-1}U^\dagger UT|0\rangle \\
&= UTC_{\ell\mathbf{a}_2,\alpha}^\dagger\mathcal{T}^{-1}U^\dagger|0\rangle K \\
&= \sum_{\alpha'} Uc_{\ell\mathbf{a}_2,\alpha'}^\dagger U^\dagger[D_{\alpha\alpha'}(\mathcal{T})]^*|0\rangle K \\
&= \sum_{\alpha'\ell'} c_{\ell'\mathbf{a}_2,\alpha'}^\dagger \delta_{\ell\ell'} e^{i\int_{r_0}^{\ell\mathbf{a}_2+\delta_{\alpha'}} \tilde{\mathbf{A}}\cdot d\mathbf{r}} |0\rangle KD_{\alpha\alpha'}(\mathcal{T}) \\
&= \sum_{\alpha'\ell'} c_{\ell'\mathbf{a}_2,\alpha'}^\dagger |0\rangle K \delta_{\ell\ell'} e^{-i\int_{r_0}^{\ell\mathbf{a}_2+\delta_{\alpha'}} \tilde{\mathbf{A}}\cdot d\mathbf{r}} D_{\alpha\alpha'}(\mathcal{T}) \\
&= \sum_{\alpha'\ell'} c_{\ell'\mathbf{a}_2,\alpha'}^\dagger |0\rangle K [D^\dagger(UT)]_{\ell'\alpha',\ell\alpha}, \quad [D^\dagger(UT)]_{\ell'\alpha',\ell\alpha} = \delta_{\ell\ell'} e^{-i\int_{r_0}^{\ell\mathbf{a}_2+\delta_{\alpha'}} \tilde{\mathbf{A}}\cdot d\mathbf{r}} D_{\alpha\alpha'}(\mathcal{T})
\end{aligned} \tag{D36}$$

with  $\ell = 0, 1$  and  $\alpha = 1, \dots, N_{orb}$  in a tensor product basis.

To determine the action of  $UT$  on the Hofstadter Hamiltonian, we use the fact that  $UT$  commutes with  $H^{\Phi/2}$ , giving

$$\mathcal{H}_{\ell\alpha,\ell'\beta}^{\Phi/2}(\mathbf{k}) = \sum_{\ell'\alpha',r'\beta'} [D(UT)]_{\ell\alpha,\ell'\alpha'} \mathcal{H}_{\ell'\alpha',r'\beta'}^{\Phi/2*}(-\mathbf{k}-\boldsymbol{\kappa}) [D^\dagger(UT)]_{r'\beta',r\beta}. \tag{D37}$$

We recognize the usual form of an anti-unitary symmetry acting on a single-particle Hamiltonian, but with a momentum shift that comes from the algebra of  $UT$  and  $T(\Phi/2)$ . We mention that the full symmetry algebra of  $H^{\Phi/2}$ ,

$$UT, T_i(\Phi/2) \tag{D38}$$

forms a *projective* representation of the magnetic space group  $1'$  at  $\phi = 0$  with the projective phases  $\phi$  and  $\boldsymbol{\kappa}$  given by

$$T_1(\Phi/2)T_2(\Phi/2) = e^{i\Phi/2}T_2(\Phi/2)T_1(\Phi/2), \quad UTT_i(\Phi/2) = e^{i\boldsymbol{\kappa}\cdot\mathbf{b}_i}T_i(\Phi/2)UT. \tag{D39}$$

For instance, we can consider the model of twisted bilayer graphene introduced in App. G1. In Fig. 14, we show that, due to the Peierls paths being taken through the center of the honeycomb, we find nonzero expression for  $\Omega_{i,\alpha}$ . Choosing a convention where the origin is fixed at the center of the honeycomb, we find that Eq. (D30) yields  $\boldsymbol{\kappa} = (\pi, \pi)$ .

### 3. Wilson Loop Proof of a Nontrivial $\mathbb{Z}_2$ Index with $\mathcal{T}$ symmetry

The crux of our proof in Sec. III is the establishment that the  $\mathbb{Z}_2$  Kane-Mele invariant of  $H^{\Phi/2}$  is trivial. App. D2 demonstrated this using the action of the magnetic translation group on the BZ. Here, we prove the same result using the Wilson loop. We assume that the magnetic periodicity is given  $\Phi = 2\pi n$ ,  $n$  odd and we will prove that  $\delta^{\phi=\Phi/2} = +1$ . In App. F2, we show when  $n$  is even,  $\delta^{\phi=\Phi/2}$  is *not* fixed to be +1.

#### a. $UT$ Constraints on the Wilson Loop

To begin, we study the constraint imposed by  $UT$  on the Wilson loop at  $\phi = \Phi/2$  in the  $1 \times 2$  gauge-invariant magnetic unit cell. To begin, we need to work in an eigenbasis of  $H^{\Phi/2}, T_1(\Phi/2), T_2^2(\Phi/2)$  which is given by

$$|m, \mathbf{k}\rangle = \sum_{\ell\alpha} |\mathbf{k}, \ell, \alpha\rangle [\mathcal{U}^\dagger(\mathbf{k})]_{\ell\alpha,m}, \quad \ell = 0, 1, \alpha = 1, \dots, N_{orb}, \text{ and } m = 1, \dots, 2N_{orb} \tag{D40}$$

where  $[\mathcal{U}(\mathbf{k})]_{\ell\alpha,m}$  is a  $2N_{orb} \times 2N_{orb}$  unitary matrix which relates the  $\ell, \alpha$  basis (in Eq. (D4)) to the  $m$  energy eigenbasis of  $\mathcal{H}^{\Phi/2}(\mathbf{k})$ . To follow the method of App. C1, we write define  $|u_j^{\Phi/2}(\mathbf{k})\rangle$ , the eigenstate of  $\mathcal{H}^{\Phi/2}(\mathbf{k})$ , by

$$\langle \mathbf{k}, \ell, \alpha | u_j^{\Phi/2}(\mathbf{k}) \rangle = [U(\mathbf{k})]_{\ell\alpha,j} \tag{D41}$$

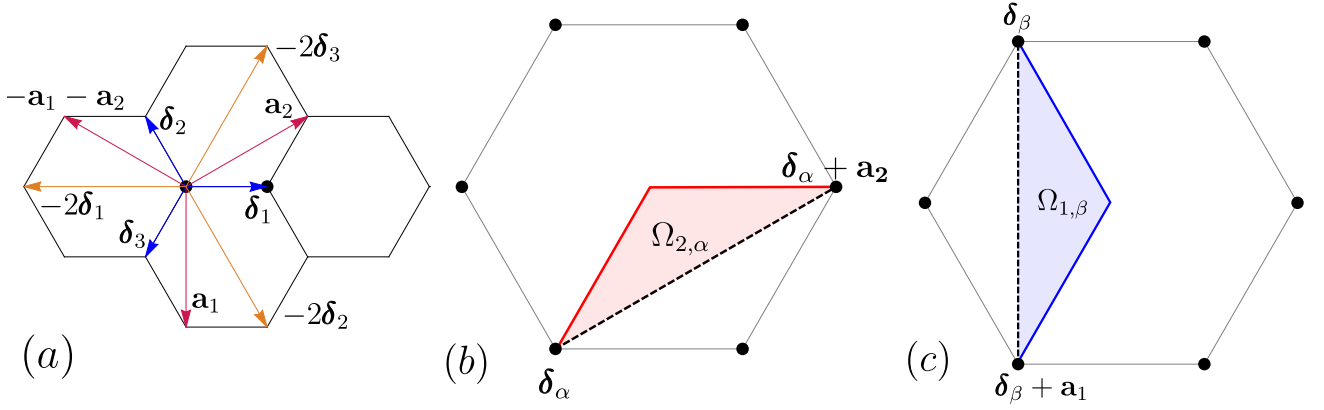


FIG. 14. (a) We show the lattice vectors and nearest neighbor vectors of the TBG model, replicated from Fig. 6c. (b) We show the area  $\Omega_{1,\alpha} = 1/6$  enclosed by the Peierls Paths (shown in solid red) and the straight-line path in dashed black for a given orbital  $\delta_\alpha$ . We recall that  $\Phi = 6\pi$ , as discussed in detail in App. G 1, so  $\Phi\Omega_{1,\alpha} = \pi$ . In the convention where the origin is at the center of the honeycomb, we calculate  $\Phi\delta_\alpha \times \mathbf{a}_1 = 6\pi(-\delta_1/2 + \mathbf{a}_1/2) \times \mathbf{a}_1 = 6\pi \times 1/3 = 0 \pmod{2\pi}$ , and hence from Eq. (D30), we find  $\kappa_1 = \pi$ . (c) We show the area  $\Omega_{2,\beta} = 1/6$  enclosed by the Peierls Paths (shown in solid blue) and the straight-line path in dashed black for a given orbital  $\delta_\beta$ . We recall that  $\Phi = 6\pi$ , as discussed in detail in App. G 1, so  $\Phi\Omega_{2,\beta} = \pi$ . In the convention where the origin is at the center of the honeycomb, we calculate  $\Phi\delta_\beta \times \mathbf{a}_2 = 6\pi(-\delta_1/2 - \mathbf{a}_1/2) \times \mathbf{a}_2 = 6\pi \times -2/3 = 0 \pmod{2\pi}$ , and hence from Eq. (D30), we find  $\kappa_2 = \pi$ .

where  $j = 1, \dots, 2N_{occ}$ , assuming the energy spectrum is gapped for  $\phi \in (0, \Phi/2)$  and we can separate the occupied bands. For convenience, we define the unitary matrix  $Q = D(UT)$  which, by Eq. (D7), satisfies

$$QK\mathcal{H}^{\Phi/2}(\mathbf{k})KQ^\dagger = \mathcal{H}^{\Phi/2}(-\mathbf{k} - \boldsymbol{\kappa}) \quad (\text{D42})$$

where  $K$  is complex conjugation. Following App. C 1, we now form the unitary sewing matrix

$$\begin{aligned} \mathcal{B}_{\mathbf{k}}^{ij} &= \langle u_i^{\Phi/2}(-\mathbf{k} - \boldsymbol{\kappa}) | QK | u_j^{\Phi/2}(\mathbf{k}) \rangle \\ &= \langle u_i^{\Phi/2}(-\mathbf{k} - \boldsymbol{\kappa}) | Q | u_j^{\Phi/2*}(\mathbf{k}) \rangle \end{aligned} \quad (\text{D43})$$

which connects eigenstates at TRS momenta [46]:

$$|u_j^{\Phi/2}(\mathbf{k})\rangle = \sum_i Q |u_i^{\Phi/2*}(-\mathbf{k} - \boldsymbol{\kappa})\rangle [\mathcal{B}^\dagger]_{-\mathbf{k}-\boldsymbol{\kappa}}^{ij}. \quad (\text{D44})$$

Using this relation, we determine that a small segment of a Wilson loop obeys

$$\begin{aligned} [W_{\mathbf{k}'_1 \leftarrow \mathbf{k}_1}^{\Phi/2}]^{ij} &= \langle u_i^{\Phi/2}(\mathbf{k}'_1) | u_j^{\Phi/2}(\mathbf{k}_1) \rangle \\ &= \sum_{rs} \mathcal{B}_{-\mathbf{k}'_1 - \boldsymbol{\kappa}}^{ir} \langle u_r^{\Phi/2*}(-\mathbf{k}'_1 - \boldsymbol{\kappa}) | Q^\dagger Q | u_s^{\Phi/2*}(-\mathbf{k}_1 - \boldsymbol{\kappa}) \rangle [\mathcal{B}^\dagger_{-\mathbf{k}_1 - \boldsymbol{\kappa}}]^{sj} \\ &= \sum_{rs} \mathcal{B}_{-\mathbf{k}'_1 - \boldsymbol{\kappa}}^{ir} [W_{-\mathbf{k}'_1 - \boldsymbol{\kappa} \leftarrow -\mathbf{k}_1 - \boldsymbol{\kappa}}^{\Phi/2*}]_{rs} [\mathcal{B}^\dagger_{-\mathbf{k}_1 - \boldsymbol{\kappa}}]^{sj}. \end{aligned} \quad (\text{D45})$$

We now want to consider a full Wilson loop. Because of the shift due to  $\boldsymbol{\kappa}$ , we will find it convenient to shift the origin of the Wilson loop. Hence we define  $\tilde{\mathbf{k}}$  by  $\mathbf{k} = -\boldsymbol{\kappa}/2 + \tilde{\mathbf{k}}$  and define a Wilson loop  $\tilde{W}^{\Phi/2}(\tilde{k}_1)$  by integrating along  $\tilde{k}_2$ :

$$\tilde{W}^{\Phi/2}(\tilde{k}_1) \equiv W_{(-\kappa_1/2 + \tilde{k}_1, -\kappa_2/2 + \pi/2) \leftarrow (-\kappa_1/2 + \tilde{k}_1, -\kappa_2/2 - \pi/2)}^{\Phi/2}. \quad (\text{D46})$$

Using Eq. (D45), we find

$$\begin{aligned} \tilde{W}^{\Phi/2}(\tilde{k}_1) &= \mathcal{B}_{(-\kappa_1/2 - \tilde{k}_1, -\kappa_2/2 - \pi/2)} \tilde{W}_{(-\kappa_1/2 - \tilde{k}_1, -\kappa_2/2 - \pi/2) \leftarrow (-\kappa_1/2 - \tilde{k}_1, -\kappa_2/2 + \pi/2)}^{\Phi/2*} \mathcal{B}_{(-\kappa_1/2 - \tilde{k}_1, -\kappa_2/2 + \pi/2)}^\dagger \\ &= \mathcal{B}_{(-\kappa_1/2 - \tilde{k}_1, -\kappa_2/2 - \pi/2)} \tilde{W}_{(-\kappa_1/2 - \tilde{k}_1, -\kappa_2/2 + \pi/2) \leftarrow (-\kappa_1/2 - \tilde{k}_1, -\kappa_2/2 - \pi/2)}^{\Phi/2* \dagger} \mathcal{B}_{(-\kappa_1/2 - \tilde{k}_1, -\kappa_2/2 + \pi/2)}^\dagger \\ &= \mathcal{B}_{(-\kappa_1/2 - \tilde{k}_1, -\kappa_2/2 - \pi/2)} [\tilde{W}^{\Phi/2}(-\tilde{k}_1)]^T \mathcal{B}_{(-\kappa_1/2 - \tilde{k}_1, -\kappa_2/2 + \pi/2)}^\dagger \end{aligned} \quad (\text{D47})$$

We now observe that from the construction of the translation eigenstates in Eq. (D10), we have  $|k_1, k_2, \ell, \alpha\rangle = |k_1 + 2\pi, k_2, \ell, \alpha\rangle = |k_1, k_2 + \pi, \ell, \alpha\rangle$ , and thus from Eq. (D5), we find that  $\mathcal{H}^{\Phi/2}(k_1, k_2) = \mathcal{H}^{\Phi/2}(k_1 + 2\pi, k_2) = \mathcal{H}^{\Phi/2}(k_1, k_2 + \pi)$ . In other words, the embedding matrices that enforce the magnetic BZ periodicity are trivial. This is due to the choice of the eigenbasis in Eq. (D10), which differ from the bases we considered in Eq. (A40) in the Landau gauge. Hence, we have

$$\mathcal{B}_{(-\kappa_1/2 - \tilde{k}_1, -\kappa_2/2 + \pi/2)}^{ij} = \mathcal{B}_{(-\kappa_1/2 - \tilde{k}_1, -\kappa_2/2 - \pi/2)}^{ij} . \quad (\text{D48})$$

Returning to Eq. (D47) with this result, we find

$$\tilde{W}^{\Phi/2}(\tilde{k}_1) = \mathcal{B}_{(-\kappa_1/2 - \tilde{k}_1, -\kappa_2/2 - \pi/2)} [\tilde{W}^{\Phi/2}(-\tilde{k}_1)]^T \mathcal{B}_{(-\kappa_1/2 - \tilde{k}_1, -\kappa_2/2 - \pi/2)}^\dagger . \quad (\text{D49})$$

We define the eigenvalues of  $\tilde{W}^{\Phi/2}(\tilde{k}_1)$  as  $\{\exp i\tilde{\vartheta}_j(\tilde{k}_1)\}$ . Using Eq. (D49), we find the usual constraint on the Wannier centers:

$$\{\tilde{\vartheta}_j(\tilde{k}_1)\} = \{\tilde{\vartheta}_j(-\tilde{k}_1)\} \quad (\text{D50})$$

emphasizing that  $\tilde{k}_1$  is the coordinate measured from  $-\kappa/2$ , i.e.  $\tilde{\vartheta}_j(\tilde{k}_1)$  is the Wilson eigenvalue of the loop at  $-\kappa/2 + \tilde{k}_1 \mathbf{b}_1$ . By re-centering the magnetic BZ around  $-\kappa/2$ , we have found that the  $UT$  symmetry behaves like  $\mathcal{T}$  at  $\phi = 0$  on the shifted Wilson loop  $\tilde{W}(\tilde{k}_1)$ . We now study the constraint on the Wilson loop spectrum due to the  $\Phi/2$  periodicity of  $k_1$  (recalling that we take  $n$  odd here). From Eq. (D6), we have

$$V_1(\Phi/2, k_2) \mathcal{H}^{\Phi/2}(\mathbf{k}) V_1^\dagger(\Phi/2, k_2) = \mathcal{H}^{\Phi/2}(\mathbf{k} + \pi \mathbf{b}_1) . \quad (\text{D51})$$

Following App. C1, we now form the unitary sewing matrix

$$B_{\mathbf{k}}^{ij} = \langle u_i^{\Phi/2}(\mathbf{k} + \pi \mathbf{b}_1) | V_1(\Phi/2, k_2) | u_j^{\Phi/2}(\mathbf{k}) \rangle \quad (\text{D52})$$

which is not to be confused with  $\mathcal{B}_{\mathbf{k}}$ , the sewing matrix for  $UT$  defined in Eq. (D43).  $B_{\mathbf{k}}$  which connects eigenstates that are  $\pi \mathbf{b}_1$  apart [46]:

$$|u_j^{\Phi/2}(\mathbf{k})\rangle = \sum_i V_1(\Phi/2, k_2) |u_i^{\Phi/2}(\mathbf{k} + \pi \mathbf{b}_1)\rangle [B_{\mathbf{k} + \pi \mathbf{b}_1}^\dagger]^{ij} . \quad (\text{D53})$$

Following the same discussion in Eq. (D45), we find

$$\tilde{W}^{\Phi/2}(\tilde{k}_1) = B_{(-\kappa_1/2 + \tilde{k}_1 + \pi, -\kappa_2/2 + \pi/2)} \tilde{W}^{\Phi/2}(\tilde{k}_1 + \pi) B_{(-\kappa_1/2 + \tilde{k}_1 + \pi, -\kappa_2/2 - \pi/2)}^\dagger . \quad (\text{D54})$$

The two embedding matrices  $B_{\mathbf{k}}$  and  $B_{\mathbf{k} - \pi \mathbf{b}_2}$  are identical:

$$\begin{aligned} B_{\mathbf{k} - \pi \mathbf{b}_2}^{ij} &= \langle u_i^{\Phi/2}(\mathbf{k} + \pi \mathbf{b}_1 - \pi \mathbf{b}_2) | V_1(\Phi/2, k_2 - \pi) | u_j^{\Phi/2}(\mathbf{k} - \pi \mathbf{b}_2) \rangle \\ &= \langle u_i^{\Phi/2}(\mathbf{k} + \pi \mathbf{b}_1) | V_1(\Phi/2, k_2) | u_j^{\Phi/2}(\mathbf{k}) \rangle \\ &= B_{\mathbf{k}}^{ij} \end{aligned} \quad (\text{D55})$$

where we have used that the eigenstates (Eq. (D10)) and the embedding matrix  $V_1(\Phi/2, k_2)$  are periodic in  $\pi \mathbf{b}_2$ , as we can see from App. D2 b. Thus in the basis of Eq. (D10), we find that Eq. (D54) enforces

$$\{\tilde{\vartheta}_j(\tilde{k}_1)\} = \{\tilde{\vartheta}_j(\tilde{k}_1 + \pi)\} \quad (\text{D56})$$

which is in contrast to Eq. (C12), which was performed in the Landau gauge. This is due to a different choice of eigenstates. In the Landau gauge, we chose to diagonalize the Hamiltonian in the basis of Eq. (A40) on which  $T_1(0)$  was diagonal (see App. A7). In contrast, the basis constructed in Eq. (D10) is diagonal under  $T_1(\Phi/2)$ .

#### b. $\mathbb{Z}_2$ Index from the Wilson Loop

We will now see that, given Eqs. (D50) and (D56), the  $\mathbb{Z}_2$  invariant must be trivial. Ref. [36] provides the following method of calculating  $\delta^{\phi = \Phi/2}$  from the Wilson loop eigenvalues. Draw an arbitrary line of arbitrary constant

$\tilde{\vartheta}(\tilde{k}_1) = \tilde{\vartheta}^*$  through the *half* Wilson spectrum  $\{\tilde{\vartheta}_j(\tilde{k}_1)\}$ ,  $\tilde{k}_1 \in (-\pi, 0)$  and count the number of times it crosses the Wilson bands;  $\delta^{\phi=\Phi/2}$  is trivial if there are an even number of crossings, and non-trivial if there are an odd number. We emphasize  $\tilde{\mathbf{k}}$  refers to the momentum  $\mathbf{k} = -\boldsymbol{\kappa}/2 + \tilde{\mathbf{k}}$  in the magnetic BZ. We will prove that all crossings of the Wilson loop spectrum with the arbitrary line  $\tilde{\vartheta}'$  occur in pairs, and hence  $\delta^{\phi=\Phi/2}$  is trivial.

Suppose a crossing occurs at the point  $(\tilde{k}_1^*, \tilde{\vartheta}^*)$  with  $\tilde{k}_1^* \in (-\pi, 0)$ , so there is a Wilson band satisfying  $\tilde{\vartheta}(\tilde{k}_1^*) = \tilde{\vartheta}^*$ . By  $U\mathcal{T}$ , Eq. (D50) ensures there is also a band satisfying  $\tilde{\vartheta}(-\tilde{k}_1^*) = \tilde{\vartheta}^*$ . Then, using Eq. (D50), there are bands satisfying  $\tilde{\vartheta}(-\tilde{k}_1^* - \pi) = \tilde{\vartheta}^*$  and  $\tilde{\vartheta}(\tilde{k}_1^* + \pi) = \tilde{\vartheta}^*$ . Note that generically,  $\tilde{k}_1^*$  and  $-\tilde{k}_1^* - \pi$  are distinct points and  $-\tilde{k}_1^* - \pi \in (-\pi, 0)$  (see Fig. 12). Thus each crossing at  $\tilde{k}_1^*$  comes with a partner at  $-\tilde{k}_1^* - \pi$  and the total number of crossing in the half spectrum  $\tilde{k}_1 \in (-\pi, 0)$  must be even. We can always avoid a crossing at the degenerate point  $\tilde{k}_1^* = -\pi/2 = -\tilde{k}_1^* - \pi$  where this argument breaks down by changing  $\tilde{\vartheta}^*$ , since it is arbitrary.

## Appendix E: $C_{2z}\mathcal{T}$ symmetry

In this Appendix, we discuss the Hofstadter topological phases protected by  $C_{2z}\mathcal{T}$  symmetry. First, we demonstrate that  $(UC_{2z}\mathcal{T})^2 = \pm(C_{2z}\mathcal{T})^2$  where the sign is determined by an integral along Peierls paths (App. E1). We discuss the topological invariants in both cases. If  $(UC_{2z}\mathcal{T})^2 = +1$ , the  $w_2$  invariant at  $\Phi/2$  can be calculated in an expanded unit cell where  $U$  is diagonal in momentum space (App. E2). When  $(UC_{2z}\mathcal{T})^2 = -1$ , we argue the phase must be trivial in real space, and then calculate the nested Wilson loop to show the triviality explicitly (App. E3).

### 1. Symmetry Properties

In Sec. , we consider Hamiltonians with the symmetry  $C_{2z}\mathcal{T}$  at  $\phi = 0$  which satisfies  $(C_{2z}\mathcal{T})^2 = +1$ . At  $\phi = \Phi/2$ , the symmetry of  $H^{\Phi/2}$  is  $UC_{2z}\mathcal{T}$ , which may square to either  $\pm 1$ . We derive a formula for this sign as follows. First, the action of  $C_{2z}$  on the annihilation operator reads

$$C_{2z}^\dagger c_{\mathbf{R},\alpha} C_{2z} = \sum_{\beta} D_{\alpha\beta}(C_{2z}) c_{-\mathbf{R}-\boldsymbol{\delta}_\alpha-\boldsymbol{\delta}_{\beta},\beta} \quad (\text{E1})$$

where  $D_{\alpha\beta}(C_{2z}) = 0$  if  $\boldsymbol{\delta}_\alpha - C_{2z}\boldsymbol{\delta}_\beta = \boldsymbol{\delta}_\alpha + \boldsymbol{\delta}_\beta$  is not a lattice vector. We let  $U = e^{i\mathcal{O}}$  as defined by Eq. (A5), and then compute

$$\begin{aligned} C_{2z}\mathcal{O} &= C_{2z} \sum_{\mathbf{R}\beta} c_{\mathbf{R},\beta}^\dagger c_{\mathbf{R},\beta} \int_{\mathbf{r}_0}^{\mathbf{R}+\boldsymbol{\delta}_\beta} \tilde{\mathbf{A}} \cdot d\mathbf{r}, \\ &= \sum_{\mathbf{R}\beta} C_{2z} c_{\mathbf{R},\beta}^\dagger C_{2z}^\dagger C_{2z} c_{\mathbf{R},\beta} C_{2z}^\dagger C_{2z} \int_{\mathbf{r}_0}^{\mathbf{R}+\boldsymbol{\delta}_\beta} \tilde{\mathbf{A}} \cdot d\mathbf{r} \\ &= \left( \sum_{\mathbf{R}\beta\beta'\beta''} c_{-\mathbf{R}-\boldsymbol{\delta}_\beta-\boldsymbol{\delta}_{\beta'},\beta'}^\dagger [D(C_{2z})^\dagger]_{\beta'\beta} [D(C_{2z})]_{\beta\beta''} c_{-\mathbf{R}-\boldsymbol{\delta}_\beta-\boldsymbol{\delta}_{\beta''),\beta''} \int_{\mathbf{r}_0}^{\mathbf{R}+\boldsymbol{\delta}_\beta} \tilde{\mathbf{A}} \cdot d\mathbf{r} \right) C_{2z} \end{aligned} \quad (\text{E2})$$

where  $\nabla \times \tilde{\mathbf{A}} = \Phi$  and the integral is taken along Peierls paths. Now we take  $-\mathbf{R} - \boldsymbol{\delta}_\beta - \boldsymbol{\delta}_{\beta'} \rightarrow \mathbf{R}$  by relabeling the sum. This takes  $c_{-\mathbf{R}-\boldsymbol{\delta}_\beta-\boldsymbol{\delta}_{\beta''),\beta''} \rightarrow c_{\mathbf{R}+\boldsymbol{\delta}_{\beta'}-\boldsymbol{\delta}_{\beta''),\beta''}$ . But because  $[D(C_{2z})^\dagger]_{\beta'\beta} [D(C_{2z})]_{\beta\beta''}$  is only nonzero when  $\boldsymbol{\delta}_{\beta'} - \boldsymbol{\delta}_{\beta''} = 0$  by unitarity, we have

$$\begin{aligned} C_{2z}\mathcal{O} &= \left( \sum_{\mathbf{R}\beta\beta'\beta''} c_{\mathbf{R},\beta'}^\dagger [D(C_{2z})^\dagger]_{\beta'\beta} [D(C_{2z})]_{\beta\beta''} c_{\mathbf{R},\beta''} \int_{\mathbf{r}_0}^{-\mathbf{R}-\boldsymbol{\delta}_\beta-\boldsymbol{\delta}_{\beta'}+\boldsymbol{\delta}_\beta} \tilde{\mathbf{A}} \cdot d\mathbf{r} \right) C_{2z} \\ &= \left( \sum_{\mathbf{R}\beta'\beta''} c_{\mathbf{R},\beta'}^\dagger \left( \sum_{\beta} [D(C_{2z})^\dagger]_{\beta'\beta} [D(C_{2z})]_{\beta\beta''} \right) c_{\mathbf{R},\beta''} \int_{\mathbf{r}_0}^{-\mathbf{R}-\boldsymbol{\delta}_{\beta'}} \tilde{\mathbf{A}} \cdot d\mathbf{r} \right) C_{2z} \\ &= \left( \sum_{\mathbf{R}\beta'} c_{\mathbf{R},\beta'}^\dagger c_{\mathbf{R},\beta'} \int_{\mathbf{r}_0}^{-\mathbf{R}-\boldsymbol{\delta}_{\beta'}} \tilde{\mathbf{A}} \cdot d\mathbf{r} \right) C_{2z}. \end{aligned} \quad (\text{E3})$$



We recall for the reader that  $\tilde{\mathbf{A}}$  is a gauge field generating  $\Phi$  flux. Hence, from Eq. (A4), we can deform the integral along Peierls paths to find

$$\int_{\mathbf{r}_0}^{-\mathbf{R}-\boldsymbol{\delta}_{\beta'}} \tilde{\mathbf{A}} \cdot d\mathbf{r} = \left( \int_{-\mathbf{r}_0}^{-\mathbf{R}-\boldsymbol{\delta}_{\beta'}} + \int_{\mathbf{r}_0}^{-\mathbf{r}_0} \right) \tilde{\mathbf{A}} \cdot d\mathbf{r} \pmod{2\pi}. \quad (\text{E4})$$

By a change of variables in the integral  $\mathbf{r} = -\mathbf{s}$ , we establish

$$\int_{-\mathbf{r}_0}^{-\mathbf{R}-\boldsymbol{\delta}_{\beta'}} \tilde{\mathbf{A}}(\mathbf{r}) \cdot d\mathbf{r} = \int_{\mathbf{r}_0}^{\mathbf{R}+\boldsymbol{\delta}_{\beta'}} \tilde{\mathbf{A}}(-\mathbf{s}) \cdot d(-\mathbf{s}) = \int_{\mathbf{r}_0}^{\mathbf{R}+\boldsymbol{\delta}_{\beta'}} \tilde{\mathbf{A}}(\mathbf{s}) \cdot d\mathbf{s} \quad (\text{E5})$$

where we have used that  $\tilde{\mathbf{A}}(\mathbf{r})$  is an odd function of  $\mathbf{r}$ . This allows us to write

$$\begin{aligned} C_{2z}\mathcal{O} &= \left( \mathcal{O} + \left[ \int_{\mathbf{r}_0}^{-\mathbf{r}_0} \tilde{\mathbf{A}} \cdot d\mathbf{r} \right] \sum_{\mathbf{R},\beta} c_{\mathbf{R},\beta}^\dagger c_{\mathbf{R},\beta} \right) C_{2z}, \\ &= \left( \mathcal{O} + \left[ \int_{\mathbf{r}_0}^{-\mathbf{r}_0} \tilde{\mathbf{A}} \cdot d\mathbf{r} \right] N \right) C_{2z}, \end{aligned} \quad (\text{E6})$$

where  $N$  is the total number of electrons in the many-body state. In this work, we study single-particle physics where  $N = 1$ . In this case, we exponentiate Eq. (E6) to find

$$\begin{aligned} C_{2z}U &= C_{2z} \sum_{n=0}^{\infty} \frac{1}{n!} (i\mathcal{O})^n \\ &= \sum_{n=0}^{\infty} \frac{1}{n!} i^n \left( \mathcal{O} + \left[ \int_{\mathbf{r}_0}^{-\mathbf{r}_0} \tilde{\mathbf{A}} \cdot d\mathbf{r} \right] \right)^n C_{2z} \\ &= \exp \left( i\mathcal{O} + i \left[ \int_{\mathbf{r}_0}^{-\mathbf{r}_0} \tilde{\mathbf{A}} \cdot d\mathbf{r} \right] \right) C_{2z} \\ &= \exp \left( i \int_{\mathbf{r}_0}^{-\mathbf{r}_0} \tilde{\mathbf{A}} \cdot d\mathbf{r} \right) UC_{2z} \end{aligned} \quad (\text{E7})$$

where in the last line we use that  $\mathcal{O}$  commutes with the  $c$ -number  $i \int_{\mathbf{r}_0}^{-\mathbf{r}_0} \tilde{\mathbf{A}} \cdot d\mathbf{r}$ . Using Eq. (E7) and the relation  $\mathcal{T}U = U^\dagger\mathcal{T}$  (see Eq. (D3)), we find

$$\begin{aligned} (UC_{2z}\mathcal{T})^2 &= UC_{2z}\mathcal{T}UC_{2z}\mathcal{T} \\ &= UC_{2z}U^\dagger\mathcal{T}C_{2z}\mathcal{T} \\ &= \exp \left( -i \int_{\mathbf{r}_0}^{-\mathbf{r}_0} \tilde{\mathbf{A}} \cdot d\mathbf{r} \right) C_{2z}UU^\dagger\mathcal{T}C_{2z}\mathcal{T} \\ &= \exp \left( -i \int_{\mathbf{r}_0}^{-\mathbf{r}_0} \tilde{\mathbf{A}} \cdot d\mathbf{r} \right) C_{2z}\mathcal{T}C_{2z}\mathcal{T} \\ &= \exp \left( -i \int_{\mathbf{r}_0}^{-\mathbf{r}_0} \tilde{\mathbf{A}} \cdot d\mathbf{r} \right) (C_{2z}\mathcal{T})^2. \end{aligned} \quad (\text{E8})$$

We recall that the integrals must be taken along the Peierls paths, and  $\mathbf{r}_0$  is a fixed but arbitrary orbital of the Hamiltonian (see Eq. (A5)). Additionally, in defining  $C_{2z}$ , we have fixed the origin of the lattice to coincide with the  $C_{2z}$ -symmetric point of  $\tilde{\mathbf{A}}$ , i.e.  $\tilde{\mathbf{A}}(C_{2z}\mathbf{r}) = -\tilde{\mathbf{A}}(\mathbf{r})$ . This fixes the origin of the lattice, so we cannot redefine  $\mathbf{r}_0$ . Eq. (E8) demonstrates that  $(UC_{2z}\mathcal{T})^2$  may differ from  $(C_{2z}\mathcal{T})^2 = 1$  by a phase

$$\gamma_2 = \int_{\mathbf{r}_0}^{-\mathbf{r}_0} \tilde{\mathbf{A}} \cdot d\mathbf{r} \pmod{2\pi} \quad (\text{E9})$$

that depends only on the Peierls paths and orbitals of the Hamiltonian. It is simple to determine  $\gamma_2$  by direct computation for a given model. But we show first that  $\gamma_2$  may only take the value 0 or  $\pi$ , on the condition that the

Peierls paths of the model are themselves  $C_{2z}$ -symmetric. Let the path  $\mathcal{C}_1$  consist of Peierls paths connecting  $\mathbf{r}_0$  to  $C_{2z}\mathbf{r}_0 = -\mathbf{r}_0$ , and define  $\mathcal{C}_2 = C_{2z}\mathcal{C}_1$  which connects  $-\mathbf{r}_0$  to  $\mathbf{r}_0$ . By the same change of variables, we have that

$$\int_{\mathcal{C}_2} \tilde{\mathbf{A}} \cdot d\mathbf{r} = \int_{C_{2z}\mathcal{C}_1} \tilde{\mathbf{A}} \cdot d\mathbf{r} = \int_{\mathcal{C}_1} -\tilde{\mathbf{A}} \cdot d(-\mathbf{r}) = \int_{\mathcal{C}_1} \tilde{\mathbf{A}} \cdot d\mathbf{r} . \quad (\text{E10})$$

With this result, it is also true that

$$\oint_{\mathcal{C}_1+\mathcal{C}_2} \tilde{\mathbf{A}} \cdot d\mathbf{r} = \int_{\mathcal{C}_1} \tilde{\mathbf{A}} \cdot d\mathbf{r} + \int_{\mathcal{C}_2} \tilde{\mathbf{A}} \cdot d\mathbf{r} = 2 \int_{\mathcal{C}_1} \tilde{\mathbf{A}} \cdot d\mathbf{r} . \quad (\text{E11})$$

Because  $\mathcal{C}_1$  and  $\mathcal{C}_2$  are both Peierls paths,  $\mathcal{C}_1 + \mathcal{C}_2 = \partial\mathcal{R}$  is a closed loop taken along Peierls paths, and thus

$$2 \int_{\mathbf{r}_0}^{-\mathbf{r}_0} \tilde{\mathbf{A}} \cdot d\mathbf{r} = \oint_{\partial\mathcal{R}} \tilde{\mathbf{A}} \cdot d\mathbf{r} = \int_{\mathcal{R}} \Phi dS \in 2\pi\mathbb{Z} \quad (\text{E12})$$

where we have used that  $\nabla \times \tilde{\mathbf{A}} = \Phi$  and, by the definition of  $\Phi$ , all closed loops along Peierls' paths enclose an integer multiple of  $2\pi$  flux. Hence find that  $\int_{\mathbf{r}_0}^{-\mathbf{r}_0} \tilde{\mathbf{A}} \cdot d\mathbf{r}$  is a multiple of  $\pi$  and thus the phase is quantized to be 0 or  $\pi$ .

The phase  $\gamma_2$  may be calculated to determine the sign of  $(UC_{2z}\mathcal{T})^2$ . In some cases however, it may be determined more simply. For instance, if there is an orbital on the  $1a = (0,0)$  position, we may choose  $\mathbf{r}_0 = (0,0)$  in which case the integration path vanishes and  $\gamma_2$  must be zero. More generally, if there are *any* Peierls paths that connect  $\mathbf{r}_0$  to the origin, then we can break up the integral into  $C_{2z}$ -symmetric parts:

$$\gamma_2 = \int_{\mathbf{r}_0}^{-\mathbf{r}_0} \tilde{\mathbf{A}} \cdot d\mathbf{r} = \int_{\mathbf{r}_0}^0 \tilde{\mathbf{A}} \cdot d\mathbf{r} + \int_0^{-\mathbf{r}_0} \tilde{\mathbf{A}} \cdot d\mathbf{r} = - \int_0^{\mathbf{r}_0} \tilde{\mathbf{A}} \cdot d\mathbf{r} + \int_0^{-\mathbf{r}_0} \tilde{\mathbf{A}} \cdot d\mathbf{r} = - \int_0^{\mathbf{r}_0} \tilde{\mathbf{A}} \cdot d\mathbf{r} + \int_0^{\mathbf{r}_0} \tilde{\mathbf{A}} \cdot d\mathbf{r} = 0 . \quad (\text{E13})$$

We find that if the origin may be reached along Peierls path, then the phase is also forced to be zero. (We emphasize that at  $\phi = \Phi$ , integrals may be arbitrarily deformed along Peierls paths.) For the the QSH model of App. F 1, orbitals lie on the  $1a$  position so the phase is trivial, and in the model of twisted bilayer graphene discussed in App. G 1, the Peierls paths are taken through the origin as shown in Fig. 15a, so the phase must also be trivial. To furnish an example where the phase is  $\pi$ , we consider an alternative model of TBG in Ref. [49] that is identical to our model of TBG *except* for the choice of Peierls' paths. In the alternative model, the Peierls paths are taken along the bonds, so that  $\Phi = 2\pi$ , as shown in Fig. 15b. We can calculate  $\gamma_2$  directly via Eq. (E9). We choose  $\mathbf{r}_0 = \frac{1}{2}\boldsymbol{\delta}_1 - \frac{1}{2}\mathbf{a}_1$ , the same as in Fig. 16, and calculate

$$\begin{aligned} \gamma_2 &= \int_{\mathbf{r}_0}^{-\mathbf{r}_0} \tilde{\mathbf{A}} \cdot m\mathbf{r} \quad \text{mod } 2\pi \\ &= \pi \end{aligned} \quad (\text{E14})$$

where the path of integration (which is arbitrary as long as it is taken along Peierls paths) is shown in Fig. 15b. This emphasizes once more that the Peierls paths are physical. Different Peierls paths in the TBG model lead to different values of  $\gamma_2$ , giving  $(UC_{2z}\mathcal{T})^2 = \pm(C_{2z}\mathcal{T})^2$ . In general,  $\gamma_2$  may be simply calculated from Eq. (E9) for any model. In coming work (Ref. [60]), we will show that similar phases  $\gamma_n$  characterize the algebra of general  $UC_n\mathcal{T}$ -symmetric point groups at high symmetry Wyckoff positions.

The sign of  $(UC_{2z}\mathcal{T})^2$  has important physical consequences. If  $(UC_{2z}\mathcal{T})^2 = +1$ , then  $UC_{2z}\mathcal{T}$  protects a  $w_2$  invariant at  $\phi = \Phi/2$  in the same way as  $C_{2z}\mathcal{T}$  protects a  $w_2$  invariant at  $\phi = 0$ . We discuss how to compute this invariant in App. E 2. If  $(UC_{2z}\mathcal{T})^2 = -1$ , then there is no  $w_2$  invariant [39]. In this case, we show in App. E 3 using the nested Wilson and the 10 Fold Way that there is *no nontrivial phase* protected by  $UC_{2z}\mathcal{T}$ , and hence  $H^{\phi=\Phi/2}$  is trivial.

## 2. Calculation of the $w_2$ invariant at $(UC_{2z}\mathcal{T})^2 = +1$

In this section, we show how to use the Wilson loop to compute the  $w_2$  index of  $H^{\phi=\Phi/2}$ . We work in the Landau gauge, which is best suited for explicit calculations. Recall from Ref. [39] that  $w_2$  may be computed at  $\phi = 0$  from the Wilson loop spectrum, which is ‘‘particle-hole’’ symmetric thanks to  $C_{2z}\mathcal{T}$  [13]. We can follow the same protocol at  $\phi = \Phi/2$ , but we will find that  $U$  acts off-diagonally in momentum space and changes the symmetries of the Wilson spectrum.

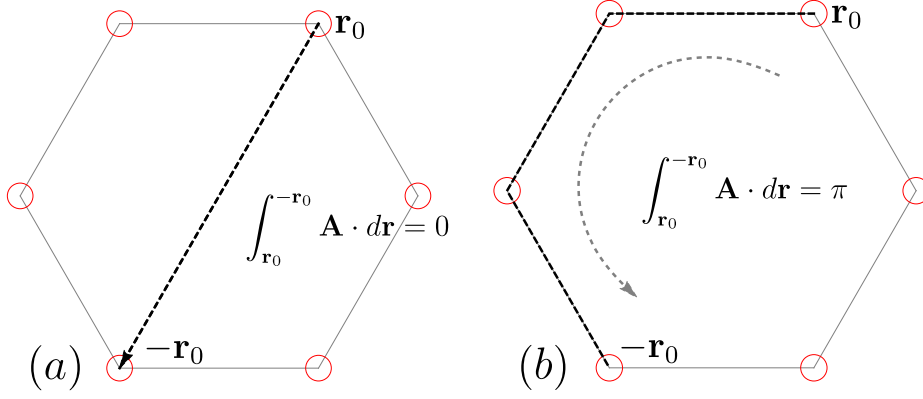


FIG. 15. We show the Peierls paths joining  $\mathbf{r}_0$  and  $-\mathbf{r}_0$  in (a) our model of twisted bilayer graphene and (b) an alternative model discussed in Ref. [49] where Peierls paths are taken along the bonds of the lattice. The different Peierls paths lead to different values of  $\gamma_2$ :  $+1$  (resp.  $-1$ ) in the case of our model (resp. the alternative model).

### a. Construction of the Extended unit cell

To compute  $w_2$  in the conventional way, we must construct  $U$  in an *extended* unit cell where it is diagonal in momentum space. We begin with the expression for  $U$  in a single-particle Hilbert space:

$$U = \sum_{\mathbf{R}\alpha} \exp\left(i \int_{\mathbf{r}_0}^{\mathbf{R}+\delta_\alpha} \tilde{\mathbf{A}} \cdot d\mathbf{r}\right) |\mathbf{R}, \alpha\rangle \langle \mathbf{R}, \alpha|, \quad \nabla \times \tilde{\mathbf{A}} = \Phi, \quad (\text{E15})$$

as is rewritten from Eq. (2) of the Main Text. Recall that the integral is taken along Peierls paths and is single-valued mod  $2\pi$ . Here we have used the single-particle bases  $|\mathbf{R}, \alpha\rangle = c_{\mathbf{R}, \alpha}^\dagger |0\rangle$ . To derive the action of  $U$  on the Hofstadter Hamiltonian  $\mathcal{H}^{\phi=\Phi/2}(\mathbf{k})$  in the Landau gauge, we could Fourier transform  $U$  over the  $1 \times q'$  unit cell at  $\phi = \Phi/2$ , where  $\phi = \mu \frac{2\pi p'}{q}$  as discussed in App. A 7. (The gauge-independent formalism introduced in App. D 2 b which ensures a  $1 \times q$  magnetic unit cell is not suited to doing numerical calculations. Thus we will rely on the Landau gauge (see App. A 7) to numerically evaluate the Wilson loop and  $w_2^{\phi=\Phi/2}$ .) However, this generically results in an expression for  $U$  that is off-diagonal in momentum space because the positionally-dependent phase in Eq. (E15) does not generically share the  $1 \times q'$  periodicity of  $H^{\phi=\Phi/2}$ . Our tactic is to find an extended  $\lambda_1 \times \lambda_2$  unit cell where  $U$  is diagonal in momentum space. Then  $UC_{2z}\mathcal{T}$  acts diagonally on the eigenstates of  $\mathcal{H}^{\phi=\Phi/2}$  when we work in a *new*  $\lambda_1 \times \frac{q'\lambda_2}{\text{gcd}(q', \lambda_2)}$  magnetic unit cell which is commensurate with the  $1 \times q'$  magnetic unit cell and the  $\lambda_1 \times \lambda_2$  unit cell where  $U$  is diagonal in momentum space.

First, we will determine in what unit cell  $U$  is diagonal in momentum space *irrespective* of  $\phi$ . Note that  $\exp(i \int_{\mathbf{r}_0}^{\mathbf{R}+\delta_\alpha} \tilde{\mathbf{A}} \cdot d\mathbf{r})$  is a single-valued function of  $\mathbf{R}$  on the lattice by the definition of  $\Phi$  (see App. A 2) and is periodic in  $\mathbf{R}$  due to the assumption of commensurate orbitals (see App. A 4). Hence it has some minimal spatial periodicity  $(\lambda_1, \lambda_2)$  with  $\lambda_1, \lambda_2 \in \mathbb{N}$  given by

$$\int_{\mathbf{r}_0}^{\lambda_1 \mathbf{a}_1 + \mathbf{R} + \delta_\alpha} \tilde{\mathbf{A}} \cdot d\mathbf{r} = \int_{\mathbf{r}_0}^{\lambda_2 \mathbf{a}_2 + \mathbf{R} + \delta_\alpha} \tilde{\mathbf{A}} \cdot d\mathbf{r} = \int_{\mathbf{r}_0}^{\mathbf{R} + \delta_\alpha} \tilde{\mathbf{A}} \cdot d\mathbf{r} \quad \text{mod } 2\pi, \quad \forall \alpha = 1, \dots, N_{orb} \quad (\text{E16})$$

with  $\mathbf{R}$  being any lattice vector. (Although it is not necessary for any of the following calculations, we can show that  $\lambda_i$  is the denominator of  $\kappa_i$ , defined in Eqs. (D30) and (D31), i.e.  $\lambda_i \kappa_i = 0 \pmod{2\pi}$ . From this perspective, the magnetic unit cell is extended so translations by  $\lambda_i \mathbf{a}_i$  commute with  $U\mathcal{T}$ , as we see from Eq. (D39).) When we Fourier transform over the Bravais lattice composed of the enlarged  $\lambda_1 \times \lambda_2$  unit cells, the BZ shrinks to  $k_1 \in (-\frac{\pi}{\lambda_1}, \frac{\pi}{\lambda_1})$ ,  $k_2 \in (-\frac{\pi}{\lambda_2}, \frac{\pi}{\lambda_2})$  which we label as  $BZ_\lambda$ . In this unit cell, the position bases are defined

$$|r_1, r_2, \ell_1, \ell_2, \alpha\rangle = c_{(\lambda_1 r_1 + \ell_1) \mathbf{a}_1 + (\lambda_2 r_2 + \ell_2) \mathbf{a}_2, \alpha}^\dagger |0\rangle, \quad \ell_1 = 0, \dots, \lambda_1 - 1, \ell_2 = 0, \dots, \lambda_2 - 1. \quad (\text{E17})$$

The momentum eigenstates are then defined by

$$|r_1, r_2, \ell_1, \ell_2, \alpha\rangle = \frac{1}{\sqrt{\mathcal{N}/\lambda_1 \lambda_2}} \sum_{k_1, k_2 \in BZ_\lambda} e^{i(k_1 \mathbf{b}_1 + k_2 \mathbf{b}_2) \cdot ((\lambda_1 r_1 + \ell_1) \mathbf{a}_1 + (\lambda_2 r_2 + \ell_2) \mathbf{a}_2 + \delta_\alpha)} |k_1, k_2, \ell, \alpha\rangle, \quad (\text{E18})$$

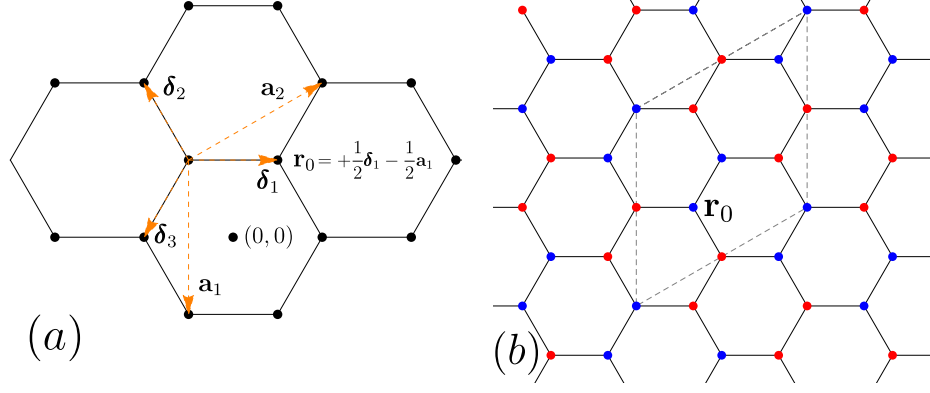


FIG. 16. (a) We show the lattice vectors  $\mathbf{a}_i$  and the nearest-neighbor vectors  $\delta_i$  for the TBG model of App. G1. The atomic sites are located at  $\pm\frac{1}{2}\delta_1 - \frac{1}{2}\mathbf{a}_1$  modulo lattice vectors, and we fix  $\mathbf{r}_0 = \frac{1}{2}\delta_1 - \frac{1}{2}\mathbf{a}_1$ . (b) We depict the value of Eq. (E22) on the lattice, with a value of +1 (−1) corresponding to blue (red). We outline the  $2 \times 2$  unit cell in dashed, gray lines which indicates the periodicity of  $U$ .

where  $\mathcal{N}$  is the number of  $1 \times 1$  unit cells in the lattice. We may now compute

$$\begin{aligned}
U &= \sum_{r_1, r_2, \ell_1, \ell_2, \alpha} \exp\left(i \int_{\mathbf{r}_0}^{(\lambda_1 r_1 + \ell_1)\mathbf{a}_1 + (\lambda_2 r_2 + \ell_2)\mathbf{a}_2 + \delta_\alpha} \tilde{\mathbf{A}} \cdot d\mathbf{r}\right) |r_1, r_2, \ell_1, \ell_2, \alpha\rangle \langle r_1, r_2, \ell_1, \ell_2, \alpha| \\
&= \frac{1}{\mathcal{N}/\lambda_1\lambda_2} \sum_{\mathbf{k}, \mathbf{k}' \in BZ_\lambda, \ell_1, \ell_2, \alpha} |\mathbf{k}, \ell_1, \ell_2, \alpha\rangle \langle \mathbf{k}', \ell_1, \ell_2, \alpha| \times \\
&\quad \left[ \sum_{r_1, r_2} \exp(i(\mathbf{k} - \mathbf{k}') \cdot ((\lambda_1 r_1 + \ell_1)\mathbf{a}_1 + (\lambda_2 r_2 + \ell_2)\mathbf{a}_2 + \delta_\alpha)) \exp\left(i \int_{\mathbf{r}_0}^{(\lambda_1 r_1 + \ell_1)\mathbf{a}_1 + (\lambda_2 r_2 + \ell_2)\mathbf{a}_2 + \delta_\alpha} \tilde{\mathbf{A}} \cdot d\mathbf{r}\right) \right] \\
&= \frac{1}{\mathcal{N}/\lambda_1\lambda_2} \sum_{\mathbf{k}, \mathbf{k}' \in BZ_\lambda, \ell_1, \ell_2, \alpha} |\mathbf{k}, \ell_1, \ell_2, \alpha\rangle \langle \mathbf{k}', \ell_1, \ell_2, \alpha| \times \\
&\quad \left[ \sum_{r_1, r_2} \exp(i(\mathbf{k} - \mathbf{k}') \cdot ((\lambda_1 r_1 + \ell_1)\mathbf{a}_1 + (\lambda_2 r_2 + \ell_2)\mathbf{a}_2 + \delta_\alpha)) \exp\left(i \int_{\mathbf{r}_0}^{\ell_1\mathbf{a}_1 + \ell_2\mathbf{a}_2 + \delta_\alpha} \tilde{\mathbf{A}} \cdot d\mathbf{r}\right) \right]
\end{aligned} \tag{E19}$$

where we have used Eq. (E16) to remove the  $r_1, r_2$  dependence of the integral. Then the sum in brackets can be explicitly evaluated and we find

$$\begin{aligned}
U &= \frac{1}{\mathcal{N}/(\lambda_1\lambda_2)} \sum_{\mathbf{k}, \mathbf{k}' \in BZ_\lambda, \ell_1, \ell_2, \alpha} |\mathbf{k}, \ell_1, \ell_2, \alpha\rangle \langle \mathbf{k}', \ell_1, \ell_2, \alpha| e^{i \int_{\mathbf{r}_0}^{\ell_1\mathbf{a}_1 + \ell_2\mathbf{a}_2 + \delta_\alpha} \tilde{\mathbf{A}} \cdot d\mathbf{r} + i(\mathbf{k} - \mathbf{k}') \cdot (\ell_1\mathbf{a}_1 + \ell_2\mathbf{a}_2 + \delta_\alpha)} \times \\
&\quad \sum_{r_1, r_2} e^{i(\mathbf{k} - \mathbf{k}') \cdot (\lambda_1 r_1 \mathbf{a}_1 + \lambda_2 r_2 \mathbf{a}_2)} \\
&= \sum_{\mathbf{k} \in BZ'} \sum_{\ell_1, \ell_2, \alpha} \mathcal{U}_{\ell_1, \ell_2, \alpha} |\mathbf{k}, \ell_1, \ell_2, \alpha\rangle \langle \mathbf{k}, \ell_1, \ell_2, \alpha|, \quad \mathcal{U}_{\ell_1, \ell_2, \alpha} = e^{i \int_{\mathbf{r}_0}^{\ell_1\mathbf{a}_1 + \ell_2\mathbf{a}_2 + \delta_\alpha} \tilde{\mathbf{A}} \cdot d\mathbf{r}}.
\end{aligned} \tag{E20}$$

We see explicitly that  $U$  is diagonal in momentum space in the  $\lambda_1 \times \lambda_2$  unit cell.

We now give an example of this calculation for model of twisted bilayer graphene (introduced in detail in App. G1). In fact, we will use this expression for  $U$  in momentum space later for Wilson loop calculations in App. G3. We recall that the nearest-neighbor vectors of the honeycomb lattice are  $\delta_\alpha$ ,  $\alpha = 1, 2, 3$  (as shown for convenience in Fig. 16a), and that there are  $s$  and  $p_z$  orbitals on the atomic sites which are located at  $\pm\frac{1}{2}\delta_1 - \frac{1}{2}\mathbf{a}_1$ . We refer to the choice of + (resp. −) as the A (resp. B) sublattice. The Peierls paths of the model (Fig. 3) enclosed multiples of a third of the unit cell, so  $n = 3$  and  $\Phi = 6\pi$ . Using our Landau gauge for  $\tilde{\mathbf{A}}$ , it is straightforward to calculate the following integrals along Peierls' paths (see Fig. 3)

$$\exp\left(i \int_{\mathbf{R} + \delta_\alpha}^{\mathbf{R} + \delta_\alpha \pm \mathbf{a}_i} \tilde{\mathbf{A}} \cdot d\mathbf{r}\right) = -1, \quad \exp\left(i \int_{\frac{1}{2}\delta_1 - \frac{1}{2}\mathbf{a}_1}^{-\frac{1}{2}\delta_1 - \frac{1}{2}\mathbf{a}_1} \tilde{\mathbf{A}} \cdot d\mathbf{r}\right) = -1. \tag{E21}$$

$U$  also requires a choice of  $\mathbf{r}_0$ , an arbitrary but fixed position of an orbital of the Hamiltonian, e.g.  $\mathbf{r}_0$  may not be a honeycomb center for  $H_{TBG}$  because there are no orbitals there. We choose  $\mathbf{r}_0 = +\frac{1}{2}\boldsymbol{\delta}_1 - \frac{1}{2}\mathbf{a}_1$ . Then by repeated application of Eq. (E21), we find

$$\begin{aligned} \exp\left(i\int_{\frac{1}{2}\boldsymbol{\delta}_1 - \frac{1}{2}\mathbf{a}_1}^{r_1\mathbf{a}_1 + r_2\mathbf{a}_2 \pm \frac{1}{2}\boldsymbol{\delta}_1 - \frac{1}{2}\mathbf{a}_1} \tilde{\mathbf{A}} \cdot d\mathbf{r}\right) &= \exp\left(i\int_{\frac{1}{2}\boldsymbol{\delta}_1 - \frac{1}{2}\mathbf{a}_1}^{\pm\frac{1}{2}\boldsymbol{\delta}_1 - \frac{1}{2}\mathbf{a}_1} \tilde{\mathbf{A}} \cdot d\mathbf{r}\right) \exp\left(i\int_{\pm\frac{1}{2}\boldsymbol{\delta}_1 - \frac{1}{2}\mathbf{a}_1}^{r_1\mathbf{a}_1 + r_2\mathbf{a}_2 \pm \frac{1}{2}\boldsymbol{\delta}_1 - \frac{1}{2}\mathbf{a}_1} \tilde{\mathbf{A}} \cdot d\mathbf{r}\right) \\ &= \pm(-1)^{r_1+r_2} \end{aligned} \quad (\text{E22})$$

which we show pictorially in Fig. 16b. According to Eq. (E16), we can choose a  $2 \times 2$  unit cell because, using Eq. (E22),

$$\exp\left(i\int_{\mathbf{r}_0}^{2r_1\mathbf{a}_1 + 2r_2\mathbf{a}_2 \pm \frac{1}{2}\boldsymbol{\delta}_1 - \frac{1}{2}\mathbf{a}_1} \tilde{\mathbf{A}} \cdot d\mathbf{r}\right) = \pm(-1)^{2r_1+2r_2} = \pm 1 \quad (\text{E23})$$

where the  $r_1, r_2$  dependence has disappeared. We index the unit cell by  $\ell_1, \ell_2 \in \{0, 1\}$  and define  $BZ_\lambda$  as  $k_1 \in (-\pi/2, \pi/2), k_2 \in (-\pi/2, -\pi/2)$ . Then following Eq. (E20), we calculate

$$\begin{aligned} U &= \sum_{\mathbf{k} \in BZ'} \sum_{\ell_1, \ell_2, \alpha} \mathcal{U}_{\ell_1, \ell_2, \alpha} |\mathbf{k}, \ell_1, \ell_2, \alpha\rangle \langle \mathbf{k}, \ell_1, \ell_2, \alpha|, \\ \mathcal{U}_{\ell_1, \ell_2, \alpha} &= \exp\left(i\int_{\mathbf{r}_0}^{\ell_1\mathbf{a}_1 + \ell_2\mathbf{a}_2 + \boldsymbol{\delta}_\alpha} \tilde{\mathbf{A}} \cdot d\mathbf{r}\right) \\ &= (-1)^{\ell_1 + \ell_2} \exp\left(i\int_{\mathbf{r}_0}^{\boldsymbol{\delta}_\alpha} \tilde{\mathbf{A}} \cdot d\mathbf{r}\right) \\ &= \text{sub}(\alpha)(-1)^{\ell_1 + \ell_2} \end{aligned} \quad (\text{E24})$$

where we have used Eq. (E21), and  $\text{sub}(\alpha) = \pm 1$  where the sign is positive (resp. negative) for  $\boldsymbol{\delta}_\alpha$  on the A (resp. B) sublattice. We will use this result in App. G3.

### b. Constraints on the Wilson loop at $\phi = \Phi/2$

Now we study how  $UC_{2z}\mathcal{T}$  symmetry constrains the Wilson loop eigenvalues. We will demonstrate that in a unit cell where  $U$  is diagonal in momentum space,  $UC_{2z}\mathcal{T}$  creates a ‘‘particle-hole’’ symmetry in the spectrum of the Wilson Hamiltonian at  $\phi = \Phi/2$ , i.e.  $\{\vartheta(k_1)\} = \{-\vartheta(k_1)\}$ . This allows the  $w_2$  invariant to be calculated by counting the number of points where  $\vartheta(k_1) = 0$  and  $\vartheta(k_1) = \pi$  as described in Ref. [39]. We emphasize that  $w_2^{\phi=\Phi/2}$  is a topological invariant and is not affected by the choice of unit cell. This is in contrast to the relative winding of the Wilson loop eigenvalues which may change when the unit cell is expanded.

To begin, we can construct the extended unit cell to be  $\lambda_1 \times \lambda_2 q' / \text{gcd}(\lambda_2, q')$  which explicitly ensures that the  $\lambda_1 \times \lambda_2$  unit cell in which  $U$  is diagonal and the  $1 \times q'$  unit cell in which we can diagonalize  $H^{\phi=\Phi/2} = \mu \frac{2\pi p}{q}$  are commensurate. For brevity, we let  $\lambda'_2 = \lambda_2 q' / \text{gcd}(\lambda_2, q')$ . In this extended unit cell, we can take  $k_1 \in (-\pi/\lambda_1, \pi/\lambda_1), k_2 \in (0, 2\pi/\lambda'_2)$  which we define as  $BZ_{\lambda'}$ . We define the  $i$ th energy eigenstate of  $H^{\phi=\Phi/2} = \mu \frac{2\pi p}{q}$  as  $|u_i^{\Phi/2}\rangle$  which is an  $N_{orb} \times \lambda_1 \lambda'_2$  vector. We call the representation of  $UC_{2z}\mathcal{T}$  on the  $|u_i^{\Phi/2}\rangle$  eigenstates  $D[UC_{2z}\mathcal{T}] = \mathcal{Q}K$  for brevity. We can derive an explicit expression by acting  $UC_{2z}\mathcal{T}$  on the momentum eigenstates:

$$\begin{aligned} UC_{2z}\mathcal{T} |\mathbf{k}, \ell_1, \ell_2, \alpha\rangle &= UC_{2z}\mathcal{T} \frac{1}{\sqrt{\mathcal{N}/\lambda_1 \lambda'_2}} \sum_{r_1, r_2} e^{-i\mathbf{k} \cdot ((\lambda_1 r_1 + \ell_1)\mathbf{a}_1 + (\lambda'_2 r_2 + \ell_2)\mathbf{a}_2 + \boldsymbol{\delta}_\alpha)} |r_1, r_2, \ell_1, \ell_2, \alpha\rangle \\ &= \frac{1}{\sqrt{\mathcal{N}/\lambda_1 \lambda'_2}} \sum_{r_1, r_2} e^{-i(-\mathbf{k}) \cdot ((\lambda_1 r_1 + \ell_1)\mathbf{a}_1 + (\lambda'_2 r_2 + \ell_2)\mathbf{a}_2 + \boldsymbol{\delta}_\alpha)} UC_{2z}\mathcal{T} |r_1, r_2, \ell_1, \ell_2, \alpha\rangle \\ &= \frac{1}{\sqrt{\mathcal{N}/\lambda_1 \lambda'_2}} \sum_{r_1, r_2, \beta} e^{-i(-\mathbf{k}) \cdot ((\lambda_1 r_1 + \ell_1)\mathbf{a}_1 + (\lambda'_2 r_2 + \ell_2)\mathbf{a}_2 + \boldsymbol{\delta}_\alpha)} \mathcal{U}_{-\ell_1, -\ell_2, \beta} [D(C_{2z}\mathcal{T})]_{\alpha\beta} | -r_1, -r_2, -\ell_1, -\ell_2, \beta\rangle K \end{aligned} \quad (\text{E25})$$

where we have used Eq. (E20) to determine the action of  $U$  on the states. Now we define

$$[\mathcal{Q}]_{\ell_1 \ell_2 \alpha, \ell'_1 \ell'_2 \beta} = \mathcal{U}_{-\ell_1, -\ell_2, \alpha} \delta_{-\ell_1, \ell'_1} \delta_{-\ell_2, \ell'_2} [D(C_{2z}\mathcal{T})]_{\alpha\beta}. \quad (\text{E26})$$

Note from Eq. (E25) that  $\mathcal{Q}_{\ell_1\ell_2\alpha,\ell'_1\ell'_2\beta}$  is only nonzero when  $\ell_1\mathbf{a}_1 + \ell_2\mathbf{a}_2 + \boldsymbol{\delta}_\alpha = -(\ell'_1\mathbf{a}_1 + \ell'_2\mathbf{a}_2 + \boldsymbol{\delta}_\beta) \bmod \lambda_1\mathbf{a}_1 + \lambda'_2\mathbf{a}_2$ . This is the usual constraint on spatial symmetries, but in the expanded unit cell. Using this property, we continue from Eq. (E25) to find

$$\begin{aligned} UC_{2z}\mathcal{T}|\mathbf{k}, \ell_1, \ell_2, \alpha\rangle &= \frac{1}{\sqrt{\mathcal{N}/\lambda_1\lambda'_2}} \sum_{r_1, r_2} \sum_{\ell'_1, \ell'_2, \beta} e^{-i(-\mathbf{k}) \cdot ((\lambda_1 r_1 - \ell'_1)\mathbf{a}_1 + (\lambda'_2 r_2 - \ell'_2)\mathbf{a}_2 - \boldsymbol{\delta}_\beta)} [Q]_{\ell_1\ell_2\alpha, \ell'_1\ell'_2\beta} | -r_1, -r_2, \ell'_1, \ell'_2, \beta\rangle K \\ &= \frac{1}{\sqrt{\mathcal{N}/\lambda_1\lambda'_2}} \sum_{r_1, r_2} \sum_{\ell'_1, \ell'_2, \beta} e^{-i\mathbf{k} \cdot ((\lambda_1 r_1 + \ell'_1)\mathbf{a}_1 + (\lambda'_2 r_2 + \ell'_2)\mathbf{a}_2 + \boldsymbol{\delta}_\beta)} [Q]_{\ell_1\ell_2\alpha, \ell'_1\ell'_2\beta} | r_1, r_2, \ell'_1, \ell'_2, \beta\rangle K \\ &= \sum_{\ell'_1, \ell'_2, \beta} [Q]_{\ell_1\ell_2\alpha, \ell'_1\ell'_2\beta} |\mathbf{k}, \ell'_1, \ell'_2, \beta\rangle K. \end{aligned} \tag{E27}$$

We assume that  $(UC_{2z}\mathcal{T})^2 = +1$  in this section, so  $\mathcal{Q}\mathcal{Q}^* = +1$ . Note that in the  $\lambda_1 \times \lambda'_2$  unit cell,  $UC_{2z}\mathcal{T}$  is also diagonal in momentum space because both  $C_{2z}$  and  $\mathcal{T}$  reverse the momentum of a state. Then we can define a unitary sewing matrix

$$\mathcal{B}_{\mathbf{k}}^{ij} = \langle u_i^{\Phi/2}(\mathbf{k}) | \mathcal{Q} | u_j^{\Phi/2*}(\mathbf{k}) \rangle \tag{E28}$$

which obeys

$$|u_j^{\Phi/2}(\mathbf{k})\rangle = \mathcal{Q} |u_i^{\Phi/2*}(\mathbf{k})\rangle [\mathcal{B}^\dagger]_{\mathbf{k}}^{ij}. \tag{E29}$$

Using Eq. (E29), we determine that a small segment of a Wilson loop obeys

$$\begin{aligned} [W_{\mathbf{k}'_1 \leftarrow \mathbf{k}_1}^{\Phi/2}]^{ij} &= \langle u_i^{\Phi/2}(\mathbf{k}'_1) | u_j^{\Phi/2}(\mathbf{k}_1) \rangle \\ &= \sum_{rs} \mathcal{B}_{\mathbf{k}'_1}^{ir} \langle u_r^{\Phi/2*}(\mathbf{k}'_1) | \mathcal{Q}^\dagger \mathcal{Q} | u_s^{\Phi/2*}(\mathbf{k}_1) \rangle [\mathcal{B}^\dagger]_{\mathbf{k}_1}^{sj} \\ &= \sum_{rs} \mathcal{B}_{\mathbf{k}'_1}^{ir} [W_{\mathbf{k}'_1 \leftarrow \mathbf{k}_1}^{\Phi/2*}]_{rs} [\mathcal{B}^\dagger]_{\mathbf{k}_1}^{sj}. \end{aligned} \tag{E30}$$

Extending this to a full Wilson loop along  $BZ_{\lambda'}$ , where we integrate along  $k_2 \in (0, 2\pi/\lambda'_2)$ , we find

$$\begin{aligned} W^{\Phi/2}(k_1) &= \mathcal{B}_{(k_1, \frac{2\pi}{\lambda'_2})} W_{(k_1, \frac{2\pi}{\lambda'_2}) \leftarrow (k_1, 0)}^{\Phi/2*} \mathcal{B}_{(k_1, 0)}^\dagger \\ &= \mathcal{B}_{(k_1, \frac{2\pi}{\lambda'_2})} W^{\Phi/2*}(k_1) \mathcal{B}_{(k_1, 0)}^\dagger. \end{aligned} \tag{E31}$$

To related the sewing matrices  $\mathcal{B}$  at points across the  $BZ_{\lambda'}$ , we need to use the embedding matrix  $V'_2(\Phi/2)$  that implements the  $2\pi/\lambda'_2$  periodicity. Following identically the calculation of the the embedding matrix  $\bar{V}_2(\phi)$  in the  $1 \times q'$  unit cell in Eq. (A44), we find

$$[V'_2(\Phi/2)]_{\ell_1\ell_2\alpha, \ell'_1\ell'_2\beta} = \delta_{\ell_1\ell'_1} \delta_{\ell_2\ell'_2} e^{i\frac{2\pi}{\lambda'_2}\ell_2} \delta_{\alpha\beta} e^{i\frac{2\pi}{\lambda'_2}\boldsymbol{\delta}_\alpha \cdot \mathbf{b}_2} \tag{E32}$$

where  $\ell_1 = 0, \dots, \lambda_1 - 1$  and  $\ell_2 = 0, \dots, \lambda'_2 - 1$  index the unit cells within the extended  $\lambda_1 \times \lambda'_2$  unit cell, respectively. We now observe that

$$\begin{aligned} \mathcal{B}_{(k_1, \frac{2\pi}{\lambda'_2})}^{ij} &= \langle u_i^{\Phi/2}(k_1, \frac{2\pi}{\lambda'_2}) | \mathcal{Q} K | u_j^{\Phi/2}(k_1, \frac{2\pi}{\lambda'_2}) \rangle \\ &= \langle u_i^{\Phi/2}(k_1, 0) | [V'_2(\Phi/2)]^\dagger \mathcal{Q} K V'_2(\Phi/2) | u_j^{\Phi/2}(k_1, 0) \rangle \end{aligned} \tag{E33}$$

By direct calculation with Eqs. (E26) and (E32), we compute

$$\begin{aligned} [V'_2(\Phi/2)]^\dagger \mathcal{Q} K V'_2(\Phi/2)_{\ell_1\ell_2\alpha, \ell'_1\ell'_2\beta} &= e^{-i\frac{2\pi}{\lambda'_2}(\ell_2\mathbf{a}_2 + \boldsymbol{\delta}_\alpha + \ell'_2\mathbf{a}_2 + \boldsymbol{\delta}_\beta) \cdot \mathbf{b}_2} [\mathcal{Q} K]_{\ell_1\ell_2\alpha, \ell'_1\ell'_2\beta} \\ &= [\mathcal{Q} K]_{\ell_1\ell_2\alpha, \ell'_1\ell'_2\beta} \end{aligned} \tag{E34}$$

where in the last line we have used that  $[\mathcal{Q} K]_{\ell_1\ell_2\alpha, \ell'_1\ell'_2\beta}$  is only nonzero if  $\ell_1\mathbf{a}_1 + \ell_2\mathbf{a}_2 + \boldsymbol{\delta}_\alpha = -(\ell'_1\mathbf{a}_1 + \ell'_2\mathbf{a}_2 + \boldsymbol{\delta}_\beta) \bmod \lambda_1\mathbf{a}_1 + \lambda'_2\mathbf{a}_2$ , so  $\ell_2 + \boldsymbol{\delta}_\alpha \cdot \mathbf{b}_2 + \ell'_2 + \boldsymbol{\delta}_\beta \cdot \mathbf{b}_2 = 0 \bmod \lambda'_2$ . Hence we obtain

$$\begin{aligned} \mathcal{B}_{(k_1, \frac{2\pi}{\lambda'_2})}^{ij} &= \langle u_i^{\Phi/2}(k_1, 0) | \mathcal{Q} K | u_j^{\Phi/2}(k_1, 0) \rangle \\ &= \mathcal{B}_{(k_1, 0)}^{ij}. \end{aligned} \tag{E35}$$

Returning to Eq. (E31), we find the desired “particle-hole” symmetry

$$\begin{aligned} W^{\Phi/2}(k_1) &= \mathcal{B}_{(k_1,0)}^\dagger W^{\Phi/2*}(k_1) \mathcal{B}_{(k_1,0)}, \\ \{\vartheta_j(k_1)\} &= \{-\vartheta_j(k_1)\} \end{aligned} \quad (\text{E36})$$

as previously stated. This is identical to the Wannier center constraint arising from  $C_{2z}\mathcal{T}$  at  $\phi = 0$  and hence we can calculate  $w_2$  directly from the Wilson loop spectrum following the discussion of Ref. [39].

### 3. Proof of a Trivial Phase when $(UC_{2z}\mathcal{T})^2 = -1$

Now we consider the case where  $(UC_{2z}\mathcal{T})^2 = -1$  and there is no  $w_2$  invariant defined. We remark that no 2D crystalline system at  $\phi = 0$  can have such a symmetry because  $(C_{2z}\mathcal{T})^2 = C_{2z}^2\mathcal{T}^2 = (\pm 1)^2 = 1$ . From the 3D perspective where  $\phi$  is interpreted as  $k_z$  and  $U$  is the embedding matrix along the  $z$  direction, the symmetry algebra at  $k_z = 0$  is always the same as at  $k_z = \pi$ , so having  $(C_{2z}\mathcal{T})^2 = +1$  and  $(UC_{2z}\mathcal{T})^2 = -1$  is also impossible. The possibility of such projective symmetry algebras (see also Eq. (D39)) is a novel feature of Hofstadter physics.

The Higher Order Topological Insulator (HOTI) phase is still characterized by Wannier flow between  $\phi = 0$  and  $\phi = \Phi/2$ . Because we assume a non-trivial  $w_2$  index at  $\phi = 0$  that protects corner states, we need only show corner states are not stable if  $(UC_{2z}\mathcal{T})^2 = -1$ . This establishes that  $H^{\Phi/2}$  is in a trivial atomic limit, and so pumping must occur between  $\phi = \Phi/2$  and  $\phi = 0$ .

First we provide a heuristic argument that  $(UC_{2z}\mathcal{T})^2 = -1$  trivializes the phase. We consider a finite crystal that preserves  $UC_{2z}\mathcal{T}$  symmetry, where  $C_{2z}$  is a rotation around the origin. Consider a high symmetry Wyckoff position  $\mathbf{w}$  with  $UC_{2z}\mathcal{T}$  in its magnetic point group. If the state has a center exactly at  $\mathbf{w}$ , then by Kramers Theorem it must have a Kramers partner at  $\mathbf{w}$  because  $(UC_{2z}\mathcal{T})^2 = -1$ . If a state has a Wannier center at  $\mathbf{w} + \boldsymbol{\delta}$ , perturbed slightly from  $\mathbf{w}$ , then by  $UC_{2z}\mathcal{T}$  there is another state at  $\mathbf{w} - \boldsymbol{\delta}$ . Hence any pair of states at  $\mathbf{w}$  can be moved adiabatically away from  $\mathbf{w}$  along  $UC_{2z}\mathcal{T}$ -symmetric paths. This indicates a trivial (Real Space Invariant) RSI [61]. In coming work (Ref. [60]), we derive expressions for the RSIs of all the 2D magnetic point groups. This indicates that the bulk is trivialized, and by the Bulk-Boundary correspondence, we expect the boundary states to be trivial [61–65].

In absence of the  $w_2$  invariant, corner states can still be diagnosed using the nested Berry phase formalism of Refs. [45, 46]. Hence, we can compute the determinant of the nested Wilson loop  $\mathcal{W}$  to confirm the heuristic argument given before. We remark that Ref. [41] demonstrated that  $C_{2z}\mathcal{T}$  symmetry quantizes  $\det \mathcal{W} = \pm 1$  (where  $-1$  is the nontrivial value of the topological phase) when  $(C_{2z}\mathcal{T})^2 = \pm 1$  and the nested Wilson loop is taken over a particle-hole symmetric configuration of Wannier bands. Here we study the specific case where  $(UC_{2z}\mathcal{T})^2 = -1$ , and we show that the determinant of the nested Wilson loop over particle-hole symmetric Wannier bands is fixed to be  $+1$ , trivial.

We define the Wannier Hamiltonian  $H_W(k_1)$  by  $W^{\Phi/2}(k_1) = e^{iH_W(k_1)}$ , and the Wannier bands as

$$H_W(k_1) |w_j(k_1)\rangle = \vartheta_j(k_1) |w_j(k_1)\rangle. \quad (\text{E37})$$

We call  $\mathcal{K} = \mathcal{B}_{(k_1,0)} K$  the representation of  $UC_{2z}\mathcal{T}$  on  $H_W(k_1)$  such that

$$\mathcal{K} H_W(k_1) \mathcal{K}^{-1} = -H_W(k_1). \quad (\text{E38})$$

The essential difference between the  $\mathcal{K}^2 = +1$  case and the  $\mathcal{K}^2 = -1$  case is that the latter creates “anti-Kramers’ pairs”, i.e. the states  $|w_j(k_1)\rangle$  and  $\mathcal{K} |w_j(k_1)\rangle$  have opposite Wilson eigenvalues,  $\pm\vartheta(k_1)$ , but are necessarily distinct even when  $\vartheta(k_1) = -\vartheta(k_1) \pmod{2\pi}$ . First we prove that the two states  $|w(k_1)\rangle$  and  $\mathcal{K} |w(k_1)\rangle$  have opposite eigenvalues. Let  $H_W(k_1) |w(k_1)\rangle = \vartheta(k_1) |w(k_1)\rangle$ . Then

$$\begin{aligned} H_W(k_1) \mathcal{K} |w(k_1)\rangle &= -\mathcal{K} H_W(k_1) |w(k_1)\rangle \\ &= -\mathcal{K} \vartheta(k_1) |w(k_1)\rangle \\ &= -\vartheta(k_1) \mathcal{K} |w(k_1)\rangle \end{aligned} \quad (\text{E39})$$

where we have used Eq. (E38) to anti-commute  $\mathcal{K}$  and  $H_W(k_1)$ . Now we prove that anti-Kramers’ pairs represent distinct states by contradiction. Suppose  $\vartheta(k_1) = 0, \pi$  and  $\mathcal{K}^{-1} |w_j(k_1)\rangle$  and  $|w_j(k_1)\rangle$  represent the same state, so  $\mathcal{K} |w_j(k_1)\rangle = e^{i\alpha} |w_j(k_1)\rangle$ . Then by acting  $\mathcal{K}$  again, we find

$$\begin{aligned} \mathcal{K}^2 |w_j(k_1)\rangle &= \mathcal{K} e^{i\alpha} |w_j(k_1)\rangle \\ - |w_j(k_1)\rangle &= e^{-i\alpha} \mathcal{K} |w_j(k_1)\rangle \\ - |w_j(k_1)\rangle &= e^{-i\alpha+i\alpha} |w_j(k_1)\rangle \\ - |w_j(k_1)\rangle &= |w_j(k_1)\rangle \end{aligned} \quad (\text{E40})$$

so we reach a contradiction because  $|w_j(k_1)\rangle \neq 0$ . Importantly, we see that for  $\vartheta = 0$  or  $\vartheta = \pi$ , where  $\vartheta = -\vartheta$ ,  $|w(k_1)\rangle$  and  $\mathcal{K}|w(k_1)\rangle$  are true Kramers' partners, meaning they are distinct states with the same eigenvalue.

Following Ref. [41], the Wilson loop bands selected to compute the nested Wilson loop should preserve  $UC_{2z}\mathcal{T}$ . By Eq. (E39), the states  $|w(k_1)\rangle$  and  $\mathcal{K}|w(k_1)\rangle$  are automatically particle-hole symmetric and hence respect  $UC_{2z}\mathcal{T}$ . We now argue that the bands of a generic nested Wilson loop can be gapped into pairs related by  $\mathcal{K}$  because there are no other unitary symmetries to protect crossings, so in general the selected bands decompose into two sets, one above  $\vartheta = 0$  and the other below  $\vartheta = 0$ . Note that there must always be an even number of bands because  $(UC_{2z}\mathcal{T})^2 = -1$ . For now, we assume that there at least 4 bands so we can calculate the nested Wilson loop on a  $UC_{2z}\mathcal{T}$ -symmetric pair of bands which is a subset of full Wilson Hamiltonian spectrum. We treat the special case of two bands later and show it is also trivial.

We now study a generic  $2 \times 2$  block to show that its determinant is always +1, which is sufficient to establish that the determinant of a generic nested Wilson loop (with at least four bands) is +1 by block diagonalization. At every  $k_1$ , we can diagonalize the Wilson Hamiltonian  $H_W(k_1)$  to find its two eigenvectors which, due to the  $UC_{2z}\mathcal{T}$  symmetry, can be written as  $|w(k_1)\rangle$  and  $\mathcal{K}|w(k_1)\rangle$ . The nested Wilson loop in the  $k_1 \in (-\pi/\lambda_1, \pi/\lambda_1), k_2 \in (0, 2\pi/\lambda'_2)$  BZ of the extended unit cell is written

$$\mathcal{W} = \tilde{U}^\dagger(2\pi/\lambda_1) \left[ \prod_{k_1}^{2\pi/\lambda_1 \leftarrow 0} \tilde{\mathcal{P}}_{k_1} \right] \tilde{U}(0), \quad \tilde{\mathcal{P}}_{k_1} = \tilde{U}(k_1)\tilde{U}^\dagger(k_1) \quad (\text{E41})$$

where  $\tilde{U}(k_1)$  is the  $\lambda_1\lambda'_2 N_{orb} \times 2$  matrix of the eigenvectors of the Wilson loop. We choose a conventional ordering where the columns of  $\tilde{U}(k_1)$  are ordered such that  $\tilde{U}(k_1) = [w_1(k_1), w_2(k_1)]$  where  $w_1(k_1)$  is the column vector of length  $\lambda_1\lambda'_2 N_{orb}$  corresponding to  $|w(k_1)\rangle$  and  $w_2(k_1)$  is the column vector corresponding to  $\mathcal{K}|w(k_1)\rangle$ . Note that in this ordering,

$$\begin{aligned} \mathcal{K}\tilde{U}(k_1) &= \mathcal{K}[w_1(k_1), w_2(k_1)] \\ &= [\mathcal{K}w_1(k_1), \mathcal{K}w_2(k_1)]K \\ &= [w_2(k_1), \mathcal{K}^2 w_1(k_1)]K \\ &= [w_2(k_1), -w_1(k_1)]K \\ &= [w_1(k_1), w_2(k_1)] \begin{pmatrix} 0 & -1 \\ 1 & 0 \end{pmatrix} K \\ &= \tilde{U}(k_1) (-i\sigma_2 K) \end{aligned} \quad (\text{E42})$$

where  $\sigma_2$  is a Pauli matrix. Acting on the projectors, we find that they commute with  $\mathcal{K}$ :

$$\begin{aligned} \mathcal{K}\tilde{\mathcal{P}}_{k_1} &= \tilde{U}(k_1)(-i\sigma_2 K)U^\dagger(k_1) \\ &= \tilde{U}(k_1)(U(k_1) \cdot i\sigma_2 K)^\dagger \\ &= \tilde{U}(k_1)(-\mathcal{K}U(k_1))^\dagger \\ &= -\tilde{U}(k_1)U^\dagger(k_1)\mathcal{K}^{-1} \\ &= \tilde{U}(k_1)U^\dagger(k_1)\mathcal{K} \\ &= \tilde{\mathcal{P}}_{k_1}\mathcal{K} \end{aligned} \quad (\text{E43})$$

so  $[\tilde{\mathcal{P}}_{k_1}, \mathcal{K}] = 0$ . Using this identity on the nested Wilson loop, we find  $(-i\sigma_2 K)\mathcal{W}(-i\sigma_2 K)^\dagger = \mathcal{W}$ . Writing

$$\mathcal{W} = e^{i\mathcal{H}_W}, \quad \mathcal{H}_W = \sum_{i=0}^3 d_i \sigma_i, \quad (\text{E44})$$

defining  $\sigma_0$  as the  $2 \times 2$  identity matrix, we find that  $\mathcal{H}_W$  must obey

$$-\sigma_2 \mathcal{H}_W^* \sigma_2 = \mathcal{H}_W. \quad (\text{E45})$$

Eq. (E45) requires  $d_0 = 0$  or  $d_0 = \pi$ , but the  $d_i$  for  $i = 1, 2, 3$ , are free. We emphasize that the anti-symmetric  $\sigma_2$  matrix appearing in Eq. (E45) is due to  $\mathcal{K}^2 = -1$ . In the other case where  $\mathcal{K}^2 = +1$ , we could choose a symmetric matrix, like  $\sigma_1$ , and we would have a different reality condition. We can now compute the determinant from Eq. (E44):

$$\det[\mathcal{W}] = \exp(i\text{Tr}[\mathcal{H}_W]) = \exp(2id_0), \quad (\text{E46})$$



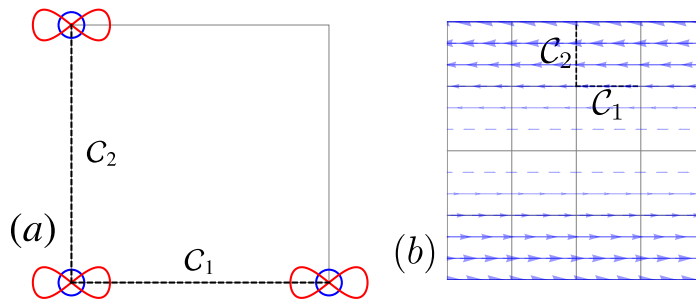


FIG. 17. (a) We show the Peierls paths for the QSH model of App. F 1 with the hopping amplitudes. All orbitals are on the  $1a$  Wyckoff position and, being  $s$  (blue) and  $p_z$  (red) orbitals, are localized near the atoms. and the only hoppings are nearest neighbor. The Peierls paths are taken along the lattice vectors, indicated by  $C_1, C_2$ . (b) We show the lattice with the vector field  $\mathbf{A} = \phi(-y, 0)$  and the two hoppings in an arbitrary unit cell. We see that along  $C_1$ , there is a nonzero phase accumulated along the hopping, but there is no phase accumulated along  $C_2$  because  $\mathbf{A}$  is always perpendicular to the path of integration.

so because  $d_0$  is quantized by  $UC_{2z}\mathcal{T}$  to be 0 or  $\pi$ , the determinant must equal  $+1$ . Thus for a Wilson loop with four or more bands, the nested Wilson loop indicates a trivial phase.

We now consider the special case of a Wilson loop  $W^{\Phi/2}(k_1) = e^{iH_W(k_1)}$  with only two bands, so it is not possible to take a  $UC_{2z}\mathcal{T}$ -symmetric subset of bands. The  $2 \times 2$  Wilson Hamiltonian  $H_W(k_1)$  obeys  $\mathcal{K}H_W(k_1)\mathcal{K}^{-1} = -H_W(k_1)$  with  $\mathcal{K}^2 = -1$ . Without loss of generality, we make take  $\mathcal{K} = i\sigma_2 K$ . We can apply the same reasoning of Eqs. (E44) and (E45) but for the Wilson Hamiltonian. We have that  $H_W(k_1)$  must be in the form

$$H_W(k_1) = \sum_{i=0}^3 h_{W,i}(k_1)\sigma_i \quad (\text{E47})$$

where  $h_{W,0}(k_1) = 0$  or  $h_{W,0}(k_1) = \pi$  but  $h_{W,i}(k_1)$  for  $i = 1, 2, 3$  are free. Because the  $h_{W,i}$  are free, there are no protected crossings (Weyl nodes) at  $\vartheta = 0$  or  $\vartheta = \pi$  and no protected winding number, unlike in the  $(C_{2z}\mathcal{T})^2 = +1$  case studied in Ref. [13]. Indeed, the Wilson Hamiltonian Eq. (E47) must be topologically trivial as a map from  $k_1 \in S^1$  to  $h_{W,i} \in S^3$  because  $\pi_1(S^3) = 0$ . Thus we have shown that with  $UC_{2z}\mathcal{T}$  symmetry satisfying  $(UC_{2z}\mathcal{T})^2 = -1$ , the Wilson loop with two bands is topologically trivial.

There is also a more abstract way to understand that  $(UC_{2z}\mathcal{T})^2 = -1$  ensures the Wilson Hamiltonian is trivial. Returning to Eq. (E38), we recognize that the Wilson Hamiltonian (assuming  $\mathcal{K}^2 = -1$  is the only symmetry of the model) is in the symmetry class  $C, d = 1$  of the Ten-fold Way [32, 33]. Therefore it has no topological index and is necessarily trivial. In comparison, when we consider  $UC_{2z}\mathcal{T}$  symmetry squaring to  $+1$ , the Wilson Hamiltonian would be in the symmetry class  $D, d = 1$  in which case there is a  $\mathbb{Z}_2$  topological invariant which we identify as the quantized determinant of the nested Wilson loop [13, 41].

## Appendix F: The Quantum Spin Hall Model

In this Appendix, we introduce the Quantum Spin Hall (QSH) model of Bernevig, Hughes, and Zhang (BHZ) as a simple lattice model to exemplify our proofs of the Hofstadter topological phase in Secs. and [30]. In App. F 1, we recap the essentials of the model before explicitly writing down the Hofstadter Hamiltonian. We enumerate the symmetries of the model and introduce onsite symmetry-breaking perturbations that isolate different topological phases: a mirror Chern insulator, a Kane-Mele insulator, and a fragile  $w_2$  insulator. We then add a next-nearest neighbor term to the Hamiltonian to break the flux periodicity from  $\Phi = 2\pi$  ( $n = 1$ ) to  $\Phi = 4\pi$  ( $n = 2$ ). Using this model, we demonstrate that when  $n$  is even, the Hofstadter phase of a zero-field  $\mathbb{Z}_2$  insulator may be a weak TI or 3D (strong) TI (App. F 2).

### 1. Hofstadter Hamiltonian

The BHZ Hamiltonian is a model with spin-1/2 electrons  $\sigma$  and  $s, p$  orbitals  $\tau$ , all at the  $1a$  Wyckoff position [30]. The momentum space Hamiltonian is

$$H_{QSH}(k_x, k_y) = (M - \cos k_x - \cos k_y)I \otimes \tau_3 + \sin k_x \sigma_3 \otimes \tau_1 + \sin k_y I \otimes \tau_2 \quad (\text{F1})$$

and realizes a Quantum Spin Hall effect with a mirror Chern number equal to  $-1$  (resp.  $+1$ ) for  $0 < M < 2$  (resp.  $-2 < M < 0$ ). We define this topological invariant using the mirror symmetry  $M_z = -i\sigma_3 \otimes I$ , the product of a rotation  $C_{2z} = -i\sigma_3 \otimes \tau_3$  and inversion  $\mathcal{I} = I \otimes \tau_3$  which satisfies  $[H_{QSH}(\mathbf{k}), M_z] = 0$  for any  $\mathbf{k}$ . Because  $M_z$  is local in the BZ, all occupied bands can be labeled by a mirror eigenvalue  $m = \pm i$ . Then we define the usual Chern number  $C$  and mirror Chern number  $C_{M_z}$

$$C = C_{m=+i} + C_{m=-i}, \quad C_{M_z} = \frac{C_{m=+i} - C_{m=-i}}{2}. \quad (\text{F2})$$

From these expressions, one can calculate that at half filling, the Chern number  $C$  is identically zero (owing to TRS) but that

$$C_{M_z} = \begin{cases} -1, & M \in (0, 2) \\ +1, & M \in (-2, 0) \\ 0, & |M| > 2 \end{cases}. \quad (\text{F3})$$

As per the discussion in Sec. , the Hofstadter Butterfly must have a gap closing when  $|M| < 2$  since each mirror block of the Hamiltonian has its own non-zero Chern number. To verify this, we construct the Hofstadter Hamiltonian explicitly.

The Hofstadter Hamiltonian is simple to construct because all hoppings are nearest neighbor and we take the Peierls path directly along the bonds for all orbitals in the model, as shown in Fig. 17a. In our Landau gauge  $\mathbf{A} = (-\phi y, 0)$ , the only term that acquires a phase the  $y$ -hopping:  $c_{x+1,y}^\dagger c_{x,y} \rightarrow e^{-i\phi y} c_{x+1,y}^\dagger c_{x,y}$  as we depict Fig. 17b. All closed loops enclose an integer area, so  $n = 1$ , and we can take  $\phi = \frac{2\pi p}{q}$  to recover a  $1 \times q$  magnetic unit cell. (Note that because  $\mu = 1$ , there is no distinction between  $q$  and  $q'$  in this gauge.) At  $\Phi = 2\pi$ , all the Peierls phases of the model are manifestly zero mod  $2\pi$ , so it can be trivially shown that the  $H^{\phi+\Phi} = H^\phi$ , and hence  $U = 1$  (Eq. (A5)). The Hofstadter Hamiltonian is

$$\begin{aligned} \mathcal{H}_{y,y'}^\phi &= \delta_{y,y'} h_y + \delta_{y,y'+1} T + \delta_{y+1,y'} T^\dagger \\ h_y &= (M - \cos(k_x - \phi y)) I \otimes \tau_3 + \sin(k_x - \phi y) \sigma_3 \otimes \tau_1, \\ T &= -\frac{1}{2} e^{-ik_y} I \otimes (\tau_3 - i\tau_2) \end{aligned} \quad (\text{F4})$$

We promote the Mirror symmetry to  $M_z = \delta_{y,y'}(-i\sigma_3 \otimes I)$  since it commutes with each block of the Hofstadter Hamiltonian. Thus we see explicitly that  $M_z$  remains a symmetry at all  $\phi$ .

As discussed in Sec. , we add symmetry-breaking terms to the QSH model Eq. (F1) to remove symmetries from the Hamiltonian. This is accomplished by enumerating all of the symmetries of the model. The elementary symmetries are  $\mathcal{I}, C_{2z}, C_{4z}, \mathcal{T}$ , and  $C_{2x}$ , and  $M_z = \mathcal{I}C_{2z}$ . We collect their representations and products in Table I. For brevity, we do not include the additional products of other symmetries with  $C_{4z}$  because they are broken if  $C_{4z}$  is broken. Similarly,  $C_{4z}$  is broken if  $C_{2z}$  is broken.

Inversion symmetry  $\mathcal{I}$  and  $C_{4z}$  also require composition with other gauge-dependent unitary operators to remain symmetries at  $\phi \neq 0$ . The Landau gauge preserves inversion symmetry. However, the  $1 \times q$  magnetic unit cell at  $\phi = \frac{2\pi p}{q}$  breaks inversion symmetry. Hence we find that  $\mathcal{I}$  acting on the Hofstadter Hamiltonian must be multiplied by a permutation matrix  $\mathcal{D}$  that inverts the order of unit cells within the  $1 \times q$  magnetic unit cell. Explicitly,  $\mathcal{D}_{\ell,\ell'} = \delta_{q-\ell,\ell'}$ . The Landau gauge explicitly breaks the  $C_{4z}$  symmetry, so a gauge transformation is necessary. In Ref. [60], we will develop the full theory of space group symmetries in the Hofstadter Butterfly. Because we do not use the  $C_{4z}$  symmetry in this work, we refer the reader to Ref. [60] for further details. Considering only the spatial structure and not the orbital character, a generic term in the  $H_{QSH}$  (Eq. (F1)) transforms as

$$\begin{aligned} \sum_{\mathbf{R}} C_{4z} \left[ \exp \left( i \int_{\mathbf{R}}^{\mathbf{R}+\mathbf{a}_i} \mathbf{A}(\mathbf{r}) \cdot d\mathbf{r} \right) c_{\mathbf{R}+\mathbf{a}_i}^\dagger c_{\mathbf{R}} \right] C_{4z}^\dagger &= \sum_{\mathbf{R}} \exp \left( i \int_{\mathbf{R}}^{\mathbf{R}+\mathbf{a}_i} \mathbf{A}(\mathbf{r}) \cdot d\mathbf{r} \right) c_{C_{4z}(\mathbf{R}+\mathbf{a}_i)}^\dagger c_{C_{4z}\mathbf{R}} \\ &= \sum_{\mathbf{R}} \exp \left( i \int_{C_{4z}^{-1}\mathbf{R}}^{C_{4z}^{-1}(\mathbf{R}+C_{4z}\mathbf{a}_i)} \mathbf{A}(\mathbf{r}) \cdot d\mathbf{r} \right) c_{\mathbf{R}+C_{4z}\mathbf{a}_i}^\dagger c_{\mathbf{R}} \\ &= \sum_{\mathbf{R}} \exp \left( i \int_{\mathbf{R}}^{\mathbf{R}+C_{4z}\mathbf{a}_i} C_{4z}^{-1} \mathbf{A}(C_{4z}\mathbf{r}) \cdot d\mathbf{r} \right) c_{\mathbf{R}+C_{4z}\mathbf{a}_i}^\dagger c_{\mathbf{R}}. \end{aligned} \quad (\text{F5})$$

TABLE I. Symmetries of the BHZ Model

Symmetry	$\phi = 0$	$\phi \neq 0$	Mapping of $\mathbf{k}, \phi$
$\mathcal{I}$	$I \otimes \tau_3$	$\mathcal{ID}$	$(-k_x, -k_y, \phi)$
$\mathcal{T}$	$i\sigma_2 \otimes IK$	$\mathcal{T}$	$(-k_x, -k_y, -\phi)$
$C_{2z}$	$-i\sigma_3 \otimes \tau_3$	$(C_{4z}G)^2$	$(-k_x, -k_y, \phi)$
$C_{4z}$	$1/\sqrt{2}(I + C_{2z})$	$C_{4z}G$	$(-k_y, k_x, -\phi)$
$M_z$	$-i\sigma_3 \otimes I$	$M_z$	$(k_x, k_y, \phi)$
$C_{2x}$	$i\sigma_1 \otimes \tau_3$	$G^{-1}C_{2x}G$	$(k_x, -k_y, -\phi)$
$M_z C_{2x}$	$i\sigma_2 \otimes \tau_3$	$G^{-1}M_z C_{2x}G$	$(k_x, -k_y, -\phi)$
$\mathcal{IT}$	$i\sigma_2 \otimes \tau_3 K$	$\mathcal{ITD}$	$(k_x, k_y, -\phi)$
$C_{2z} \mathcal{T}$	$-i\sigma_1 \otimes \tau_3 K$	$(C_{4z}G)^2 \mathcal{T}$	$(k_x, k_y, -\phi)$
$M_z \mathcal{T}$	$-i\sigma_1 \otimes IK$	$M_z \mathcal{T}$	$(-k_x, -k_y, -\phi)$
$\mathcal{IC}_{2x}$	$i\sigma_1 \otimes I$	$\mathcal{IC}_{2x}$	$(-k_x, k_y, -\phi)$
$\mathcal{IM}_z C_{2x}$	$i\sigma_2 \otimes I$	$\mathcal{IM}_z C_{2x}$	$(-k_x, k_y, -\phi)$
$\mathcal{TC}_{2x}$	$-i\sigma_3 \otimes \tau_3 K$	$\mathcal{T}G^{-1}C_{2x}G$	$(-k_x, k_y, \phi)$
$\mathcal{T}M_z C_{2x}$	$-I \otimes \tau_3 K$	$\mathcal{T}G^{-1}M_z C_{2x}G$	$(-k_x, k_y, \phi)$
$\mathcal{ITC}_{2x}$	$-i\sigma_3 \otimes IK$	$\mathcal{ITC}_{2x}$	$(k_x, -k_y, \phi)$
$\mathcal{ITM}_z C_{2x}$	$K$	$\mathcal{ITM}_z C_{2x}$	$(k_x, -k_y, \phi)$

We list the symmetries of the BHZ model in column 1 and their representations on the Bloch Hamiltonian in column 2. In column 3, we provide their representations on the Hofstadter Hamiltonian  $\mathcal{H}_{QSH}$  in the presence of nonzero flux. The symmetries listed in column 3 refer to the  $4 \times 4$  representations defined in column 2. Note that for  $\phi \neq 0$ , some of the symmetries are broken, and take  $\phi \rightarrow -\phi$ . The mapping of  $\mathbf{k}$  and  $\phi$  under the action of the symmetries is shown in column 4.

This shows us that, because the Peierls phase acquired from the hopping  $\mathbf{R} \rightarrow \mathbf{R} + \mathbf{a}_i$  is different from the phase acquired from  $C_{4z}\mathbf{R} \rightarrow C_{4z}(\mathbf{R} + \mathbf{a}_i)$ , a gauge transformation  $G$  is required. We define

$$G c_{\mathbf{R},\alpha} G^{-1} = e^{-i\lambda(\mathbf{R})} c_{\mathbf{R},\alpha}, \quad G = \exp \left( i \sum_{\mathbf{R}} c_{\mathbf{R},\alpha}^\dagger c_{\mathbf{R},\alpha} \lambda(\mathbf{R}) \right), \quad (\text{F6})$$

which acts as a gauge transformation of the vector potential in the Peierls substitution:  $G c_{\mathbf{R}+\mathbf{a}_i}^\dagger c_{\mathbf{R}} G^{-1} = \exp(i \int_{\mathbf{R}}^{\mathbf{R}+\mathbf{a}_i} \nabla \lambda \cdot d\mathbf{r}) c_{\mathbf{R}+\mathbf{a}_i}^\dagger c_{\mathbf{R}}$ .  $\lambda(\mathbf{r})$  must satisfy

$$C_{4z}^{-1} \mathbf{A}(C_{4z}\mathbf{r}) - \nabla \lambda(\mathbf{r}) = \mathbf{A}(\mathbf{r}). \quad (\text{F7})$$

It is trivial to check that  $\lambda(\mathbf{r}) = \phi xy$  satisfies Eq. (F7). This completes our discussion of the symmetries.

From Table I, it can be checked that the Hamiltonian with onsite perturbation

$$H'_{QSH} = H_{QSH} + \epsilon_1 I \otimes \tau_1 + \epsilon_2 \sigma_3 \otimes \tau_2 \quad (\text{F8})$$

breaks all symmetries except  $M_z, \mathcal{T}, M_z \mathcal{T}$ . Thus  $H'_{QSH}$  can have no Chern number that would enforce a gap closing, but does still have a Mirror Chern number. If we also add a mirror-breaking term, defining

$$H''_{QSH} = H'_{QSH} + \epsilon_3 \sigma_2 \otimes \tau_2, \quad (\text{F9})$$

then we lose the mirror Chern number and a bulk gap may open (see Fig. 1). As demonstrated in Sec. III,  $H''_{QSH}$  – which has only  $\mathcal{T}$  symmetry – can be classified as a 3D TI with gapless surface states in  $\phi$  for open boundary conditions, but it need not have gapless bulk states. Finally, we also can break all symmetries except  $C_{2z} \mathcal{T}$ . Explicitly, we let

$$H'''_{QSH} = H_{QSH} + \epsilon_4 I \otimes \tau_2 + \epsilon_5 (\sigma_1 + \sigma_2) \otimes I + \epsilon_6 (\sigma_1 \otimes \tau_2 + \sigma_2 \otimes \tau_2 + \sigma_1 \otimes \tau_3) \quad (\text{F10})$$

which preserves  $C_{2z} \mathcal{T}$  only and opens a gap at all  $\phi$ . We show the Hofstadter Butterfly for this model in Fig. 18 and confirm the pumping of corner states that characterizes a HOTI. Note that because  $U = 1$  (Eq. (A5)) in our gauge and  $H^{\phi=\Phi}$  is identical to  $H^{\phi=0}$ , we trivially have  $(UC_{2z}\mathcal{T})^2 = (C_{2z}\mathcal{T})^2 = 1$ , which agrees with our general calculation in Eq. (E13). We list the values of the parameters in these perturbed Hamiltonians in Table II.

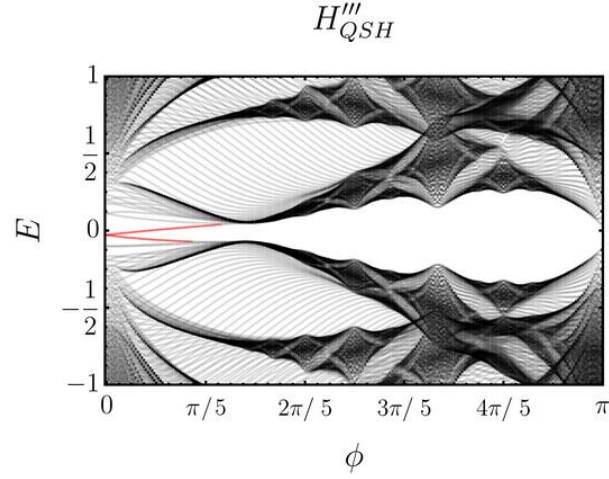


FIG. 18. We show the Hofstadter Butterfly for  $H'''_{QSH}$  computed on a  $25 \times 25$  unit cell lattice with open boundary conditions along both directions. The model as defined in Table II is in the topological phase and exhibits corner modes (red) that are pumped into the bulk (grey) as  $\phi$  is increased.

TABLE II. QSH Hamiltonians and their Symmetries

Hamiltonian	Symmetries	Parameters
$H'_{QSH} = H_{QSH} + \epsilon_1 I \otimes \tau_1 + \epsilon_2 \sigma_3 \otimes \tau_2$	$M_z, \mathcal{T}$	$\epsilon_1 = .1, \epsilon_2 = .11, M = 1.5$
$H''_{QSH} = H_{QSH} + \epsilon_1 I \otimes \tau_1 + \epsilon_2 \sigma_3 \otimes \tau_2 + \epsilon_3 \sigma_2 \otimes \tau_2$	$\mathcal{T}$	$\epsilon_1 = .1, \epsilon_2 = .11, \epsilon_3 = .12, M = 1.5$
$H'''_{QSH} = H_{QSH} + \epsilon_4 I \otimes \tau_2 + \epsilon_5 (\sigma_1 + \sigma_2) \otimes I + \epsilon_6 (\sigma_1 \otimes \tau_2 + \sigma_2 \otimes \tau_2 + \sigma_1 \otimes \tau_3)$	$C_{2z} \mathcal{T}$	$\epsilon_4 = .1, \epsilon_5 = .11, \epsilon_6 = .05, M = 1.6$

We list the variations of the BHZ model (column 1), the symmetries they retain from the perturbations (column 2), and the values of the parameters that realize their nontrivial Hofstadter topology (column 3). The Hofstadter Butterflies of the models may be found in Fig. 1 and Fig. 18.

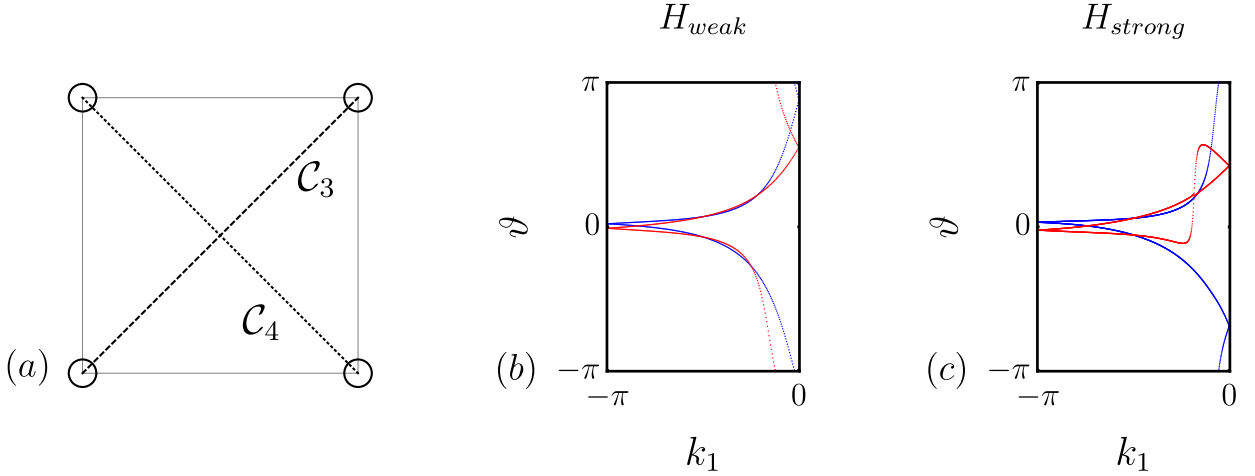


FIG. 19. (a) In App. F 2, we introduce two next-nearest neighbor hoppings of amplitude  $\lambda$  whose Peierls paths are taken along the diagonals and are indicated by  $\mathcal{C}_3, \mathcal{C}_4$ . We calculate the Peierls phase in Eq. (F12). (b) We show the Wilson loop spectra for the model  $H_{weak}$  of Table III which is  $4\pi$ -periodic in flux at  $\phi = 0$  (blue) and  $\phi = 2\pi$  (red). We calculate the  $\mathbb{Z}_2$  invariant by observing that any line of constant  $\vartheta$  intersects an odd number of eigenvalues. We find that both phases at 0 and  $2\pi$  are nontrivial, and the model is a weak TI. (c) By tuning the parameters to  $H_{strong}$  of Table III, the model can reach a strong 3D TI phase where the  $\phi = 0$  model is  $\mathbb{Z}_2$  nontrivial, but the  $\phi = 2\pi$  model is trivial because lines of constant  $\vartheta$  intersect an even number of eigenvalues. In both cases, the 3D topology is nontrivial.

TABLE III. Weak and Strong TI Hamiltonians

Hamiltonian	Symmetries	Parameters
$H_{weak} = H_{QSH} + \epsilon_1 I \otimes \tau_1 + \epsilon_2 \sigma_3 \otimes \tau_2 + \epsilon_3 \sigma_2 \otimes \tau_2 + \lambda H_{diag}$	$\mathcal{T}$	$\epsilon_1 = .2, \epsilon_2 = .21, \epsilon_3 = .22, \lambda = -.1, M = 1.7$
$H_{strong} = H_{QSH} + \epsilon_1 I \otimes \tau_1 + \epsilon_2 \sigma_3 \otimes \tau_2 + \epsilon_3 \sigma_2 \otimes \tau_2 + \lambda H_{diag}$	$\mathcal{T}$	$\epsilon_1 = .2, \epsilon_2 = .21, \epsilon_3 = .22, \lambda = -.2, M = 1.85$

We list two variants of BHZ model which realize a weak and strong 3D TI phase (column 1). Each has only  $\mathcal{T}$  symmetry (column 2). The values of the parameters for these phases are found in column 3.

## 2. Discussion of the Proof for $\mathcal{T}$ -symmetric TIs with General Flux Periodicity $\phi \rightarrow \phi + 2\pi n$

In this section, we discuss how our proof of the trivial  $\mathbb{Z}_2$  invariant at  $\phi = \Phi/2, \Phi = 2\pi n$  (see Sec. III) relies on  $n \in \mathbb{N}$  being odd. This leads to a  $k_1 \rightarrow k_1 + \pi$  periodicity in the magnetic BZ which ensures every gap closing comes in pairs. If  $n$  is even, this proof fails because there is no increased periodicity along  $k_1$ . In this case, it is unclear a priori whether the  $\phi = \Phi/2$  model may be trivial or nontrivial. We show an example of a model with  $n = 2$  that can realize either a trivial or nontrivial phase at  $\phi = \Phi/2$ , confirming that the Hofstadter topology is not uniquely determined by the zero-field topology when  $n$  is even.

We begin with the QSH model of App. F1. To break the  $\Phi = 2\pi$  periodicity to a  $\Phi = 4\pi$  periodicity, we add next nearest-neighbor diagonal hoppings as shown in Fig. 19a. This term breaks the  $\phi \rightarrow \phi + 2\pi$  periodicity because now half a unit cell can be encircled along Peierls paths. However, it does not change  $\mu$  because the new hoppings obey  $\mathbf{b}_1 \cdot ((\mathbf{R} + \boldsymbol{\delta}_\alpha) - (\mathbf{R}' + \boldsymbol{\delta}_\beta)) = \mathbf{b}_1 \cdot (\mathbf{a}_1 + \mathbf{a}_2) = 1$ , which does not affect Eq. (A28). We couple  $s$  orbitals to  $p$  orbitals, preserving  $\mathcal{T}$  symmetry, and find that in momentum space, the appropriate term is

$$H_{diag}(\mathbf{k}) = \lambda I \otimes \tau_1 (\cos(k_x + k_y) + \cos(k_x - k_y)). \quad (\text{F11})$$

Consulting App. F1, we see that this term breaks a number of the zero-field symmetries ( $\mathcal{I}, C_{2z}, C_{4z}, C_{2x}, M_z C_{2x}, \mathcal{IT}, C_{2z}\mathcal{T}, C_{2x}\mathcal{T}, M_z C_{2x}\mathcal{T}$ ) but preserves  $\mathcal{T}, M_z, M_z\mathcal{T}, \mathcal{IC}_{2x}, M_z\mathcal{IC}_{2x}, \mathcal{IT}C_{2x}, M_z\mathcal{IT}C_{2x}$ . We break all the remaining symmetries except  $\mathcal{T}$  using the perturbations shown in Table III. The Peierls phase for the two diagonal hoppings are found to be

$$\lambda \rightarrow \lambda(\phi) = \lambda \exp \left( i \int_{(x,y)}^{(x+1,y\pm 1)} \mathbf{A} \cdot d\mathbf{r} \right) = t \exp \left( -i\phi y \pm i\frac{\phi}{2} \right). \quad (\text{F12})$$

At  $\phi = 2\pi$  where the new model is  $\mathcal{T}$  symmetric, the magnetic unit cell is the same as at  $\phi = 0$ . Indeed, adding the new hopping has not changed  $\mu = 1$ , thus *not* requiring an enlarged magnetic unit cell at  $\phi = 2\pi$ , and the Hamiltonian is the same except for the diagonal coupling which obeys  $\lambda(2\pi) = -\lambda$ . We now construct two models:  $H_{weak}$  is characterized by the parameters  $\lambda = -0.1, M = 1.7$  and  $H_{strong}$  is characterized by  $\lambda = -0.2, M = 1.85$  (see Table III), each of which has a nontrivial  $\mathbb{Z}_2$  invariant at  $\phi = 0$ . We show in Fig. 19b that the first model  $H_{weak}$  exhibits a weak Hofstadter TI phase where both the  $\phi = 0$  and  $\phi = \Phi/2 = 2\pi$  Hamiltonians have nontrivial  $\mathbb{Z}_2$  invariants, so  $\theta = 0$ . On the contrary, we show in Fig. 19c that the second model  $H_{strong}$  exhibits a strong Hofstadter TI phase where the  $\mathbb{Z}_2$  invariant at  $\phi = \Phi/2$  is trivial, and hence  $\theta = \pi$ . From these two examples, we see that the topology at  $\Phi/2 = n\pi$  cannot be uniquely determined from the  $\phi = 0$  topology when  $n$  is even, and thus the Hofstadter Hamiltonian may be either a weak or strong TI.

## Appendix G: A Model of Twisted Bilayer Graphene

In this Appendix, we introduce a model of twisted bilayer graphene on the Moiré lattice. Briefly, we review the fragile topology in zero field, and then we move on to construct the Hofstadter Hamiltonian (App. G1). In App. G2, we introduce terms that isolate various symmetries of the model, and use these perturbed Hamiltonians to illustrate the results of Sec. . We also provide a detailed discussion of the  $UC_{2z}\mathcal{T}$  symmetry at  $\phi = \Phi/2$  and its constraints on the Wilson loop in both the Landau gauge magnetic unit cell and an expanded unit cell (App. G3). We discuss the bulk gap closings enforced by  $C_{2z}$  as mentioned in Sec. and the Wannier flow protected by  $C_{2z}\mathcal{T}$  from a real space perspective (App. G4). Finally, we also argue that  $C_{2x}\mathcal{T}$  can protect a bulk gapless point in App. G5.

## 1. The Hofstadter Hamiltonian

In Ref. [13], a 4-band model of twisted bilayer graphene was constructed on the Moiré lattice to capture the phenomenology of the fragile topology inherent to the system. In momentum space, the model is written

$$\begin{aligned}
H_{TBG}(\mathbf{k}) = & \Delta\mu_3 \otimes \sigma_0 + \mu_0 \otimes \sigma_1 \sum_{i=1}^3 t \cos(\boldsymbol{\delta}_i \cdot \mathbf{k}) + t' \cos(-2\boldsymbol{\delta}_i \cdot \mathbf{k}) \\
& - \mu_0 \otimes \sigma_2 \sum_{i=1}^3 t \sin(\boldsymbol{\delta}_i \cdot \mathbf{k}) + t' \sin(-2\boldsymbol{\delta}_i \cdot \mathbf{k}) - 2\lambda\mu_2 \otimes \sigma_3 \sum_{i=1}^3 \sin(\mathbf{d}_i \cdot \mathbf{k}).
\end{aligned} \tag{G1}$$

Here,  $\mu$  (resp.  $\sigma$ ) are the  $s, p$  orbital (resp. sublattice) Pauli matrices, and the Moiré lattice vectors are  $\mathbf{a}_1 = \sqrt{3}(0, -1)D$ ,  $\mathbf{a}_2 = (\frac{3}{2}, \frac{\sqrt{3}}{2})D$  where  $D$  is the length of the Moiré superlattice unit cell edge. The nearest-neighbor vectors are  $\boldsymbol{\delta}_1 = \frac{1}{3}\mathbf{a}_1 + \frac{2}{3}\mathbf{a}_2$ ,  $\boldsymbol{\delta}_2 = -\frac{2}{3}\mathbf{a}_1 - \frac{1}{3}\mathbf{a}_2$ ,  $\boldsymbol{\delta}_3 = \frac{1}{3}\mathbf{a}_1 - \frac{1}{3}\mathbf{a}_2$  and second-nearest-neighbors are  $\mathbf{d}_1 = \mathbf{a}_1$ ,  $\mathbf{d}_2 = \mathbf{a}_2$ ,  $\mathbf{d}_3 = -\mathbf{a}_1 - \mathbf{a}_2$ . We depict the hopping amplitudes in Fig. 20a-Fig. 20d and the vectors in Fig. 20e. From here forward, we normalize  $\mathbf{a}_1$  and  $\mathbf{a}_2$  to have unit area matching the convention established earlier, so we take  $\mathbf{a}_i \rightarrow \mathbf{a}_i/\Omega$ ,  $\Omega = \mathbf{a}_1 \times \mathbf{a}_2 = \frac{3\sqrt{3}}{2}D^2$ . The Peierls paths  $\mathcal{C}_1, \mathcal{C}_2, \mathcal{C}_3$  and  $\mathcal{C}_4$  of the model are sketched in Fig. 20.

We define the lattice with the center of the honeycomb at the origin, so the orbitals are located at  $(r_1 - \frac{1}{2})\mathbf{a}_1 + r_2\mathbf{a}_2 \pm \frac{1}{2}\boldsymbol{\delta}_1$ . Following Ref. [13], we choose parameters  $t' = -t/3$ ,  $\lambda = \sqrt{2/27}t$  in which case the onsite splitting  $\Delta$  determines the topology. For  $|\Delta| < 2t$ , there is a fragile pair winding of 1 in the Wilson loop of the occupied bands at half filling, which we plot in Fig. 2b. The winding is protected by a  $C_{2z}\mathcal{T} = I \otimes \sigma_1 K$  symmetry, and the model also has physical  $C_{3z} = I$ ,  $C_{2x} = \mu_3 \otimes I$  symmetries [13]. As written, this model also exhibits the ‘‘accidental’’ symmetries  $C_{2z} = I \otimes \sigma_1$ ,  $\mathcal{T} = K$  which are separately preserved in the model but need not be preserved in the physical system. Note that  $C_{2z}^2 = \mathcal{T}^2 = +1$ , indicating spinless particles.

Now we discuss the construction of the Hofstadter Hamiltonian. We proceed in the Landau gauge  $\mathbf{A}(\mathbf{r}) = -\phi\mathbf{b}_1(\mathbf{r} \cdot \mathbf{b}_2)$  which we emphasize is centered at the  $1a$  position in the center of the honeycomb although there is no orbital there. As argued in Ref. [49], the path of integration of the Peierls phases should be taken through the centers of the honeycomb cells because, from microscopics, the orbital overlap is greatest there. This is depicted in Fig. 3. Calculating the Peierls phases along those paths, we write the model in position space with the magnetic field as

$$\begin{aligned}
H_{TBG}^\phi = & \sum_{\mathbf{R}} \left( c_{\mathbf{R}}^\dagger \Delta\mu_3 \otimes \sigma_0 c_{\mathbf{R}} + \sum_{i=1}^3 \frac{t_i}{2} c_{\mathbf{R}+\boldsymbol{\delta}_i}^\dagger \mu_0 \otimes \sigma_1 c_{\mathbf{R}} + \frac{t'_i}{2} c_{\mathbf{R}-2\boldsymbol{\delta}_i}^\dagger \mu_0 \otimes \sigma_1 c_{\mathbf{R}} \right. \\
& \left. - i \sum_{i=1}^3 \frac{t_i}{2} c_{\mathbf{R}+\boldsymbol{\delta}_i}^\dagger \mu_0 \otimes \sigma_2 c_{\mathbf{R}} + \frac{t'_i}{2} c_{\mathbf{R}-2\boldsymbol{\delta}_i}^\dagger \mu_0 \otimes \sigma_2 c_{\mathbf{R}} - i \sum_{i=1}^3 c_{\mathbf{R}+\mathbf{d}_i}^\dagger \mu_2 \otimes \text{diag}(\lambda_i, -\lambda'_i) c_{\mathbf{R}} + h.c. \right)
\end{aligned} \tag{G2}$$

where the new hopping elements at each  $\mathbf{R} = r_1\mathbf{a}_1 + r_2\mathbf{a}_2$  are calculated using Eq. (A1) and the Peierls paths are given in Fig. 20f,g,h. We compute the Peierls phases along these paths to be

$$\begin{aligned}
t_i = & t \cos\left(\frac{\phi}{6}\right) \left\{ e^{-i\phi\frac{r_2}{3}}, e^{i\phi(\frac{2r_2}{3}-\frac{1}{3})}, e^{i\phi(-\frac{r_2}{3}+\frac{1}{6})} \right\}, t'_i = t' \left\{ e^{i\phi(\frac{2r_2}{3}-\frac{2}{3})}, e^{-i\phi\frac{4r_2}{3}}, e^{i\phi\frac{2r_2}{3}} \right\}, \\
\lambda_i = & \lambda \left\{ e^{-i\phi(r_2-\frac{1}{6})}, e^{-i\frac{\phi}{6}}, e^{i\phi(r_2-1)} \right\}, \lambda'_i = \lambda \left\{ e^{-i\phi(r_2+\frac{1}{6})}, e^{i\frac{\phi}{6}}, e^{i\phi r_2} \right\}.
\end{aligned} \tag{G3}$$

In particular, the nearest-neighbor hoppings have two Peierls paths taken in superposition (see Fig. 20f). For example, the paths  $\mathcal{C}_1, \mathcal{C}_2$  for the  $t_1$  hopping are shown in Fig. 21a, and the Peierls substitution reads

$$\begin{aligned}
t_1 \rightarrow t_1(\phi) = & \frac{t}{2} \left( e^{i\int_{\mathcal{C}_1} \mathbf{A} \cdot d\mathbf{r}} + e^{i\int_{\mathcal{C}_2} \mathbf{A} \cdot d\mathbf{r}} \right) \\
= & \frac{t}{2} \left( 1 + e^{i\int_{\mathcal{C}_2-\mathcal{C}_1} \mathbf{A} \cdot d\mathbf{r}} \right) e^{i\int_{\mathcal{C}_1} \mathbf{A} \cdot d\mathbf{r}}.
\end{aligned} \tag{G4}$$

Noting that  $\mathcal{C}_2 - \mathcal{C}_1 = \partial\mathcal{R}$ , where  $\mathcal{R}$  is marked as the grey rhombus in Fig. 21a, is a closed loop of area  $1/3$  (recalling that we normalized the area of the unit cell to 1), we find

$$\begin{aligned}
t_1(\phi) = & \frac{t}{2} \left( 1 + e^{i\phi/3} \right) e^{i\int_{\mathcal{C}_1} \mathbf{A} \cdot d\mathbf{r}} \\
= & \frac{t}{2} \left( e^{-i\phi/6} + e^{i\phi/6} \right) e^{i\frac{\phi}{6} + i\int_{\mathcal{C}_1} \mathbf{A} \cdot d\mathbf{r}} \\
= & t \cos\left(\frac{\phi}{6}\right) e^{i\frac{\phi}{6} + i\int_{\mathcal{C}_1} \mathbf{A} \cdot d\mathbf{r}}.
\end{aligned} \tag{G5}$$

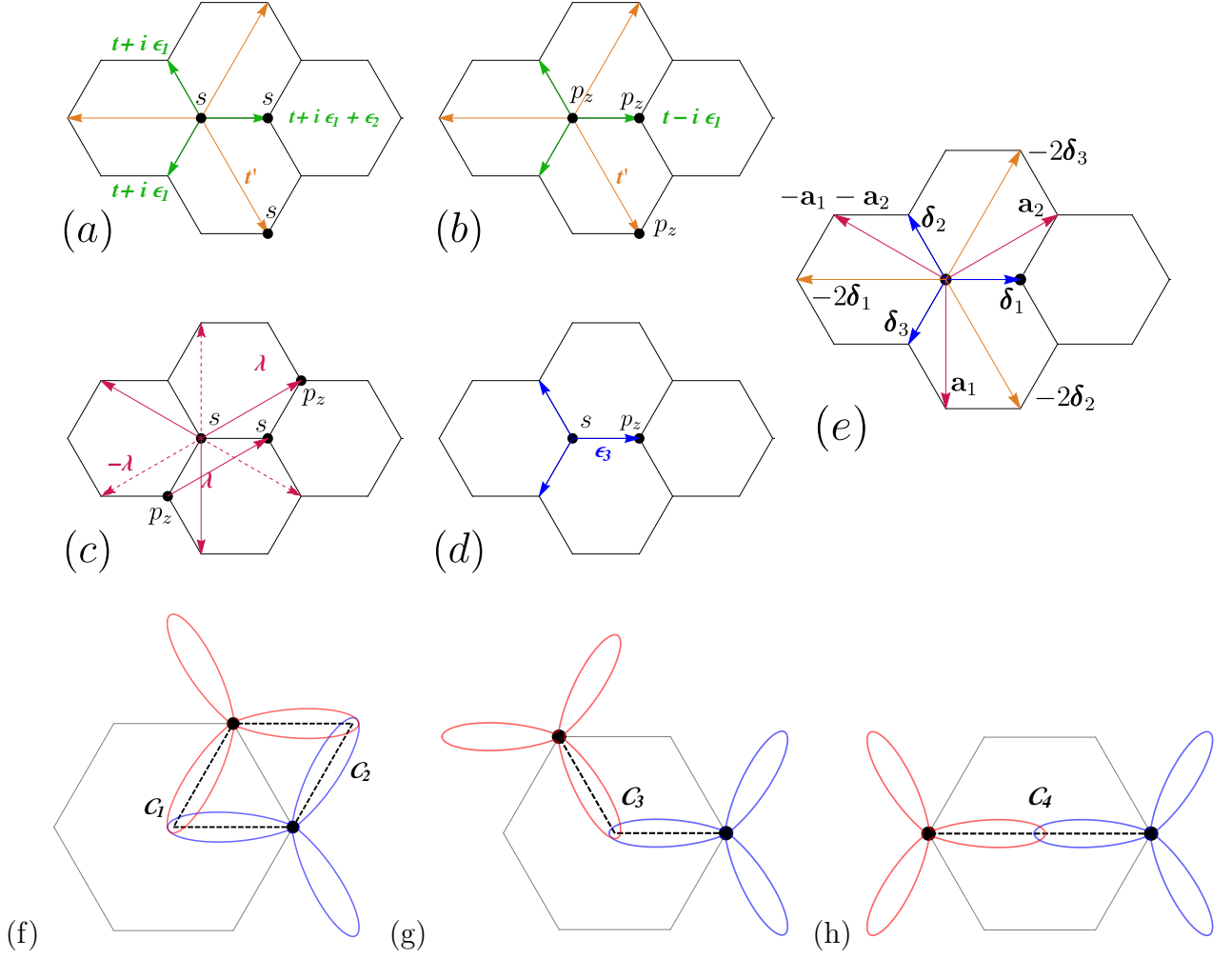


FIG. 20. (a) – (d) We depict the hoppings  $t, t'$ , and  $\lambda$  for the  $s$  and  $p_z$  orbitals of the model in Ref. [13]. We also show the amplitudes  $\epsilon_1, \epsilon_2$ , and  $\epsilon_3$  of the symmetry breaking terms which are discussed in App. G2. For visual clarity, the arrows denoting the hoppings do *not* correspond to the Peierls paths which are instead shown in Fig. 3. (e) We also depict the first-, second-, and third-nearest neighbor vectors of the model. (f) We show the two Peierls paths of the nearest-neighbor hopping,  $C_1$  and  $C_2$ , we are taken in superposition as we discuss in Fig. 3. (g) We show the second nearest-neighbor path  $C_3$ . (h) We show the second nearest-neighbor path  $C_4$ .

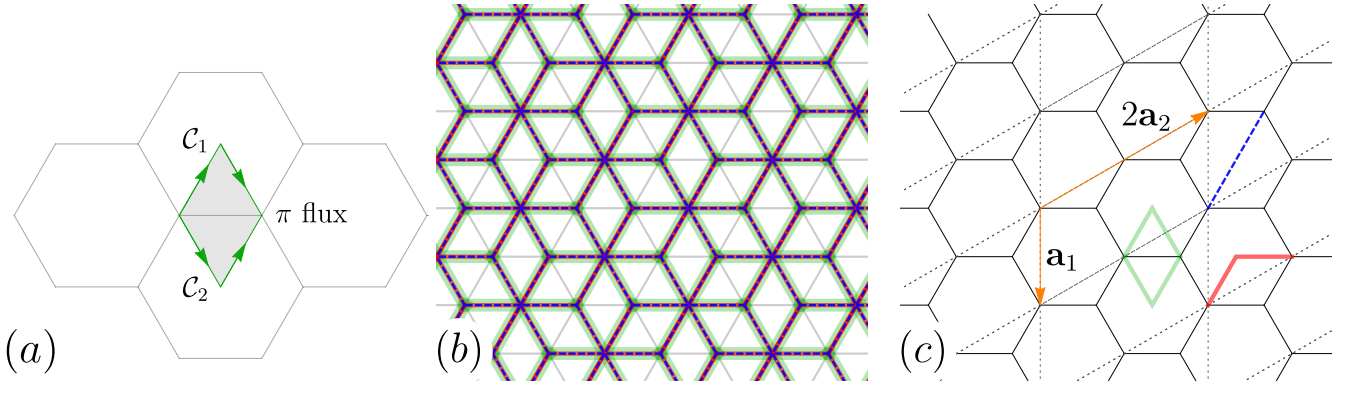


FIG. 21. (a) We sketch the two paths ( $C_1$  and  $C_2$ ) of a nearest-neighbor hopping which are taken in superposition. At  $\phi = \Phi/2 = 3\pi$ , the phase difference between  $C_1$  and  $C_2$  is equal to  $3\pi \times \frac{1}{3} = \pi$  because the paths enclose  $1/3$  of a unit cell. Thus, their contributions to the amplitude add with exactly opposite signs, and the hopping vanishes. (b) We depict the Peierls paths of the model with the nearest-neighbor hoppings in green, the second nearest-neighbor hoppings in red, and the third nearest-neighbor hoppings in dashed blue. The honeycomb is shown in light grey. We see that any closed loop along the Peierls' paths encloses an integer number of rhombuses, each of which is  $1/3$  of the unit cell. Hence  $n = 3$  and  $\Phi = 6\pi$ . (c) We show the  $1 \times 2$  magnetic unit cell of the model at  $\phi = \mu \frac{2\pi p'}{q} = 3 \frac{2\pi}{2}$  outlined in dotted grey lines. In addition for visual clarity, we also show examples of the first-, second-, and third nearest neighbor paths shown with the same colors as in (b).

Computing the remaining integral gives Eq. (G3). We emphasize in the  $\lambda$  hopping term,  $\sigma_z \rightarrow \text{diag}(\lambda, -\lambda')$  because the different sublattice sites have different hopping paths. We refer to the phases of the hoppings as  $\arg t_i = \varphi_{t_i}(\ell)$ ,  $\arg t'_i = \varphi_{t'_i}(\ell)$ ,  $\arg \lambda_i = \varphi_{\lambda_i}(\ell)$ ,  $\arg \lambda'_i = \varphi_{\lambda'_i}(\ell)$ .

To Fourier transform Eq. (G2) in momentum space in the Landau gauge, we compute  $\mu$  using Eq. (A28). To do so, we only need the vectors between orbitals connected by hoppings, which for nearest neighbors are  $\delta_i$ , second nearest neighbors are  $\mathbf{a}_i$ , and third nearest neighbors are  $-2\delta_i$ . From Eq. (A28), we calculate  $\mu = \text{lcd} \{ \mathbf{b}_1 \cdot \delta_i, \mathbf{b}_1 \cdot \mathbf{a}_i, \mathbf{b}_1 \cdot (-2\delta_i) \}_{i=1}^3 = \text{lcd} \{ \frac{1}{3}, -\frac{2}{3}, \frac{1}{3}, 1, 0, -\frac{2}{3}, \frac{4}{3}, -\frac{2}{3} \} = 3$ . Hence, we can form the Hofstadter Hamiltonian by taking  $\phi = 3 \frac{2\pi p'}{q}$  for  $p', q'$  coprime, and define the magnetic BZ as  $k_1 \in (-\pi, \pi), k_2 \in (0, 2\pi/q')$  with a  $1 \times q'$  magnetic unit cell. Indeed, one can check that  $\phi = 3 \frac{2\pi p'}{q}$  explicitly gives a  $r_2 \rightarrow r_2 + q'$  periodicity in the Peierls phases from Eq. (G3). Note that in Ref. [49], the Hofstadter of the model was constructed in the square lattice gauge  $\mathbf{A}_{sq}(\mathbf{r}) = \phi(0, x)$ , which is not the form of our Landau gauge,  $\mathbf{A}(\mathbf{r}) = -\phi \mathbf{b}_1(\mathbf{r} \cdot \mathbf{b}_2)$ . In the square lattice gauge, Ref. [49] found it was necessary to rationalize the flux as  $\phi = 2 \frac{2\pi p'}{q}$ . There is no contradiction because the rationalization is gauge-dependent.

The flux periodicity  $\Phi$  is gauge invariant and is determined by the possible loops along Peierls paths. We overlay all possible Peierls paths in Fig. 21b, from which we can see that all paths enclose a multiple of  $1/3$  of a unit cell. Hence  $n = 3$  and  $\Phi = 6\pi$ . Note that  $\mu$  and  $n$  being identical is coincidental, as can be seen by considering the gauge choice of Ref. [49] where this explicitly does not hold.

We now construct the Hofstadter Hamiltonian. As required, there is no dependence on  $r_1$  and the Hamiltonian can be Fourier transformed over  $\mathbf{a}_1$  immediately. At  $\phi = 3 \frac{2\pi p'}{q}$ , we choose the unit cell to be indexed by  $\ell = 0, \dots, q' - 1$ . An example of the  $\phi = 3\pi$  ( $q' = 2$ ) magnetic unit cell is shown in Fig. 21c. Keeping track of how the hoppings connect different atoms in the magnetic unit cell, we derive the Hofstadter Hamiltonian

$$[\mathcal{H}^\phi(\mathbf{k})]_{\ell, \ell'} = \delta_{\ell \ell'} h_\ell + \delta_{\ell-1, \ell'} T_\ell^\dagger + \delta_{\ell'-1, \ell} T_{\ell'} + \delta_{\ell-2, \ell'} S_\ell^\dagger + \delta_{\ell'-2, \ell} S_{\ell'} \quad (\text{G6})$$

where the  $4 \times 4$  blocks are given by

$$\begin{aligned} h_\ell &= \Delta \mu_3 \otimes \sigma_0 + \mu_0 \otimes \sigma_1 (|t_i| \cos(\mathbf{k} \cdot \delta_1 - \varphi_{t_1}(\ell)) + t' \cos(2\mathbf{k} \cdot \delta_2 + \varphi_{t_2}(\ell)) + t' \cos(2\mathbf{k} \cdot \delta_3 + \varphi_{t_3}(\ell))) \\ &\quad - \mu_0 \otimes \sigma_2 (|t_i| \sin(\mathbf{k} \cdot \delta_1 - \varphi_{t_1}(\ell)) + t' \sin(-2\mathbf{k} \cdot \delta_2 - \varphi_{t_2}(\ell)) + t' \sin(-2\mathbf{k} \cdot \delta_3 - \varphi_{t_3}(\ell))) \\ &\quad - \lambda \mu_2 \otimes \text{diag}(\sin(\mathbf{k} \cdot \mathbf{d}_1 - \varphi_{\lambda_1}(\ell)), -\sin(\mathbf{k} \cdot \mathbf{d}_1 - \varphi_{\lambda_1}(\ell))) \\ T_\ell &= \frac{|t_i|}{2} (\mu_0 \otimes \sigma_1 - i\mu_0 \otimes \sigma_2) (e^{i\varphi_{t_2}(\ell) - i\mathbf{k} \cdot \delta_2} + e^{i\varphi_{t_3}(\ell) - i\mathbf{k} \cdot \delta_3}) \\ &\quad - i\lambda \mu_2 \otimes (-\text{diag}(e^{-i\varphi_{\lambda_2}(\ell-1)}, -e^{-i\varphi_{\lambda_2}(\ell-1)}) e^{i\mathbf{k} \cdot \mathbf{d}_2} + \text{diag}(e^{i\varphi_{\lambda_3}(\ell)}, -e^{i\varphi_{\lambda_3}(\ell)}) e^{-i\mathbf{k} \cdot \mathbf{d}_3}) \\ S_\ell &= \frac{t'}{2} (\mu_0 \otimes \sigma_1 - i\mu_0 \otimes \sigma_2) e^{i\varphi_{t_1}(\ell) + 2i\mathbf{k} \cdot \delta_1} . \end{aligned} \quad (\text{G7})$$



TABLE IV. Symmetries of the TBG Model

Symmetry	$\phi = 0$	$\phi \neq 0$	Mapping of $\mathbf{k}, \phi$
$C_{3z}$	$I$	$C_{3z}G_{2\pi/3}$	$R_{2\pi/3}\mathbf{k}, \phi$
$C_{2x}$	$\mu_3 \otimes I$	$C_{2x}$	$(k_x, -k_y), -\phi$
$C_{2z}$	$I \otimes \sigma_1$	$C_{2z}\mathcal{D}$	$-\mathbf{k}, \phi$
$\mathcal{T}$	$K$	$\mathcal{T}$	$-\mathbf{k}, -\phi$
$C_{2z}\mathcal{T}$	$I \otimes \sigma_1 K$	$C_{2z}\mathcal{DT}$	$\mathbf{k}, -\phi$
$C_{2x}\mathcal{T}$	$-i\mu_3 \otimes IK$	$C_{2x}\mathcal{T}$	$(-k_x, k_y), \phi$
$C_{2x}C_{2z}$	$i\mu_3 \otimes \sigma_1$	$C_{2x}C_{2z}\mathcal{D}$	$(-k_x, k_y), -\phi$
$C_{2x}C_{2z}\mathcal{T}$	$\mu_3 \otimes \sigma_1 K$	$C_{2x}TC_{2z}\mathcal{D}$	$(k_x, -k_y), \phi$

We list the symmetries of the TBG model Eq. (G2) in column 1 and their representations on the Bloch Hamiltonian in column 2. In column 3, we provide their representations on the Hofstadter Hamiltonian  $\mathcal{H}_{TBG}$  in the presence of nonzero flux. The symmetries listed in column 3 refer to the  $4 \times 4$  representations defined in column 2. Note that for  $\phi \neq 0$ , some of the symmetries are broken, and take  $\phi \rightarrow -\phi$ . The mapping of  $\mathbf{k}$  and  $\phi$  under the action of the symmetries is shown in column 4.

This completes the construction of the Hofstadter Hamiltonian. We can now discuss the symmetries of the  $H_{TBG}^\phi$  at nonzero flux. The  $\phi = 0$  symmetries are promoted to those in Table IV (third column) when  $\phi \neq 0$  with the additional  $\mathcal{D}$  and  $G'$  factors. For brevity, we do not include product symmetries with  $C_{3z}$  and the other symmetries since they are broken when we break  $C_{3z}$ . Again,  $\mathcal{D}_{\ell\ell'} = \delta_{\ell, q' - \ell'}$  acts on the (enlarged) magnetic unit cell indices to flip the magnetic unit cell under  $C_{2z}$ . Additionally,  $C_{3z}$  requires a gauge transformation because our Landau gauge explicitly breaks  $C_{3z}$  symmetry. To determine the appropriate gauge transformation  $G'$ , we refer to the discussion around Eq. (F5) which shows that

$$G' = \exp\left(i \sum_{\mathbf{R}\alpha} c_{\mathbf{R}\alpha}^\dagger c_{\mathbf{R}\alpha} \chi(\mathbf{R} + \boldsymbol{\delta}_\alpha)\right) \quad (\text{G8})$$

where  $\chi(\mathbf{r}) = -\phi xy$  is the solution to

$$C_{3z}^{-1} \mathbf{A}(C_{3z}\mathbf{r}) - \nabla\chi(\mathbf{R}) = \mathbf{A}(\mathbf{r}) . \quad (\text{G9})$$

We refer the reader to Ref. [60] for a detailed treatment of space group symmetries in the presence of magnetic fields. We note that there is also a particle-hole symmetry  $Ph = \mu_1 \otimes \sigma_3$  that obeys

$$Ph^\dagger H_{TBG}^\phi(\mathbf{k}) Ph = -H_{TBG}^{-\phi*}(-\mathbf{k}) \quad (\text{G10})$$

which exists at  $\phi = 0$  and  $\phi = \Phi/2$ .

Using these expressions, one can check explicitly that the symmetries in Table IV are preserved. For symmetries that take  $\phi \rightarrow -\phi$ , the zero-field symmetry is restored at  $\Phi/2 = 3\pi, p'/q' = 1/2$ . At this point,  $\cos \frac{\Phi/2}{6} = 0$ , so nearest neighbor couplings vanish due to the interference of their Peierls paths. Fig. 21a illustrates that the phase difference between the two paths is  $\pi$ , and they destructively interfere.

## 2. Breaking Symmetries

Like in the case of the QSH model, we may add symmetry-breaking terms to  $H_{TBG}$  in order to isolate the effects of various symmetries. In Sec. , we showed that  $C_{2z}\mathcal{T}$  symmetry alone was responsible for the HOTI classification of the Hofstadter phase, and thus we build perturbations to destroy all other symmetries of the model. By coupling nearest neighbor atoms with an imaginary coupling that takes opposite signs for the  $s$  and  $p_z$  orbitals, we break  $C_{2z}$  and  $\mathcal{T}$  symmetry individually. In momentum space at  $\phi = 0$ , this term reads

$$H_1(\mathbf{k}) = \mu_3 \otimes \sum_i (\sigma_1 \sin \boldsymbol{\delta}_i \cdot \mathbf{k} + \sigma_2 \cos \boldsymbol{\delta}_i \cdot \mathbf{k}) . \quad (\text{G11})$$

One may check that this term breaks  $C_{2z}, \mathcal{T}, C_{2x}\mathcal{T}, C_{2x}C_{2z}$ . To break  $C_{3z} = I \otimes I$ , we add an anisotropic term that alters only the  $\boldsymbol{\delta}_1$  hopping,

$$H_2(\mathbf{k}) = \mu_0 \otimes (\sigma_1 \cos \boldsymbol{\delta}_1 \cdot \mathbf{k} - \sigma_2 \sin \boldsymbol{\delta}_1 \cdot \mathbf{k}) . \quad (\text{G12})$$

TABLE V. TBG Hamiltonians and their Symmetries

Hamiltonian	Symmetries	Parameters
$H'_{TBG} = H_{TBG} + \epsilon_1 H_{1,im}(\mathbf{k}) + \epsilon_2 H_2(\mathbf{k}) + \epsilon_3 H_3(\mathbf{k})$	$C_{2z}\mathcal{T}$	$\epsilon_1 = .12, \epsilon_2 = .11, \epsilon_3 = .1, \Delta = 1.6$
$H''_{TBG} = H_{TBG} + \epsilon_2 H_2(\mathbf{k}) + \epsilon_3 H_3(\mathbf{k})$	$C_{2z}, \mathcal{T}, C_{2z}\mathcal{T}$	$\epsilon_2 = .11, \epsilon_3 = .1, \Delta = 1.6$
$H'''_{TBG} = H_{TBG} + \epsilon_2 H_2(\mathbf{k}) + \epsilon_4 H_4(\mathbf{k})$	$C_{2x}\mathcal{T}$	$\epsilon_2 = .11, \epsilon_4 = .1, \Delta = 1.6$

We list the variations of the TBG model (column 1), the symmetries they retain from the perturbations (column 2), and the values of the parameters that realize their nontrivial Hofstadter topology (column 3). The Hofstadter Butterflies of the models may be found in Fig. 2, Fig. 23, and Fig. 24.

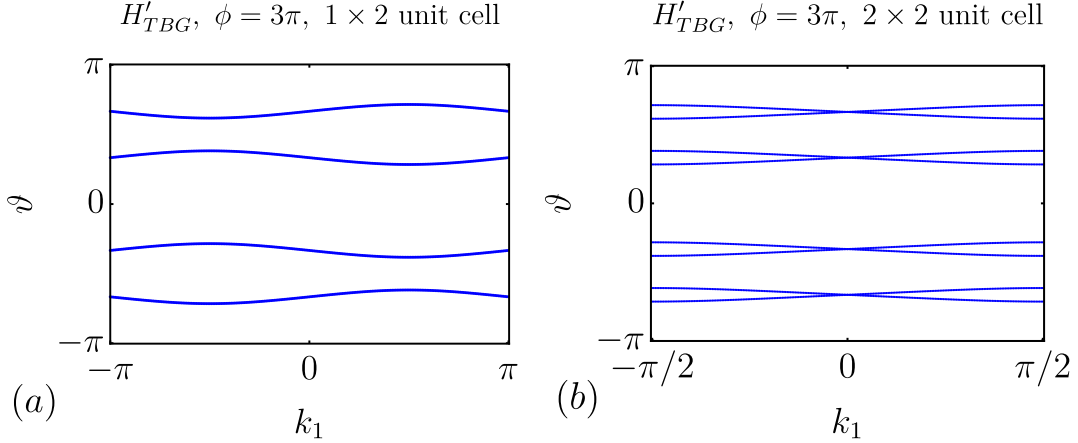


FIG. 22. (a) We show the Wilson Loop spectrum for  $H'_{TBG}$  in the  $1 \times 2$  magnetic unit cell of our Landau gauge at  $\phi = \Phi/2$  where  $UC_{2z}\mathcal{T}$  is not diagonal in momentum space. Hence there is no “particle-hole” symmetry. (b) To make  $U$  diagonal in momentum space such that the Wilson spectrum realizes the “particle-hole” symmetry of a conventional  $w_2$  insulator, we diagonalize  $H^{\Phi/2}$  in a  $2 \times 2$  unit cell where  $k_1$  is defined in  $(-\pi/2, \pi/2)$ . We calculate the Wilson loop for this Hamiltonian and observe that it matches the spectrum of (a) with the Wilson bands folded so  $k_1$  is defined only mod  $\pi$ . Note that  $(UC_{2z}\mathcal{T})^2 = +1$ , so we may calculate  $w_2^{\phi=\Phi/2}$  as described in App. E 2 without calculating the nested Wilson loop.

To break  $C_{2x}$  and all the remaining product symmetries, we use the term

$$H_3(\mathbf{k}) = \mu_1 \otimes \sum_i (\sigma_1 \cos \delta_i \cdot \mathbf{k} - \sigma_2 \sin \delta_i \cdot \mathbf{k}). \quad (\text{G13})$$

One may check that all these perturbations preserve the particle-hole symmetry Eq. (G10). This is desirable for stabilizing the corner modes at zero energy, although this is not essential to the physics of the model. We will show in App. G 4 that if  $C_{2z}$  and  $\mathcal{T}$  are maintained, then a bulk gap closing is enforced by the  $C_{2z}$  eigenvalues. To show this, we remove  $H_1$  to create the Hamiltonian  $H''_{TBG}$  which possesses  $C_{2z}, \mathcal{T}$ , and their product  $C_{2z}\mathcal{T}$ .  $H''_{TBG}$  has a gapless bulk due to  $C_{2z}$  (see Fig. 23). Note that although  $H''_{TBG}$  has a  $\mathcal{T}$  symmetry, this model is spinless and thus  $\mathcal{T}^2 = +1$  so there is no Kane-Mele invariant. The models in this section are summarized in Table V.

### 3. Computing the $w_2$ index protected by $UC_{2z}\mathcal{T}$ symmetry

From Table V, we see that  $H'_{TBG}$  has a  $C_{2z}\mathcal{T}$  symmetry and hence has  $UC_{2z}\mathcal{T}$  symmetry at  $\phi = \Phi/2$ . As shown in Fig. 15a,  $(UC_{2z}\mathcal{T})^2 = e^{i\gamma_2}(C_{2z}\mathcal{T})^2 = +1$ , so the phase at  $\phi = \Phi/2$  is characterized by the  $w_2$  invariant. Following the discussion of App. E 2 where we used this model as an example, we can compute this invariant in a  $2 \times 2$  unit cell where  $UC_{2z}\mathcal{T}$  acts diagonally in momentum space. For pedagogical purposes, we also compute the Wilson loop in the  $1 \times 2$  unit cell at  $\phi = \Phi/2$  where  $UC_{2z}\mathcal{T}$  is not diagonal and there is no particle-hole symmetry in the Wilson spectrum. We plot the Wilson loop spectra using these two possible unit cells in Fig. 22. From the spectrum of Fig. 22b, we observe that there are no crossings at  $\vartheta = 0$  or  $\vartheta = \pi$  and thus  $w_2^{\phi=\Phi/2} = 0$ . Note that the number of crossings at  $\vartheta = 0$  must equal the number at  $\vartheta = \pi$  because  $\{\vartheta(k_1 + \phi)\} = \{\vartheta(k_1) + \pi\}$  (see Eq. (C12)). From here,

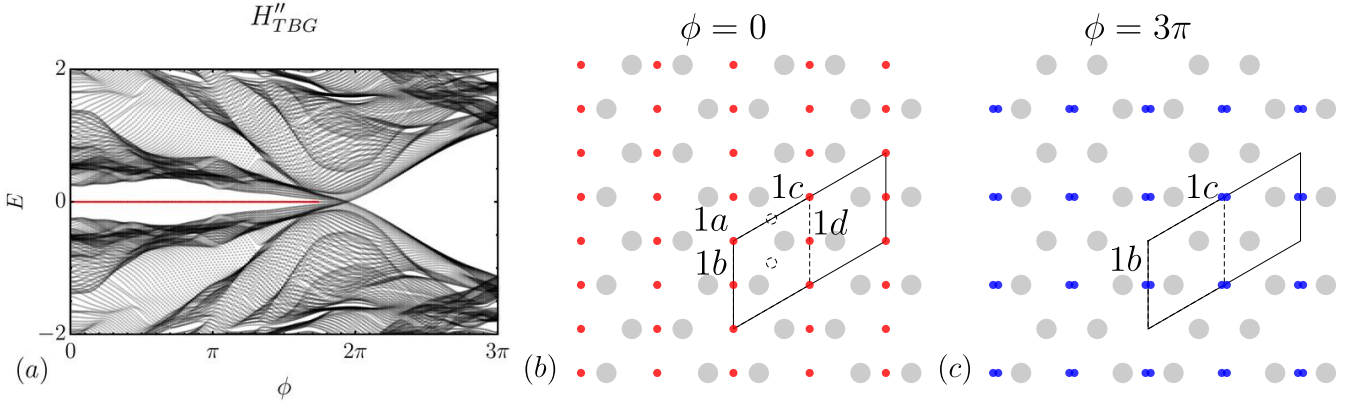


FIG. 23. The Hofstadter Butterfly is calculated on a  $20 \times 20$  lattice in the topological phase for  $H''_{TBG}$ , described in App. G 1, which has both  $C_{2z}$  and  $\mathcal{T}$ . Because  $C_{2z}\mathcal{T}$  remains, there is still corner mode pumping, but the model is not a HOTI due to the bulk gap closing enforced by  $C_{2z}$  eigenvalues. We demonstrate this in (b) and (c), where the Wannier centers of the phases at  $\phi = 0, 3\pi$  are shown in red and blue respectively in *magnetic* unit cell. (We show the boundary of the *standard* unit cell and its  $1c, 1d$  orbitals with dashed lines.) A possible Wannierization is shown in (b), with  $s$  and  $p_z$  orbitals at the  $1b$  and  $1c$  positions. Without breaking  $C_{2z}$  symmetry, pairs of orbitals may be moved to other high symmetry Wyckoff positions, but it is impossible to reach the state at  $\phi = 0$ .

we can calculate the Hofstadter HOTI invariant

$$\theta = w_2^{\phi=0} - w_2^{\phi=\Phi/2} = 1 \quad (\text{G14})$$

recalling that  $H^{\phi=0}$  is nontrivial. Thus corner states are pumped into the bulk as the flux is tuned from 0 to  $\Phi/2$  as we see in Fig. 2a of the Main Text. We discuss the signatures of this phase in the following section App. G 4 from a real-space perspective.

#### 4. $C_{2z}$ Symmetry Eigenvalues

When  $C_{2z}$  and  $\mathcal{T}$  remain symmetries of the model as in  $H'_{TBG}$ , a gap closing may be enforced by the symmetry eigenvalues of  $C_{2z}$ , as we observe from the Hofstadter Butterfly in Fig. 23a. We will prove this gap closing for  $H''_{TBG}$  (see Table V) using the framework of Topological Quantum Chemistry [50–52]. To obtain the band representations of this model, we calculate the  $C_{2z}$  eigenvalues directly from  $H''_{TBG}$  (see Table V) for  $\phi = 3\pi$  at the 4 inversion invariant points in the  $\phi = 3\pi$  BZ. The calculation is straightforward at  $\phi = 3\pi$  using the embedding matrices and symmetries defined in Sec. A 8 and App. G 1 respectively. At  $\phi = 0$ , note that we must artificially extend the  $1 \times 1$  unit cell to the  $1 \times 2$  magnetic unit cell to compare the atomic limits of the band representations at  $\phi = 0$  and  $\phi = 3\pi$  in the same unit cell.

We collect the eigenvalues of the occupied bands in Table VI. We note that at  $\phi = 0$  and  $\phi = 3\pi$ , all bands are connected energetically. We emphasize that Wyckoff positions correspond to the *magnetic* unit cell, i.e.  $1a = (0, 0)$ ,  $1b = \mathbf{a}_1/2$ ,  $1c = 2\mathbf{a}_2/2$ ,  $1d = \mathbf{a}_1/2 + 2\mathbf{a}_2/2$  taking the center of the hexagonal plaquette ( $1a$ ) as the origin.

TABLE VI. TBG  $C_{2z}$  eigenvalues

	$(0, 0)$	$\pi\mathbf{b}_1$	$\frac{\pi}{2}\mathbf{b}_2$	$\pi\mathbf{b}_1 + \frac{\pi}{2}\mathbf{b}_2$	Band Representation
$\xi^{\phi=0}$	$-1, -1, +1, +1$	$+1, +1, +1, +1$	$-1, -1, +1, +1$	$-1, +1, -1, +1$	$BR^{\phi=0} = 2\Gamma_1 + 2\Gamma_2 + 4B_1 + 2Y_1 + 2Y_2 + 2A_1 + 2A_2$
	$(0, 0)$	$\pi\mathbf{b}_1$	$\frac{\pi}{2}\mathbf{b}_2$	$\pi\mathbf{b}_1 + \frac{\pi}{2}\mathbf{b}_2$	Band Representation
$\xi^{\phi=3\pi}$	$-1, -1, +1, +1$	$-1, -1, +1, +1$	$-1, -1, +1, +1$	$-1, -1, +1, +1$	$BR^{\phi=3\pi} = 2\Gamma_1 + 2\Gamma_2 + 2B_1 + 2B_2 + 2Y_1 + 2Y_2 + 2A_1 + 2A_2$

In columns 1-4, we show the  $C_{2z}$  eigenvalues calculated from  $H''_{TBG}$  (see Table V) at half filling in the  $1 \times 2$  magnetic unit cell at both  $\phi = 0$  and  $\phi = 3\pi$ . Column 5 shows the (spinless) band representations determined from the eigenvalues.

We see that we may obtain the momentum space band representations of Table VI by inducing atomic orbitals from high symmetry Wyckoff positions to the full space group [66, 67]. First we consider the  $\phi = 0$  band representation.

Because no  $B_2$  irreps appear, the possible atomic orbitals are  $A_{1a}, B_{1b}, A_{1c}, B_{1d}$ , recalling that  $A(B)$  is the even (odd) irrep under  $C_{2z}$ . There is only one Wannierization possible:

$$BR^{\phi=0} = (A_{1a} \oplus B_{1b} \oplus A_{1c} \oplus B_{1d}) \uparrow G. \quad (\text{G15})$$

We show the location of the Wannier centers in Fig. 23b.

Next, we consider the bands at  $\phi = 3\pi$  forming  $BR^{\phi=3\pi}$ . In this case, there are many non-unique atomic limits that recover the band structure. Note that any pair of locally even irreps ( $s$  orbitals) and locally odd irreps ( $p_z$  orbitals) at the same Wyckoff position  $w$  yields the band representation  $(A_w \oplus B_w) \uparrow G = \Gamma_1 + \Gamma_2 + B_1 + B_2 + Y_1 + Y_2 + A_1 + A_2$  when induced to the space group. Thus placing both an  $s$  and  $p_z$  orbital at any two high symmetry Wyckoff positions  $w_1, w_2$  will yield  $(A_{w_1} \oplus B_{w_1} \oplus A_{w_2} \oplus B_{w_2}) \uparrow G = BR^{\phi=3\pi}$ . In fact, these limits  $A_{w_1} \oplus B_{w_1} \oplus A_{w_2} \oplus B_{w_2}$  are the only possible atomic limits. This may be shown by exhaustion. In Fig. 23b, we show one such Wannierization to the  $1b$  and  $1c$  Wyckoff positions within the magnetic unit cell.

We conclude that there must be an odd number of irreps at the  $1a$  position for  $\phi = 0$ , but there must be an even number of irreps at the  $1a$  position for  $\phi = 3\pi$ . Under  $C_{2z}$ -preserving perturbations that preserve the gap, electrons may be moved off the high symmetry Wyckoff positions into the  $2e = (x, y), (1-x, 1-y)$  position *in pairs*, so necessarily only an even number of electrons can be deformed to another high symmetry Wyckoff position. We see that  $BR^{\phi=0}$  and  $BR^{\phi=3\pi}$  are incompatible in this manner, and a gap closing must occur at an intermediate  $\phi$  while  $C_{2z}$  is preserved, as we see in Fig. 23a. We underscore that although the magnetic unit and the magnetic BZ do not evolve smoothly as the flux is increased, the Wannier centers do evolve smoothly, which our argument relies on.

We can also use this position-space argument to understand the Wannier flow that characterizes the Hofstadter HOTI phase when  $C_{2z}$  is broken but  $C_{2z}\mathcal{T}$  is preserved. For instance, we can take  $H''_{TBG}$  and break its  $C_{2z}$  symmetry by adding a small perturbation Eq. (G11), resulting in the new model  $H'_{TBG}$  which only has  $C_{2z}\mathcal{T}$  symmetry. Let us first consider the Wannier centers of  $H'_{TBG}$  at  $\phi = 0$  and  $\phi = 3\pi$  where  $UC_{2z}\mathcal{T}$  still pins Wannier centers to the high-symmetry Wyckoff positions (which are invariant under the magnetic point group  $2'$  (a proper subset of the point group  $2$ ) symmetries). Then as argued in App. G3, the Wannier centers must flow nontrivially between  $\phi = 0$  and  $\phi = 3\pi$  where there are different Wannierizations. However, with  $C_{2z}$  broken, this Wannier flow does *not* require a gap closing as the flux is tuned from 0 to  $3\pi$ . This is because the Wannier centers are not constrained to obey  $C_{2z}$  symmetry at all  $\phi$ . Instead, the Wannier flow is  $C_{2z}\mathcal{T}$ -symmetric: if there is a Wannier center at  $\mathbf{r}$  at flux  $\phi$ , then by  $C_{2z}\mathcal{T}$ , there is a Wannier center at  $-\mathbf{r}$  and  $-\phi$ . So each trajectory  $\mathbf{r}(\phi)$  must obey  $\mathbf{r}(\phi) = -\mathbf{r}(-\phi)$ . Thus as we tune the flux through its full period, we find nontrivial Wannier flow that pumps electrons between unit cells. We depict an example in Fig. 24a of two electrons interpolating between the  $1a, 1d$  Wyckoff positions at  $\phi = 0$  and the  $1c, 1b$  positions at  $\phi = \Phi/2$ . On open boundary conditions, this induces corner state flow. The corner states must be degenerate in energy at  $\phi = 0$  because they are  $C_{2z}\mathcal{T}$  partners, and are pinned to zero energy when particle-hole symmetry exists. As the flux is increased, the pumping converts an occupied energy level to a hole on one of the boundaries with the reverse process happening on the other boundary by  $C_{2z}\mathcal{T}$ , matching the energy splitting in Fig. 2.

## 5. $C_{2x}\mathcal{T}$ -Protected Gap Closing

While we have not paid much attention to the  $C_{2x}$  and  $C_{3z}$  symmetries of the model, it is important to break the composite symmetry  $C_{2x}\mathcal{T}$  to realize the HOTI phase. (Note  $C_{2x}\mathcal{T}$  exists in  $H_{TBG}$  due to the accidental  $\mathcal{T}$  symmetry.) We argue now that because both  $C_{2x}$  and  $\mathcal{T}$  take  $\phi \rightarrow -\phi$  in the Hofstadter Hamiltonian (see Table IV),  $C_{2x}\mathcal{T}$  is preserved at all flux and may protect a gap closing [? ].

Let  $\mathcal{H}^\phi(\mathbf{k})$  be the Hofstadter Hamiltonian of the  $H_{TBG}$ . It obeys

$$C_{2x}\mathcal{T}\mathcal{H}^\phi(k_x, k_y)(C_{2x}\mathcal{T})^{-1} = \mathcal{H}^\phi(-k_x, k_y), \quad C_{2x}\mathcal{T} = I_{q'} \otimes (-i\mu_3 \otimes I_2K), \quad (\text{G16})$$

with  $I_{q'}$  the  $q' \times q'$  identity matrix. Our strategy for understanding the bulk gap closing is to study an effective two band Hamiltonian that models the low energy behavior near the Fermi level. We will show that generically,  $C_{2x}\mathcal{T}$  symmetry is sufficient to prove a gap closing between the two bands at some  $\phi$ , but this is only a proof of local stability. In particular, the assumption of an effective two band model assumes the two bands are close to each other and well separated from all other bands. This is certainly false when  $\Delta$ , the onsite potential, is large and the conduction bands are far from the valence bands. As such no gap closing need exist. This is similar to the local stability of a Weyl node, which is locally protected but can be gapped out in pairs.

Because  $C_{2x}\mathcal{T}$  acts as the identity on the sublattice index but as  $-i\mu_3$  on the spin indices (see Eq. (G16)), the minimal low energy Hamiltonian consists of two bands which adequately models the highest energy valence band and lowest energy conduction band. The most general effective Hamiltonian is then

$$\mathcal{H}_{eff}(k_x, k_y, \phi) = d_0(\mathbf{k}, \phi)\mu_0 + d_1(\mathbf{k}, \phi)\mu_1 + d_2(\mathbf{k}, \phi)\mu_2 + d_3(\mathbf{k}, \phi)\mu_3 \quad (\text{G17})$$

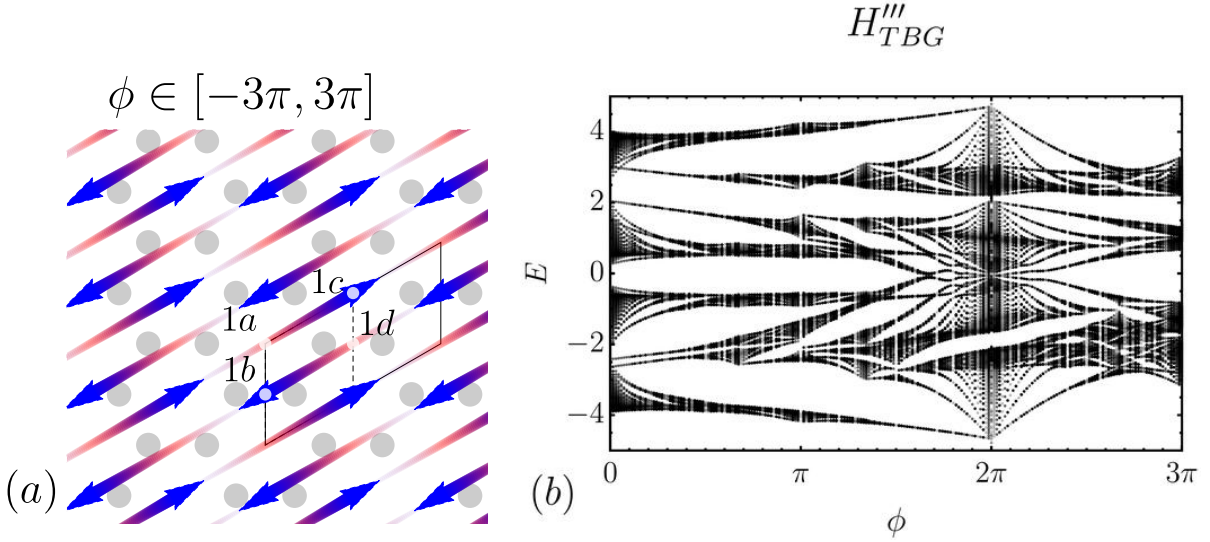


FIG. 24. (a) We show an example of  $C_{2z}\mathcal{T}$  symmetric Wannier flow from  $\phi = -3\pi$  to  $\phi = 3\pi$ , going from the  $1b, 1c$  positions at  $\phi = -3\pi$  (blue) to the  $1a, 1d$  positions (red), and back to the  $1b, 1c$  positions at  $\phi = 3\pi$ . When we break  $C_{2z}$ , the orbitals may move slightly from the maximal Wyckoff positions. However, with  $C_{2z}\mathcal{T}$  intact, the Wannier flow is still protected. (b) We show the Hofstadter Butterfly for  $H'''_{TBG}$  on periodic boundary with only  $C_{2x}\mathcal{T}$  symmetry, and observe the bulk gap closing. The exact Hamiltonian is given in Table V. Because  $C_{2z}\mathcal{T}$  is broken, there is also no  $w_2^{\phi=0}$  invariant to protect winding in the Wilson loop. Thus the Hofstadter Topology is trivial, although the the bulk gap closing at finite flux is locally protected by  $C_{2x}\mathcal{T}$ .

and acting on this Hamiltonian,  $C_{2x} = -i\mu_3K$ . At  $k_x = 0$ , Eq. (G16) mandates that  $C_{2x}\mathcal{T}$  commute with  $H_{eff}$  at all  $k_y, \phi$ . Using Eq. (G17), we compute

$$C_{2x}\mathcal{T}\mathcal{H}_{eff}(0, k_y, \phi)(C_{2x}\mathcal{T})^{-1} = d_0(0, k_y, \phi)\mu_0 - d_1(0, k_y, \phi)\mu_1 + d_2(0, k_y, \phi)\mu_2 + d_3(0, k_y, \phi)\mu_3. \quad (\text{G18})$$

But  $[C_{2x}\mathcal{T}, \mathcal{H}_{eff}(0, k_y, \phi)] = 0$ , so  $d_1 = 0$ . There are two free parameters,  $k_y \in (-\pi, \pi), \phi \in (0, 6\pi)$ , which we fix by the requirement that  $d_2(0, k_y^*, \phi^*) = d_3(0, k_y^*, \phi^*) = 0$ . Generically, such a  $k_y^*$  and  $\phi^*$  will exist because the  $d_1, d_2$  space is of codimension 0. In this case,  $\mathcal{H}_{eff}(0, k_y^*, \phi^*) \propto \mu_0$ , and the two bands must be degenerate in energy.

We substantiate this argument with a numerical calculation of the Hofstadter Butterfly. We build  $H'''_{TBG}$  by adding terms to  $H_{TBG}$  that break all symmetries except  $C_{2x}\mathcal{T}$ . We make use of the new perturbation

$$H_4(\mathbf{k}) = \mu_0 \otimes \sigma_3 + \mu_2 \otimes \sigma_0 + \mu_3 \otimes \sigma_3 \quad (\text{G19})$$

which is onsite and preserves  $C_{2x}\mathcal{T}$ . Explicitly, it breaks  $C_{2z}, C_{2x}, \mathcal{T}, C_{2z}\mathcal{T}, C_{2x}C_{2z}, C_{2x}C_{2z}\mathcal{T}$ , and particle-hole symmetry. Using these perturbations, we build  $H'''_{TBG} = H_{TBG} + \epsilon_2 H_2(\mathbf{k}) + \epsilon_4 H_4(\mathbf{k})$  and include precise values of the parameters in Table V. We show the spectrum in Fig. 24b and observe that the bulk is gapless due to the Weyl node at  $(k_x, k_y, \phi) = (0, k_y^*, \phi^*)$ .